Precise Spike Timing in Complex Neural Networks

Dissertation

zur Erlangung des Doktorgrades
der Mathematisch-Naturwissenschaftlichen Fakultäten
der Georg-August-Universität zu Göttingen

vorgelegt von

Raoul-Martin Memmesheimer

aus Duisburg

Göttingen 2007

D7

Referent	:	Prof. Dr. Theo Geisel
Koreferent	:	Prof. Dr. Reiner Kree
Tag der mündlichen Prüfung	:	18.12.2007

Contents

Chapter 1

Introduction

Humans and other animals have a sensory system that is stimulated by their environment. The sensory system is highly selective and already pre-processes inputs. Further processing by the central nervous system ultimately leads to sensory and possibly conscious perception. Neurons and their interconnections are the biological basis for these and all related processes, ranging from the initiation of simple reflexes to the construction of high-level knowledge about the world.[1]

A crucial, established assumption about brain function is that it is not the overwhelming diversity of neurons which is responsible for complex behavior but their number and their interconnectivity, i.e. the *neural network* [104]. This suggests that it might be possible to capture basic properties of the functionality of the nervous system by studying the dynamics of neural networks with comparably simple neuron and connection models, although single neurons are highly complicated and their detailed microbiological architecture and dynamics are a subject of present research. This approach may enable us to clarify mechanisms which otherwise would remain obscured beneath the complexity of detailed description. Some tools for a quantitative description have been developed in physics and mathematics, in particular in statistical physics, dynamical systems theory and in the theory of stochastic processes.

For the understanding of a neural network, as for many other complex systems with underlying network structure (ranging from gene regulatory networks [80] to food webs of species [56]), it is crucial to understand how the dynamics of single elements together with couplings and network structure give rise to the collective dynamics. In studies of neural networks, the most common and also a very successful approach is to assess the dynamics generated by a predefined network analytically or numerically. Important examples in spiking neural networks include studies on emerging collective phenomena such as synchronization (cf. e.g.

[1] We note that here and in the following we adopt a "third person" perspective of an objective observer on the nervous system. Of course, subjects experience directly and immediately, in the "first person" perspective (see e.g. [134]). It is unclear if and how the individual, private experience can be explored in – generically intersubjective – natural sciences.

[190, 197, 195, 182]), on changes of the dynamics due to modification of the model, e.g. by introducing delayed coupling [58, 166] or short term synaptic plasticity [189, 191], on mean field theories (as reviewed e.g. in [33, 84]) or on networks with dynamical topology that changes according to learning schemes (cf., e.g., [10, 161, 138, 47, 139]). The inverse problem is to find networks that give rise to a predefined dynamics. A classical example is provided by an artificial Hopfield neural network [88]. Such a network is trained and, by gradually adapting its coupling strengths, it becomes an associative memory, fulfilling pattern recognition tasks. The network typically consists of binary units. In spiking neural networks, the inverse problem is less understood. Some studies constructed networks that give rise to dynamics similar to microscopic dynamics found in experiments: Reference [159] studies a three unit model for a central pattern generator, a neural network that produces rhythmic activity. Numerically, it was shown that the qualitative spiking dynamics is independent of both the details of the neuron model and the details of synaptic coupling. In [119], a method was presented to construct neural network models so that the neurons exhibit irregular spike trains with statistical properties similar to neurons in extracellular recordings.

However, the precise spike dynamics in neurobiological neural networks might also be important: In experimental recordings, precisely timed patterns of spikes are embedded in seemingly irregular spike trains of neurons in vivo and in vitro [6, 66, 152, 67]. Thus they have to be detected using advanced statistical methods [6, 89, 164]. Some of the methods have been criticized as producing false positives mainly due to violations of the underlying statistical assumptions in the spike trains [148, 137] and only recently statistical methods that are not subject to this criticism have been developed [66, 151]. Since the patterns of spikes are correlated with phases of activity, they might be important for neural processing [5, 6, 164, 152, 68]. Their dynamical origin, however, is unknown. A possible explanation for their occurrence is the existence of underlying 'synfire chains'. In these models, networks are designed by embedding chains of neuron groups with strong excitatory projections from one group to the next. These feedforward structures allow synchronous activity to stably propagate along the chain [3, 83, 54, 18]. So far, however, there is no experimental evidence for the existence of the underlying feedforward connected structures. Underlying recurrent networks that exhibit precisely timed patterns of spikes might be another explanation for the occurrence of precisely timed patterns of spikes. The construction of recurrent networks which give rise to a predefined, precisely timed pattern of spikes would be a possible first approach to such a model. Only few articles consider this problem. Reference [123] provides an algorithm to construct one specific, fully connected network that can realize one predefined simple periodic pattern of spikes, i.e. a pattern in which each neuron spikes once within a period. Another article showed how to construct networks realizing patterns close to the fully synchronous state [50] in networks of complicated connectivity.

Is it possible to determine spiking neural networks that give rise to arbitrary spike patterns with an analytical approach? Is it possible to determine the entire

set of such networks? In chapter 4 we positively answer these questions for a class of spiking neural networks. The method is very general, it covers strongly heterogeneous networks with different types of neurons and connections and allows to realize arbitrarily complicated patterns. Since the set of networks that give rise to one predefined spike pattern is typically high dimensional, we can impose additional restrictions on the realizing network, for instance a predefined detailed network connectivity, or we can design networks that optimize network properties such as wiring costs. This suggests applications to biological neural networks such as central pattern generators.

Crucial for the occurrence of some neural activity in general and of spike patterns in particular are the stability properties of the corresponding orbits and trajectories, especially under noisy conditions in biological systems or when the network that realizes a certain pattern is embedded in another neural network. The stability properties also determine the computational abilities of the network, where computation is not only possible with stable states, cf. [114, 14, 15]. In spiking neural networks, stability has been mostly analyzed in simple systems with a few neurons [136, 197, 195] or for collective states, such as oscillatory and synchronous states [190, 195, 31, 30, 176] or the asynchronous state [2, 31, 79, 30, 196, 105]. Only a few studies assess the stability properties of the precise spiking dynamics in larger networks. In purely excitatory networks, long chaotic transients and switching dynamics (unstable attractors) have been found [209, 180]. For purely inhibitory networks of leaky integrate-and-fire neurons with instantaneous coupling, i.e. coupling without transmission delay, and synaptic currents of infinitesimal temporal extent, several studies indicate that the dynamics is stable. Recent numerical investigations of weakly diluted networks show the stability of trajectories underlying irregular dynamics [208]. Also, in globally coupled networks, the periodic dynamics is stable [98]. The results in [98] further indicate that the irregular dynamics converges to a periodic orbit. For more general classes of networks, in [123], it was shown that the stored pattern of spikes (see above) is even a global attractor. The stability of the near-synchronous state in networks with delay (delayed coupling can significantly change the dynamical properties [58, 166]) was studied in [50], in particular showing that it is stable in inhibitory networks of leaky integrate-and-fire neurons. However, related numerical results were interpreted as indicating instability of the irregular dynamics when delayed couplings are included [76].[2]

We present a more general analytical investigation on the stability properties of trajectories underlying the spiking dynamics valid even in heterogeneous networks with delay. Given the complicating network properties, we study first periodic orbits in chapter 5. We analytically assess the stability properties of orbits underlying arbitrary non-degenerate periodic patterns of spikes, i.e. periodic patterns of spikes without simultaneous spike sendings and receivings. We show that in large and important classes of networks such patterns are either all stable or all unstable and numerically illustrate and interpret our results. For instance, in arbitrary purely inhibitory networks of neurons with normal dissipation such as leaky

[2]We explain these results in appendix A on the basis of the analytical results derived in ch. 6.

integrate-and-fire neurons, every periodic non-degenerate spike pattern, no matter how complicated, is stable.

The spiking dynamics of cortical neurons shows high temporal irregularity (cf. sec. 2.3). One possible explanation is that this irregularity occurs due to a balance of excitatory and inhibitory input to the neurons [198, 199, 30]. In this *balanced state* the mean input is subthreshold and spikes result from fluctuations of the membrane potential. The highly irregular dynamics generated is often associated with chaotic dynamics and chaoticity was conjectured to be an emergent phenomenon of large, sparse balanced networks [198, 199]. A state of highly irregular dynamics also occurs in purely inhibitory networks of neurons with normal dissipation. Orbits underlying non-degenerate periodic patterns of spikes are stable in these networks (see above). Are trajectories underlying irregular activity also stable? For fully connected networks without delay, ref. [98] indicates that this is the case and that the dynamics converges to a periodic orbit. Also, in weakly diluted networks without delay there is numerical evidence that the irregular spiking dynamics is stable and finally converges to a periodic orbit [208]. In contrast, as mentioned above, numerical simulations in diluted networks with delay were interpreted to show chaotic dynamics [76].

In chapter 6, we analytically show that in purely inhibitory networks with inhomogeneous delay distribution and arbitrary, strongly connected network topology, any trajectory underlying generic irregular spike dynamics is asymptotically stable. We give strong analytical evidence that finally the dynamics converges to a periodic orbit. We further numerically investigate the dynamics and discuss transitions to chaotic dynamics through introduction of excitatory couplings and finite synaptic decay time. Our results show that the dynamics in purely inhibitorily coupled networks differs substantially from the dynamics of networks which explicitly include sufficiently many excitatory couplings, even though the mean field descriptions [199, 30] of both network types are nearly identical when the parameters are suitably chosen. Thus, our results further emphasize the necessity to study the microscopic dynamics of neural networks if precise spike timing is indeed important.

As mentioned above, an important model for the generation of precise spike timing in neural networks is the synfire model, that assumes the presence of embedded feedforward networks which give rise to propagation of synchrony. Another modeling study investigated the construction of feedforward structures by strengthening already existing connections in a random network [201]. In the network models considered, only very large strengthening of synapses between neuron groups and further modification of neurons within the groups led to propagation of synchrony over a few groups. Neurobiological experiments, however, show that concurrent excitatory inputs to a neuron can be nonlinearly enhanced due to active dendrites [82, 13, 159]. Some forms of this nonlinear enhancement only occur if the input is synchronous. If a neuron responds to such an enhanced input with a spike, this response has high temporal precision [13]. Thus, simultaneous synchronous inputs to a group of neurons will generate synchronous responses. This led to the fruitful

idea that nonlinear dendritic enhancement might cause stable propagation of synchrony even in purely random neural networks. Up to now, highly detailed neuron models for neurons with nonlinear dendrites exist as well as very abstract ones suited e.g. for studies in discrete time or in rate networks [128, 129, 154, 153, 81]. However, the effect of nonlinear dendritic interactions on the dynamics of recurrent spiking neural networks has not yet been studied. In chapter 7, we introduce a spiking neuron model with nonlinear dendritic interactions based on [13] that is suitable for studying a spiking neural network in continuous time. We show analytically and numerically that a network of nonlinearly coupled neurons indeed gives rise to stable propagation of synchrony for biologically realistic parameters. As expected from previous work [3, 83, 54, 18, 201], this is not the case for a linearly coupled network with similar parameters. In contrast to a synfire chain model, the synchrony is not bound to fixed groups but propagates freely in the network. We numerically and analytically study the propagation and the emergence of the propagating state when the nonlinearity is strengthened.

Our model predicts certain patterns of activity in certain brain regions. Due to the response properties of neurons investigated in [13], the synchronous pulses in our model have temporal difference of about 5ms, a rather short time difference for a neuronal network. Thus, a pattern of activity characterized by strongly synchronous pulses with this time difference is predicted in the hippocampal regions where the pyramidal neurons motivating our model were found [13]. If the synchronous pulses are large enough, the propagation of synchrony would even be reflected in neural mass signals such as the local field potential. Indeed, the region in question shows a prominent pattern of activity, sharp waves/ripples, sharp increases of overall activity [35] with a superposed oscillation of frequency 200Hz (ripples [206, 116, 37]), where the troughs have temporal distance about 5ms and are assumed to originate from highly synchronous activity of pyramidal neurons. Sharp wave/ripples are a neurobiologically very well studied pattern of activity (see, e.g., [206, 117, 143, 21]) and are considered to play an important role in learning [37]. Two different mechanisms based on oscillating networks of inhibitory neurons [206, 39] and electrical synapses [184, 186, 115] have been proposed to explain their occurrence.

In chapter 8, we propose a new model for sharp wave ripples, based on nonlinear dendritic interactions. Based on [13], we develop a more detailed neuron model and show that for biologically realistic parameters spontaneous sharp-wave/ripple-like patterns of spiking activity occur. We highlight that, in contrast to existing models, the precise ripple frequency is predicted. Further, we expect our model to fit well with the role conjectured for sharp wave/ripples in learning. We discuss our model, partially together with the existing models, in the context of electrophysiological findings about sharp wave/ripples and neuroanatomical knowledge about the involved hippocampal regions. We emphasize that combinations of the three existing models for sharp wave/ripples are possible. We finally conclude that, regarding present knowledge, our model provides a plausible explanation for the occurrence of sharp wave/ripples.

This thesis is structured as follows. The first part starts with an introduction (current chapter 1) and provides the neurobiological background as well as mathematical and physical concepts used throughout the thesis (chapter 2). Also, the rather general neuron model used in most of the thesis is introduced (chapter 3). In the second part, we consider the dynamics of neural networks as an inverse problem by predefining an invariant dynamics and determining the class of networks that gives rise to it (chapter 4). In the third part, we analytically derive general statements about the stability properties of periodic and irregular spike dynamics for large classes of networks (chapters 5 and 6). The appendix of the thesis explains some implications of these statements for the interpretation of a recent publication. In the fourth part (chapters 7 and 8), we study the implications of experimentally found nonlinear dendritic enhancement on network dynamics. We show that it can lead to the propagation of precisely synchronous pulses of spikes (chapter 7). This predicts certain patterns of neural activity in a hippocampal region of the brain. Indeed, the predicted patterns are found there (chapter 8). Each chapter of the second, third and fourth part starts with a short introduction, an overview of the state of current research and a model section; it closes with a conclusion and an outlook. In the fifth part (chapter 9) we give summarizing conclusions and outlooks.

Chapter 2

Fundamentals

This chapter summarizes some basic concepts used throughout the thesis. We start with neurobiological foundations about neurons and their interconnections [104, 160] and motivate the neural network models considered [48, 72, 113]. Basic graph theory [20], the notion of hybrid dynamical systems [19, 28] and Markov chains [144] will provide means to study their microscopic dynamics. For the global, mean field, perspective, we introduce stochastic differential equations and derive the diffusion approximation to the network dynamics [97, 165, 69].

2.1 Single neurons

The nervous system has two types of cells, nerve cells or neurons and glial cells. The neurons are directly responsible for most of the information transmission while glia cells have rather auxiliary functions.[1]

Typical neurons can be divided into four morphologically distinct regions: i) The cell body or soma, the metabolic center also containing the nucleus. ii) The dendrites, processes of the soma, which branch out to collect input from other neurons. iii) The axon, a process which can extend over long distances and conducts signals to other neurons. iv) The presynaptic terminals, swellings of the axon where the contact to the postsynaptic cells is established by forming synapses with postsynaptic terminals e.g. at the dendrite of another, postsynaptic neuron.

Neurons in higher animals mainly communicate by sending and receiving electrical pulses, action potentials. This is generically a digital communication pathway. Analog pathways of communication also exists, e.g. the direct electrical coupling via gap junctions, cf. sec. 2.5. Action potentials are fast and short-lived electrical

[1] Glial functions include e.g. sustaining and separating neurons, taking up neurotransmitter from the synaptic cleft or forming the Myelin sheath isolating many axons. Besides, there is two-way signaling between glial cells and neurons which leads e.g. to neuromodulation and glial cells communicate via intracellular calcium waves and intercellular diffusion of chemical messengers (cf. Ref. [63, 62, 200] for recent reviews).

pulses with amplitudes of $70 - 100$mV and durations about $1 - 10$ms. Remarkably, the action potentials or spikes and the mechanism of their generation are highly stereotypical throughout the brain: At rest, neurons maintain a potential difference of approximately -65mV relative to the extracellular medium at their external membrane. This resting membrane potential results from an excess of large organic anions and chloride inside and sodium and calcium cations outside the cell. Additionally, there is an excess of potassium cations inside the cell which is however not sufficient to balance the potential difference. The cell membrane is riddled with ion channels. Some of them are rather unspecific (though impermeable for the large organic ions) and always open, so that there is a continued passive outward flow of K^+ and an inward flow of Na^+ ions due to the concentration gradient which is compensated by ion pumps actively transporting K^+ in, and Na^+ out of the cell. Others are voltage gated and only open when the polarization of the cell is decreased.[2] These channels are responsible for the generation of action potentials. If the cell is depolarized, voltage gated, Na^+ specific channels open and the resulting Na^+ influx increases the depolarization so that even more channels open. The resulting positive feedback process leads to a strong depolarization. At the same time, although a bit slower, voltage gated K^+ channels begin to open and the outflux of positive ions repolarizes the cell, a process supported by the reduction of Na^+ influx due to in- and deactivation of sodium channels.

Action potentials are usually generated in the initial segment of the axon.[3] Here, inputs conducted from the input zones are summed up and if a large enough number of depolarizing, excitatory signals has been integrated, the depolarization of this trigger zone is large enough and an action potential is generated. This action potential is an all-or-none event and thus highly nonlinear. The action potential then travels down the axon to the presynaptic terminals. Since the variability of the depolarization needed to generate an action potential is fairly small, the action potential initiation is often modeled as beginning if the depolarization exceeds a sharp threshold.[4]

However, action potentials can also be generated in dendrites [112, 173]. Dendritic sodium spikes can boost the effect of inputs by a factor of $2 - 3$ and induce sharply peaked depolarizations in the somatic membrane potential [82, 13, 142]. Remarkably, in [13] this boosting was found only if the inputs are rather synchronous in time, within less than 2ms. The resulting depolarization moves down the dendrite and can trigger an action potential at the initial segment of the axon. Due to the sharply peaked initiating depolarization, the timing of the action potential is precise in the sub-millisecond range. Other dendritic spikes are mediated by voltage gated Ca^{2+} or NMDA channels, the latter are ligand gated but also have

[2] In fact, there are usually a number of closed and open states so that the kinetics of channels can be modeled as a Markovian system. The transition between several states before the channel opens can cause additional delays and shapes the onset of the action potential [86, 51].

[3] The position of the action potential generation is still subject to recent research, see, e.g., [44].

[4] The onset variability and the speed of onset have nevertheless a strong influence on the response properties of neurons [141, 140, 64].

a voltage dependence due to a Mg^{2+} ion blocking the channel if the membrane is polarized [82, 157]. These spikes have longer time courses up to several hundreds of milliseconds and often occur together with fast spikes. They have particularly interesting implications on the computing abilities of neurons when only the spike rate and not the spike timing is considered because a pyramidal neuron then can be modeled as two or more layered feed-forward network instead of a single threshold element [154, 153, 81]. In the last part of the thesis we will study consequences of fast dendritic spikes on the spike timing dynamics of a neural network.

2.2 Synaptic interaction

Synapses allow signal transmission between different neurons. There are two types of synapses, electrical and chemical synapses.

In the area of an electrical synapse, the extracellular space between two neighboring cells is extraordinary small and bridged by ion channels called gap junctions. These connections allow direct ion flux between the cells and thus signaling of even subthreshold potential fluctuations with nearly zero time delay. Therefore, they are considered to be particularly important for synchronizing large populations of neurons [46, 23, 65]. Nevertheless, electrical synapses in general do not allow inhibitory actions or long-lasting changes in effectiveness,[5] require large contact areas and are usually responsible for rather stereotyped functions.

In contrast, chemical synapses are highly flexible. They can act excitatorily or inhibitorily, show plasticity on short and long timescales, a basis for longer lasting memory, and they can amplify signals. Indeed, chemical synapses are considered most important for the nervous system (cf. [104], p. 111). We will therefore concentrate on chemical synapses.

Chemical synapses transmit the information that an action potential has reached the presynaptic terminal.[6] If an action potential reaches a presynaptic terminal of a chemical synapse, the depolarization induces the influx of calcium ions which in turn leads to the fusion of synaptic vesicles and to the exocytosis of the contained neurotransmitter into the synaptic cleft.[7] The neurotransmitter reacts with receptors on the postsynaptic side before it is quickly removed from the cleft. This either leads directly to ion influx into the postsynaptic cell if receptor and channel form one macromolecule (receptor channel, ligand gated ion channel, ionotropic receptor) or to the generation of a second messenger cascade (metabotropic receptors and Tyrosinkinases). Ionotropic receptors have rapid postsynaptic effects we are interested in, such as rapid changes in the post synaptic potential which last for several milliseconds. In contrast, metabotropic receptors mediate effects on longer timescales of seconds or minutes.

The fusion of a single synaptic vesicle at an action potential arrival can be seen as a random event with a given probability. Indeed, the number of fusing

[5] See, however, [106].

[6] Recently, also analog transmission components have been found in chemical synapses [8, 170].

[7] For a detailed presentation of vesicle fusion and exocytosis, see, e.g., [104], ch. 13.

vesicles follows approximately a Binomial distribution and often no vesicle fuses which leads to a failure of synaptic transmission. On the other hand, the fusion of multiple vesicles need not be reflected in a higher post-synaptic current because the channels on the postsynaptic side can be saturated already by the neurotransmitter contained in one vesicle.

Also, the mechanism of synaptic transmission implies that chemical synapses are unidirectional and the complex steps needed for the signal transmission at a chemical synapse entail a synaptic delay, which ranges from 0.3ms to several milliseconds or longer [104], p. 131.

The probability for a synaptic connection from one neuron to another neuron within range is between $1 - 25\%$, i.e. the neural network is sparsely connected. Multiple, but few synaptic couplings between two neurons exist. The number of synapses per neuron ranges from several thousands to several ten thousands, depending on the cell type and the organism ([4] ch. 2, [26] chs. 2,20,34).

The rise times of the postsynaptic current are in the sub-millisecond to millisecond range, the decay of the current after the neurotransmitter has been removed from the synaptic cleft are several milliseconds (AMPA, $GABA_A$ channels) or several hundreds of milliseconds (NMDA channels)[8].

Neurons project either always excitatory (e.g. pyramidal neurons) or always inhibitory (cf. the diversity of inhibitory interneurons [149, 122]) on postsynaptic neurons. Thus, in the classical view, there is a clear separation between excitatory and inhibitory neuron populations.[9]

2.3 Cortical neural network dynamics

Spontaneous cortical activity is highly irregular. Single neurons spike at low rates of several Hz per neuron[10] and the spike train statistics often agree with a Poissonian process, where deviations are mostly due to refractory effects ([172, 169], [48] p. 32). The spike trains of different neurons however can be significantly correlated, as has been found in numerous experiments studying different brain areas and animals. Recently, it has been found that these correlations increase with higher spiking frequency. The mechanisms underlying the correlations as well as their implications for neural processing are not yet understood (cf. [49] and references therein). There are several sources for stochasticity. An external source for stochasticity is the unreliability and stochastic nature of synaptic transmission, cf. sec. 2.2. Internal

[8] The variability is however large between neurons in different areas and even between different trials [183, 188]

[9] Recently microcircuits have been discovered, where pyramidal neurons act inhibitorily on other pyramidal neurons. Here an axo-axonal gap junction between the pyramidal neuron and an inhibitory interneuron is present near a synapse from the interneuron to another pyramidal neuron. The first pyramidal neuron thus activates an inhibitory synapse to another pyramidal neuron with virtually no time delay so that the connection is equivalent to a direct inhibitory pyramid-pyramid connection [163].

[10] We note that even this low value is biased and probably estimated too large, because many experiments are selective to firing neurons, preferentially to firing neurons with higher rate.

sources are thermal noise and channel noise. Channel noise results from stochastic opening of voltage gated channels and is the dominating internal source generating noise with amplitude up to 0.5mV [92]. Since the internal stochasticity is weak, the dynamics of a single neuron to a given direct stimulation is rather reliable ([118, 145, 100]). This may lead to patterns of spikes which are reliably repeated in the network dynamics [61]. Indeed, there is increasing evidence for the existence of such spike patterns. Since the patterns are correlated with stimuli they might be important for neural processing [5, 68, 6]. However, the statistical analysis to prove their significance is non-trivial, in particular if the rates change during trials and observations of spike patterns have often been criticized or proven to be artefacts of the statistical methods used [148, 137]. Recently however, reliable methods that are independent of the spike train statistics and partially also robust against changes in the firing frequency have been developed [66, 151]. The application to newly derived and existing data revealed the presence of statistically significant repeated patterns of spikes in particular during phases of alertness or during stimulation of a neuronal population [152, 66, 67].

2.4 Model neurons

Neuron models exist on many levels of abstraction from highly detailed models with a large number of compartments and precise ion channel distributions, to simple threshold elements with only two discrete states (see e.g. [88, 120]). Simulations of highly detailed models may yield a good picture of the neural dynamics but the crucial mechanisms can remain obscure. Of course, oversimplified models may lead to wrong results, i.e. model artefacts, but also detailed models are not immune against this, because the crucial properties may simply be unknown on a microscopic level, cf. [141].

The level of abstraction appropriate for our investigations is the level of single compartment integrate-and-fire neurons. This means, we only consider one compartment, the zone of the neuron where the action potential is triggered. The inputs as collected and mediated by the input zone, are described by their effective action on the trigger zone. The trigger zone acts as an integrator and if the total excitation is large enough, the neuron is reset and an action potential is artificially added.

These models have a reasonable degree of accuracy. Still, they are often analytically tractable, have only a small number of free parameters to be fixed and allow simulations of larger networks.

The first, and a very successful and well studied integrate-and-fire model is the leaky integrate-and-fire (LIF) model (cf. [107, 192, 1], an extensive review about the state of research is given in [33, 34]). The neuron is modeled as an electrical RC-circuit consisting of i) a capacitor with capacitance C_m representing the charge separating membrane with the potential difference $V(t)$ interpreted as membrane potential, ii) parallel to the conductance a resistor with leak conductance g_L rep-

resenting the passive open ion channels and iii) a battery generating a potential difference equal to the resting potential V_{rest} representing the electromotive force due to diffusion currents of ions, cf. section 2.1. An external current models the inputs and charges the capacitor. Taken together, the subthreshold dynamics is governed by

$$C_m \frac{dV(t)}{dt} = g_L(V_{\text{rest}} - V(t)) + I_e(t). \tag{2.1}$$

When the potential difference at the capacitor reaches a certain threshold Θ_U, the generation of an action potential is postulated and the capacitor is reset to a reset potential $V_{\text{r}} < \Theta_U$. (The index U at the threshold is introduced for consistency with the phase oscillator representation, see ch. 3.2.) The battery can be omitted by interpreting the capacitance's potential as the potential $V(t) - V_{\text{rest}}$ relative to the resting potential which is equivalent to setting $V_{\text{rest}} = 0$. Despite its simplicity, this model reproduces aspects of the response properties of real neurons to constant current injection and to fluctuating inputs with not too high frequencies fairly well ([48] p. 165, [162, 140]).

The leaky-integrate-and fire neuron is characterized by its leak current dependency, the $I-V$ curve $I(V) = g_L(V_{\text{rest}} - V)$. Improved models introduce different leak current dependencies. An important example is the quadratic integrate-and-fire (QIF) model, which has the normal form of the saddle node bifurcation and describes the behavior of higher models near such a bifurcation,

$$C_m \frac{dV(t)}{dt} = \frac{g_L}{2\Delta_T}(V(t) - V_T)^2 - I_T + I_e(t), \tag{2.2}$$

where V_T the threshold potential, at which the $I-V$ curve gets positive slope, I_T is the threshold current (and bifurcation parameter) above which tonic firing occurs, Δ_T is a parameter characterizing the inverse curvature of the $I-V$ curve at V_T [57, 140, 90]. Another model is the exponential integrate-and-fire model which adds the spike generating current $g_L\Delta_T \exp((V - V_T)/\Delta_T)$, where the parameters have the same meaning as in the QIF model, to the $I-V$ curve of the LIF neuron [64]. In the quadratic and exponential integrate-and-fire models, $V(t)$ can escape to infinity in finite time, the upstroke corresponds to the upstroke of the action potential. It is often sensible to put a finite spike cutoff Θ_U past which the neuron is reset since infinite voltages have no physical meaning and it can simplify considerations. Further improved models include refractory periods, dynamic thresholds or time constants (see, e.g., [172, 29, 64, 72, 100]).

In most of this thesis, we will deal with Mirollo-Strogatz phase oscillators covering an entire class of integrate-and-fire models including oscillatory leaky integrate-and-fire and quadratic or exponential integrate-and-fire neurons with spike cutoff. In chapters 7 and 8, we concentrate on leaky integrate-and-fire neurons.

2.5 Models of synaptic interaction

We consider standard models of fully reliable synapses without plasticity.[11] While the neurotransmitter it is in the cleft, the fast postsynaptic receptor channels open at a high constant rate.[12] After removal, they close with lower rate $1/\tau_s$. There is thus first a rapid exponential increase and thereafter a slower exponential decay of the channel open probability and therewith of the conductance due to the receptor channels. Often, the time of conductance increase is negligible and thus the number of open channels and therewith the conductance is proportional to a single exponential function $\exp(-t/\tau_s)$. If the rise time is not negligible, the synaptic conductance can be described by the difference of two exponentials, a triangular pulse or by an alpha function to model dendritic filtering effects (cf. [192], p. 97ff, [91], p. 46ff, [48], p. 182ff). We now consider one type of ions, and channels which are permeable for these ions (cf. [104], p. 89ff). Due to the different ionic concentrations (different chemical potentials) inside and outside the cell, the diffusion of ions through open channels leads to a charge separation. This charge separation is the source of an electromotive force. An electromotive force generated by a difference in the chemical potential is just a battery. So, a population of ionic channels can be modeled as a battery in series with a conductance $\bar{g}_i(t)$ due to the open channels. $\bar{g}_i(t)$ is proportional to the fraction of open channels, so if the channels were activated at time $t = 0$, we have

$$\bar{g}_i(t) = \bar{g}_{i,\max} \exp(-t/\tau_s), \tag{2.3}$$

where $\bar{g}_{i,\max}$ is the maximal conductivity due to ion i. The ionic current through the channels stop when the electrical and chemical driving forces are equal, i.e. when the membrane potential equals the potential E_i generated by the battery. E_i is called the reversal potential of the ions i. From Ohms law we derive the ionic current through the channels due to ion i as

$$I_i(t) = \bar{g}_i(t)(E_i - V(t)). \tag{2.4}$$

2.6 Networks of leaky integrate-and-fire neurons

We now consider networks of $N \in \mathbb{N}$ neurons with arbitrary connectivity. Taking together the results Eqs. (2.1, 2.4) from sections 2.4 and 2.5 yields the conductance based single compartment leaky integrate-and-fire neuron model, for a neuron $l \in \{1, \ldots, N\}$,

$$C_m \frac{dV_l(t)}{dt} = g_L(V_{\text{rest}} - V_l(t)) + \sum_i \bar{g}_{li}(t)(E_i - V_l(t)), \tag{2.5}$$

[11] A model for synapses with short term plasticity has been introduced in [189] and the implications of the networks dynamics were studied in a series of subsequent articles (see, e.g. [111]).

[12] Also in ligand gated channels there are usually a number of closed and open states which can cause additional delays and shape the post-synaptic current [86, 51].

where the unspecific external current has been replaced by the synaptic input currents. The sum over i is over the various channel types and the various ions, and the values of C_m, g_L, $V_{\rm rest}$ are neuron specific. For simplicity, we will assume that each channel is selective for one ion type in the following. Further, we collect multiple synaptic couplings a neuron sometimes forms with another neuron into one, assuming that the transmission delay is identical. After division by the leak conductance g_L, we get

$$\tau_{\rm mem}\frac{dV_l(t)}{dt} = V_{\rm rest} - V_l(t) + \sum_i g_{li}(t)(E_i - V_l(t)), \tag{2.6}$$

where $g_{li}(t) = \bar{g}_{li}(t)/g_L$ is the conductance of channels i in units of the resting membrane conductance. $\tau_{\rm mem}$, the membrane time constant, is the time constant of the RC-circuit described by Eq. (2.1) and yields the typical time scale for changes in $V_l(t)$. Neglecting the membrane potential dependence of the synaptic input currents yields the current based single compartment leaky integrate-and-fire neuron model

$$\tau_{\rm mem}\frac{dV_l(t)}{dt} = V_{\rm rest} - V_l(t) + \sum_i g_{li}(t)(E_i - V_{\rm rest}). \tag{2.7}$$

Networks of current and conductance based neurons can generate quite different network dynamics [201]. If we use synapses as given by Eq. (2.3), the interactions between neurons in the network are specified by the rule that on arrival of a spike from another neuron k at time θ, the conductance jumps according to

$$g_{li}(\theta) = g_{li}(\theta^-) + \Delta g_{lki}, \tag{2.8}$$

with coupling strength Δg_{lki} which describes the activation of the channels i at neuron l due to a spike from neuron k. The dynamics between arrivals of spikes can be written as differential equation

$$\tau_{{\rm s},i}\frac{dg_{li}(t)}{dt} = -g_{li}(t), \tag{2.9}$$

with the decay time $\tau_{{\rm s},i}$ of the synaptic current for channels i. Due to the synaptic transmission delay, a spike sent at time $t^{\rm s}$ arrives at the postsynaptic neurons some time later, at $\theta = t^{\rm s} + \tau_{lk}$, where τ_{lk} is the delay of the coupling from neuron k to neuron l.

A further approximation (cf., e.g., [33] for a review) neglects the time course of the synaptic current and assumes that the entire charge is deposited in infinitesimal time. In the current based synapse with single exponential time course, Eq. (2.3), the charge deposited by a single spike due to channels i is $\Delta g_{lki}\tau_{{\rm s},i}(E_i - V_{\rm rest})$ so that the conductance of the synapse with infinitesimal time course is

$$g_{li}(t) = \Delta g_{lki}\tau_{{\rm s},i}\delta(t-\theta). \tag{2.10}$$

This leads to a jump in the membrane potential at θ

$$\begin{aligned} V_l(\theta^-) \to & V_l(\theta) = V_l(\theta^-) + \sum_i \Delta g_{lki} \frac{\tau_{\mathrm{s},i}}{\tau_m} (E_i - V_{\mathrm{rest}}) \\ & =: V_l(\theta^-) + \varepsilon_{lk}, \end{aligned} \tag{2.11}$$

where we used that we do not need to distinguish the different channels activated by a spike from neuron k anymore but can express the action of neuron k on neuron l by a single coupling strength ε_{lk}. For the conductance based model, the charge depends on the membrane potential of the neuron. Here, a rule similar to Eq. (2.11) can be introduced,

$$V_l(\theta^-) \to V_l(\theta) = V_l(\theta^-) + \frac{(E_i - V_l(\theta^-))}{(E_i - V_{\mathrm{rest}})} \varepsilon_{lki}, \tag{2.12}$$

where channels with different reversal potentials have still to be distinguished.[13]

2.7 Systems with impulse effect

Neural networks containing synapses with infinitesimal course are typical examples for hybrid systems, or more precisely, systems with impulse effect. This is also true for networks with synapses with finite time course, even if the time course of the post-synaptic current is smooth, because the synaptic delay make re-orderings of the variables at spike sendings and receiving necessary to keep the phase space finite dimensional and an instantaneous reset may introduce further discontinuities [14]. Hybrid dynamical systems combine continuous dynamics, defined e.g. by a set of differential equations, with discrete dynamics, such as switching between different sets of dynamical equations in *switching systems*, or jumping and reset of states in *systems with impulse effect* [167, 19]. Systems with impulse effect naturally occur in models where the timescale of some interactions is negligible, examples are found e.g. in mechanics (billiards, clockworks, separation of a stage of a rocket), theoretical biology (sudden exterior changes in a population), in control theory (impulse control) or in theoretical physics (neural networks). Networks with synapses of the type Eq. (2.10) are autonomous systems with impulse effect which can be described by equations

$$\frac{dx(t)}{dt} = f(x(t)), \;\; x(t) \in \Omega \backslash M, \tag{2.13}$$

$$x(t) = I(x(t^-)), \;\; x(t^-) \in M, \tag{2.14}$$

[13] We note that an expression of the kind $dV(t)/dt = f(V(t)) + V(t)\bar{\varepsilon}\delta(t)$ as appearing in the conductance based case is strictly speaking undefined, because the delta distribution is given on the space of continuous functions and $V(t)$ will not be continuous at $t = 0$. It can be given sense by rewriting the equation as $d \ln V(t)/dt = f(V(t))/V(t) + \bar{\varepsilon}\delta(t)$, by formally integrating from 0^- to 0^+, where the integral over the bounded function $f(V(t))/V(t)$ vanishes in the limit, and by concluding $\ln V(0^+) - \ln V(0^-) = \bar{\varepsilon}$ or $V(0^+) = V(0^-)e^{\bar{\varepsilon}}$, where $\bar{\varepsilon} = \ln(\varepsilon)$, cf. [99, 177].

where $f : \Omega \backslash M \to \mathbb{R}^n$, $I : M \to N$, with n-dimensional phase space Ω and $M, N \subset \Omega$ (class three in [19], p. 21; [27]). Between hits of the trajectory $x(t)$ on the set M, it follows the smooth time evolution given by the differential equation (2.13), this corresponds to the time evolution of the neural network between spike sendings or spike arrivals. When the trajectory hits the set M at times t_n, e.g. when a neuron reaches the threshold or a spike reaches the end of its run time given by the delay of the coupling, some jump event occurs.

We now introduce the notions of stability, attractivity and asymptotic stability (see, e.g., [97], p. 53 for smooth dynamical systems) in hybrid dynamical systems. We note that the notions are not appropriate to describe certain phenomena such as unstable attractors (cf. [177]). In systems with impulse effect, we face the complication that even for trajectories staying near each other for most of the time, if the jump or event times t_n in one and t'_n in the other trajectory are not identical, there can be a macroscopic deviation within the interval $[\min(t_n, t'_n), \max(t_n, t'_n))$ where in one trajectory the event has already occurred, while in the other trajectory it has not. This leads to the following definitions of stability which allow for macroscopic deviations in arbitrarily small environments around the event times t_n (cf. [19], p. 60). Let $\varphi(t)$ be a solution of the dynamical equations (2.13) and (2.14) that hits M at times t_n, $n \in \mathbb{N}$. Further, let $x_0 \in \Omega$ be a point in phase space and $x(t; t_0, x_0)$, $t \in \mathbb{R}$ a solution of the dynamical equations (2.13) and (2.14) that assumes at time t_0 the value x_0.

(i) Stability. A solution $\varphi(t)$ is stable if for all $\eta > 0$, for all $\epsilon > 0$ and for all $t_0 > 0$ with $|t_0 - t_n| > \eta$, there is a $\delta > 0$ so that for all x_0 with $|x_0 - \varphi(t_0)| < \delta$,

$$|x(t; t_0, x_0) - \varphi(t)| < \epsilon \text{ for all } t \text{ with } t \geq 0 \wedge \forall_n |t - t_n| > \eta. \tag{2.15}$$

(ii) Attractivity. A solution $\varphi(t)$ is attractive if for all $\eta > 0$ and for all $t_0 > 0$ with $|t_0 - t_n| > \eta$, there is a $\delta > 0$ so that for all $\epsilon > 0$: For all x_0 with $|x_0 - \varphi(t_0)| < \delta$ there is a $D > 0$, so that

$$|x(t; t_0, x_0) - \varphi(t)| < \epsilon \text{ for all } t \text{ with } t \geq D \wedge \forall_n |t - t_n| > \eta. \tag{2.16}$$

(iii) Asymptotic stability. A solution is asymptotically stable if it is stable and attractive.

(iv) Instability. A solution $\varphi(t)$ is unstable if there is a $\epsilon > 0$, a $\eta > 0$ and a $t_0 > 0$ with $|t_0 - t_n| > \eta$ so that for all $\delta > 0$, there is a $x_0 \in \Omega$ with $|x_0 - \varphi(t_0)| < \delta$,

$$|x(t; t_0, x_0) - \varphi(t)| \geq \epsilon \text{ for some } t \text{ with } t \geq 0 \wedge \forall_n |t - t_n| > \eta. \tag{2.17}$$

Since we consider time translation invariant systems, we will consider the dynamics as stable or asymptotically stable also if it converges to some equivalent dynamics which is shifted in time, and unstable only if it departs from all equivalent dynamics (cf. also [19], p. 124). As for smooth dynamical systems, stability of trajectories can be established by considering the smooth Poincaré-map and its linearization [177, 75], we will however often chose a direct nonlinear proof of stability or instability.

2.8 Some notions from graph theory

A neural network has the structure of a weighted directed graph, where the nodes are the neurons, the directed edges are the directed synaptic connections from one neuron to another and the weights are the coupling strengths. We introduce some basic concepts from the theory of graphs and directed graphs [20, 41, 102].

A graph $G = (V, E)$ is a pair consisting of a non-empty finite set V of elements called nodes or vertices and a finite set E of two element subsets, pairs of elements of V called edges. We label the vertices of a graph or the neurons in the network by natural numbers so that $V = \{1, ..., N\}$ with $N = |V|$. In a directed graph, the set E consists of ordered pairs of elements of V, also often called arcs to distinguish the directed from undirected case. One can further introduce a weighting function $c : E \to \mathbb{R}$ on the edges of the graph. The triple (V, E, c) is called a weighted graph. Since a graph can be considered as a special digraph, where to any edge $e_1 = (i, j)$, from i to j, $i \neq j$, $i, j \in V$, there is also an edge $e_1 = (j, i)$, we consider only digraphs in the following. The definitions allows digraphs to have edges starting and ending at the same vertex, but it does not allow parallel edges, i.e. multiple edges with the same start- and end-vertex, which matches the neural network structure because we collected multiple synaptic couplings from one neuron to another in a single coupling.[14] The coupling matrix of our network is the matrix ε with $\varepsilon_{ji} = c((i, j))$ if $(i, j) \in E$ and $\varepsilon_{ji} = 0$ otherwise. We call the set of neurons $\mathrm{Pre}(j) = \{i|(i, j) \in E\} = \{i|\varepsilon_{ji} \neq 0\}$ having a connection to neuron j the set of presynaptic neurons of j and the set $\mathrm{Post}(j) = \{i|(j, i) \in E\} = \{i|\varepsilon_{ij} \neq 0\}$ the set of postsynaptic neurons of j.

We are often interested only in the presence or absence of a coupling and not in the particular weight. Indeed, the definitions for distance and diameter for a weighted graph are not suitable for our purposes[15]. We thus give the following definitions for unweighted graphs. A subgraph $G' = (V', E')$ of $G = (V, E)$ is a graph with $V' \subset V$ and $E' \subset E|V'$, where $E|V'$ denotes the subset of edges in E whose endpoints lie in V'. For neural networks, we use the term subnetwork in the same sense. Now, consider a special subgraph with $L + 1 = |V'|$ vertices, where the L elements of E' have the structure $e_k = (i_{k-1}, i_k)$ for $k = 1, ..., L$ with $i_0, ..., i_L \in V'$ and $v_k \neq v_{k'}$ for $k \neq k'$. Such a subgraph is called a path of length L from i_0 to i_L. The distance $d(i, j)$ from vertex i to vertex j is the length of the shortest path from i to j and the diameter of a graph is the maximal distance from one vertex to another, $\mathrm{diam}(G) = \max_{ij} d(i, j)$. If there is no path one defines $d(i, j) = \infty$.

A directed graph is called strongly connected if the distance from any vertex i to any other vertex j is smaller than infinity, $d(i, j) < \infty$, which is equivalent to $\mathrm{diam}(G) < \infty$. If a network is strongly connected, then the coupling matrix is

[14] When parallel arcs and edges are allowed, one speaks of pseudographs.

[15] The weight of a subgraph is the sum over the coupling weights, and the distance is defined via the minimum weight of all paths between two vertices. While this definition is sensible e.g. for the traveling salesman problem, the sum over the couplings of a subgraph has no obvious meaning in interacting neural networks.

irreducible, i.e. there is no permutation or renumbering of vertices, that brings the coupling matrix into the form $\varepsilon = \begin{pmatrix} X & 0 \\ Y & Z \end{pmatrix}$ with square matrices X, Z. This property reflects the fact that each subnetwork at least indirectly influences all other subnetworks and is influenced by them. Further, the property of irreducibility allows conclusions on the eigenvalues of the matrix [125].

2.9 Markov chains

In this section, we introduce the concept of discrete time Markov chains and stochastic matrices (cf., e.g., [144]) as needed in chapter 7. Let the state space I be a countable set, where each $i \in I$ is a state. In our applications, i will be the size of a synchronous group, and I will be the set of natural numbers $\{1, ..., N\}$, where N is the network size. A sequence $\lambda = (\lambda_i)_{i \in I}$ with elements $0 \leq \lambda_i < \infty$ is called a distribution if it is normalized to one, $\sum_{i \in I} \lambda_i = 1$. Similarly, a matrix W with elements p_{ij}, $i, j \in I$ is called stochastic if $0 \leq p_{ij} < \infty$ and every row is normalized $\sum_{j \in I} p_{ij} = 1$. Let $(\Omega, \mathcal{F}, P)$ be a probability space, i.e Ω is a set, $\mathcal{F}$ a σ-Algebra on this set, and P probability measure on $\mathcal{F}$. Further define $(X_n)_{n \in \mathbb{N}}$, a family of random variables on $(\Omega, \mathcal{F}, P)$ with values in the measurable space I endowed with the natural σ-Algebra, the powerset of I. The quadruple $(\Omega, \mathcal{F}, P, (X_n)_{n \in \mathbb{N}})$ is a stochastic process. Let λ be a distribution. Then, $(\Omega, \mathcal{F}, P, (X_n)_{n \in \mathbb{N}})$ is called a Markov chain with initial distribution λ if (i) $P(X_0 = i) = \lambda_i$ for $i \in I$ and (ii) for the conditional probabilities $P(X_{n+1} = i_{n+1} | X_n = i_n, ..., X_0 = i_0) = P(X_{n+1} = i_{n+1} | X_n = i_n)$ holds, for all $i_0, ..., i_{n+1} \in I$. The latter condition implies that the state at $n + 1$ only depends on n and on the state at n but not on the states before. If $P(X_{n+1} = i_{n+1} | X_n = i_n)$ is independent of n, the Markov chain is called homogeneous. Via $p_{ij} = P(X_{n+1} = j | X_n = i)$ the transition probabilities $P(X_{n+1} = j | X_n = i)$ of a homogeneous Markov chain yield a stochastic matrix with entries p_{ij}, the transition matrix. Vice versa, if W is a stochastic matrix, and λ a distribution, then there is a a homogeneous Markov chain with W as transition matrix and λ as initial distribution.

2.10 Diffusion approximation

We now consider stationary neural activity. As mentioned above, the neural network is sparse and the number of synapses a neuron receives is large (of the order of 10^4). Thus, we assume that the temporal correlations of the inputs to each neuron are sufficiently small and consider the limiting case of uncorrelated synaptic inputs (cf., however, sec. 2.3). Further, the activity of a neuron is generated by many small inputs which sum up to a Gaussian distributed total input when integrated over small times as a consequence of the negligible correlation of the inputs and the central limit theorem. We assume that all inputs have Poissonian statistics (cf. sec. 2.3) and therefore also superpose to an input spike train with Poissonian

statistics.[16]

We concentrate on a current based network of leaky integrate-and-fire neurons with synapses of infinitesimal time course (δ-coupling) following [31, 30] to derive the results needed later. Multiplying Eqs. (2.7, 2.10) by $\gamma = 1/\tau_{\text{mem}}$ and setting $V_{\text{rest}} = 0$ leads together with Eq. 2.11 to

$$\frac{dV_l(t)}{dt} = -\gamma V_l + \sum_{j=1}^{N} \sum_{k \in \mathbb{Z}} \varepsilon_{lj} \delta(t - t_{jk}^{\text{s}} - \tau_{lj}), \tag{2.18}$$

where ε_{lj} is the coupling strength from neuron j to neuron l, t_{jk}^{s} is the time when neuron j sends its kth spike and τ_{lj} is the delay of the coupling from neuron j to neuron l. For simplicity of presentation, we assume that all neurons are identical and each excitatory coupling and each inhibitory coupling has the same value, $\varepsilon_{\text{Ex}} > 0$ and $\varepsilon_{\text{In}} < 0$ respectively, and we consider additional external excitatory spike trains with frequency ν_{ext} and the same coupling strength ε_{Ex} as the internal connections. Each neuron has C_{Ex} excitatory, C_{In} inhibitory inputs from the network and C_{ext} external inputs where the external neurons fire with frequency ν_{ext}. Neurons within the network fire with frequency ν. Assuming the abovementioned idealized input properties, the absence of filtering or influence of the membrane potential allows us to model the input current directly by a constant current together with additive Gaussian white noise.[17] For very small input amplitudes and high input frequencies, Eq. (2.18) can be approximated by the Langevin equation

$$\frac{dV_l(t)}{dt} = -\gamma V_l(t) + \mu_l + \sigma_l \eta_l(t), \tag{2.19}$$

where μ_l is the constant current and $\eta_l(t)$ is a Gaussian white noise with $\langle \eta_l(t) \rangle = 0$ and $\langle \eta_l(t) \eta_l(t') \rangle = \delta(t - t')$. Formally integrating $\sigma_l \eta_l(t)$ over time yields a Wiener process $W_l(t) = \sigma_l \int_0^t \eta_l(s) ds$ with $W_l(t) \sim \mathcal{N}(0, \sigma_l^2 t)$, where $\mathcal{N}(0, \sigma_l^2 t)$ is the Gaussian distribution centered at zero with variance $\sigma_l^2 t$. We assumed that each of the input spike trains is Poissonian, so we can collect them into three Poissonian spike trains, an excitatory, and inhibitory and an external spike train. The number of inputs in these trains up to a time t is Poissonian distributed with expected number of inputs $C_{\text{Ex}} \nu t$, $C_{\text{In}} \nu t$, $C_{\text{ext}} \nu_{\text{ext}} t$ and variance $C_{\text{Ex}} \nu t, C_{\text{In}} \nu t, C_{\text{ext}} \nu_{\text{ext}} t$. Thus, the input strengths summed up to time t by each of the trains are distributed with mean $C_{\text{Ex}} \varepsilon_{\text{Ex}} \nu t$, $C_{\text{In}} \varepsilon_{\text{In}} \nu t$, $C_{\text{ext}} \varepsilon_{\text{Ex}} \nu_{\text{ext}} t$ and variance $C_{\text{Ex}} \varepsilon_{\text{Ex}}^2 \nu t, C_{\text{In}} \varepsilon_{\text{In}}^2 \nu t, C_{\text{ext}} \varepsilon_{\text{Ex}}^2 \nu_{\text{ext}} t$. This distribution is approximated (and matched in the limit of infinitely many infinitesimal inputs) by the Gaussian distribution $\mathcal{N}(\mu_l t, \sigma_l^2 t)$ of the Wiener process' $W_l(t)$ finite dimensional distribution at time t, $\mathcal{N}(0, \sigma_l^2 t)$, together with the constant drift $\mu_l t$. μ_l and σ_l^2, equal the mean and variance of the input strengths

[16] For non-Poissonian processes, the superposition is in general not a Poissonian process, although the inter-spike-interval-distribution becomes exponential [110, 40].

[17] The models can be adapted for the conductance based models and to the presence of synaptic filtering, the subsequent analysis however becomes more involved (cf. [33] and references therein).

distribution per time which is

$$\mu_l = C_{\mathrm{Ex}}\varepsilon_{\mathrm{Ex}}\nu + C_{\mathrm{In}}\varepsilon_{\mathrm{In}}\nu + C_{\mathrm{ext}}\varepsilon_{\mathrm{Ex}}\nu_{\mathrm{ext}}, \tag{2.20}$$

$$\sigma_l^2 = C_{\mathrm{Ex}}\varepsilon_{\mathrm{Ex}}^2\nu + C_{\mathrm{In}}\varepsilon_{\mathrm{In}}^2\nu + C_{\mathrm{ext}}\varepsilon_{\mathrm{Ex}}^2\nu_{\mathrm{ext}}, \tag{2.21}$$

since the three input trains are uncorrelated.

White noise η is not a random process in the classical theory of random processes but a random distribution, because its values are almost everywhere infinitely large and uncorrelated. Formally integrating Eq. (2.19) and using $W(t) = \int_0^t \eta(s)ds$, yields the well defined stochastic differential equation

$$dV(t) = -\gamma V(t)dt + \mu dt + \sigma dW(t) \tag{2.22}$$

where no neuron index l is necessary since the considerations are identical for each neuron. The solution for the stochastic differential equation Eq. (2.22) is the Ornstein-Uhlenbeck process [194]. In addition to the stochastic differential equation, we have the condition that $V(t)$ is reset to zero when it reaches the threshold Θ_U. Due to this boundary hitting reset, the model is often denoted as hybrid stochastic model [155]. It can be analyzed analogously to an ordinary stochastic model using the Fokker-Planck formalism with appropriate boundary conditions [31, 30].

Let $P(V,t)$ be the probability density (often also called probability distribution in physical literature) of the membrane potentials in the limit $N \to \infty$. The Fokker-Planck equation is the continuity equation of the probability density,

$$\frac{\partial P(V,t)}{\partial t} = -\frac{\partial S(V,t)}{\partial V}, \tag{2.23}$$

where $S(V,t)$ is the probability current through V at time t as determined by Eq. (2.22),

$$S(V,t) = (-\gamma V + \mu)P(V,t) - \frac{\sigma^2}{2}\frac{\partial}{\partial V}P(V,t), \tag{2.24}$$

with the drift $(-\gamma V + \mu)P(V,t)$ and the diffusion current in the direction of the negative gradient $-\frac{\partial}{\partial V}P(V,t)$ (see, e.g., [165], p. 72). We now have to consider the boundary conditions at $-\infty$, at the threshold Θ_U and at the reset potential V_{r}. For $V \to -\infty$ to ensure integrability of $P(V,t)$, the boundary conditions are

$$\lim_{V\to-\infty} P(V,t) = 0, \quad \lim_{V\to-\infty} VP(V,t) = 0. \tag{2.25}$$

Since the diffusion current drives the neurons over the threshold, but cannot drive it to flow back, the probability density at the threshold is zero,

$$P(\Theta_U, t) = 0, \tag{2.26}$$

while the probability current over the threshold equals the number of neurons firing per time,

$$S(\Theta_U, t) = \nu \Leftrightarrow \frac{\partial}{\partial V}P(V,t) = -\frac{2}{\sigma^2}\nu. \tag{2.27}$$

Finally, $P(V,t)$ has to be continuous at the reset potential V_r, while $S(V,t)$ has to change about $S(\Theta_U,t)$, the number of neurons passing the threshold per time and being reset,

$$S(V_\mathrm{r}^+,t) - S(V_\mathrm{r}^-,t) = \nu \Leftrightarrow \frac{\partial}{\partial V}P(V_\mathrm{r}^+,t) - \frac{\partial}{\partial V}P(V_\mathrm{r}^-,t) = -\frac{2}{\sigma^2}\nu. \tag{2.28}$$

Following refs. [31, 30], we derive stationary, normalized solutions $P(V,t) = P(V)$ of Eq. (2.23) with boundary conditions (2.25-2.28) by first observing that Eq. (2.23) implies $S(V) = \text{const}$ except at $V = V_\mathrm{r}$, because there are no additional sinks or sources. The boundary conditions (2.27, 2.28) are fulfilled if $S(V) = 0$ on $(-\infty, V_\mathrm{r})$ and $S(V) = \nu$ on $(V_\mathrm{r}, \Theta_U]$. This yields together with Eq. (2.24) ordinary differential equations which are solved using the remaining boundary conditions and written as one solution for $P(V)$ on $(-\infty, \Theta_U]$,

$$P(V) = \frac{2\nu}{\sigma^2}\exp\left(-\frac{(\gamma V-\mu)^2}{\gamma\sigma^2}\right)\int_V^{\Theta_U}\Theta\left(s-V_\mathrm{r}\right)\exp\left(\frac{(\gamma s-\mu)^2}{\gamma\sigma^2}\right)ds, \tag{2.29}$$

where $\Theta\left(s-V_\mathrm{r}\right)$ is the Heaviside step function. The normalization condition

$$\int_\infty^{\Theta_U} P(V)dV = 1 \tag{2.30}$$

yields a self-consistency condition determining the frequency ν of the neurons. Introducing the error function $\mathrm{erf}(u) = \frac{2}{\sqrt{\pi}}\int_0^u \exp(-t^2)dt$, it can be rewritten as

$$1 = \nu\frac{\sqrt{\pi}}{\gamma}\int_{\frac{\gamma V_\mathrm{r}-\mu}{\sqrt{\gamma}\sigma}}^{\frac{\gamma\Theta_U-\mu}{\sqrt{\gamma}\sigma}}\exp(u^2)(1+\mathrm{erf}(u))du, \tag{2.31}$$

which allows numerical solution for ν. Since ν is the the only free parameter $P(V)$ depends on, $P(V)$ is fully determined.

Chapter 3

Mirollo-Strogatz neurons

In chapters 4-6 we use the Mirollo-Strogatz phase oscillator model. In this model, the state of the neuron is given by a phase $\phi(t)$ which increases linearly during free time evolution, while the interactions are nonlinear. This linearization of the free dynamics simplifies the analytical description. Further, the general framework allows to treat entire classes of models in one formalism and also allows for simple and fast event based numerical simulations. Due to these advantages, the model has has been used in a number of studies about synchronization properties [136, 182], stability of the synchronous and near synchronous state [177, 50], the influence of delay on the network dynamics [58, 59], chaotic dynamics [209] and unstable attractors [180, 181]. We note that the class of models considered was also suggested to describe other natural systems ranging from earthquakes over flashing fireflies to chirping crickets [32, 85, 113].

3.1 Networks of oscillating neurons

The current based networks of leaky integrate-and-fire neurons and of quadratic or exponential integrate-and-fire models with spike cutoff as introduced in section 2.4 are contained in a class of models described by the differential equation

$$\frac{dV_l(t)}{dt} = f_l(V_l(t)) + S_l(t), \tag{3.1}$$

with reset potential at

$$V_\mathrm{r} = 0. \tag{3.2}$$

Indeed, also some conductance based and more general models given by differential equations of the form

$$\frac{dV_l(t)}{dt} = A(V_l(t)) + B(V_l(t))S_l(t), \tag{3.3}$$

where A, B in general depend on l, can be brought into the form Eq. (3.1) by a transformation of variables

$$\bar{V}_l(t) = \int_0^{V_l(t)} B(v)^{-1} dv \tag{3.4}$$

possible under weak conditions on $A(V_l), B(V_l)$ [195, 177, 181]. This leads to a differential equation

$$\frac{d\bar{V}_l(t)}{dt} = \bar{A}(\bar{V}_l(t)) + S_l(t), \tag{3.5}$$

where $\bar{A}(\bar{V}) := A(V(\bar{V}))/B(V(\bar{V}))$, $V(\bar{V})$ is given by solving Eq. (3.4) for V and the threshold $\Theta_{U,l}$ has to be transformed into $\bar{\Theta}_{U,l} := \int_0^{\Theta_{U,l}} B(v)^{-1} dv$.

We will now model the fast synaptic dynamics by pulses with negligible time course (2.10) and the slow, e.g. NMDA, currents as summing up to a constant input current. A constant input current may also arise from an external source or from faster inputs where the fluctuations are negligible. The explicit interactions between the neurons in the network are then given by

$$S_l(t) = \sum_{k=1}^{N} \sum_{n \in \mathbb{Z}} \varepsilon_{lk} \delta(t - t_{kn}^{\mathsf{s}} - \tau_{lk}), \tag{3.6}$$

where ε_{lk} is the coupling strength from neuron k to neuron l, t_{kn}^{s} is the time when neuron k sends its nth spike and τ_{lk} is the delay of the coupling from neuron k to neuron l. If $V_l(t)$ reaches the threshold $\Theta_{U,l}$, the neuron is reset to the reset potential $V_{\mathrm{r}} < \Theta_{U,l}$. An input prolongs the time to next firing of neuron l if $\varepsilon_{lk} < 0$ (inhibitory coupling from k to l), it leaves it unchanged if there is no coupling, $\varepsilon_{lk} = 0$, and it excites the neuron to earlier firing if $\varepsilon_{lk} > 0$ (excitatory coupling from k to l). The constant current is included in $f_l(V_l)$. We assume that $f_l(V_l)$ satisfies

$$f_l(V_l) > 0 \tag{3.7}$$

for all $V_l \leq \Theta_{U,l}$ i.e. that the neuron reaches the threshold also if there are no time dependent network inputs. If the neurons are not firing without explicit time dependent network input, the firing times are always at arrival times of spikes. Only at an arrival of an excitatory spike, the neuron can reach or exceed the threshold. This leads to a firing dynamics highly determined by the initial conditions, namely by the spikes sent and not received at time $t = 0$.

A too large inhibition could be inconsistent with a possible lower bound for V as present, e.g., for the leaky integrate-and-fire neuron with anomalous dissipation $\gamma < 0$ (sec. 3.4). This does not change the methods developed in the subsequent chapter 4 using the phase representation. For the stability analysis of the irregular network dynamics in inhibitory networks, chapter 6, we assume that the lower bound is small enough so that this case does not occur in the dynamics.

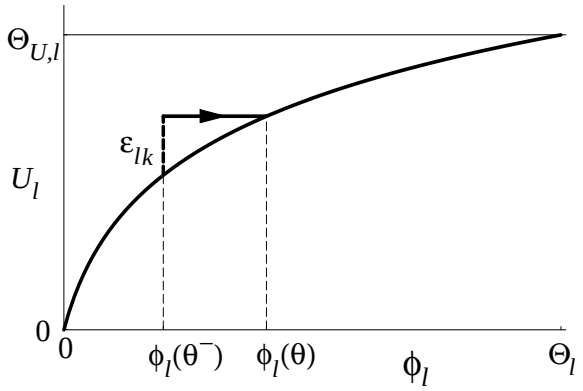

Figure 3.1: Response of the phase dynamics to an incoming excitatory spike. The rise function U_l of neuron l is plotted as a function of its phase ϕ_l. The membrane potential is given by $U_l(\phi_l(t))$. In the absence of interactions, $\phi_l(t)$ increases uniformly with time t according to Eq. (3.8). If a spike sent by neuron k is received by neuron l at time θ, it induces a phase jump $\phi_l(\theta^-) \to \phi_l(\theta)$ mediated by the rise function U_l and its inverse according to (3.16) and (3.17). $\Theta_{U,l} = U_l(\Theta_l)$ is the threshold for the membrane potential.

3.2 The Mirollo-Strogatz model

The dynamics of such a neuron can be equivalently described by a phase model proposed by Mirollo and Strogatz [136]. Here, the state of a neuron l is characterized by a single phase-like variable $\phi_l(t)$. In the absence of interactions, the phases increase uniformly obeying

$$d\phi_l/dt = 1. \tag{3.8}$$

When ϕ_l reaches the phase threshold of neuron l at time t, $\phi_l(t^-) = \Theta_l > 0$, it is reset,

$$\phi_l(t) = 0, \tag{3.9}$$

and a spike is emitted. The membrane potential is defined as $U_l(\phi_l(t))$ with the strictly monotonic increasing rise function U_l. We can connect this definition to the one given by Eq. (3.1) via the solution $\tilde{V}_l(t)$ of the free $S_l(t) \equiv 0$ dynamics that satisfies the initial condition

$$\tilde{V}_l(0) = 0. \tag{3.10}$$

We continue this solution $\tilde{V}_l$ as far as possible to a real interval $(B_l, T_{0,l}]$, i.e. to negative real arguments t with infimum $B_l \in \mathbb{R}_- \cup \{-\infty\}$ and to positive real t until $T_{0,l} \in \mathbb{R}_+$ where $T_{0,l}$ is the free period of neuron l,

$$\tilde{V}_l(T_{0,l}) = \Theta_{U,l}\,. \tag{3.11}$$

We define the phase threshold to equal the free period,

$$\Theta_l := T_{0,l}, \tag{3.12}$$

the rise function U_l is then defined via the solution $\tilde{V}_l$,

$$U_l(\phi) := \tilde{V}_l(\phi), \tag{3.13}$$

where now $\phi \in (B_l, \Theta_l]$. This definition together with Eq. (3.8), Eqs. (3.9, 3.2) and Eqs. (3.11, 3.12) implies that for $V_l(0) = U_l(\phi_l(0))$, the free dynamics satisfies

$$V_l(t) = U_l(\phi_l(t)) \tag{3.14}$$

during free time evolution, when reaching the threshold and after reset, i.e. for all t. We now translate the jump in the potential into a jump in the phases. We first note that since $\tilde{V}_l(t)$ is strictly monotonically increasing in t, this also holds for $U_l(\phi)$ in ϕ, and the inverse U_l^{-1} exists on the interval $(B_{U,l}, \Theta_{U,l}]$, where

$$B_{U,l} := \lim_{\phi \searrow B_l} \tilde{V}_l(\phi), \tag{3.15}$$

$B_{U,l} \in \mathbb{R}_- \cup \{-\infty\}$. Suppose a spike sent by neuron k arrives at neuron l at time θ. We i) transform the phase before the interaction, $\phi_l(\theta^-)$ into the potential before the interaction, $V_l(\theta^-) = U_l(\phi_l(\theta^-))$, then ii) add the potential jump, ε_{lk}, $V_l(\theta) = V_l(\theta^-) + \varepsilon_{lk}$, and finally iii) transform back to phase representation via U_l^{-1}, $\phi_l(\theta) = U_l^{-1}(V_l(\theta))$. Taken together,

$$\phi_l(\theta) = U_l^{-1}(U_l(\phi_l(\theta^-)) + \varepsilon_{lk}) = H^{(l)}_{\varepsilon_{lk}}\left(\phi_l\left(\theta^-\right)\right), \tag{3.16}$$

where we introduced the continuous transfer function

$$H^{(l)}_{\varepsilon}(\phi) := U_l^{-1}(U_l(\phi) + \varepsilon) \tag{3.17}$$

that is strictly monotonic increasing, both as a function of ε and of ϕ. If $U_l(\phi) + \varepsilon > \Theta_{U,l}$, which is possible for $\varepsilon > 0$, we call the input supra-threshold, neuron l emits a spike and it is reset. We assume that $U_l(\phi) + \varepsilon < B_{U,l}$ (possible only for $\varepsilon < 0$ and $B_{U,l} \neq -\infty$) does not occur in the spike dynamics considered. Supra-threshold input leads to immediate spiking and reset of the neuron. We thus extend the definition of the transfer function to

$$H^l_{\varepsilon}(\phi) = U_l^{-1}(U_l(\phi) + \varepsilon) \quad \text{for } U_l(\phi) + \varepsilon < \Theta_{U,l}, \tag{3.18}$$

$$H^l_{\varepsilon}(\phi) = 0 \quad \text{for } U_l(\phi) + \varepsilon \geq \Theta_{U,l}. \tag{3.19}$$

From the construction, equivalence, Eq. (3.14), between both phase and potential representations holds also in the system with interaction when the phase interaction is mediated by the transfer function, cf. Fig. 3.2. Throughout this thesis, we will assume that $\phi_l(t)$ is piecewise linear so that in any finite interval there are only a finite number of spikes, i.e. there are no Zeno states [207].

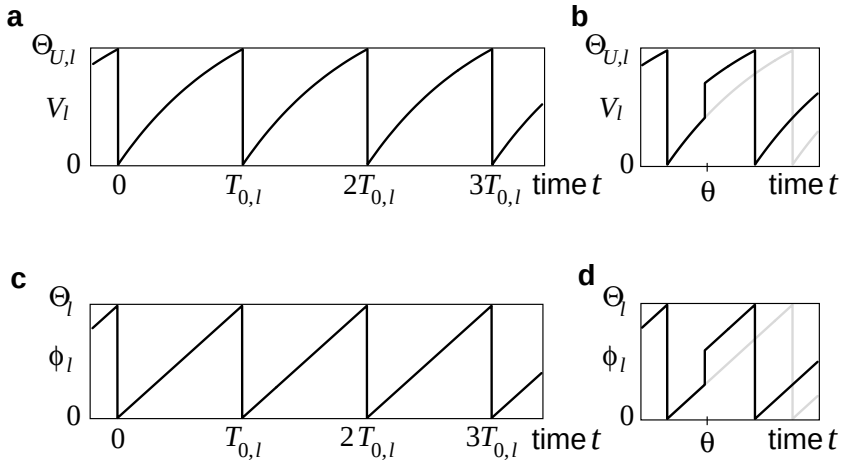

Figure 3.2: Comparison of potential representation (a,b) and phase representation (c,d). The free dynamics of (a) the potential$V_l(t)$ and (b) the phase $\phi_l(t)$ are periodic with period $T_{0,l}$. (b) Potential dynamics in response to an incoming excitatory spike at time θ. (d) Phase dynamics in response to input has a jump with size given by (3.16).

3.3 Benefits of the Mirollo-Strogatz phase model

The advantages of the Mirollo-Strogatz phase representation originate from two facts

(i) Sending and receiving of spikes are the only nonlinear events.

(ii) It is possible to study an entire class of models in one scheme.

Both facts simplify analytical considerations in chapters 4, 5 and 6. For our studies of the stability properties of the dynamics we can choose an event based framework and concentrate exclusively on the interaction points since distances between trajectories only change at these points. The Mirollo-Strogatz model allows to derive analytical results that are valid for the entire class of models.

Additionally, numerical simulations can be done using a simple event based algorithm. The algorithm is outlined as follows [58, 179, 176, 181]: We keep track of the "pseudo-spike times" [98] of a neuron l, the times $\Theta_l - \phi_l(t)$ remaining to the next hypothetical spike of neuron l without interaction. Further, of the spike arrival times together with the neurons that sent the spike. In each step, the smallest pseudo-spike time is compared with the time remaining until the next spike arrives. If the next event is i) a spike sending event, the dynamics is linearly evolved to this event and the pseudo-spike times of the sending neurons are reset to Θ_l. The newly sent spikes are stored in the spike list. If the next event is ii) a spike

receiving event, the dynamics is linearly evolved to this event and the pseudo-spike times of the receiving neurons are actualized following Eq. (3.17). The received spikes are deleted from the list.

3.4 Explicit examples

In this section we will derive the phase oscillator representation of several neural models following the rules given in sec. 3.2. We start with the *leaky integrate-and-fire neuron*, given by Eq. (2.1). As in sec. 2.10, we set $\gamma = 1/\tau_{\mathrm{mem}}$ and introduce a constant current I_{ext} (cf. sec. 3.1). In the form Eq. (3.1) with $S(t) = 0$ and $I = \gamma V_{\mathrm{rest}} + I_{\mathrm{ext}}/C_m$, Eq. (2.1) reads

$$\frac{dV}{dt} = -\gamma V + I, \tag{3.20}$$

so $f(V) = -\gamma V + I$. Solving the differential equation with initial conditions $\tilde{V}(0) = 0$ and using Eq. (3.14) yields the rise function

$$U_{\mathrm{IF}}(\phi) = \frac{I}{\gamma}(1 - e^{-\gamma\phi}). \tag{3.21}$$

We extend the range of the inverse time constant γ to the entire real axis, $\gamma \in \mathbb{R}$. γ specifies the dissipation in the system. For normal dissipation, $\gamma > 0$, $U_{\mathrm{IF}}(\phi)$ is concave, $U''_{\mathrm{IF}}(\phi) < 0$, bounded above by I/γ and it asymptotically approaches this value for $\phi \to \infty$. Condition 3.7 implies that $I/\gamma > \Theta_U$ to have an intrinsically oscillatory neuron. For $\gamma < 0$, $U_{\mathrm{IF}}(\phi)$ is convex, $U''_{\mathrm{IF}}(\phi) > 0$, and bounded below by $I/\gamma < 0$. The membrane potential $U_{\mathrm{IF}}(\phi)$ grows exponentially with ϕ so that, apart from $\Theta_U > V_{\mathrm{r}}$, no condition is necessary to obtain a self-oscillatory neuron. Without dissipation, $\gamma = 0$, the membrane potential dynamics of an isolated neuron is linear and specified by $U_{\mathrm{IF}}(\phi) = I\phi$. The phase threshold (3.12) for a particular integrate-and-fire neuron m is given by

$$\Theta_m = U_m^{-1}(\Theta_{U,m}) = \frac{1}{\gamma_m} \ln\left(\frac{I_m}{I_m - \gamma_m \Theta_{U,m}}\right) \tag{3.22}$$

if the parameters are I_m and γ_m; for $\gamma_m = 0$ we have $\Theta_m = \Theta_{U,m}/I$, the limit $\gamma_m \to 0$ in (3.22).

For the *conductance based leaky-integrate-and-fire neuron* with purely inhibitory coupling (and only one type of ions), we have

$$\frac{dV}{dt} = -\gamma V + I + \frac{E_i - V}{E_i} S(t), \tag{3.23}$$

where $E_i < V_{\mathrm{r}} = V_{\mathrm{rest}} = 0$ and V is bounded to $(E_i, \Theta_U]$. The steps described in sec. 3.1 for the transformation to $\bar{V}(t)$ can be done explicitly (cf. [177]) giving

$$\bar{V}(V) = (-E_i)\left[\ln(V - E_i) - \ln(-E_i)\right], \tag{3.24}$$

with $\bar{V} \in (-\infty, \bar{V}(\Theta_U)]$, and the transformed differential equation reads

$$\frac{d\bar{V}(t)}{dt} = [I + \gamma(-E_i)] \exp\left(-\frac{\bar{V}(t)}{(-E_i)}\right) - \gamma(-E_i). \tag{3.25}$$

It can be solved by separation of variables to derive $\tilde{V}(t)$ and thus U_{CoIF} for the transformed system,

$$U_{\mathrm{CoIF}}(\phi) = (-E_i) \ln\left(1 + \frac{I}{\gamma(-E_i)} \left(1 - \exp(-\gamma\phi)\right)\right). \tag{3.26}$$

The phase threshold for some neuron m is

$$\begin{aligned} \Theta_m &= U_m^{-1}(\bar{V}_m(\Theta_{U,m})) \\ &= -\frac{1}{\gamma} \ln\left(\frac{\gamma(-E_i)}{I}\left(1 - \exp\left(\frac{\bar{V}_m(\Theta_{U,m})}{(-E_i)}\right)\right) + 1\right). \end{aligned} \tag{3.27}$$

For the *quadratic integrate-and-fire neuron*, with $a = g_L/(2\Delta_T C_m)$ and $I = -I_T/C_m + I_{\mathrm{ext}}/C_m$, Eq. 2.2 reads

$$\frac{dV}{dt} = a(V - V_T)^2 + I.$$

The construction of the neuron model implies $V_{\mathrm{r}} < V_T < \Theta_U$ which results in an oscillatory neuron if $I > 0$. The rise function can be computed to

$$U_{\mathrm{QIF}}(\phi) = V_T + \sqrt{\frac{I}{a}} \tan(\sqrt{Ia}t + b), \tag{3.28}$$

where $b = -\arctan(\sqrt{a/I}V_T)$ fixed by $\tilde{V}(0) = 0$ and the phase threshold for a neuron m reads

$$\begin{aligned} \Theta_m &= U_m^{-1}(\Theta_{U,m}) \\ &= \frac{1}{\sqrt{Ia}} \left(\arctan\left(\sqrt{\frac{a}{I}}V_T\right) + \arctan\left(\sqrt{\frac{a}{I}}(\Theta_{U,m} - V_T)\right)\right). \end{aligned} \tag{3.29}$$

Another interesting and analytically useful example are *Mirollo-Strogatz biological oscillators* introduced in [136]. We generalize the rise function to

$$U_{\mathrm{MS}}(\phi) = \frac{1}{b} \ln\left(1 + \frac{1}{a}\phi\right), \tag{3.30}$$

where $ab > 0$. This corresponds to a differential equation

$$\frac{dV}{dt} = \frac{1}{ab} \exp(-bV) \tag{3.31}$$

for V (cf. Eq. 3.1). $U_{\mathrm{MS}}(\phi)$ is concave for $a, b > 0$ and convex for $a, b < 0$. In the former case, $B = -a$, the domain of U_{MS} is $\phi \in (-a, \infty]$, with $U_{\mathrm{MS}}(\phi) \to \infty$ as

$\phi \to \infty$. If $a, b < 0$, the domain is $\phi \in (-\infty, |a|)$, where $U_{\mathrm{MS}}(\phi) \to \infty$ as $\phi \nearrow |a|$. Therefore, in both cases, the neuron is oscillating for any $\Theta_U > V_{\mathrm{r}}$. The threshold for the phase of a specific neuron m is given by

$$\Theta_m = U_m^{-1}(\Theta_{U,m}) = a_m(\exp(b_m \Theta_{U,m}) - 1) \tag{3.32}$$

for parameters a_m, b_m.

Interestingly, there is a direct relation between neural oscillators of leaky integrate-and-fire type and Mirollo-Strogatz biological oscillators: the rise function of a Mirollo-Strogatz biological oscillator is the inverse of the rise function of a leaky integrate-and-fire neuron [131]. For all $x > -a$ we have

$$U_{\mathrm{MS}}(x) = \frac{1}{b} \ln\left(1 + \frac{x}{a}\right) = -\frac{1}{\gamma} \ln\left(1 - \frac{\gamma}{I} x\right) = U_{\mathrm{IF}}^{-1}(x) \tag{3.33}$$

when setting $b = -\gamma$, $a = -\gamma/I$. This can be directly verified by explicitly inverting U_{IF} . It might be useful to establish such equivalences because the interaction function H (3.17) contains both, the rise function U and its inverse U^{-1}.

Chapter 4

Designing complex neural networks

In this chapter we investigate the inverse problem to the relations between structure and dynamics of a complex spiking neural network: We determine the set of networks that exhibit an arbitrary predefined precise spiking dynamics.

Is it possible to modify the features of interactions so that a neural network gives rise to a given dynamics? We will assume that all neuron parameters (U_m, Θ_m) and delay times τ_{ml} (cf. sec. 4.2) are given and fixed in a network; the task is to find networks with these given features that exhibit a desired pattern as an invariant dynamics. We present a method to analytically find the set of all networks as defined by the neurons' coupling strengths that exhibit a given pattern of spikes as an invariant solution. We explicitly carry the construction out for periodic patterns, but this restriction can be relieved by omitting the periodicity conditions. In the predefined pattern of spikes, all spike times of all the neurons are exactly specified, the pattern may be arbitrary long and have complicated temporal structure. However, very long patterns will usually not be realizable since they imply too many conditions which will in general be incompatible. It is further possible to store multiple patterns in one network, where the initial conditions of the dynamics decide which pattern will be recalled. The analysis presented is very general. We allow for inhomogeneous networks with different types of neurons, heterogeneously distributed delays and thresholds (and thus intrinsic neuron frequencies), combinations of inhibitory and sub- and supra-threshold excitatory interactions as well as for complicated patterns that include degenerate event times, multiple spiking of the same neuron within the pattern and silent neurons that never fire.

We further show how to design networks if additional restrictions are imposed, for instance by predefining the detailed network connectivity. We illustrate the applicability of the method by examples of Erdös-Rényi and scale-free random networks. Finally, the method can be used to design networks that optimize network properties. To illustrate the idea we design networks that exhibit a predefined

pattern dynamics and at the same time minimize the networks' wiring costs.

The design method sees immediate application when numerically studying the stability properties of periodic patterns (sec. 4.8) and illustrating analytical results (ch. 5). A generalization for temporally extended couplings that is valid in inhibitory networks of leaky integrate-and-fire neurons is employed in sec. 6.7.

We partially presented the results derived in this chapter in a letter [132] and in an exhaustive publication [131].

4.1 State of the art

A number of studies have been addressed to determining networks that give rise to a desired kind of network activity. An example are synfire chains. In these models, networks that give rise to propagation of synchronous activity are constructed by connecting groups of neurons with strongly excitatory directed projections to a chain [3, 83, 54, 18]. Other studies were dedicated to finding networks that realize different stable activity patterns, such as an asynchronous, irregular state [79, 105]. Closer related to our work, a recent article [119] captures the effective coupling between neurons in a biological neural network. A method was presented to construct a network of leaky integrate-and-fire neurons that exhibits irregular spike trains with statistical properties similar to the spike trains found in extracellular recordings of a subset of neurons in a biological neural network. Further, a neurobiologically oriented work studied a three unit model for the central pattern generator in the stomatogastric ganglion of the lobster [159]. Central pattern generators are neural circuits that produce stereotypic spike pattern and thus control the generation of rhythmic, stereotypic motor actions e.g. for locomotion, respiration, heartbeat, mastication or digestion [146, 77, 158]. Extensive numerical investigations showed that the qualitative spiking dynamics produced by the network does not depend on the details of the neuron model and the synaptic coupling, i.e. that an entire class of networks produced similar dynamics [159].

A few studies show how to design a network that gives rise to a predefined, precisely timed pattern of spikes. In [123], an algorithm is given that allows to construct one specific, fully connected network realizing one predefined simple periodic pattern of spikes. In such a pattern each neuron fires once within a period. The network model has purely inhibitory couplings without transmission delay (cf. sec. 4.2 for further description). A second study showed how to construct networks with purely excitatory or purely inhibitory connections realizing patterns close to the fully synchronous state [50]. Starting with a network of normalized connections that gives rise to the fully synchronous state, small heterogeneities are introduced that cause the synchronous state to split up. If the heterogeneities are too large, the near-synchronous state breaks down and the network assumes an irregular firing state. The near synchronous pattern is predicted from the network heterogeneity or, inversely, the network heterogeneities can be derived from a predefined near-synchronous firing pattern.

4.2 The model

We consider a complex network of N neurons in the Mirollo-Strogatz phase representation, cf. sec. 3.2. The phase of a neuron $l \in \{1, ..., N\}$ at time t is given by $\phi_l(t)$, the strength of the coupling from neuron k to neuron l is ε_{lk} and the coupling delay is given by τ_{lk}. In particular, the delay distribution can be inhomogeneous. The effect of a spike arriving at neuron l is mediated by the transfer function $H^{(l)}$ given in Eqs. (3.16, 3.17). In ref. [123] the interaction is instantaneous, there is no synaptic delay. Besides, the authors use a network model given by Eq. (3.3) with synapses Eq. (3.6), but the differential equation is directly transformed into a model with linear free time evolution through the transformation $\bar{V}(V) \propto \int_0^V A(v)^{-1} dv$, which is always possible since $A(V) > 0$ for the entire range of V, and the nonlinearity is collected in a V-dependent coefficient of the coupling term[1]. In [50], the near synchronous state is studied in networks of Mirollo-Strogatz neurons with homogeneous delay distribution $\tau_{lk} = \tau$ and almost normalized coupling $\sum_{j=1}^{N} \varepsilon_{ij} \approx \varepsilon$ for all i.

4.3 Admissible networks

Given a predefined spike pattern, we call a network that exhibits this pattern as an invariant dynamics an *admissible* network. An admissible network will show the predefined periodic pattern of spikes when the dynamics is started at the correct initial conditions. Assuming that all neuron parameters (U_m, Θ_m) and delay times τ_{ml} (cf. sec. 4.2) are given and fixed in a network, we determine the networks admissible for a given pattern by designing the coupling strengths ε_{ml}. It turns out that there is often a multi-dimensional family of solutions so that networks with very different configurations of the coupling strengths are admissible; below we derive analytical restrictions that define the set of all networks exhibiting such a pattern. Of course, there might be situations, where other parameters, such as the delays [60] are desired to be variable as well (or only). The key aspects of the approach presented below can be readily generalized to such design tasks.

4.4 Degenerate event timing

In the Mirollo-Strogatz phase representation, sending and receiving of spikes are the only nonlinear events. These events sometimes occur simultaneously, a case which

[1] There is a problem in the derivation of the coefficient Eq. (4) in [123]. In an equation of the form $dV(t)/dt = F(V(t)) + G(V(t))\varepsilon\delta(t)$, the size of the jump in V at zero is not given by $V(0^+) - V(0^-) = \varepsilon G(V(0))$ but, in generalization of the conductance based case, sec. 2.6, it is implicitly given by $\int_{V(0^-)}^{V(0^+)} G(v)^{-1} dv = \varepsilon$. This problem can be easily solved by defining the network dynamics, Eq. (1) in [123] by $dx_i(t)/dt = F_i(x_i(t)) + \sum_{j=1}^{N} \sum_f G_i(x_i(t_j^{f-}))J_{ij}\delta(t - t_j^f)$ instead of $dx_i(t)/dt = F_i(x_i(t)) + G_i(x_i(t)) \sum_{j=1}^{N} \sum_f J_{ij}\delta(t - t_j^f)$, as it is also done after the transformation of variables, in Eq. (3).

we call degenerate. In the presence of degenerate events, care has to be taken in the definition of the model's dynamics. Simultaneous events occurring at different neurons do not cause any difficulties because an arbitrary order of processing does not affect the collective dynamics at any future time. However, if two or more events occur simultaneously at the same neuron, we need to specify a convention for the order of processing. We will therefore go through the possible combinations in the following (cf. [131]):

(i) *spike sending due to spike reception*: The action of a received spike might be strong enough so that the excitation is supra-threshold,

$$U_m\left(\phi_m\left((t+\tau_{ml})^-\right)\right)+\varepsilon_{ml}\geq U_m\left(\Theta_m\right). \tag{4.1}$$

We use the convention that neuron m sends a spike simultaneous to the reception of the spike from neuron l at time $t+\tau_{ml}$ and is reset to

$$\phi_m\left(t+\tau_{ml}\right)=0. \tag{4.2}$$

(ii) *spike received at sending time*: If neuron m receives a spike from neuron l exactly at the same time when m was about to send a spike anyway,

$$\phi_m\left((t+\tau_{ml})^-\right)=\Theta_m, \tag{4.3}$$

we take the following convention for the order processing: first the spike is sent and the phase is reset to zero, then the incoming spike is received so that

$$\phi_m\left(t+\tau_{ml}\right)=H^{(m)}_{\varepsilon_{ml}}\left(0\right). \tag{4.4}$$

If the spike received causes again a supra-threshold excitation, we neglect this second spike generated at time $t+\tau_{ml}$ and just reset the neuron m to zero as in (4.2).

(iii) *simultaneous reception of multiple spikes*: If multiple spikes are received simultaneously by the same neuron and each subset of spikes does *not* cause a supra-threshold excitation (as in (4.1)), a convention about the order of treatment is not necessary as can be seen from the following argument. If neuron m at time θ simultaneously receives $h\in\mathbb{N}$ spikes from neurons $l_1,...,l_h$, and $\sigma:\{1,...,h\}\to\{1,...,h\}$ is an arbitrary permutation of the first h integers, we have

$$\begin{aligned}
&H^{(m)}_{\varepsilon_{ml_{\sigma(1)}}}(H^{(m)}_{\varepsilon_{ml_{\sigma(2)}}}(...H^{(m)}_{\varepsilon_{ml_{\sigma(h)}}}(\phi_m(\theta^-))...))\\
=&U_m^{-1}[U_m(U_m^{-1}[U_m(...U_m^{-1}[U_m(\phi_m(\theta^-))+\varepsilon_{ml_{\sigma(h)}}]...)+\varepsilon_{ml_{\sigma(2)}}])+\varepsilon_{ml_{\sigma(1)}}]\\
=&U_m^{-1}[U_m(\phi_m(\theta^-))+\varepsilon_{ml_{\sigma(h)}}+...+\varepsilon_{ml_{\sigma(2)}}+\varepsilon_{ml_{\sigma(1)}}]\\
=&H^{(m)}_{\varepsilon_{ml_1}+\varepsilon_{ml_2}+...+\varepsilon_{ml_h}}(\phi_m(\theta^-)).
\end{aligned} \tag{4.5}$$

Treating the incoming spikes separately in arbitrary order is therefore equivalent to treating them as one spike from a hypothetical neuron with coupling strength

$\varepsilon_{ml_1} + \varepsilon_{ml_2} + ... + \varepsilon_{ml_h}$ to neuron m. Moreover, upon sufficiently small changes to the spike reception times, the sub-threshold response of neuron m continuously changes with these reception times. This is because the neuron's response function $H^{(m)}$ is identical for different incoming spikes. We note that in a generalized model one might introduce different transfer functions for different couplings. This would reflect the fact that, dependent e.g. on the position of the synapse, incoming spikes may have different effects on the postsynaptic neuron even if they generate the same amount of charge flowing into (or out of) the neuron. We extend the definition

$$\phi_m(\theta) = H^{(m)}_{\varepsilon_{ml_1}+\varepsilon_{ml_2}+...+\varepsilon_{ml_h}}(\phi_m(\theta^-)) \tag{4.6}$$

for the processing of multiple spike arrivals to more involved cases, where a subset of spikes generates a spike. Treating this subset first would result in a different dynamics than summing up all couplings strength, e.g. if the remaining couplings balance the strong excitatory subset. In this case the order of treatment is not arbitrary and the phase as well as the spikes generated in response to the receptions do not depend continuously on the spike arrival times; as a convention, we sum the coupling strengths first, as in (4.6). The generalization of (i) and (ii) to the case of multiple spikes received simultaneously is straightforward. The dynamics however will in general also *not* depend continuously on the arrival times.

(iv) *simultaneous sending of multiple spikes:* As we exclude the simultaneous sending of multiple spikes by the same neuron, if several spikes are sent simultaneously, they are sent by different neurons; therefore no difficulties arise and we need no extra convention.

4.5 Characterizing periodic spike patterns

What characterizes a periodic pattern of precisely timed spikes? Let $t_{i'}$, $i' \in \mathbb{Z}$, be an ordered list of times at which a neuron emits the i'th spike occurring in the network, so that $t_{j'} \geq t_{i'}$ if $j' > i'$. Assume a periodic pattern consists of M spikes. Such a pattern is then characterized by its period T, by the times $t_i \in [0, T)$ of spikes $i \in \{1, ..., M\}$, and by the indices $s_i \in \{1, \ldots, N\}$ identifying the neuron that sends spike i at t_i. If two or more neurons in the network simultaneously emit a spike, i.e. $t_i = t_j$ with $i \neq j$, the above order is not unique and we fix it arbitrarily. The periodicity of the pattern then entails

$$t_i + nT = t_{i+nM} \text{ and } s_i = s_{i+nM} \tag{4.7}$$

for all $n \in \mathbb{Z}$, where the definition of s is appropriately extended. Due to the periodicity of the pattern, we can assume without loss of generality that the delay times are smaller than the patterns period, otherwise, we take them modulo T without changing the invariant dynamics. Further, to avoid extensively many case distinctions we require that between any two subsequent spike times t, t' of a neuron l, that neuron receives at last one spike in the interval $(t, t') \cap (t, t + \Theta_l)$. We will employ the indexing method also in chapter 5 to study the stability properties of periodic patterns of spikes.

4.6 Firing pattern and phase dynamics

A predefined pattern of spikes imposes conditions on the time evolution of the neurons' phases. Suppose a specific neuron l fires at $K(l)$ different times $t_{i_k} \in [0, T)$, $k \in \{1, ..., K(l)\}$ within the first period. For non-degenerate event times this implies

$$\phi_l(t_{i_k}^-) = \Theta_l, \tag{4.8}$$

whereas at any other time $t \in [0, T)$, $t \neq t_{i_k}$ for all k,

$$\phi_l(t^-) < \Theta_l, \tag{4.9}$$

to prevent untimely firing.

If the network is fixed, in general there will not be a phase dynamics that gives rise to a predefined pattern. If there is a phase dynamics which gives rise to a certain pattern, then this dynamics is unique for an important subset of neurons in the network:

Lemma 1: Let $S \subset \{1, ..., N\}$ be the set of neurons that (i) do not receive any supra-threshold excitations and (ii) are firing at least once in the pattern. Predefining the firing dynamics of the network determines the phase dynamics of the neurons in S uniquely.

Proof: We disprove the opposite: There may be a phase dynamics $\tilde{\phi}_m(t)$, $m \in \{1, ..., N\}$ which is different from the original phase dynamics $\phi_m(t)$, $m \in \{1, ..., N\}$ but generates the same spike pattern. We assume that also for some $l \in S$ the phase dynamics $\tilde{\phi}_l(t)$ is different from $\phi_l(t)$. Further, assume for some t_0, $\phi_l(t_0) > \tilde{\phi}_l(t_0)$. Then this inequality remains true for all future times t_0. First, it remains true during free time evolution. But also the inputs are the same (input times and strengths) for both dynamics and the $H_\varepsilon^{(l)}(\phi)$ are strictly monotonically increasing as function of ϕ, so the relation $\phi_l(t) > \tilde{\phi}_l(t)$ for $t \geq t_0$ remains true also after arbitrarily many interactions. Therefore, denoting the next firing time of neuron l after time t_0 by t_j, we conclude that $\Theta_l = \phi_l(t_j^-) > \tilde{\phi}_l(t_j^-)$, violating neuron l's firing pattern. An analogous argument shows that if $\phi_l(t_0) < \tilde{\phi}_l(t_0)$ for some t_0, the firing pattern would be also violated.

If a neuron that (i) receives one or more supra-threshold inputs or (ii) is silenced (i.e. has no firing time in the pattern) has a perturbed phase dynamics, its spike sub-pattern can still remain the predefined one. (i) If a neuron l receives a supra-threshold input, a small initial deviation from the original phase dynamics that occurs sufficiently briefly before the input, will only change the phase ϕ_l of that neuron but not its next spike time as long as the input remains supra-threshold. Since the dynamics continues without deviations with respect to the original phase dynamics, all future events will also take place at the predefined times. Thus there are different initial conditions that lead to the same spike pattern. (ii) A sufficiently small initial deviation from original dynamics that occurs at a silenced neuron can decay without making the neuron fire so that the spike pattern stays unchanged, although the phase of the silenced neuron is different.

In this chapter, we are mainly interested in periodic dynamics. Indeed, we can show that a periodic spike pattern implies a periodic phase dynamics in the neurons in S.

Theorem 2: For all neurons l that (i) do not receive any supra-threshold excitations and (ii) are firing at least once in the pattern, i.e. for all $l \in S$, the periodicity T of the entire firing pattern is sufficient for the periodicity of the phases,

$$\phi_l(t) = \phi_l(t + nT), \tag{4.10}$$

for all $n \in \mathbb{Z}$ and all $t \in [0, T)$.

Proof: We compare for some $l \in S$ the phase dynamics of $\phi_l(t)$ and $\phi_l(t + T)$ and assume without loss of generality for some t_0, $\phi_l(t) > \phi_l(t + T)$. Again, this inequality remains true for all $t > t_0$ and at the next firing time t_j, $\Theta_l = \phi_l(t_j^-) > \phi_l((t_j+T)^-)$ violating the patterns periodicity. Therefore, if the pattern is periodic, the phases of neurons $l \in S$ are also periodic and the phases have the period of the pattern.

How far does, on the other hand, periodicity of the phase dynamics imply periodicity of the spike pattern?

Theorem 3: The periodicity of the phases of all neurons in the network is sufficient for the periodicity of the spiking times of each neuron. Further, if there are no supra-threshold excitations in the network, the spike pattern has the period of the phase dynamics.

Proof: If the phase dynamics is periodic with period T and no supra-threshold excitations occur, it satisfies in particular $\phi_l((t_{i_k} + nT)^-) = \Theta_l$ and $\phi_l((t+nT)^-) < \Theta_l$ for $t \neq t_{i_k}$, where $t \in [0, T)$ and $t_{i_k} \in [0, T)$, $k \in \{1, \ldots, K(l)\}$, are the firing times of neuron l in the first period. Therefore the sub-pattern of spikes generated by neuron l is periodic with period T. Since l is arbitrary, the entire pattern is periodic with period T.

Interestingly, if there are supra-threshold excitations, the sub-pattern of a neuron need not have the period T of the phases, as can be seen from a simple, albeit constructed example: Consider a neuron l, which is coupled only to itself and receives input from itself as well as once per phase period T from only one other neuron m. If neuron l receives a supra-threshold input from neuron m at time θ, we have $\phi_l(\theta^-) < \Theta_l$ and $U_l(\phi_l(\theta^-)) + \varepsilon_{lm} \geq U_l(\Theta_l)$. Leaving aside the assumption $\tau_{ij} < T$ made in sec. 4.5, suppose the delay of the coupling from l to l is $\tau_{ll} = T$, i.e. equal to the period of the phases. Further, the coupling strength ε_{ll} is inhibitory and so that $H^{(l)}_{\varepsilon_{lm}+\varepsilon_{ll}}(\phi_l(\theta^-)) = 0$, i.e. $\varepsilon_{ll} = -U_l(\phi_l(\theta^-)) - \varepsilon_{lm} < 0$. Then the phase of neuron l can be periodic, whether or not it receives a spike from itself because $\phi_l(\theta) = 0$ in each case, either due to the reset of neuron l or due to the inhibitory spike received from itself. Now, if neuron l sent a spike at time θ, there will be no spike sending at $\theta + T$ because of the inhibition by its self-interaction. Since the self-interaction spike is then missing at time $\theta + 2T$, a spike will be emitted at that later time and so on. So the spike sub-pattern of this neuron (consisting of all those spikes in the total pattern that are generated by neuron l) has period $2T$, and not T.

However, the spike sub-pattern of any neuron l has to be periodic even if it receives supra-threshold input. This can be seen as follows: Due to the conventions above, a spike can only be emitted when there is a discontinuity in the phase ϕ_l (after a supra-threshold excitation, the phase is always zero, after a simultaneous reception and spiking it is always unequal to Θ_l) or if the neuron receives a supra-threshold input when its phase is $\phi_l(\theta^-) = 0$. Since $\phi_l(t)$ is piecewise continuous, in every (finite) time interval $[t, t+T)$ there are only finitely many discontinuities, as well as only finitely many times with $\phi_l(\theta^-) = 0$ because the phase is monotonous otherwise. Therefore, given a certain phase dynamics, spikes can be emitted by the network only at finitely many times in any interval $[t, t+T)$. This implies that there are only finitely many combinations of spikes which can be emitted by the network within a period T of the phases. Because the network is a finite-dimensional deterministic dynamical system, after a finite integer multiple of T, the spike patterns have to recur. After this has happened, not only the phases but (because here we can choose T to be an arbitrary integer multiple of the phase period so that $\tau_{lm} < T$ without loss of generality) also all spikes in transit are the same as at some time before. Since at any time the state of the network is fixed by the phases and the spikes in transit, the entire dynamics must repeat. So, the pattern is periodic with some period nT, $n \in \mathbb{N}$.

As a direct consequence from the two preceding theorems we note the important special case $S = \{1, ..., N\}$.

Corollary 4: If all neurons in the network receive only subthreshold input and are firing at least once in a pattern, periodicity of the entire pattern is equivalent to the periodicity of the phase dynamics and the periods are equal.

For simplicity, we impose in the following that the phase dynamics of all neurons, including those neurons that are silent (i.e. never send a spike) and those that receive supra-threshold inputs, are periodic with period T. We consider $\phi_l(t)$ for $t \in [0, T)$ with periodic boundary conditions. All times are measured modulo T and spike time labels j are reduced to $\{1, ..., M\}$ by subtracting a suitable integer multiple of M.

4.7 Indexing periodic spike patterns

Setting out from sec. 4.5, in this section we provide a method of indexing all spike reception times, and of ordering them in time. The input coupling strengths are indexed accordingly. Based on this scheme, we will be able to derive conditions ensuring the sending of a spike at the pre-defined spike times, periodicity of the phase dynamics, and quiescence (non-spiking) of the neurons between their desired spike times in sec. 4.8.

Let $\theta_{l,j} := t_j + \tau_{ls_j}$ be the time when neuron l receives the spike labeled j from neuron s_j. Then, for inhomogeneous delay distribution the $\theta_{l,j}$ might not be ordered in j. Therefore, we define a permutation $\sigma_l : \{1, ..., M\} \to \{1, ..., M\}$ of

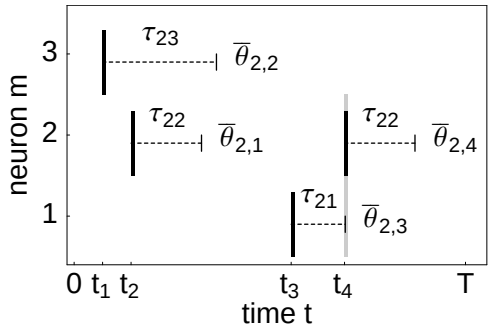

Figure 4.1: Pattern of $M = 4$ spikes in a network of $N = 3$ neurons illustrating the indexing of spike sending and reception times. The spike (sending) times t_i, marked by black bars, are indexed with increasing i according to their temporal order of occurrence in the network (the neuron identities play no role for this index). The ordered spike reception times $\bar{\theta}_{l,i}$ are displayed for neuron $l = 2$. They are generally different for other receiving neurons ($l \neq 2$, not shown) and obtained by adding the delay times τ_{lm} (dashed lines) to the spike sending times t_j and then ordering the resulting set for each neuron. Here, there is one degenerate event: neuron $l = 2$ receives a spike from $m = 1$ exactly at its second spike sending time t_4 (light gray vertical bar).

the indices of spikes received by neuron l, so that

$$\bar{\theta}_{l,j} := \theta_{l,\sigma_l(j)} \tag{4.11}$$

is ordered, i.e. $\bar{\theta}_{l,j} \geq \bar{\theta}_{l,i}$ if $j > i$. If multiple spikes are received at one time, σ_l is not unique. This, however, has no consequence for the collective dynamics because all the associated spike receptions are treated as one according to Eq. (4.6). If neuron l receives multiple, say $p(l, j)$ spikes at time $\bar{\theta}_{l,j}$, we only consider the lowest of all indices j' with reception time $\bar{\theta}_{l,j'} = \bar{\theta}_{l,j}$. If neuron l receives spikes at M_l different times, we denote the smallest index of each reception time by $j_1(l), ..., j_{M_l}(l)$ so that

$$j_n(l) := j_{n-1}(l) + p(l, j_{n-1}(l)). \tag{4.12}$$

for $n \in \{2, \ldots, M_l\}$ and $j_1(l) = 1$. The first set of equal reception times starts with index $j_1(l) = 1$ and contains $p(l, 1)$ spikes. Therefore, the second set of equal reception times has first index $j_2(l) = p(l, 1) + 1 = p(l, j_1(l)) + j_1(l)$ and contains $p(l, j_2(l))$ spikes. This way all indices are defined recursively. To keep the notation concise, we skip the argument l in the following (where it is clear) as the argument or index of some quantity which is itself a further index or a subindex, e.g., of $\bar{\theta}_l$ or ε_l. For instance, we abbreviate $\bar{\theta}_{l,j_i(l)}$ by $\bar{\theta}_{l,j_i}$ and $p(l, j_k(l))$ by $p(j_k)$ where appropriate. Furthermore, indices denoting different spike receptions of neuron l are reduced to $\{1, ..., M_l\}$ by subtracting a suitable multiple of M_l. We define

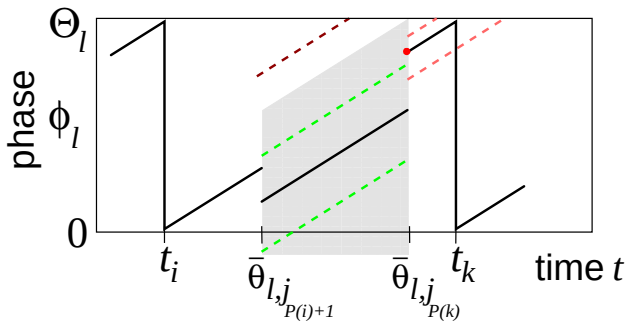

Figure 4.2: Restriction of a neuron's dynamics between its firing events, cf. Eqs. (4.17) and (4.18). In this example, two spikes arrive between the firing times t_i and t_k of neuron l. The solid line indicates one possible time evolution of the phase $\phi_l(t)$. Between the firing times, $\phi_l(t)$ may follow any path within the possibly semi-infinite polygon (gray shaded; green dashed lines show other possible trajectories). A too large phase at $\bar{\theta}_{l,j_{P(i)+1}}$ contradicts Eq. (4.18) and will lead to early firing (dark red dashed line). The phase at $\bar{\theta}_{l,j_{P(k)}}$ is fixed (red dot). Any other phase inconsistent with the equality (4.17) would lead to a firing time earlier or later than predefined (light red dashed lines).

$P_l(i) \in \{1, ..., M_l\}$ (cf. also Fig. 4.2) as the index of the last reception time for neuron l before its firing time t_i,

$$P_l(i) := \text{argmin}\{t_i - \bar{\theta}_{l,j_k} \,|\, k \in \{1, ..., M_l\}, t_i - \bar{\theta}_{l,j_k} > 0\}. \tag{4.13}$$

If there are no simultaneous spikes received by neuron l and if there is no spike received at the firing time t_i itself, $P_l(i)$ is given by

$$P_l(i) = \text{argmin}\{t_i - \bar{\theta}_{l,j} \,|\, j \in \{1, ..., M\}\}. \tag{4.14}$$

4.8 Determining all admissible networks

Using the indexing methods developed in sec. 4.7 and 4.5, in this section we give an analytical restriction of the set of all admissible networks for a given spike pattern. The principle idea is that Eqs. (4.17) and (4.18) can be reduced to restrictions on the phases at the arrival times of spikes and thus yield the admissible networks as illustrated in Fig. 4.2.

In the following, if two or more reception times are equal, we will select the smallest index and restrict the dynamics only *once*, using Eqns. (4.5, 4.6) and the definition of $j_i(l)$ above. Only the total action of all spikes received by a neuron l at a particular $\bar{\theta}_{l,j_i}$ will be restricted, by a single condition. We therefore define the sum of the coupling strengths of all spikes received by neuron l at time $\bar{\theta}_{l,j_i}$ as

$$\bar{\varepsilon}_{l,i} = \varepsilon_{l s_{\sigma(j_i)}} + ... + \varepsilon_{l s_{\sigma(j_i + p(j_i) - 1)}}. \tag{4.15}$$

Indeed, $\sigma_l(j_i(l)+k)$, $k \in \{0,...,p(l,j_i(l))-1\}$, are the indices of the $p(l,j_i(l))$ different spikes received by neuron l at the ith reception time $\bar{\theta}_{l,j_i}$, $i \in \{1,...,M_l\}$. If neuron l receives all spikes at different times, we have $\bar{\varepsilon}_{l,i} = \varepsilon_{ls_{\sigma(i)}}$. Let

$$\Delta_{l,i} = \bar{\theta}_{l,j_{i+1}} - \bar{\theta}_{l,j_i} \tag{4.16}$$

be the time differences between two successive different reception times, where $i+1$ has to be reduced to $\{1,...,M_l\}$ by subtracting a suitable integer multiple of M_l. We now rewrite Eqns. (4.8) and (4.9) for neuron l as a set of conditions on the phases $\phi_l(\bar{\theta}_{l,j_i})$ at the different spike reception times $\bar{\theta}_{l,j_i}$ in terms of the firing times t_{i_k} of that neuron and the spike reception times $\bar{\theta}_{l,j_{i'}}$, $i' \in \{1,...,M_l\}$.

If the given pattern does not imply the reception of a spike precisely at the firing time t_{i_k} (together with the firing times and the delays also the reception times are fixed), this results in

$$\phi_l(\bar{\theta}_{l,j_{P(i_k)}}) = \Theta_l - (t_{i_k} - \bar{\theta}_{l,j_{P(i_k)}}), \tag{4.17}$$

$$\phi_l(\bar{\theta}_{l,j_i}) < \Theta_l - \Delta_{l,i}, \tag{4.18}$$

where $k \in \{1,...,K(l)\}$ and $i \in \{1,...,M_l\} \backslash \{P(i_k) | k \in \{1,...,K(l)\}\}$. We note that, by definition (4.13), there is no input to neuron l between the spike(s) received at $\bar{\theta}_{l,j_{P(i_k)}}$ and the neuron's next firing time t_{i_k}.

The firing time condition (4.17) states that the neuron at time $\bar{\theta}_{l,j_{P(i_k)}}$ is as far away from its threshold Θ_l as it needs to be in order to exactly evolve there freely in the remaining time $t_{i_k} - \bar{\theta}_{l,j_{P(i_k)}}$. The inequalities (4.18) guarantee that the neuron does not spike between the firing times determined by the predefined pattern: They ensure that neuron l is far enough from its threshold at all other spike reception times and is not firing at any time that is not in the desired pattern, $t \neq t_{i_k}$.

Above, we had fixed the convention, that if a spike is received by a neuron when it is just about to fire, the spike received is processed after the sending of the new spike. If we had used the convention that first the received spike is considered, the "$<$" in inequality (4.18) would have been replaced by a "$\leq$". Here equality, $\phi_l(\bar{\theta}_{l,j_i}) = \Theta_l - \Delta_{l,i}$, means that the neuron approaches the threshold at $\bar{\theta}^-_{l,j_{i+1}}$, i.e. $\phi_l(\bar{\theta}^-_{l,j_{i+1}}) = \Theta_l$, but since the received spike is processed first, an untimely spike can be prevented by an inhibitory input.

If there is one or several spikes received precisely at a predefined firing time t_{i_k}, supra-threshold excitation can be used to realize the pattern. To account for this, the firing time condition (4.17) and the silence condition (4.18) with $i = P_l(i_k)+1$ have to be replaced by the conditions

$$\phi_l(\bar{\theta}_{l,j_{P(i_k)}}) < \Theta_l - (t_{i_k} - \bar{\theta}_{l,j_{P(i_k)}}), \tag{4.19}$$

$$U_l(\phi_l(t^-_{i_k})) + \bar{\varepsilon}_{l,P(i_k)+1} \geq U_l(\Theta_l). \tag{4.20}$$

Here, the strict inequality (4.19) prevents untimely spiking (cf. the dark red dashed line in Fig. 4.2) and guarantees that the neuron does not reach the threshold by its

intrinsic dynamics. The second, inequality (4.20), ensures the spiking at t_{i_k}. However, (4.20) is not an inequality on the phases depending at the reception times only, but involves the total coupling of the incoming spikes. We note that expression (4.19) with an equal sign, "=", describes the case that the neuron spikes without supra-threshold excitation, because due to our above convention, the firing is treated before the spike reception. Then, inequality (4.20) is obsolete. So Eq. (4.17) is the appropriate spike time condition also if spikes are received by neuron l when it just reaches threshold. Now, there are two cases possible (i) the spikes do not cause a supra-threshold excitation $U_l(0) + \bar{\varepsilon}_{l,P(i_k)+1} < U_l(\Theta_l)$ from the reset phase of the neuron or (ii) they cause a supra-threshold excitation, $U_l(0) + \bar{\varepsilon}_{l,P(i_k)+1} \geq U_l(\Theta_l)$. In the first case, $\phi_l(t_{i_k}) = \phi_l(\bar{\theta}_{l,j_{P(i_k)+1}}) = H^{(l)}_{\bar{\varepsilon}_{l,P(i_k)+1}}(0)$, in the second $\phi_l(t_{i_k}) = \phi_l(\bar{\theta}_{l,j_{P(i_k)+1}}) = 0$. In the first case, the silence condition (4.18) with $i = P(i_k) + 1$ applies so that this case does not need a special treatment, in the second, we have the inequality $\bar{\varepsilon}_{l,P(i_k)+1} \geq U_l(\Theta_l)$ instead.

Specifying conditions on the phases at these ordered and clustered (simultaneous) spike reception times is equivalent to specifying the phases at the unordered and unclustered times because $\phi_l(\theta_{l,i}) = \phi_l(\theta_{l,j})$ if $\theta_{l,i} = \theta_{l,j}$.

If there are no simultaneous events, the strengths of coupling onto a particular neuron l, $\varepsilon_{ll'}$, $l' \in \{1, \ldots, N\}$, are restricted by $K(l)$ nonlinear equations and $M - K(l)$ inequalities originating from (4.17) and (4.18). All the coupling strengths in the network realizing a given pattern are thus restricted by a system of $\sum_{l=1}^{N} K(l) = M$ nonlinear equations and $\sum_{l=1}^{N}(M - K(l)) = (N-1)M$ inequalities.

We conclude that the constraints (equations and inequalities) restricting the coupling strengths of the network (to be consistent with a predefined pattern) *separate into disjoint constraints* for the couplings onto each individual neuron.

In the presence of simultaneous events, for each neuron there are $M_l - K(l) + S(l)$ inequalities originating from (4.19), (4.20) and (4.18), (where $S(l)$ is the number of supra-threshold excitations, not counting the ones where the spike is omitted) and $K(l) - S(l)$ equations originating from the spikings described by (4.17). We see that simultaneous receptions decrease the number of constraints. Again, these constraints separate. This property is due to the fact that the pattern is fixed; it turns out (see below) that because of this separation, it is easier to find a solution for the coupling strengths that satisfy these constraints.

Fig. 4.2 illustrates the constraints. After a firing of neuron l at time t_i where its phase is zero, conditions (4.17) and (4.18) impose restrictions on the phases at the spike reception times while the time evolution proceeds towards the subsequent firing time t_k of neuron l.

If we now compute explicitely the dynamics of neuron l between two successive firing times t_i and t_k and evaluate the dynamics at the times occurring in (4.17) and (4.18), we obtain

$$
\begin{aligned}
H^{(l)}_{\bar\varepsilon_{l,P(i)-1}}(\bar\theta_{l,j_{P(i)-1}} - t_i) &< \Theta_l - \Delta_{l,P(i)-1}\,,\\
H^{(l)}_{\bar\varepsilon_{l,P(i)-2}}(H^{(l)}_{\bar\varepsilon_{l,P(i)-1}}(\bar\theta_{l,j_{P(i)-1}} - t_i) + \Delta_{l,P(i)-1}) &< \Theta_l - \Delta_{l,P(i)-2}\,,\\
&\vdots\\
H^{(l)}_{\bar\varepsilon_{l,P(k)}}(...H^{(l)}_{\bar\varepsilon_{l,P(i)-2}}(H^{(l)}_{\bar\varepsilon_{l,P(i)-1}}(\bar\theta_{l,j_{P(i)-1}} - t_i)\\
+\Delta_{l,P(i)-1}) \ldots + \Delta_{l,P(k)-1}) &= \Theta_l - (t_k - \bar\theta_{l,j_{P(k)}})
\end{aligned}
\tag{4.21}
$$

in the case of no spike reception at time t_i and no supra-threshold excitation that generates the spike at t_k. Now we consider the case that there was a spike reception at time t_i. If a supra-threshold spike generated the spike time t_i from a phase $\phi_l(t_i^-) < \Theta_l$ and the intrinsic dynamics generates the spike at t_k, the set of equations and inequalities reads

$$
\begin{aligned}
H^{(l)}_{\bar\varepsilon_{l,P(i)-2}}(\Delta_{l,P(i)-1}) &< \Theta_l - \Delta_{l,P(i)-2}\,,\\
&\vdots\\
H^{(l)}_{\bar\varepsilon_{l,P(k)}}(...H^{(l)}_{\bar\varepsilon_{l,P(i)-2}}(\Delta_{l,P(i)-1}) \ldots + \Delta_{l,P(k)-1}) &= \Theta_l - (t_k - \bar\theta_{l,j_{P(k)}}).
\end{aligned}
\tag{4.22}
$$

Alternatively, at t_i, the threshold can be reached by the intrinsic dynamics $\phi_l(t_i^-) = \Theta_l$ although a spike is arriving. Here we have to consider two different cases: (i) $U_l(0) + \bar\varepsilon_{l,P(i)-1} < U_l(\Theta_l)$, i.e. the spike is subthreshold. This is just a special case of (4.21) with $\bar\theta_{l,j_{P(i)-1}} - t_i = 0$. (ii) $U_l(0) + \bar\varepsilon_{l,P(i)-1} \geq U_l(\Theta_l)$, i.e. the spike is supra-threshold. In this case, we fixed the convention that the second spike is omitted and the neuron is reset to zero; therefore system (4.22) is supplemented with the condition

$$
\bar\varepsilon_{l,P(i)-1} \geq U_l(\Theta_l) \tag{4.23}
$$

on $\bar\varepsilon_{l,P(i)-1}$.

The above equations also cover the case that a spike is received by neuron l at the spike time t_k when neuron l already reached Θ_l, i.e. $\bar\theta_{l,j_{P(k)-1}} = t_k$. However, also supra-threshold excitation can then be used to generate the spike t_k. Then, if no spike is received at t_i, or if a spike is received when the threshold is already reached and no supra-threshold excitation takes place, the couplings are restricted by (4.21) where the last equation has to be replaced by the inequalities

$$
\begin{aligned}
&H^{(l)}_{\bar\varepsilon_{l,P(k)}}(...H^{(l)}_{\bar\varepsilon_{l,P(i)-2}}(H^{(l)}_{\bar\varepsilon_{l,P(i)-1}}(\bar\theta_{l,j_{P(i)-1}} - t_i)\\
&\qquad +\Delta_{l,P(i)-1}) \ldots + \Delta_{l,P(k)-1}) < \Theta_l - (t_k - \bar\theta_{l,j_{P(k)}}),\\
&U_l(H^{(l)}_{\bar\varepsilon_{l,P(k)}}(...H^{(l)}_{\bar\varepsilon_{l,P(i)-2}}(H^{(l)}_{\bar\varepsilon_{l,P(i)-1}}(\bar\theta_{l,j_{P(i)-1}} - t_i)\\
&+\Delta_{l,P(i)-1}) \ldots + \Delta_{l,P(k)-1}) + \Delta_{l,P(k)}) + \bar\varepsilon_{l,P(k)+1} \geq U_l(\Theta_l).
\end{aligned}
\tag{4.24}
$$

If supra-threshold excitation occurred at time t_i and supra-threshold input generated the spike at t_k, the couplings are restricted by (4.22) (possibly completed by

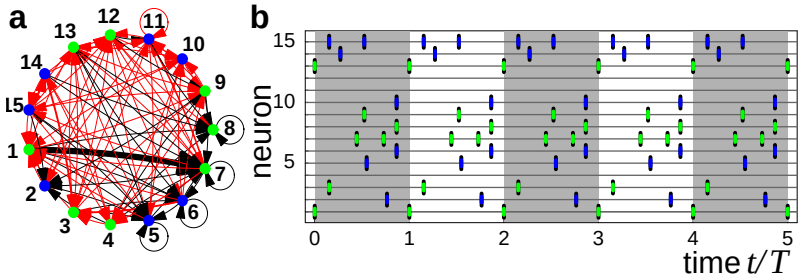

Figure 4.3: Complicated spike pattern in a small network ($N = 15$). (a) Network of eight integrate-and-fire neurons (green) and seven Mirollo-Strogatz biological oscillators (blue) with uniformly distributed thresholds $\Theta_l \in [0.5, 2.0]$ and delays $\tau_{ml} \in [0.1, 0.9]$ (further parameters see text). Each directed connection between any two neurons is randomly chosen to be present with probability $p = 0.6$. Connections are either excitatory (black) or inhibitory (red) (thicknesses proportional to coupling strengths). (b) The spiking dynamics (green and blue bars according to neuron type) of the network shown in (a) perfectly agrees with the predefined pattern (period $T = 1.3$) of precisely timed spikes (black bars underlying the colored ones). The pattern includes several simultaneous spikes. Three neurons, $l \in \{4, 11, 12\}$, are switched off (non-spiking).

(4.23)), where the last equation has to be replaced by the inequalities

$$\begin{aligned} H^{(l)}_{\bar{\varepsilon}_{l,P(k)}}(...H^{(l)}_{\bar{\varepsilon}_{l,P(i)-2}}(\Delta_{l,P(i)-1}) \\ \ldots + \Delta_{l,P(k)-1}) < \Theta_l - (t_k - \bar{\theta}_{l,j_{P(k)}}), \\ U_l(H^{(l)}_{\bar{\varepsilon}_{l,P(k)}}(...H^{(l)}_{\bar{\varepsilon}_{l,P(i)-2}}(\Delta_{l,P(i)-1}) \\ \ldots + \Delta_{l,P(k)-1}) + \Delta_{l,P(k)}) + \bar{\varepsilon}_{l,P(k)+1} \geq U_l(\Theta_l). \end{aligned} \tag{4.25}$$

We have thus shown:

Theorem 5: The set of solutions to the systems (4.21)–(4.25) for all $K(l)$ pairs of subsequent firing times (t_i, t_k), where $i = i_n$, $k = i_{n+1}$, $n \in \{1, \ldots, K(l)\}$, provides the set of all admissible coupling strengths $\varepsilon_{ll'}$, $l' \in \{1, \ldots, N\}$, of incoming connections to neuron l. Solutions to systems analogous to (4.21)–(4.25) for all neurons $l \in \{1, \ldots, N\}$ define all coupling strengths of an admissible network.

Roughly speaking, in the absence of supra-threshold excitation, the time of each spike of each neuron provides one "hard" (equality) constraint on the in general N-dimensional set of input coupling strengths of that neuron. The silence conditions provide "soft" (inequality) constraints, often not lowering the dimensionality of the solution space of coupling strengths. Intuitively a hard restriction can be understood by considering a simple example: Consider a network of $N = 3$ neurons. If one neuron m receives two spikes in a fixed time interval in which it does not send a spike itself, the coupling strengths of these spikes are arbitrary as long as

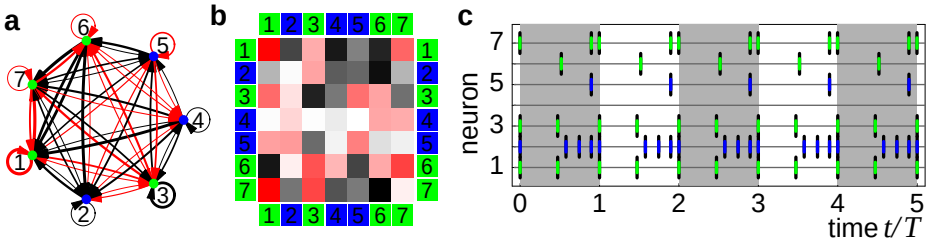

Figure 4.4: Spike pattern in a small network ($N = 7$) randomly chosen from a subset of the admissible networks. (a,b) Network of four leaky integrate-and-fire neurons (green) and three Mirollo-Strogatz biological oscillators (blue) in graph and matrix representation. Thresholds and delays are uniformly distributed in $\Theta_l \in [0.5, 1.5]$ and $\tau_{ml} \in [0.1, 0.9]$ (further details see text). (c) The spiking dynamics (green and blue bars according to neuron type) of the network shown in (a) and (b) perfectly agrees with the predefined pattern of period $T = 1.3$ (black bars).

their *total impact* on the neuron's phase ϕ_m (advancing or retarding) is the same, cf. also Fig. 4.2. This provides one, and not two, hard restrictions to the set of input coupling strengths to neuron m.

There are patterns for which the systems (4.21)–(4.25), with predefined neuron properties and predefined delay distribution, do not have a solution. This means that if the delays and neural parameters are specified, no network, independent of how the coupling strengths are chosen, exhibits that predefined pattern. This can already be observed from a simple example: consider a non-degenerate pattern where neuron l sends three successive spikes and between each two successive of these spike times there is precisely one spike received, each sent by the same neuron m. Then, the coupling strength ε_{lm} is fixed (by the firing time condition to which (4.21) reduces) to ensure the correct time of the second spike of neuron l and cannot be modified to ensure the third one. So, if the interval between the second and third spike time does not by coincidence match the one determined by the input, the pattern will not be realizable by any network. Other, more complicated examples follow immediately. This implies that certain predefined patterns may not be realizable in any network, no matter how its neurons are interconnected. We note that if we allow the neural parameters and delay times to vary as well, the system again might have a solution.

In the case of leaky integrate-and-fire neurons or Mirollo-Strogatz biological oscillators, a solution of (4.21)–(4.25), if one exists, can be found in a simple way, because the system is then reducible to be linear in the coupling strengths or polynomial in its exponentials, respectively. Instances for solutions of the equations and inequalities describing the set of admissible networks can then be found by standard methods as e.g. implemented in recent computer algebra programs.[2] We

[2] To specify a single solution, we gave an additional function to be optimized, some wiring cost function, and proceeded as described in sec. 4.12. We use the software MATHEMATICA 5, Wolfram

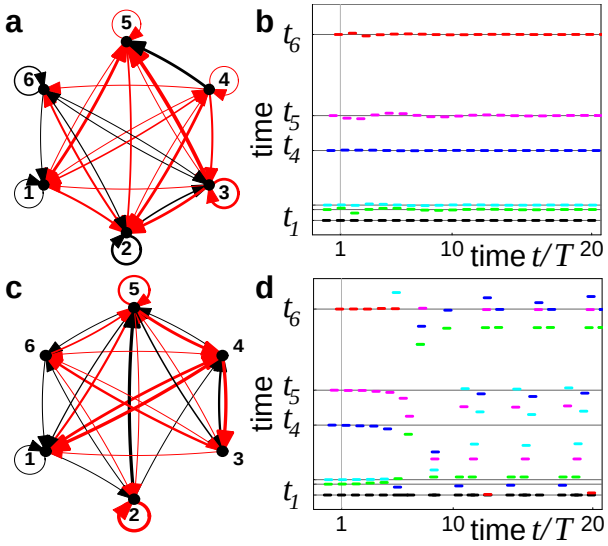

Figure 4.5: Two different networks (a), (c) realize the same predefined pattern ((b), (d) grey lines) [132]. The networks consist of six identical leaky integrate-and-fire neurons with $I_m = 1.2$, $\gamma_m = 1$, $\Theta_m = 1$. In one network realization the pattern is stable, in the other it is unstable. Further comments see text.

will therefore concentrate on these two neuron types for our explicit examples.

Examples for complex networks realizing predefined patterns are given in Figs. 4.3, 4.4. In Figs. 4.3, 4.4, the parameters of the leaky integrate-and-fire neurons are uniformly distributed within $\gamma_m \in (0.5, 1.5)$, $I_m = (1.08, 2.08)$. (If $\gamma_m = 1$ and $I_m = e/(e-1) \approx 1.58$ as well as $\Theta_m = 1$ then $\Theta_{U,m} = 1$.) The parameters b_m of the Mirollo-Strogatz biological oscillators are uniformly distributed within $b_m \in (0.7, 1.5)$, then a_m is chosen according to a uniform distribution within $a_m \in (1/(e^{b_m} - 1) - 0.1, 1/(e^{b_m} - 1) + 0.1)$. Connections are either excitatory (black) or inhibitory (red). Fig. 4.4 shows the network in graph (a) and matrix (b) representation. In (a) the line widths of the links, in (b) the color intensities are proportional to the coupling strengths. The network of Fig. 4.4 is a realization randomly drawn from those networks with couplings in the range $\varepsilon_{lm} \in (-1.5, 1.5)$ that exhibit the predefined pattern displayed in (c) (black bars underlying the colored ones). The pattern includes several simultaneous spikes. One neuron, $l = 4$, is silenced (non-spiking).

Often (4.21)–(4.25) are under-determined systems so that many solutions exist, implying that many different networks realize the same predefined pattern, cf. Fig. 4.5. The networks in Fig. 4.5 are realizations of random graphs where each

Research 2003 for the solution. Linear optimization problems are solved with linear programming methods; for polynomial problems, cylindrical algebraic decomposition is used.

coupling is present with probability $p = 0.8$; the coupling delay is $\tau_{ml} = 0.125$. A small random perturbation is applied at the beginning of the second period. The network dynamics (spike times relative to the spikes of neuron $l = 1$, color coded for each neuron), found by exact numerical integration (cf. sec. 3.3) shows that in network (a) the pattern is stable and thus regained after a few periods (b); in network (c) the pattern is unstable and eventually another pattern is assumed (d). We conclude that the stability properties of the pattern depend on the specific network it is realized in. Our method allows to store multiple patterns in one network. The network admissible for all pattern is given by the intersection of all sets of networks admissible for a single network, cf. Fig. 4.6. The maximal storage capacity for random patterns can be easily estimated from above. Each firing time yields one equation restriction on the coupling strengths. The number of possible firing times sampled over all firing patterns is bounded from above by the number of couplings that can be chosen freely, i.e. by N^2. Due to the presence of inequalities and the separation of restricting conditions for each neuron, also sets of spike patterns with a total of less firing times will often be incompatible so that no network realizing them exists.

4.9 Simple periodic pattern

In this section, we will show that an entire class of patterns can, under few weak requirements always be realized by a (typically multi-dimensional) family of networks and this family of networks can be analytically parameterized: The class of simple periodic patterns, in which every neuron fires exactly once before the pattern repeats [131].

For a simple periodic pattern, we label, without loss of generality, the neuron firing at time t_l by l, i.e. $s_l = l$ for $l \in \{1, ..., M = N\}$. Accordingly, we have $\theta_{l,m} = t_m + \tau_{lm}$. The time differences between two successive spike times of the same neuron equal the period of the simple periodic pattern. Thus, for each neuron l the reception times of spikes from all neurons of the network are guaranteed to lie between two successive firings of neuron l. We note again, that due to the periodicity of the pattern, we can assume without loss of generality that the delay times are smaller than the patterns period; otherwise, we take them modulo T without changing the invariant dynamics. In the following, we require that two simple criteria are met.

i) For each neuron its self-interaction delay is smaller than its free period, i.e. $\tau_{ll} < T_{0,l}$ for $l \in \{1, \ldots, N\}$.

This criterion ensures that the spike time of each neuron can be modified, at least by the self-coupling. If, as we assume throughout this chapter (see section 4.8), a neuron l firing only once in the period (here at t_l) receives at least one spike in the interval $(t_l, t_l + \Theta_l)$ (or, if $\Theta_l \geq T$ in $(t_l, t_l + T)$), this criterion is not necessary to hold for the existence of solutions. Indeed, solutions exist as stated below for any presynaptic neuron sending the spike modifying the spike time (with

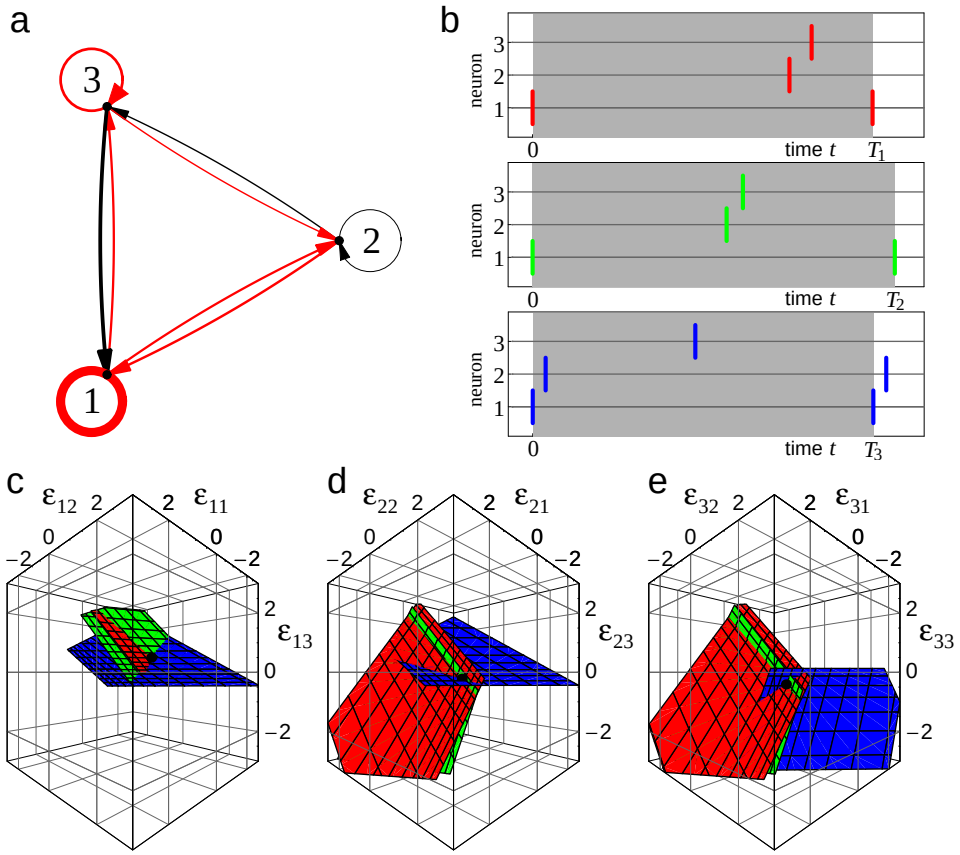

Figure 4.6: Network (a) realizing three different spike patterns (b). The network consists of three leaky integrate-and-fire neurons with $I_m = e/(e-1)$, $\gamma_m = 1$, $\Theta_m = 1$, I_m is chosen so that the free period $T_{0,l} = 1$ (large arrowhead omitted at self-coupling from neuron one to neuron one). Three different periodic patterns of spikes (b) are predefined. The sets of admissible networks for each of the pattern are displayed in coupling space in (c),(d),(e). The admissible set is colored like the corresponding pattern. The separation of constraints allows for each neuron l a separate presentation of the sets $\varepsilon_{l1}, \varepsilon_{l2}, \varepsilon_{l3}$ of incoming couplings satisfying (4.21)–(4.25). For leaky-integrate-and fire neurons the admissible sets are half-planes in the coupling space. The intersections of the planes give the actual coupling strength in the network realizing all three patterns as marked by the black ball.

the second criterion appropriately modified).

ii) The threshold minus a possible lower bound of the phase plus the self-interaction delay for each neuron l is larger than the pattern's period, $\Theta_l - B_l + \tau_{ll} > T$.

This second condition is obsolete if there is no finite lower bound of the phase, as e.g. for leaky integrate-and-fire neurons.

Given these weak constraints, the following statement holds.

Theorem 6: For simple periodic patterns, if conditions (i) and (ii) are satisfied, solutions to (4.21) exist and the set of admissible networks contains an $N(N-1)$ dimensional submanifold of the space of coupling strengths. This means that all simple periodic patterns are typically realizable by a high-dimensional family of networks. The set of all networks satisfying the systems (4.21-4.25) can be explicitly parameterized.

Proof: We first show that one solution exists, then show another statement, which explicitly shows that the solution space contains an $N(N-1)$-dimensional submanifold. We explicitly construct a trivial solution, where only self-interaction is present, while all the other coupling strengths are zero. We consider the one neuron system consisting of neuron l. Because of $\phi_l(t_l) = 0$ and condition (i) at the reception time of the spike from neuron l to itself, $\phi_l((t_l + \tau_{ll})^-) = \tau_{ll}$ holds. At time $t_l + \tau_{ll}$ the neuron's phase is set to $\phi_l(t_l + \tau_{ll}) = \Theta_l - (T - \tau_{ll}) < \Theta_l$ by choosing the coupling strength $\varepsilon_{ll} = H^{(l)-1}_{\phi_l(t_l+\tau_{ll})}(\phi_l((t_l + \tau_{ll})^-))$. Here, $H^{(l)-1}_{\psi}(\phi) = U_l(\psi) - U_l(\phi)$ is the inverse of $H^{(l)}_{\varepsilon}(\phi)$ with respect to ε, which exists for any ψ and ϕ in the domain of U_l. Indeed, $0 \leq \phi_l((t_l + \tau_{ll})^-) < \Theta_l$ is in the domain of U_l as well as $\phi_l(t_l + \tau_{ll})$. The latter is true, even if a lower bound is present, because $\phi_l(t_l + \tau_{ll}) = \Theta_l - (T - \tau_{ll}) > B_l$ due to condition (ii). Now, since no further spike is received, the condition Eq. (4.17) for the spike sending time is satisfied and the next spiking will take place at $t_l + T$. Since there are no further spike receptions there are no silence conditions (4.18) to be satisfied. All neurons taken together as a network without couplings between different neurons the pattern is invariant. We now set out to parameterize the entire nonempty class of solutions realizing the given pattern. Indeed, for simple periodic patterns this can be done analytically. The parameterization for each neuron $l \in \{1, \ldots, N\}$ is given as follows: (i) in the case $\theta_{l,j} \neq t_l$ for all $j \in \{1, ..., N\}$,

$$\begin{aligned}
\bar{\varepsilon}_{l,P(l)-1} &= H^{(l)-1}_{\phi_l(\bar{\theta}_{l,j_{P(l)-1}})}(\bar{\theta}_{l,j_{P(l)-1}} - t_l), \\
\bar{\varepsilon}_{l,P(l)-k} &= H^{(l)-1}_{\phi_l(\bar{\theta}_{l,j_{P(l)-k}})}(\phi_l(\bar{\theta}_{l,j_{P(l)-k-1}}) + \Delta_{l,P(l)-k-1}), \\
\bar{\varepsilon}_{l,P(l)} &= H^{(l)-1}_{\Theta_l-(t_l-\bar{\theta}_{l,j_{P(l)}})}(\phi_l(\bar{\theta}_{l,j_{P(l)-1}}) + \Delta_{l,P(l)-1}),
\end{aligned} \tag{4.26}$$

where $k \in \{2, ..., M_l - 1\}$ and the neurons' phases $\phi_l(\bar{\theta}_{l,j_i})$, $i \in \{1, ..., M_l\} \backslash \{P_l(l)\}$ at the spike reception times are the parameters that are subject to the restrictions (4.18). These equations also hold with $\bar{\theta}_{l,j_{P(l)-1}} - t_l = 0$ if there is a spike reception

at t_l but no supra-threshold excitation. (ii) If there is a spike reception at t_l, neuron l already reaches threshold due to its intrinsic dynamics $\phi_l(t_l^-) = \Theta_l$, and there is supra-threshold excitation immediately after the reset, we have

$$\begin{aligned}
\bar{\varepsilon}_{l,P(l)-1} \geq & U_l(\Theta_l) - U_l(0), \\
\bar{\varepsilon}_{l,P(l)-2} = & H^{(l)-1}_{\phi_l(\bar{\theta}_{l,j_{P(l)-2}})}(\bar{\theta}_{l,j_{P(l)-2}} - t_l), \\
\bar{\varepsilon}_{l,P(l)-k} = & H^{(l)-1}_{\phi_l(\bar{\theta}_{l,j_{P(l)-k}})}(\phi_l(\bar{\theta}_{l,j_{P(l)-k-1}}) + \Delta_{l,P(l)-k-1}), \\
\bar{\varepsilon}_{l,P(l)} = & H^{(l)-1}_{\Theta_l-(t_l-\bar{\theta}_{l,j_{P(l)}})}(\phi_l(\bar{\theta}_{l,j_{P(l)-1}}) + \Delta_{l,P(l)-1}),
\end{aligned} \tag{4.27}$$

where $k \in \{3, ..., M_l - 1\}$. The parameters are the neurons' phases $\phi_l(\bar{\theta}_{l,j_i})$, $i \in \{1, ..., M_l\} \backslash \{P_l(l), P_l(l) + 1\}$ at the spike reception times that are subject to the restrictions (4.18) and $\bar{\varepsilon}_{l,P(l)-1}$ which is bounded below by $\bar{\varepsilon}_{l,P(l)-1} \geq U_l(\Theta_l)$. (iii) If there is a spike reception at $\theta_{l,j} = t_l$, and the spike at t_l is generated by supra-threshold excitation:

$$\begin{aligned}
\bar{\varepsilon}_{l,P(l)-2} = & H^{(l)-1}_{\phi_l(\bar{\theta}_{l,j_{P(l)-2}})}(\bar{\theta}_{l,j_{P(l)-2}} - t_l), \\
\bar{\varepsilon}_{l,P(l)-k} = & H^{(l)-1}_{\phi_l(\bar{\theta}_{l,j_{P(l)-k}})}(\phi_l(\bar{\theta}_{l,j_{P(l)-k-1}}) + \Delta_{l,P(l)-k-1}), \\
\bar{\varepsilon}_{l,P(l)-1} \geq & U_l(\Theta_l) - U_l(\phi_l(\bar{\theta}_{l,j_{P(l)}}) + \Delta_{l,P(l)}),
\end{aligned} \tag{4.28}$$

where $k \in \{3, ..., M_l\}$. Here the parameters are the neurons' phases $\phi_l(\bar{\theta}_{l,j_i})$, $i \in \{1, ..., M_l\} \backslash \{P_l(l) + 1\}$ at the spike reception times that are subject to the restrictions (4.18), (4.19) and $\bar{\varepsilon}_{l,P(l)-1}$, which is not parameterized but only bounded below by a function of $\phi_l(\bar{\theta}_{l,j_{P(l)}})$ unless we require that the spike precisely excites the neuron to the threshold, i.e. the "=" in the last equation is valid. These relations follow directly from (4.21-4.25) by inversion and (4.17-4.19). Since the $\bar{\varepsilon}_{l,i}$ are disjoint sums of couplings ε_{lj} , the couplings towards neuron l can be parameterized using the parameters for $\bar{\varepsilon}_{l,i}$ and $p(l, j_i) - 1$ independent couplings per reception time $\bar{\theta}_{l,j_i}$. We now demonstrate that a $N(N-1)$-dimensional submanifold is contained in the set of solutions. In case (i) above, the Jacobian of the couplings with respect to the phases can be directly seen to have full rank $M_l - 1$. Therefore, parameterization (4.26) gives an $M_l - 1$-dimensional submanifold of the M_l-dimensional space of $\bar{\varepsilon}_{l,i}$. Since the $\bar{\varepsilon}_{l,i}$ are just disjoint sums of couplings ε_{lj}, an $(N-1)$-dimensional submanifold of networks realizing the pattern exists in N-dimensional ε_{lj}-space, $j \in \{1, \ldots, N\}$, l fixed. We further know that the trivial solution of uncoupled neurons with self-interaction constructed above is contained in case (i). Therefore, the set of parameters subject to the restrictions (4.18) is nonempty. Since it is open, there is an $(N-1)$-dimensional open set parameterizing the submanifold. The product of these submanifolds of all couplings is an $N(N-1)$-dimensional submanifold which is contained in the set of solutions.

4.10 Implementing additional network features

As we have seen above, the systems of equations and inequalities (4.21)–(4.25) defining the set of admissible networks is often underdetermined. We can then require additional properties from the neurons and their interactions. So far we assumed that neurons and delays were given but arbitrary, but network coupling strengths, and therefore the connectivity, were not restricted. Now, we provide examples of how to require in advance additional features that are controlled by the coupling strengths. A connection from a neuron l to m can be absent (requiring the coupling strength $\varepsilon_{ml} = 0$), taken to be inhibitory ($\varepsilon_{ml} < 0$) or excitatory ($\varepsilon_{ml} > 0$) or to lie within an interval; in particular, we can specify inhibitory and excitatory subpopulations.

Additional features entail additional conditions on the phases at the spike reception times which can be exploited for network parameterization, as we here and in the subsequent section demonstrate for simple periodic patterns, where we employ the same conventions as in section 4.9.

(i) If the pattern is non-degenerate, *exclusion of self-interaction* is guaranteed by the conditions

$$\phi_l(\theta_{l,l}) = \tau_{ll} \tag{4.29}$$

if there is no spike-reception in (t_l, θ_l), and

$$\phi_l(\theta_{l,l}) - \phi_l(\theta_{l,\sigma(\sigma^{-1}(l)-1)}) = \Delta_{l,\sigma^{-1}(l)-1} \tag{4.30}$$

otherwise, typically reducing the dimension of the submanifold of possible networks by N.

(ii) Requiring purely inhibitory networks leads to the accessibility conditions

$$\phi_l(\bar{\theta}_{l,j_{P(l)-1}}) \leq \bar{\theta}_{l,j_{P(l)-1}} - t_l, \tag{4.31}$$

$$\phi_l(\bar{\theta}_{l,j_{i-1}}) - \phi_l(\bar{\theta}_{l,j_i}) \leq \Delta_{l,i}, \tag{4.32}$$

where $i \in \{1, ..., M_l\} \backslash \{P_l(l)\}$. Since $\phi_l(\bar{\theta}^-_{l,j_{P(l)-1}}) = \bar{\theta}_{l,j_{P(l)-1}} - t_l$, the first inequality is equivalent to $\phi_l(\bar{\theta}_{l,j_{P(l)-1}}) \leq \phi_l(\bar{\theta}^-_{l,j_{P(l)-1}})$. This guarantees $\bar{\varepsilon}_{l,P(l)-1} = H^{(l)-1}_{\phi_l(\bar{\theta}_{l,j_{P(l)-1}})}\left(\phi_l(\bar{\theta}^-_{l,j_{P(l)-1}})\right) = U_l(\phi_l(\bar{\theta}_{l,j_{P(l)-1}})) - U_l(\phi_l(\bar{\theta}^-_{l,j_{P(l)-1}})) \leq 0$, due to the monotonicity of U_l, so that the couplings summing up to $\bar{\varepsilon}_{l,P(l)-1}$ can be chosen to be inhibitory or zero. Analogously, the second inequality ensures $\phi_l(\bar{\theta}_{l,j_i}) \leq \phi_l(\bar{\theta}^-_{l,j_i})$. We note that (4.31) also covers the case of spikes received at time t_l. Since their action is inhibitory, no supra-threshold excitation can occur and (4.31) yields $\phi_l(t_l) = \phi_l(\bar{\theta}_{l,j_{P(l)-1}}) \leq \bar{\theta}_{l,j_{P(l)-1}} - t_l = 0$. To parameterize all networks we can therefore successively choose $\phi_l(\bar{\theta}_{l,j_{P(l)-m}})$, $m \in \{1, ..., M_l - 1\}$, starting with $m = 1$. Inequalities (4.31) and (4.32) hold with reversed relations for *purely excitatory coupling* if no supra-threshold excitation occurs. Otherwise, they have to be replaced by

$$\phi_l(\bar{\theta}_{l,j_{P(l)-2}}) \geq \bar{\theta}_{l,j_{P(l)-2}} - t_l, \tag{4.33}$$

$$\phi_l(\bar{\theta}_{l,j_{i-1}}) - \phi_l(\bar{\theta}_{l,j_i}) \geq \Delta_{l,i}, \tag{4.34}$$

where $i \in \{1, ..., M_l\} \backslash \{P_l(l), P_l(l)+1\}$. An additional condition at time $t_l = \bar{\theta}_{l,j_{P(l)-1}}$ is not necessary, since the condition that the spike has a supra-threshold action already ensures the excitatory coupling. In general, purely inhibitory realizations can exist if the minimal inter-spike-interval of each single neuron l is larger than the neuron's free period, i.e.

$$\min\left\{t_{i_{k+1}} - t_{i_k} | k \in \{1, ..., K(l)\}\right\} \geq \Theta_l, \tag{4.35}$$

for all $l \in \{1, ..., N\}$, where the index $k+1$ has to be reduced to $\{1, ..., K(l)\}$ subtracting a suitable multiple of $K(l)$. If (4.35) is not satisfied, for some k, $\phi_l(t^-_{i_{k+1}}) = \Theta_l$ is not reachable from $\phi_l(t_{i_k}) = 0$. For the same reason, purely excitatory realizations can exist if

$$\max\left\{t_{i_{k+1}} - t_{i_k} | k \in \{1, ..., K(l)\}\right\} \leq \Theta_l. \tag{4.36}$$

In the case of simple periodic patterns, for purely inhibitory coupling the inequalities (4.35) reduce to $T \geq \max_m \Theta_m$. If even

$$T > \max_m \Theta_m \tag{4.37}$$

holds, the trivial solution is purely inhibitory with couplings $\varepsilon_{ll} < 0$. Therefore, from the statements in sec. 4.5 and the corresponding proof, we conclude that there is a submanifold of purely inhibitory networks in the set of solutions. Analogously, if

$$T < \min_m \Theta_m, \tag{4.38}$$

there is a submanifold of purely excitatory networks in the set of solutions.

4.11 Network design on predefined connectivities

A particularly interesting special case of implementing additional network features is requiring the absence of certain connections. This just enters the restricting conditions (4.21-4.25) as simple additional equalities $\varepsilon_{ml} = 0$ specifying that there is no connection from l to m. By specifying absent connections we generally also specify which connections are *present* (except in cases where $\varepsilon_{ml} = 0$ by coincidence), i.e. the *connectivity* of the network. Though very simple to implement, specifying the absence of connections is thus a very powerful tool. Since the absence of each of the N^2 connections ε_{ml}, $m, l \in \{1, \ldots, N\}$, can be pre-specified independently, we can typically *specify in advance any arbitrary connectivity* of the network. A particular predefined pattern is of course not always realizable in such a network.

We illustrate this network design with predefined connectivities by a few examples (cf. [131]). The two small networks of Figure 4.5 are both networks with pre-specified absent links. Here we chose random networks of $N = 6$ neurons where each connection is present with probability $p = 0.8$. The figure displays two different networks that exhibit the same pattern. One network has been chosen so that the pattern is stable the other so that it is unstable. Interestingly, on the one hand the same pattern can be invariant in two different networks with similar statistics, on the other hand their stability properties depend on the details of the coupling configurations.

We also considered large networks by predefining exactly the presence or absence of each link according to very different degree distributions. We designed them, by varying the remaining (non-zero) coupling strengths, so that all network examples exhibit the same predefined simple-periodic pattern. Network design on specific connectivities is of course not restricted to the example cases presented here, because the sets of input coupling strengths can be specified independently from each other.

For illustration, we present four large networks of $N = 1000$ neurons realizing the same predefined periodic pattern of spikes. For simplicity, we took for all networks the in-degree equal to the out-degree for each neuron. A random degree sequence was drawn from the given degree distribution (see below) and the degrees assigned to the neurons. The networks were then generated using a Monte-Carlo method similar to those discussed in Ref. [135].

Approximately 50% of the neurons are of integrate-and-fire type, the remaining are Mirollo-Strogatz biological oscillators. The parameters of the leaky integrate-and-fire neurons are randomly chosen within $I_m \in (1.08, 2.08)$, $\gamma_m \in (0.5, 1.5)$, the parameters b_m of the Mirollo-Strogatz biological oscillators are randomly chosen in $b_m \in (0.9, 1.2)$, then $a_m \in (1/(e^{b_m} - 1) - 0.1, 1/(e^{b_m} - 1) + 0.1)$. The thresholds of both neuron types are uniformly distributed within the interval $\Theta_l \in (0.8, 1.2)$. The delay distribution is heterogeneous, delays are uniformly distributed in the interval $\tau_{lm} \in (0.1, 0.3)$, $l, m \in \{1, ..., N\}$.

Two network examples (Figs. 4.7,4.8) have random connectivity with different exponential degree distributions

$$p(k) \propto e^{-\alpha k} \tag{4.39}$$

where k is the neuron degree. The other two networks (Figs. 4.9,4.10) have power-law degree distribution, according to

$$p(k) \propto k^{-\gamma} \tag{4.40}$$

For both distributions, we fixed a lower bound on the degree $k_c = 6$ so that each neuron has $k \geq k_c$ input and output connections. For networks of both distributions, we realized one with purely inhibitory coupling strengths (Figs. 4.7,4.9) and one with mixed inhibitory and excitatory coupling strengths (Figs. 4.8,4.10).

All network examples are constructed to realize the same predefined spike pattern with period $T = 1.5$. The numerical simulations (Figs. 4.7-4.10c, green or

blue bars for spiking integrate-and-fire neurons or Mirollo-Strogatz biological oscillators) agree perfectly with the predefined pattern (Figs. 4.7-4.10c, underlying black bars).

Due to the simplicity of imposing absence of links, the same method can be applied to a wide variety of network connectivities. In particular, a connectivity can be randomly drawn from any kind of degree distribution; a connectivity can also be structured (e.g. correlated degrees) and one may want to implement a very detailed specific form of it, e.g., as given by real data.

As noted above, however, not all networks can be designed for any pattern; in particular it is in general necessary to have sufficiently many incoming links to each neuron so that the interaction delay times and the input coupling strengths can account for the desired phase dynamics consistent with the predefined spike pattern.

4.12 Designing optimal networks

In section 4.8 we derived analytical constraints specifying the set of all networks that exhibit a predefined pattern and found that often there is a multi-dimensional family of solutions in the space of networks (as defined by all coupling strengths). In the previous section we exploited this freedom to design networks the connectivity of which is specified in detail. We may also exploit the freedom of choosing a solution among many possibilities by optimizing certain network properties.

Can we design networks that optimize certain structural features and at the same time exhibit a predefined pattern dynamics? This question is a very general one and it can be addressed by considering a variety of features of neuroscientific or mathematical interest. To briefly illustrate the idea, we here focus on optimizing convex 'cost' functions of the coupling strengths ε_{lm} and look for those networks among the admissible ones that minimize wiring costs.

Even for this very specific problem there are a number of different approaches we can take. For instance, we can consider networks with the same type of interactions, inhibitory or excitatory, or allow for a mixture of both, or optimize for different features of the connectivity. For simplicity, we here consider small networks whose neurons are exclusively of integrate-and-fire type and allow for a mixture of inhibitory and excitatory coupling. Integrate-and-fire neurons have the advantage (for both analysis and optimization) that the constraints (4.21)–(4.25) are linear.

The most straightforward goal for optimizing wiring costs is to minimize the quadratic cost function

$$G(\varepsilon) := \sum_{l=1}^{N} \sum_{m=1}^{N} \varepsilon_{lm}^2 \,, \tag{4.41}$$

A similar approach has already been successfully used when minimizing wiring costs of biological neural networks based on anatomical and physical constraints but neglecting dynamics issues, see, e.g. [42]. When minimizing the Euclidian

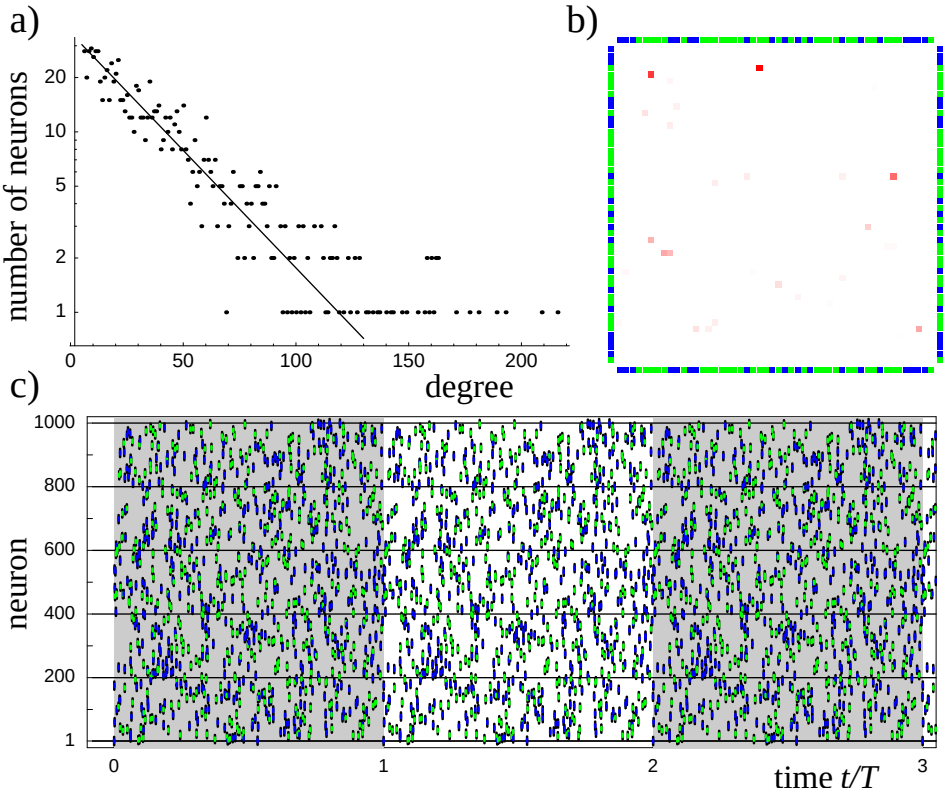

Figure 4.7: Network design with given connectivity. Predefined pattern in a network ($N = 1000$) with exponential degree distribution (panel (a), $\alpha = 0.03$) and purely inhibitory coupling. Panel (b) displays the sub-matrix of coupling strengths between the first 50 neurons. Inhibitory couplings are red, excitatory couplings are gray. The intensity of the color is proportional to the coupling strength. Due to too faint color, some very weak couplings are invisible in the plot. The frame shows integrate-and-fire neurons in green and Mirollo-Strogatz biological oscillators in blue. (c) The numerical simulations of the designed networks (green and blue bars for integrate-and-fire neurons and Mirollo-Strogatz biological oscillators) show perfect agreement with the predefined pattern (black bars).

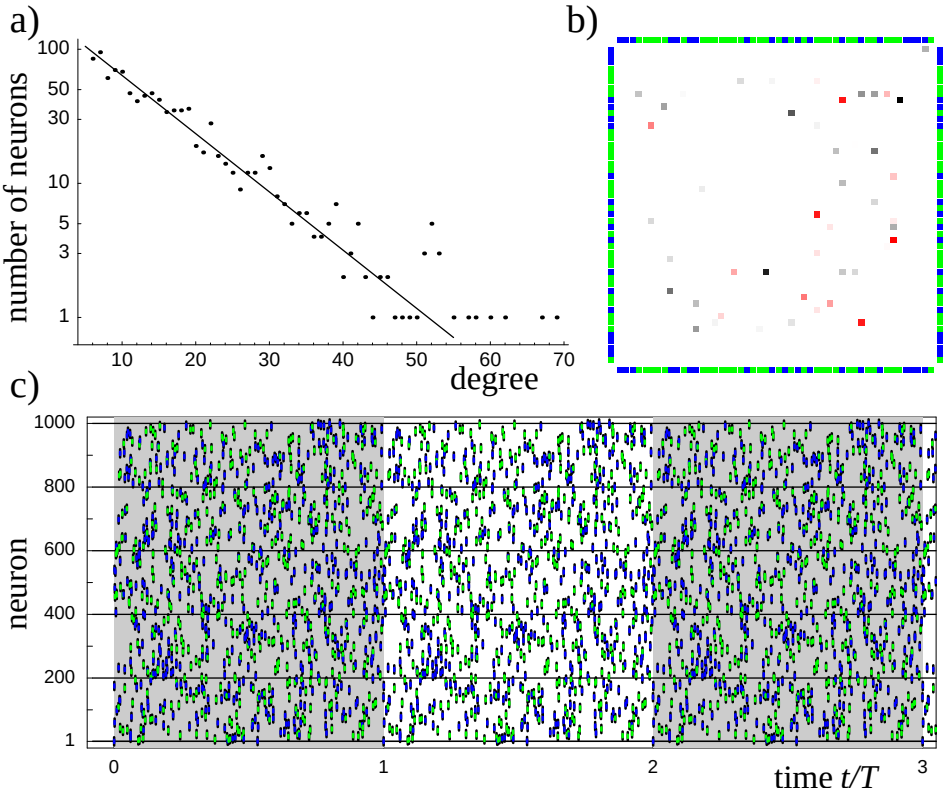

Figure 4.8: Network design with given connectivity. Predefined pattern in a network ($N = 1000$) with exponential degree distribution (panel (a), $\alpha = 0.1$) and mixed inhibitory and excitatory coupling. Other panels as in Figure 4.7.

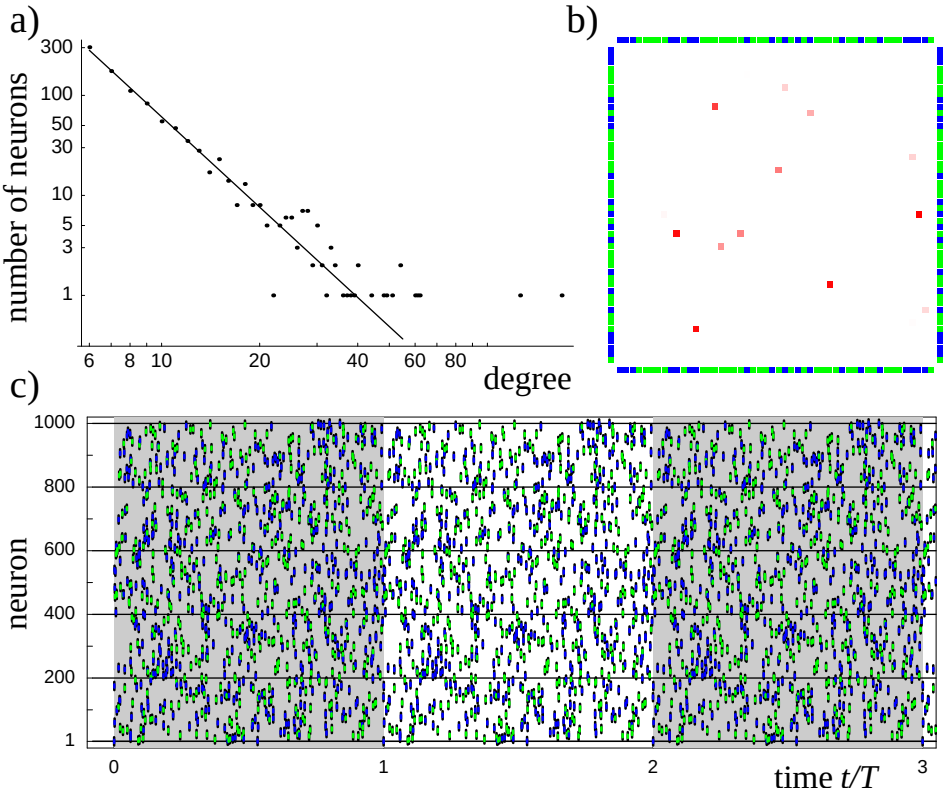

Figure 4.9: Network design with given connectivity. Predefined pattern in a network ($N = 1000$) with power-law degree distribution (panel (a), $\gamma = 3.0$) and purely inhibitory coupling. Other panels as in Figure 4.7.

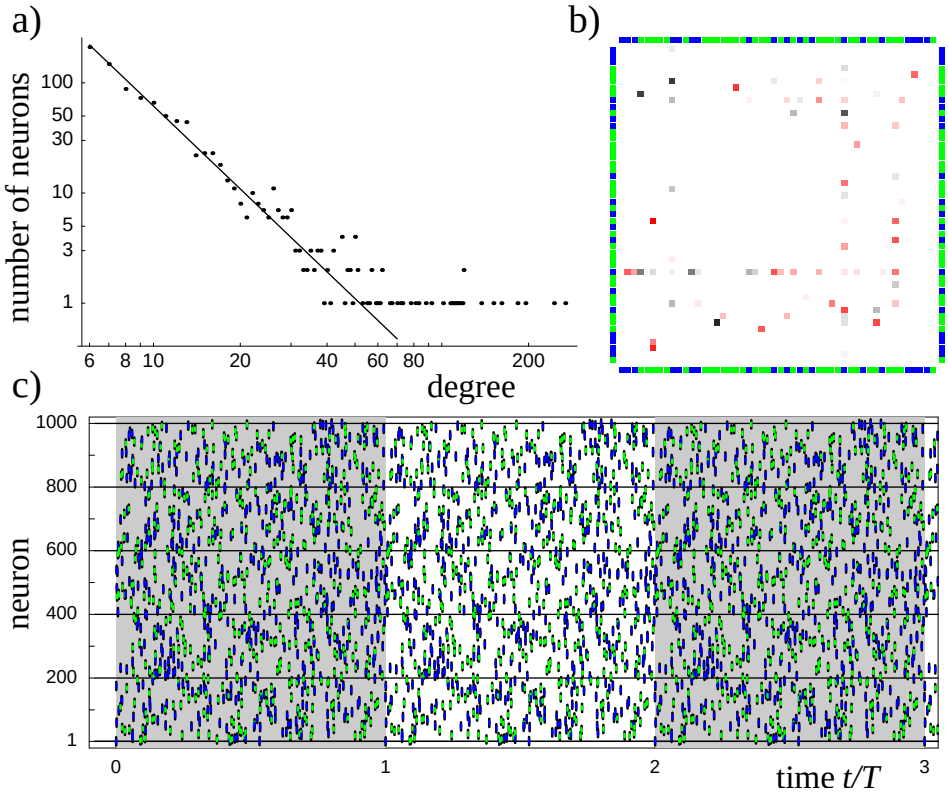

Figure 4.10: Network design with given connectivity. Predefined pattern in a network ($N = 1000$) with power-law degree distribution (panel (a), $\gamma = 2.5$) and mixed inhibitory and excitatory coupling. Other panels as in Figure 4.7.

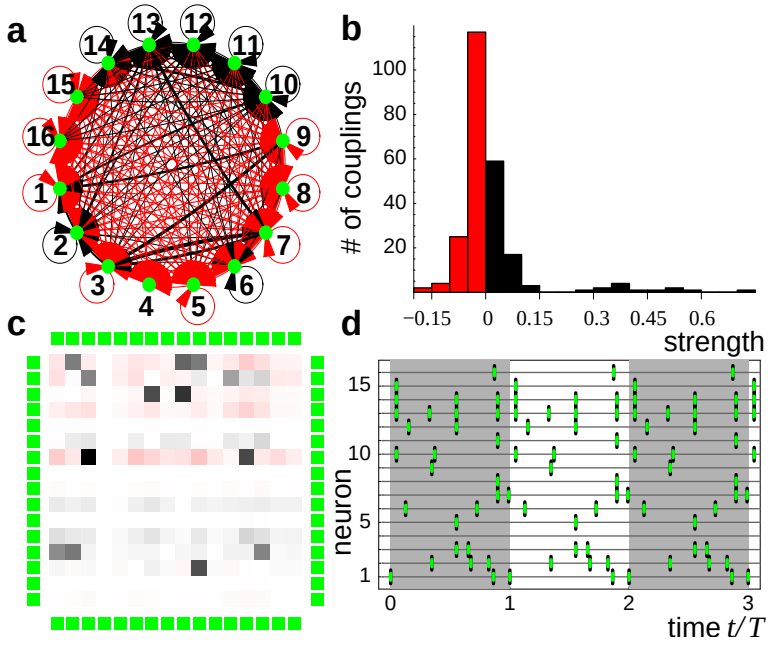

Figure 4.11: Network of leaky integrate-and-fire neurons that minimizes the wiring cost in Euclidean norm by minimizing (4.41). The parameters are randomly chosen within $I_m \in (1.0, 2.0)$, $\gamma_m \in (0.5, 1.5)$ and $\Theta_m \in (0.8, 1.2)$. The delays are uniformly distributed in $\tau_{lm} \in (0.1, 0.9)$, $l, m \in \{1, ..., N = 16\}$. Panels (a) and (c) show the network and the coupling matrix ε_{lm}. Panel (b) shows the histogram of the strengths of existing connections in the network. The bin size is 0.05. Panel (d) displays the predefined spike pattern (black bars) that is accurately reproduced (green bars). In the optimal network every neuron is connected to every other except the silenced neuron $l = 4$. This neuron has no outgoing connections: Since it generates no spikes, outgoing connections would be superfluous and do not appear in the optimal network.

(L_2) norm $\sqrt{G(\varepsilon)}$ by minimizing (4.41) for each row vector $(\varepsilon_{l,m})_{m\in\{1,\ldots,N\}}$ of the coupling matrix, a solution is searched among the admissible ones that is closest to the origin in the space of networks (defined by the coupling strengths).

Figure 4.11 shows an example of such an optimization. The network is almost globally connected and shows moderate variation among the individual coupling strengths. The predefined pattern dynamics is exactly reproduced. Such a network, while optimizing the wiring cost according to (4.41) does not appear to have any special features apart from apparently homogeneous and relatively small coupling strengths.

It seems that nature often designs networks in a different way, possibly so that they serve a dynamical purpose especially well. In particular evolution has not optimized most biological neural networks in the above manner: they are not close to globally coupled.

An alternative goal for optimizing wiring costs is to minimize the cost function

$$G(\varepsilon) := \sum_{l=1}^{N}\sum_{m=1}^{N} |\varepsilon_{lm}|\,, \tag{4.42}$$

that is, the L_1-norm of each row vector of the coupling matrix. When minimizing the L_1-norm (4.42), as before, a solution is searched among the admissible ones that is closest to the origin in the space of networks, but this time 'close' is defined by the L_1 distance measure. Interestingly, under weak conditions on the linear equality constraints, an optimal solution (4.42), searched under these constraints only, has many entries ε_{lm} equal to zero, cf. [25]. Because we typically also have many inequalities which depend on details of the pattern dynamics and are therefore uncontrolled, we cannot guarantee the zero entries for the full optimization problem (defined by equalities and inequalities) here. However, our numerics suggests that the solution in fact gives a network with many links absent and the number of links present being typically of the order of number of *equality* constraints.

Thus a network optimized by minimizing the L_1-norm is sparse, see, e.g., Fig. 4.12. Moreover, compared to the optimal L_2-norm solution above, this network has more heterogeneous connection strengths. Given some type of dynamics, a sparse network possibly is what biological systems would optimize for. In biological neural networks for instance, creating an additional synapse would probably use more resources (energy, biological matter, space, time, etc.) than making an existing synapse stronger.

Sparseness might possibly also be optimized in biological neural networks where requirements are met enabling other specific, functionally relevant dynamics. In general, of course, this dynamics may or may not consist of spike patterns.

The optimization problem, (4.41) and (4.42) with constraints (4.21)–(4.25), does typically not have a true optimum.

If a pattern is predefined that has more than one reception times between two successive sending events of some neuron, there usually are strict inequalities among the constraints (4.21)–(4.25). Because the functions $H_\varepsilon^{(l)}$ in (4.21)–(4.25) are local

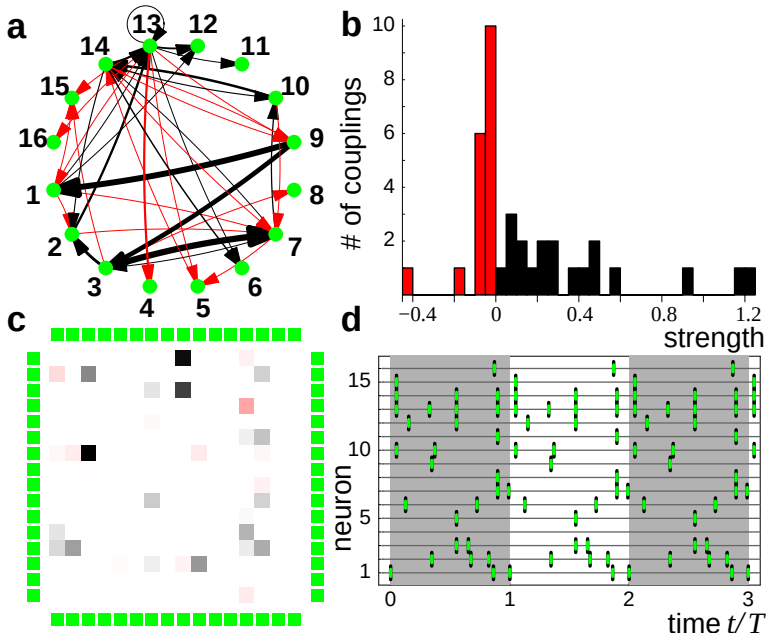

Figure 4.12: Network that minimizes the wiring cost in L_1-norm (4.42). The parameters are randomly chosen within $I_m \in (1.0, 2.0)$, $\gamma_m \in (0.5, 1.5)$ and $\Theta_m \in (0.8, 1.2)$. The delays are uniformly distributed in $\tau_{lm} \in (0.1, 0.9)$, $l, m \in \{1, ..., N = 16\}$. Panels (a) and (c) show the network and the coupling matrix ε_{lm}. Panel (b) shows the histogram of the strengths of existing connections in the network. The bin size is 0.05. Panel (d) displays the predefined spike patterns (black bars) that is accurately reproduced (green bars). The optimal network is very sparsely connected. In fact the network has one large strongly connected component, containing the neurons $\{1, 2, 3, 5, 7, 9, 10, 13, 14\}$, while the remaining neurons receive connections exclusively from this component and do not have any outgoing connections.

homeomorphisms (i.e. are continuous with local inverses that are continuous) the set of admissible coupling strengths is then not closed and thus does not contain its boundary.

During optimization, typically a solution is searched that is as close to such a boundary as possible. For instance, suppose one connection from m to l is inhibitory and its strength ε_{lm} is desired as small as possible. Then a solution is searched where the phase ϕ_l of the neuron l that receives a spike from m is so that the phase jump that spike induces is maximal (in absolute value) when ε_{lm} is held constant. This way a given desired phase jump would be achieved by a minimal coupling strength. Typically, the phase ϕ_l sought-after corresponds to a boundary of the set of admissible phases. For instance, if U_l is concave, an inhibitory spike has the largest possible effect on ϕ_l (largest phase jump) at $\phi_l = \Theta_l$. The corresponding phase constraint, however, may read $\phi_l < \Theta_l$. Thus the boundary phase and therefore also the boundary coupling strength cannot be assumed. As a consequence, the optimization problem has no true solution.

We fix this problem by imposing, instead of (4.21)–(4.25) and possible additional constraints with inequalities of the type $\phi_l > x$ or $\phi_l < y$, constraint sets that are closed, i.e. $\phi_l \geq x + \kappa$ or $\phi_l \leq y - \kappa$, where $\kappa > 0$, κ is a small cutoff (compared e.g. to the threshold). We fixed $\kappa = 0.001$ in the optimal design problems considered here.

4.13 Conclusion and outlook

For a general class of spiking neural network models we presented a method to determine the set of networks realizing a predefined, precisely timed periodic pattern of spikes.

In contrast to previous work on spiking neural networks which could construct one specific network realizing a simple periodic or a simple periodic and near synchronous pattern (cf. sec. 4.1), we analytically derived constraints on the coupling strengths defining the entire set of networks that give rise to an arbitrarily chosen periodic spike pattern. Our method is very general and covers networks of arbitrary size, with different types of neurons, heterogeneously distributed delays and thresholds, combinations of inhibitory and sub- and supra-threshold excitatory interactions as well as complicated stored patterns that include degenerate event times, multiple spiking of the same neuron within the pattern and silent neurons that never fire.

We have shown that there are patterns for which the set of admissible networks is empty. Once the features of individual neurons and all delays are fixed, this implies that these patterns cannot exist in any network, no matter how the neurons are interconnected. A predefined simple periodic pattern is particularly interesting because under weak assumptions, the constraint system has a solution for any such pattern. Thus, for any simple periodic pattern a realizing network is typically guaranteed to exist; we analytically parameterized all such networks and showed

that the set of admissible networks contains a $N(N-1)$-dimensional submanifold in the space of coupling strengths.

The class of networks giving rise to a particular spike pattern is typically high dimensional. This allows to further restrict the realizing network, for instance to predefine a detailed network connectivity (fixing the absence or presence of links between each pair of neurons). We illustrated the applicability of the method by examples of Erdös-Rényi and power-law random networks that were designed to exhibit the same spike pattern.

Another important new possibility is to design networks that exhibit a predefined dynamics and are at the same time optimized in some way. As a first example, we considered networks minimizing wiring cost. The connectivity of biological neural networks that exhibit precise spatio-temporal spiking dynamics is typically sparse. The work presented here suggests that this sparseness may result from an optimization process that takes into account dynamical aspects. If biological neural networks indeed optimize connectivity for dynamical purposes, our results may suggest that these networks minimize the total number of connections (rather than, e.g., their total strengths) and at the same time still realize specific spiking dynamics.

One important direction of future research concerns generalizations of the methods presented. Our method used the fact that the synaptic currents have infinitesimal temporal extent. This also implies that we have to employ neurons which oscillate on their own, otherwise they will only spike if they receive supra-threshold excitation and only few and degenerate spike patterns are possible. We already derived a generalization for temporally extended couplings valid in inhibitory networks of leaky integrate-and-fire neurons and employ it in sec. 6.7.

Other questions regard dynamical network topology. The presented method was an artificial network design method. Is it also possible to learn the patterns using established learning rules or algorithms? We already derived preliminary results in this direction. Biological neural networks undergo continued changes. Can the pattern dynamics be stabilized against these changes? This would require that the changing network follows a path or discrete steps within the set of admissible networks.

Also, the dynamical properties of the stored periodic patterns of spikes have to be investigated. Of particular importance are the stability properties. Are the patterns stable? Do they persist in a noisy environment? If a network that gives rise to a particular spike pattern is embedded in a larger network: Is the original pattern still detectable? We have seen, that for arbitrary networks, the stability of the pattern depends on the specific network realization (cf. Fig. 4.5). In the next chapter we will see that it is possible to analytically derive general statements about stability properties independent of the special pattern and the special network it is realized in.

Finally, our method suggest applications to biological neural networks. Indeed, for some biological neural networks such as the stomatogastric system of crustaceans [146], the entire coupling structure as well as the desired dynamics are

known. However, the neural dynamics is high dimensional, includes bursting and non-bursting neurons, electric and chemical coupling. Generalizing and partially redeveloping the derivation presented in the current chapter, we aim at determining the class of spiking neural networks that gives rise to the dynamics. A comparison with the neurobiological anatomy could reveal optimizing principles underlying network topology found in nature.

Chapter 5

Stability properties of periodic patterns

Is a pattern of spikes generated by a heterogeneous network stable or unstable? We numerically investigated patterns in a variety of networks and found that in general the stability properties depend on the details of the network it is realized in, see Fig. 4.5 for an illustration. Given a particular orbit, the linear stability properties can also be determined analytically, similar to the exact perturbation analyses for much simpler dynamics in more homogeneous networks [179, 180]. Depending on the network architecture, the same pattern can be exponentially stable or unstable, or exhibit oscillatory stable or unstable dynamics.

In this chapter we show that for large and important classes of networks general statements about the stability properties of periodic non-degenerate patterns of spikes (i.e. patterns where no simultaneous spikings and receivings occur, cf. sec. 4.4) are possible. In every network of neurons with congenerically curved rise functions and with purely inhibitory (or purely excitatory) coupling, a nonlinear stability analysis shows that the possible non-degenerate patterns are either *all* stable or *all* unstable. For instance, in purely inhibitory networks of neurons with rise functions of negative curvature, such as standard leaky integrate-and-fire neurons, Eq. (3.21) with $\gamma > 0$, every periodic non-degenerate spike pattern, no matter how complicated, is stable.

5.1 State of the art

For spiking neural networks, stability analyses have mostly been done in small systems with a few neurons [136, 197, 195] or for collective states, such as oscillatory and synchronous states [190, 195, 31, 30, 176] or the asynchronous state [2, 31, 79, 30, 196, 105]. Only a few studies assess the stability properties of the precise spiking dynamics in larger networks. The stability of a near-synchronous

precisely timed periodic pattern of spikes was shown in inhibitory networks with normal dissipation and in excitatory networks with anomalous dissipation in [50] (cf. also sec. 4.1). Reference [208] studies purely inhibitory networks of leaky integrate-and-fire neurons (normal dissipation) without delay. For homogeneous fully connected networks the stability of the 'splay state' [174], characterized by evenly spaced spike times of all network neurons, is analytically proven. Numerical investigations of weakly diluted networks show that although the dynamics may be irregular, its Lyapunov exponent is negative and the dynamics finally converges to a stable periodic orbit. Also, in globally coupled networks of leaky integrate-and-fire neurons without delay, any non-degenerate periodic of spikes has been shown to be stable [98]. (We note that in [98] each coupling may contain an excitatory component, but the inhibitory action has to dominate.) Finally, in [123], for a more general class of neuron models without delay (cf. also secs. 4.1, 4.2) it was shown that a stored simple periodic pattern of spikes is even a global attractor.

5.2 The model

We study complex networks of $N \geq 2$ neurons in Mirollo-Strogatz phase representation as introduced in sec. 3.2 and also considered in the previous chapter, cf. sec. 4.2. The neurons interact via directed delayed connections. To avoid technicalities that are not essential related to the stability properties of periodic orbits, we focus on homogeneous delays $\tau_{ij} = \tau$ for $i, j \in \{1, \ldots, N\}$. Inhomogeneous delays complicate in particular the indexing of spike patterns (cf. sec. 4.7) and the tracking of perturbations (cf. sec. 6.3). The state of a neuron $l \in \{1, \ldots, N\}$ at time $t \in \mathbb{R}$ is characterized by one variable $\phi_l(t) \in (B_l, \Theta_l]$, the phase of neuron l, that is piecewise linear in time. In addition, there are state variables $\sigma_l(t)$ that carry information about the sending times of spikes; these will be introduced below. The membrane potential of neuron l is computed from the phase by the strictly monotonic increasing rise function U_l as $U_l(\phi_l)$ (cf. sec. 3.2) which maps $(B_l, \Theta_l]$ bijectively onto $(B_{U,l}, \Theta_{U,l}]$, $B_{U,l} \in \mathbb{R}_- \cup \{-\infty\}$. We assume that for all neurons l in the network U_l is a C^1-diffeomorphism that is either strictly concave (normal dissipation) or strictly convex (anomalous dissipation). In secs. 5.9, 5.10 we study purely inhibitory networks with $\varepsilon_{ml} \leq 0$ and in secs. 5.11, 5.12 purely excitatory networks with $\varepsilon_{ml} \geq 0$ for all $m, l \in \{1, ..., N\}$. If there is no connection from neuron m to neuron l we have $\varepsilon_{ml} = 0$.

Together with U_m and U_m^{-1}, the transfer function $H_\varepsilon^{(m)}(\phi)$ is strictly monotonic increasing and differentiable both as a function of ε and of ϕ so that

$$(H_\varepsilon^{(m)})'(\phi) = \frac{U_m'(\phi)}{U_m'(U_m^{-1}(U_m(\phi) + \varepsilon))} = \frac{U_m'(\phi)}{U_m'(H_\varepsilon^{(m)}(\phi))} > 0, \tag{5.1}$$

$$\frac{\partial H_\varepsilon^{(m)}(\phi)}{\partial \varepsilon} = \frac{1}{U_m'(U_m^{-1}(U_m(\phi) + \varepsilon))} = \frac{1}{U_m'(H_\varepsilon^{(m)}(\phi))} > 0, \tag{5.2}$$

where $(H_\varepsilon^{(m)})'(\phi)$ denotes the derivative with respect to ϕ. This general scheme covers as special cases e.g. the leaky integrate-and-fire neuron with $\gamma > 0$ for normal dissipation, $\gamma < 0$ for anomalous dissipation and the biological oscillator model introduced by Mirollo and Strogatz [136] and generalized in sec. 3.4, with rise function $U_{\mathrm{MS}}(\phi) = b^{-1}\ln(1 + a^{-1}\phi)$, where $ab > 0$. U_{MS} is concave for $b > 0$ and convex for $b < 0$ (cf. sec. 3.4).

We assume that the spiking frequency of the neurons in the network is bounded above so that each neuron can only fire a limited amount of times within a time interval of the length of the delay time τ. Consequently, the number of spikes which have been sent before time t, but have not been received before time t, the number of *spikes in transit* at time t taken over the entire network, is bound above by some $N_{\mathsf{sp}} \in \mathbb{N}$, cf. [14].

Sending and receiving of spikes are the only events occurring in these systems. These events interrupt the continuous linear time evolution and constitute the only nonlinearities of the system. We here focus on the stability properties of periodic spike patterns with non-degenerate events, i.e. (i) all spikes are sent at non-identical times and (ii) are received at non-identical times and (iii) neurons receiving a spike do not generate a new spike at the same time. We now introduce the space of spike patterns of period $T \in \mathbb{R}_+$ containing $M \in \mathbb{N}$ spikes. Since each of the spikes can be sent by one neuron in the network, this space is naturally given by $[0,T)^M \times \{1,...,N\}^M$. (Different patterns in this space can be indistinguishable when generated by a network and are thus equivalent.) We assume that this space is endowed with a continuous probability density for choosing a pattern. Then, the chosen periodic spike pattern that is to be stored in a network will be non-degenerate with probability one. This in particular excludes spikes generated by supra-threshold excitation. Patterns including such spikes need to be studied separately (cf. ch. 4, [131]). Furthermore, for brevity of presentation, we exclude neurons that do not spike in the pattern.

We now define the phase space similar to [14]. The state of the system at time t is characterized by the phases of the neurons at time t, $\phi_l(t) \in (B_l, \Theta_l]$, $l \in \{1,\dots,N\}$ and the spikes sent by each neuron in the past. We number the firing times with respect to the order of their occurrence, t_i, $i \in \mathbb{Z}$, where $t_i < t_j$ for $i < j$ and denote the neuron firing the ith spike by s_i. The arrival time of the jth spike is denoted by

$$\theta_j = t_j + \tau. \tag{5.3}$$

In fact, not all firing times $t_i \leq t$ are necessary to characterize the state at time t but only those with $t - \tau < t_i \leq t$, i.e. the spikes in transit at time t. Since their number is bounded from above, the state space is finite dimensional. We introduce additional variables

$$\sigma_j(t) := t - t_j \tag{5.4}$$

within $[0,\infty)$ which track the time elapsed since the sending of the jth spike until its arrival [14]: When the spike is sent at time t_j,

$$\sigma_j(t_j) = 0, \tag{5.5}$$

for all $t_j < t < \theta_j$ and $t > \theta_j$, $\sigma_j(t)$ increases uniformly with unit derivative,

$$d\sigma_j/dt = 1. \tag{5.6}$$

In particular

$$\sigma_j(\theta_j^-) = \tau \tag{5.7}$$

holds just before spike arrival. At $t = t_j + \tau$,

$$\sigma_j(\theta_j) = \tau + 1, \tag{5.8}$$

i.e. the variable jumps about one. The original definition in [14] does not include such a jump. However, we will consider small perturbations, that are in maximum norm smaller than one. This definition of $\sigma_j(t)$ together with the definition of the norm in phase space ensures that trajectories in which the number of spikes in transit is different have large distance (at least one). If necessary, an arbitrarily large jump can be introduced.

We tag the index of the spike arriving first after t by

$$\kappa_0(t) = \min\{j|\theta_j - t > 0\} \tag{5.9}$$

and the index of the spike sent latest before t as

$$\kappa_1(t) = \max\{j|t - t_j \geq 0\}. \tag{5.10}$$

Then, $\kappa_1(t) - \kappa_0(t) + 1$ is the number of spikes in transit at t and if $\kappa_1(t) - \kappa_0(t) + 1 > 0$, $\kappa_0(t), \kappa_1(t)$ label the spikes in transit to arrive first and latest after t. The future of the system is therefore fully determined by the phases $\phi_1(t), ..., \phi_N(t)$ at time t and the spikes in transit described by $\sigma_{\kappa_1(t)}(t), ..., \sigma_{\kappa_0(t)}(t)$ together with the neurons $s_{\kappa_1(t)}, ..., s_{\kappa_0(t)}$ that sent them. From our assumption we have $\max_t(\kappa_1(t) - \kappa_0(t) + 1) \leq N_{\mathsf{sp}}$, therefore we can define:

The state of the system is given by the state space vectors

$$\begin{aligned} x(t) \quad := \quad & (\phi_1(t), ..., \phi_N(t), \sigma_{\kappa_1(t)}(t), ..., \sigma_{\kappa_1(t)-N_{\mathsf{sp}}+1}(t), \\ & s_{\kappa_1(t)}, ..., s_{\kappa_1(t)-N_{\mathsf{sp}}+1}) \end{aligned} \tag{5.11}$$

in the state space $\mathbb{X} = (B_1, \Theta_1] \times ... \times (B_N, \Theta_N] \times \mathbb{R}_{+,0}^{N_{\mathsf{sp}}} \times \{1, \ldots, N\}^{N_{\mathsf{sp}}}$ with the neurons' phases as first N entries, the times since each of the past N_{sp} spikes has been sent as entries $N+1, ..., N+N_{\mathsf{sp}}$ and the indices of the neurons which sent these spikes as entries $N + N_{\mathsf{sp}} + 1, ..., N + 2N_{\mathsf{sp}}$. We endow the state space with the maximum norm $||\,.\,||$, which is in particular also taken over the last N_{sp} entries. These last entries are the discrete indices of sending neurons. Deviations in the discrete indices generate differences between state space vectors of at least one. We will consider this as large perturbation and concentrate on small perturbations where the last N_{sp} sending neurons of the state space vectors are equal. If necessary, the norm can be given arbitrary large weight in the last N_{sp} so that a perturbation

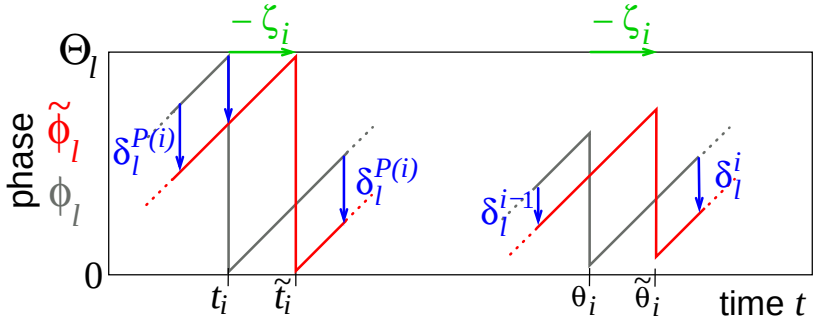

Figure 5.1: Sample spiking and receiving of neuron l. Neuron l sends the ith spike at time t_i and receives it at time $\theta_i = t_i + \tau$. In the perturbed dynamics (red), neuron l has perturbation $\delta_l^{P(i)}$ relative to the unperturbed dynamics (gray) before and after sending the spike. Due to $\delta_l^{P(i)} < 0$ and the free linear time evolution with slope one, the spike is sent about $-\zeta_i = -\delta_l^{P(i)}$ later than in the unperturbed case, at $\tilde{t}_i = t_i - \zeta_i$. It therefore also arrives about $-\zeta_i$ later than $\theta_i = t_i + \tau$, at $\tilde{\theta}_i = \theta_i - \zeta_i$. Due to the inhibitory coupling, neuron l's perturbation after the spike arrival is a weighted mean of the perturbation δ_l^{i-1} before the interaction and the spike's perturbation ζ_i, $\delta_l^i = c_{li}\delta_l^{i-1} + (1 - c_{li})\zeta_i$, where $0 < c_{li} < 1$, cf. Eqs. (5.51, 5.67).

in the spike sending neurons becomes arbitrarily large. The norm ensures together with Eq. (5.8) that states with small distance at time t have the same number and kind of spikes in transit: The senders of the last N_{sp} spikes have to be identical, otherwise the perturbation is large due to our definition of the phase space norm. If some spike has arrived in the one state and not yet arrived in the other state, the perturbation is large due to Eq. (5.8).

5.3 Notation

We now characterize the network dynamics underlying a non-degenerate periodic spike pattern and its perturbation.

First, we consider the *unperturbed dynamics* generating a non-degenerate periodic spike pattern of period T analogous to sec. 4.5. The periodicity of the pattern implies that also the phase dynamics is periodic with the same period (cf. sec. 4.6). Again, without loss of generality we can assume that the delay τ is smaller than T, otherwise we choose some sufficiently large integer multiple of T as new period of the pattern. The periodic spike pattern is characterized by the firing times $t_i \in [0, T)$, $i \in \{1, ..., M\}$ of the M spikes within the first period and the corresponding sending neurons s_i. Firing events in different periods are related by $t_i + nT = t_{i+nM}$ and $s_i = s_{i+nM}$, where $n \in \mathbb{Z}$. We further recall definition Eq. (4.14) of $P(i)$, the index

of the spike arriving last before the firing time t_i, for the case of non-degenerate patterns and homogeneous delay. For the current chapter, we slightly modify the definition since we are mainly interested in events with $t \geq 0$,

$$P(i) := \max(\kappa_0(0) - 1, \max\{j | t_i - \theta_j > 0\}). \tag{5.12}$$

This definition also applies if $\varepsilon_{is_{P(i)}}$ is zero.

We now consider another trajectory defined by the state at time $t = 0 \in (t_0, t_1)$ that we name *perturbed dynamics*. (Without loss of generality, we choose $t = 0$ to lie between t_0 and t_1.) $t = 0$ is chosen so that there is no event precisely at this time. We define the perturbed phases

$$\tilde{\phi}_l(t) := \phi_l(t) + \delta_l(t), \tag{5.13}$$

for $l \in \{1, \ldots, N\}$ by the phases $\tilde{\phi}_l(0)$. The phase perturbations are $\delta_l(t)$. Further, we denote the perturbed spike variables

$$\tilde{\sigma}_j(t) := \sigma_j(t) + \zeta_j(t), \tag{5.14}$$

where the spike perturbations are $\zeta_j(t)$. The state at time $t = 0$ is completed by specifying $\tilde{\sigma}_j(0)$ for $j \in \{\kappa_1(0) - N_{\mathsf{sp}} + 1, ..., \kappa_1(0)\}$ and by the corresponding sending spikes. We want to study the future evolution of trajectories close to each other at some point of time. So, the state of the perturbed dynamics should have small distance to the unperturbed dynamics at time $t = 0$. Changes in the last N_{sp} discrete variables would imply large distances in the maximum norm on state space. Indeed, the perturbed dynamics should be interpretable as generated by applying a small perturbation to all phases and to all spikes in transit at time $t = 0$. (Perturbations to already arrived spikes still present in $x(t)$ do not influence the future time evolution and can thus be specified arbitrarily.) Changes in the last N_{sp} variables, i.e. changes in the neurons that sent spikes, would be changes in the past and thus non-physical. We therefore consider perturbed trajectories where the neurons which sent the last N_{sp} spikes $j \in \{\kappa_1(0) - N_{\mathsf{sp}} + 1, ..., \kappa_1(0)\}$ are the same as in the unperturbed dynamics. To track the future evolution of the perturbations after $t = 0$ and to compare it to the unperturbed trajectory, we now introduce some additional concepts and notations. Together with the phases $\tilde{\phi}_l(t)$ and spike-in-transit variables $\tilde{\sigma}_i(t)$, the firing times $\tilde{t}_i$ and the arrival times $\tilde{\theta}_i$ of the perturbed system are distinguished from the unperturbed ones by superscribing a tilde. Analogously, $\tilde{\kappa}_0(t), \tilde{\kappa}_1(t)$ denote the spikes in transit to arrive first and latest after t in the perturbed system. As long as the perturbations are small, they do not alter the order of events, so this notation is appropriate and we need not introduce an extra symbol for the neuron that sent the ith spike in the perturbed dynamics. The perturbed trajectory

$$\begin{aligned}\tilde{x}(t) :=& (\tilde{\phi}_1(t), ..., \tilde{\phi}_N(t), \tilde{\sigma}_{\tilde{\kappa}_1(t)}(t), ..., \tilde{\sigma}_{\tilde{\kappa}_1(t)-N_{\mathsf{sp}}+1}(t), \\ & s_{\tilde{\kappa}_1(t)}, ..., s_{\tilde{\kappa}_1(t)-N_{\mathsf{sp}}+1})\end{aligned} \tag{5.15}$$

for $t \geq 0$ evolves according to the network time evolution described in the model section.

Because the order of events stays unchanged for the future evolution from $t = 0$ as long as the perturbations remain small, it is convenient to work with reduced phase space vectors

$$y(t) := (\phi_1(t), ..., \phi_N(t), \sigma_{\kappa_1(t)}(t), ..., \sigma_{\kappa_1(t)-N_{\mathsf{sp}}+1}(t)), \tag{5.16}$$

where the unchanged part, containing the indices of firing neurons, is left out. We collect the perturbations of reduced vectors at time t into the reduced perturbation vector

$$\begin{aligned} \delta(t) \quad = \quad & (\tilde{\phi}_1(t), ..., \tilde{\phi}_N(t), \tilde{\sigma}_{\tilde{\kappa}_1(t)}(t), ..., \tilde{\sigma}_{\tilde{\kappa}_1(t)-N_{\mathsf{sp}}+1}(t)) \\ & -(\phi_1(t), ..., \phi_N(t), \sigma_{\kappa_1(t)}(t), ..., \sigma_{\kappa_1(t)-N_{\mathsf{sp}}+1}(t)), \end{aligned} \tag{5.17}$$

and tag the minimal and maximal entries

$$\delta_{\max}(t) = \max(\delta(t)), \tag{5.18}$$

$$\delta_{\min}(t) = \min(\delta(t)). \tag{5.19}$$

It is of particular interest to consider unperturbed and perturbed trajectories with the same spikes in transit, where $\delta(t), \delta_{\max}(t), \delta_{\min}(t)$ are given by

$$\delta(t) = (\delta_1(t), ..., \delta_N(t), \zeta_{\kappa_1(t)}(t), ..., \zeta_{\kappa_1(t)-N_{\mathsf{sp}}+1}(t)), \tag{5.20}$$

$$\delta_{\max}(t) = \max\{\delta_1(t), ..., \delta_N(t), \zeta_{\kappa_1(t)}(t), ..., \zeta_{\kappa_1(t)-N_{\mathsf{sp}}+1}(t)\}, \tag{5.21}$$

$$\delta_{\min}(t) = \min\{\delta_1(t), ..., \delta_N(t), \zeta_{\kappa_1(t)}(t), ..., \zeta_{\kappa_1(t)-N_{\mathsf{sp}}+1}(t)\}. \tag{5.22}$$

In particular, the initial perturbation vector reads

$$\delta(0) = (\delta_1(0), ..., \delta_N(0), \zeta_{\kappa_1(0)}(0), ..., \zeta_{\kappa_1(0)-N_{\mathsf{sp}}+1}(0)). \tag{5.23}$$

The perturbations do not change in the intervals between events due to the piecewise linear time evolution. It is therefore convenient to introduce some notion of *event based perturbation* tracking for $i \geq \kappa_0(0) - 1$ and sufficiently small perturbations that leave the order of events unchanged.

We first define the perturbations of the spike variables $\zeta_i(t)$ for $i \geq \kappa_1(0) - N_{\mathsf{sp}} + 1$. We note that these definitions are extended to time points before $t = 0$, where the trajectories are not necessarily close to each other but the single events considered are already similar because the trajectories will be close at $t = 0$. Since the $\zeta_i(t)$ are constant except for time intervals between their receiving in the perturbed and the unperturbed dynamics, we define $\zeta_i := \zeta_i(t)$ for $t \in [\max(t_i, \tilde{t}_i), \infty) \backslash [\min(\theta_i, \tilde{\theta}_i), \max(\theta_i, \tilde{\theta}_i))$ and note that

$$\tilde{\theta}_i = \tilde{t}_i + \tau = \theta_i - \zeta_i, \tag{5.24}$$

holds.

We now consider $i \geq \kappa_0(0)$ and the perturbations of the phases $\delta_l(t)$. We denote the perturbation of neuron l's phase after the ith spike has arrived in both the perturbed and the unperturbed dynamics by

$$\delta_l^i = \tilde{\phi}_l(\max(\theta_i, \tilde{\theta}_i)) - \phi_l(\max(\theta_i, \tilde{\theta}_i)), \tag{5.25}$$

The spike which arrives last before $t = 0$ is the spike labeled with $\kappa_0(0) - 1$. We define

$$\delta_l^{\kappa_0(0)-1} := \delta_l(0). \tag{5.26}$$

The perturbation can change if neuron l sends or receives a spike. If neuron l sends a spike the perturbation is changed for the interval $[\min(t_j, \tilde{t}_j), \max(t_j, \tilde{t}_j))$ because the neuron is reset in one, e.g. the unperturbed, system, while it is not yet reset in the other, e.g. the perturbed, system. After it is reset in both systems the original perturbation is recovered. We conclude that except for intervals between unperturbed and perturbed spike sendings of neuron l, the perturbation δ_l^i remains constant and equals $\delta_l(t)$ until the next spike arrives, for $i \geq \kappa_0(0)$,

$$\begin{aligned}\delta_l^i = \delta_l(t) \text{ for } t \in \mathbb{R}_{+,0} \cap [&\max(\theta_i, \tilde{\theta}_i), \min(\theta_{i+1}, \tilde{\theta}_{i+1})) \\ &\setminus \bigcup_{j: t_j \in [\theta_i, \theta_{i+1}) \wedge s_j = l} [\min(t_j, \tilde{t}_j), \max(t_j, \tilde{t}_j)).\end{aligned} \tag{5.27}$$

For $i = \kappa_0(0) - 1$, θ_i and $\tilde{\theta}_i$ have to be replaced by 0. If some neuron s_i has perturbation $\delta_{s_i}^{P(i)}$, with $i > \kappa_1(0)$ before it fires at $t_i > 0$, the spike inherits this perturbation since

$$\tilde{t}_i = t_i - \delta_{s_i}^{P(i)}, \tag{5.28}$$

which implies that

$$\zeta_i = \delta_{s_i}^{P(i)}, \tag{5.29}$$

cf. Fig. 5.1. We note that this definition implies the minus sign before ζ_i.[1]

The event based perturbation vector δ^i and the extremal perturbations $\delta_{\max}^i, \delta_{\min}^i$ are taken directly after the arrival of ith spike in both the perturbed and the unperturbed dynamics, for $i \geq \kappa_0(0)$,

$$\delta^i = (\delta_1^i, ..., \delta_N^i, \zeta_{\kappa_1(\theta_i)}, ..., \zeta_{\kappa_1(\theta_i) - N_{\mathsf{sp}} + 1}), \tag{5.30}$$

$$\delta_{\max}^i = \max\{\delta_1^i, ..., \delta_N^i, \zeta_{\kappa_1(\theta_i)}, ..., \zeta_{\kappa_1(\theta_i) - N_{\mathsf{sp}} + 1}\}, \tag{5.31}$$

$$\delta_{\min}^i = \min\{\delta_1^i, ..., \delta_N^i, \zeta_{\kappa_1(\theta_i)}, ..., \zeta_{\kappa_1(\theta_i) - N_{\mathsf{sp}} + 1}\}. \tag{5.32}$$

We note that the event-based perturbation vector δ^i equals the time-based perturbation vector $\delta(t)$ in general only within the interval

$$\begin{aligned}\delta^i = \delta(t) \text{ for } t \in \mathbb{R}_{+,0} \cap [&\max(\theta_i, \tilde{\theta}_i), \\ &\min(\min\{t_{k'} | t_{k'} > \theta_i\}, \min\{\tilde{t}_{k'} | \tilde{t}_{k'} > \theta_i\}, \theta_{i+1}, \tilde{\theta}_{i+1})),\end{aligned} \tag{5.33}$$

[1] For our subsequent consideration ζ_i has to be defined as given in Eq. (5.29). If defined with a minus, '$\zeta_i = -\delta_{s_i}^{P(i)}$, complications arise e.g. from maximal perturbations in the phases that are transformed into minimal perturbations in the spikes.

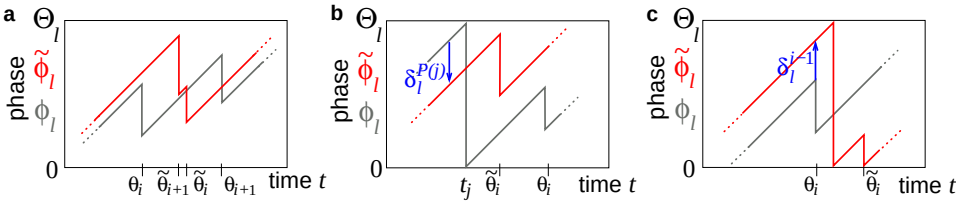

Figure 5.2: Perturbations that cause the event order to change for purely inhibitory networks. Sample time evolution of neuron l's phase shown for the perturbed (red) and the unperturbed dynamics (gray). a) The order of two arrival times θ_i, θ_{i+1} is not preserved in the perturbed dynamics, i.e. $\tilde{\theta}_i \geq \tilde{\theta}_{i+1}$, if $\zeta_{i+1} - \zeta_i \geq \theta_{i+1} - \theta_i$, cf. Eq. (5.34). b) A spike sending at t_j is passed by an early spike arrival $\tilde{\theta}_i$ if $-(\delta_l^{i-1} - \zeta_i) \geq \theta_i - t_j$, where $i = P(j)+1$, cf. Eq. (5.35). c) An early spike sending occurs instead of some spike arrival θ_i, if the perturbed dynamics reaches the threshold before the spike arrives at $\tilde{\theta}_i$, i.e. if $\delta_l^{j-1} - \zeta_j \geq \Theta_l - \phi(\theta_j^-)$, cf. Eq. (5.37).

because as soon as spikes have been newly sent, the spike variables are changed. For $i = \kappa_0(0) - 1$ an analogous expression ($\theta_i, \tilde{\theta}_i$ replaced by 0) holds. Equality of the phase perturbations holds up to the next spike arrival, cf. Eq. (5.27).

5.4 Estimating the order preserving neighborhood

We will now concentrate on purely inhibitory and purely excitatory networks and determine the maximal perturbations of phases and spikes in transit so that the perturbed dynamics keeps the same order of events as the unperturbed dynamics. In other words, we determine the maximal perturbations of phases and spikes in transit so that the order of events is preserved whenever and to whatever neurons or spikes in transit they are applied. This is just half the minimal distance between possible events in the unperturbed dynamics. We concentrate on events after $t = 0$. There are only two types of events, spike arrivals and spike sendings. So, the order of events will change (or two events will overlap) for the first time in the dynamics due to a too early spike arrival or due to a too early spike sending. In both cases, the early event can happen instead of a spike arrival or instead of a spike sending event. To avoid these changes on the order of events, restrictions on the size of the perturbations are to be imposed. The strictest restrictions arise from avoiding changes in the order of *subsequent* events. If the order of any pair of subsequent events is conserved, also the order of every pair of events (not necessarily subsequent) is conserved. There are four possible violations of the order conservation:

i) a spike arrives where in the original order of events a different spike arrives,

ii) a spike arrives where in the original order of events a spike is sent,

iii) a spike is sent where in the original order of events a spike arrives,

iv) a spike is sent where in the original order of events a different spike is sent.

The first three cases are illustrated in Fig. 5.2 for an inhibitory network, in the fourth case the spikes of two different neurons interchange, besides it is analogous to the first case. To avoid the occurrence of case i) in subsequent arrivals, it is sufficient to ensure that the perturbations of spikes in transit are so small that $\tilde{\theta}_i < \tilde{\theta}_{i+1}$. Together with Eq. (5.24) this leads to the restriction

$$\zeta_{i+1} - \zeta_i < \theta_{i+1} - \theta_i \tag{5.34}$$

on the perturbations of spikes arriving at θ_i, θ_{i+1} for all i. As an example, we here note that conditions (5.34) imply that also exchanges of higher order are excluded, e.g. $\tilde{\theta}_{i+1} > \tilde{\theta}_i$ for all i implies that $\tilde{\theta}_{i+2} > \tilde{\theta}_i$ for all i, since $\tilde{\theta}_{i+2} > \tilde{\theta}_{i+1}$.

To avoid ii), the perturbed spike times and the perturbed subsequently arriving spikes must satisfy $\tilde{t}_j < \tilde{\theta}_{P(j)+1}$. This implies together with Eqs. (5.28, 5.24) that the perturbation of the neuron's phase $\delta_l^{P(j)}$ before spiking and the perturbation of the spike arriving at $\theta_{P(j)+1}$ have to obey

$$\zeta_{P(j)+1} - \delta_l^{P(j)} < \theta_{P(j)+1} - t_j. \tag{5.35}$$

Case iii) leads to different restrictions for purely inhibitory and purely excitatory networks. For purely inhibitory networks, the perturbed trajectory must not reach the threshold before the spike arrives due to the intrinsic increase of the phase with time. If we first do not include a reset due to the possible reaching of the threshold, the perturbed phase of neuron l just before the arrival time $\tilde{\theta}_j$, of the perturbed spike is

$$\tilde{\phi}_l(\tilde{\theta}_j^-) = \phi_l(\theta_j^-) + \delta_l^{j-1} + \tilde{\theta}_j - \theta_j \tag{5.36}$$

because the phase increases with slope one. To indeed avoid passing the threshold, $\Theta_l > \phi_l(\theta_j^-) + \delta_l^{j-1} + \tilde{\theta}_j - \theta_j$ must hold, or, equivalently,

$$\delta_l^{j-1} - \zeta_j < \Theta_l - \phi_l(\theta_j^-). \tag{5.37}$$

For excitatory coupling, also supra-threshold excitation can take place and thus lead to an overlap of spike arrival and spike sending. Therefore, the phase may not have reached the minimal phase $U_l^{-1}(\Theta_{U,l} - \varepsilon)$ at which a supra-threshold excitation takes place when a spike with strength ε arrives. This is guaranteed by replacing Θ_l in Eq. (5.37) by $U_l^{-1}(\Theta_{U,l} - \varepsilon)$ which leads to the condition

$$\delta_l^{j-1} - \zeta_j \leq U_l^{-1}(\Theta_{U,l} - \varepsilon_{ls_j}) - \phi(\theta_j^-) \tag{5.38}$$

for the jth spike arrival.

Case iv), the change of the order of two spike sendings, can be inferred analogously to case i). Two subsequent spike times t_i, t_{i+1}, where $i > \kappa_1(0)$ sent by any

two neurons $k, l \in \{1, \ldots, N\}$ do not interchange their order if $\tilde{t}_i < \tilde{t}_{i+1}$, i.e. if the perturbations of the neurons phases $\delta_k^{P(i)}, \delta_l^{P(i+1)}$ before sending obey

$$\delta_l^{P(i+1)} - \delta_k^{P(i)} \leq t_{i+1} - t_i, \tag{5.39}$$

cf. Eq. (5.28).

There is yet another restriction to the perturbed dynamics. In networks with inhibition where the neurons have a lower bound for the potential, we have to ensure that also in the perturbed dynamics the inputs do not force the membrane potential below the lower bound, i.e.

$$U_l(\tilde{\phi}_l(\tilde{\theta}_j^-)) + \varepsilon_{ls_j} > B_{U,l}, \tag{5.40}$$

where $\varepsilon_{ls_j} < 0$, which yields using Eq. (5.36)

$$\zeta_j - \delta_l^{j-1} < \phi_l(\theta_j^-) - U_l^{-1}(B_{U,l} - \varepsilon_{ls_j}). \tag{5.41}$$

Taken together, Eqs. (5.34, 5.35, 5.37, 5.39, 5.41) imply for inhibitory networks that the order of events does not change and the dynamics does not fall below the lower threshold for a perturbation applied at any time t as long as $\|\delta(t)\| < d_{\max}^{\text{In}}$ with

$$\begin{aligned} d_{\max}^{\text{In}} =& \frac{1}{2} \min\{\min_{l,j}[\Theta_l - \phi_l(\theta_j^-)], \min_j(t_{j+1} - t_j), \min_j(\theta_{P(j)+1} - t_j), \\ & \min_{l,j}(\phi_l(\theta_j^-) - U_l^{-1}(B_{U,l} - \varepsilon_{ls_j}))\}, \end{aligned} \tag{5.42}$$

where $l = \{1, ..., N\}$, $j = \{1, ..., M\}$ and we used that $t_{j+1} - t_j = \theta_{j+1} - \theta_j$ due to the homogeneous delay. We note for many neurons models $B_{U,l} = -\infty$, so that no restrictions arise from taking $\min_{l,j}(\phi_l(\theta_j^-) - U_l^{-1}(B_{U,l} - \varepsilon_{ls_j}))$. For excitatory neurons, Eq. (5.37) has to be replaced by Eq. (5.38) and Eq. (5.41) can be omitted so that the order is guaranteed for $\|\delta(t)\| < d_{\max}^{\text{Ex}}$ where

$$\begin{aligned} d_{\max}^{\text{Ex}} =& \frac{1}{2} \min\{\min_{l,j}[U_l^{-1}(\Theta_{U,l} - \varepsilon_{ls_j}) - \phi_l(\theta_j^-)], \min_j(t_{j+1} - t_j), \\ & \min_j(\theta_{P(j)+1} - t_j)\}, \end{aligned} \tag{5.43}$$

We computed the size of the order preserving neighborhood for purely inhibitory and purely excitatory networks. However, the generalization for mixed networks is straightforward. In considerations applying to purely excitatory, purely inhibitory and to mixed networks, we write the upper bound of the order preserving neighborhood as $d_{\max}$. We note that (in contrast to irregular activity for infinite time, ch. 6) $d_{\max} > 0$ due to the requirement that the spike pattern is periodic and non-degenerate.

In the following, we consider perturbations smaller than $d_{\max}$ so that the order of events is preserved. In particular, we show below that for stable spike patterns

the open cubic neighborhood $||\delta(0)|| < d_{\max}$ of dimension $N + N_{\mathsf{sp}}$ is contained in the basin: Since $t = 0$ was arbitrary (without an event at this time), a trajectory reaching this neighborhood at any time will not leave it again and, for strongly connected networks, approach the periodic spike pattern. Thus, $d_{\max}$ yields a lower estimate of the linear extension of the basin in the reduced phase space. For unstable spike patterns, we will show that we can find arbitrarily small perturbations with $||\delta(0)|| < d_{\max}$ which grow and finally leave any d_1-neighborhood with $d_1 < d_{\max}$.

5.5 Propagation of the perturbation

We study how perturbations change when interactions take place under the condition that they are smaller than $d_{\max}$ before interaction.

We explicitly compute the perturbation δ_l^j of some neuron l after the reception of spike j, $j \geq \kappa_0(0)$ in terms of its perturbation δ_l^{j-1}, $|\delta_l^{j-1}| < d_{\max}$, before the reception and the perturbation ζ_j, $|\zeta_j| < d_{\max}$, of the spike times. For sufficiently small perturbations as considered below we have

$$\delta_l^i = \tilde{\phi}_l(\theta_i + |\zeta_i|) - \phi_l(\theta_i + |\zeta_i|) \tag{5.44}$$

because $\theta_i + |\zeta_i| \geq \max(\theta_i, \tilde{\theta}_i)$ and there is no event within $(\max(\theta_i, \tilde{\theta}_i), \theta_i + |\zeta_i|)$. We now evaluate the original and perturbed trajectories after this reception took place in both dynamics:

$$\begin{aligned}
\delta_l^j &= \tilde{\phi}_l(\theta_j + |\zeta_j|) - \phi_l(\theta_j + |\zeta_j|) && (5.45)\\
&= \tilde{\phi}_l(\tilde{\theta}_j) - \phi_l(\theta_j) + \zeta_j && (5.46)\\
&= H^l_{\varepsilon_{ls_j}}(\tilde{\phi}_l(\tilde{\theta}_j^-)) - H^l_{\varepsilon_{ls_j}}(\phi_l(\theta_j^-)) + \zeta_j && (5.47)\\
&= H^l_{\varepsilon_{ls_j}}(\phi_l(\theta_j^-) + \delta_l^{j-1} - \zeta_j) - H^l_{\varepsilon_{ls_j}}(\phi_l(\theta_j^-)) + \zeta_j && (5.48)\\
&= (H^l_{\varepsilon_{ls_j}})'(\phi_l(\theta_j^-) + \xi)(\delta_l^{j-1} - \zeta_j) + \zeta_j && (5.49)\\
&= c_{lj}(\delta_l^{j-1} - \zeta_j) + \zeta_j && (5.50)\\
&= c_{lj}\delta_l^{j-1} + (1 - c_{lj})\zeta_j, && (5.51)
\end{aligned}$$

where $\xi \in [\min(\delta_l^{j-1} - \zeta_j, 0), \max(\delta_l^{j-1} - \zeta_j, 0)]$ and

$$c_{lj} = (H^l_{\varepsilon_{ls_j}})'(\phi_l(\theta_j^-) + \xi). \tag{5.52}$$

The perturbations of spikes, ζ_j remain unchanged due to an interaction event. We note that c_{lj} depends not only on l, j but also on the perturbations, the spike pattern, and the interaction strength ε_{ls_j}.From (5.45) to (5.46), we use a case distinction for the absolute value, which yields together with $d\phi_l/dt = 1$ for the free evolution and $\tilde{\theta}_j = \theta_j - \zeta_j$, the subsequent Eq. (5.46) for both cases $\zeta_j \geq 0$

and $\zeta_j < 0$. The employed relations together with Eq. (5.27) also lead to $\tilde{\phi}_l(\tilde{\theta}_j^-) = \phi_l(\theta_j^-) + \delta_l^{j-1} - \zeta_j$ in (5.48). From (5.48) to (5.49) the intermediate value theorem is applied.

If $\varepsilon_{ls_j} = 0$, i.e. neuron l is not a postsynaptic neuron of neuron s_j, we have

$$c_{lj} = 1, \tag{5.53}$$

and the perturbation of neuron l's phase stays unchanged. Eq. (5.51) also directly implies that the perturbations do not change if they are all identical. This reflects the time translation invariance of the system.

5.6 Lyapunov stable spike patterns

We now formulate and prove a Theorem about the Lyapunov stability of periodic orbits in networks with arbitrary (i.e. not necessarily strongly connected) topology.

Theorem 1: Consider a network with arbitrary topology where $0 < (H_{\varepsilon_{lm}}^{(l)})'(\phi_l) \leq 1$ for all $l, m \in \{1, ..., N\}$, $\phi_l \in (B_l, \Theta_l]$. Then, any non-degenerate periodic pattern of spikes is Lyapunov stable. The event-based perturbations originating from an initial perturbation within the order preserving neighborhood, i.e. $||\delta(0)|| < d_{\max}$, are bounded by $||\delta(0)||$.

Proof: We show by induction that the event-based perturbation does not grow in time. We consider a trajectory within the order preserving neighborhood at time $t = 0$, i.e. $||\delta(0)|| < d_{\max}$. Our induction assumption is that the maximum-norm of the event-based perturbation δ^j does not exceed the maximum norm of the initial perturbation for $j \geq \kappa_0(0)$, i.e. for future evolution. Within time intervals between the same events in the perturbed and the unperturbed dynamics, the perturbation $\delta(t)$ will in general be larger. The assumption is fulfilled after the first spike arrival after zero: Just before the spike arrival at $\min(\theta_{\kappa_0(0)}, \tilde{\theta}_{\kappa_0(0)})$, the perturbation vector $\delta(\min(\theta_{\kappa_0(0)}, \tilde{\theta}_{\kappa_0(0)})^-)$, has phase perturbation entries $\delta_l(\min(\theta_{\kappa_0(0)}, \tilde{\theta}_{\kappa_0(0)})^-) = \delta_l(0) = \delta_l^{\kappa_0(0)-1}$. As spike perturbation entries it has the spike perturbation entries of $\delta(0)$ where perhaps some of the entries have been replaced by newly sent ones at possible sending times $t_1, t_2, ... < \theta_{\kappa_0(0)}$. According to Eq. (5.29), these new entries equal perturbations already present in the phase perturbations, so that in particular $||\delta(\min(\theta_{\kappa_0(0)}, \tilde{\theta}_{\kappa_0(0)})^-)|| \leq ||\delta(0)||$ holds. Application of Eq. (5.51) implies for the event-based perturbation after the arrival of the $\kappa_0(0)$th spike

$$\begin{aligned}
||\delta^{\kappa_0(0)}|| &= \max_{l,i}\{|\delta_l^{\kappa_0(0)}|, |\zeta_i|\} && (5.54)\\
&= \max_{l,i}\{|c_{l\kappa_0(0)}\delta_l^{\kappa_0(0)-1} + (1 - c_{l\kappa_0(0)})\zeta_{\kappa_0(0)}|, |\zeta_i|\} && (5.55)\\
&= \max_{l,i}\{|c_{l\kappa_0(0)}\delta_l(\min(\theta_{\kappa_0(0)}, \tilde{\theta}_{\kappa_0(0)})^-) \\
&\quad + (1 - c_{l\kappa_0(0)})\zeta_{\kappa_0(0)}|, |\zeta_i|\} && (5.56)
\end{aligned}$$

$$
\begin{aligned}
&\leq \max_{l,i}\{c_{l\kappa_0(0)}|\delta_l(\min(\theta_{\kappa_0(0)},\tilde{\theta}_{\kappa_0(0)})^-)| \\
&\quad + (1-c_{l\kappa_0(0)})|\zeta_{\kappa_0(0)}|,|\zeta_i|\} && (5.57)\\
&\leq \max_{l}\{c_{l\kappa_0(0)}||\delta(\min(\theta_{\kappa_0(0)},\tilde{\theta}_{\kappa_0(0)})^-|| \\
&\quad + (1-c_{l\kappa_0(0)})||\delta(\min(\theta_{\kappa_0(0)},\tilde{\theta}_{\kappa_0(0)})^-)||, \\
&\quad ||\delta(\min(\theta_{\kappa_0(0)},\tilde{\theta}_{\kappa_0(0)})^-)||\} && (5.58)\\
&= ||\delta(\min(\theta_{\kappa_0(0)},\tilde{\theta}_{\kappa_0(0)})^-|| && (5.59)\\
&\leq ||\delta(0)|| && (5.60)
\end{aligned}
$$

where the maximum is taken over the phase perturbations and the perturbations of the spikes in transit, $i \in \{\kappa_0(\theta_{\kappa_0(0)}),...,\kappa_1(\theta_{\kappa_0(0)})\}$ if $\kappa_0(\theta_{\kappa_0(0)}) \leq \kappa_1(\theta_{\kappa_0(0)})$. We used the triangle inequality for the absolute value and $0 < (H^l_{\varepsilon_{ls_{\kappa_0(0)}}})'(\phi_l) \leq 1$, thus $0 < c_{l\kappa_0(0)} \leq 1$, to derive (5.57) from (5.56). We now show that $||\delta^{j-1}|| < d_{\max}$ implies $||\delta^j|| \leq ||\delta^{j-1}||$ for $j > \kappa_0(0)$. Indeed, for any interaction, $0 < (H^l_{\varepsilon_{ls_j}})'(\phi_l) \leq 1$ and therefore $0 < c_{lj} \leq 1$. Similarly to the begin of induction, according to Eq. (5.51) this implies after the arrival of the jth spike,

$$
\begin{aligned}
||\delta^j|| &= \max_{l,i}\{|\delta^j_l|,|\zeta_i|\} && (5.61)\\
&\leq \max_{l,i}\{c_{lj}|\delta^{j-1}_l| + (1-c_{lj})|\zeta_j|,|\zeta_i|\} && (5.62)\\
&\leq \max_{l}\{c_{lj}||\delta^{j-1}|| + (1-c_{lj})||\delta^{j-1}||,||\delta^{j-1}||\} && (5.63)\\
&= ||\delta^{j-1}||, && (5.64)
\end{aligned}
$$

where the maximum is taken over the phase perturbations and the perturbations of the spikes in transit, $i \in \{\kappa_0(\theta_j),...,\kappa_1(\theta_j)\}$ if $\kappa_0(\theta_j) \leq \kappa_1(\theta_j)$. Therefore, $||\delta^j|| \leq ||\delta(0)|| < d_{\max}$ for all j. In particular, the perturbations of the spike timings do not grow larger than $||\delta(0)||$ and the spike pattern is Lyapunov stable according to the definition of Lyapunov stability, def. (i) in sec. 2.7, where we may apply the maximum norm since norms are equivalent in finite dimensional spaces [203]. To show this, in the following short paragraph, we use δ and ε without arguments and indices in the sense of sec. 2.7. We choose $\delta = \min(\eta, \varepsilon)$, then

$$
||\delta(0)|| < \delta. \tag{5.65}
$$

$t = 0$ was chosen arbitrarily so that no event occurred at this time, in particular the following holds for time origins with distance more than η from any event. We note that we do not need to choose the time origin 'far enough' from an event, because the definition of phase space already ensures that nearby trajectories have the same N_{sp} spikes sent and the same spikes in transit. According to Eqs. (5.29, 5.60, 5.64), differences between spike sending and arrival times after $t = 0$ equal phase perturbations bound from above by $||\delta(0)||$. Thus, the lengths of the intervals $[\max(\theta_i,\tilde{\theta}_i),\min(\theta_{i+1},\tilde{\theta}_{i+1}))$ and $[\min(t_j,\tilde{t}_j),\max(t_j,\tilde{t}_j))$ are bounded above

by $||\delta(0)|| < \delta$. Outside these intervals however, the perturbations are bound by $||\delta(0)|| < \delta$: Perturbations of phases equal event based perturbations outside these intervals (cf. Eq. 5.27) and perturbations of spikes equal previous event based perturbations of phases (cf. Eq. (5.29)). This implies that for $t > 0$ with distance more than δ from any event, i.e. $|t - t_i| > \delta$, for all $i \geq \kappa_0(0)$, and $|t - \theta_j| > \delta$, for all $j > \kappa_1(0)$, we have $||\delta(t)|| < \delta$. Due to $\eta \geq \delta$ and $\varepsilon \geq \delta$, also for all $t > 0$ with distance more than η from any event, $|t-t_i| > \eta$, for all $i \geq \kappa_0(0)$, and $|t-\theta_j| > \eta$, for all $j > \kappa_1(0)$, we have

$$||\delta(t)|| < \varepsilon \tag{5.66}$$

and thus Lyapunov stability in the sense of def. (i) in sec. 2.7.

5.7 Asymptotically stable spike patterns

We now prove a theorem stating that under certain sufficient conditions in networks that are strongly connected, almost all periodic orbits are asymptotically stable, i.e. sufficiently small perturbations to any non-degenerate periodic spike pattern decay to zero. For weakly but not strongly connected networks, this is in general not the case due to their inherent hierarchical structure [178].

Theorem 2: Consider a strongly connected network (with irreducible adjacency matrix) where $0 < (H^{(l)}_{\varepsilon_{lm}})'(\phi_l) < 1$ for all $l, m \in \{1, ..., N\}$ with $\varepsilon_{lm} \neq 0$, $\phi_l \in (B_l, \Theta_l]$. Then, any non-degenerate periodic pattern of spikes is asymptotically stable. Moreover, for initial states in the order preserving neighborhood of a periodic orbit, the dynamics converges to that orbit. In particular, a perturbed dynamics asymptotically decays to a dynamics identical to the original one up to a time shift, i.e. there is some $c_0 < ||\delta(0)||$, so that for almost (see proof) all t there is convergence with $n \to \infty$ of the phases $\tilde{\phi}_l(t + nT) - \phi_l(t + c_0 + nT) \to 0$ for $l \in 1, ..., N$ and of the spike variables $\tilde{\sigma}_{j+nM}(t + nT) - \sigma_{j+nM}(t + c_0 + nT) \to 0$ for $j \in \{\kappa_1(t) - N_{\mathsf{sp}} + 1, ..., \kappa_1(t)\}$.

Proof: We study the evolution of perturbations of phase and spike variables on an event by event basis. Since the perturbations are bound and the original orbit is periodic, the perturbed and unperturbed phases are bound, so that

$$0 < c_{\min} < c_{lj} < c_{\max} < 1 \tag{5.67}$$

holds, because $H'_\varepsilon(.)$ is continuous. Since Lyapunov stability follows from Theorem 1, it is sufficient to consider $j > \kappa_1(0)$ for the asymptotic stability. According to Eqs. (5.29, 5.51),

$$\delta_l^j = c_{lj}\delta_l^{j-1} + (1 - c_{lj})\delta_{s_j}^{P(j)}, \tag{5.68}$$

so that each interaction leads to evaluating some weighted mean of the perturbation of the sending neuron at the time of sending and the perturbation of the receiving neuron at the time of receiving. In particular, Eqs. (5.67, 5.68) imply that the perturbation of a neuron l postsynaptic to neuron s_j remains unchanged at the arrival of the jth spike only if $\delta_l^{j-1} = \delta_{s_j}^{P(j)}$, i.e. if its perturbation at the time of

receiving equals the perturbation of the sending presynaptic neuron at the time of sending the spike. Further, from Eqs. (5.53, 5.67, 5.68), we infer that a neuron l with perturbation $\delta_l^j < \delta_{\max}^j$ will have a perturbation smaller than $\delta_{\max}^j$ later on, i.e.

$$\delta_l^{j+n} < \delta_{\max}^j, \tag{5.69}$$

for all $n \in \mathbb{N}$.

If after the arrival of the jth spike, all neurons' phases $\phi_1, ..., \phi_N$ and all spikes in transit $\sigma_{\kappa_1(\theta_j)}, ..., \sigma_{\kappa_0(\theta_j)}$ possess identical perturbations, the perturbed dynamics is identical to the unperturbed one up to a time shift, so that the statement of Theorem 2 holds for identical perturbations.

From now on, we thus assume that at least one neuron's phase or spike in transit has non-maximal perturbation. We show that the *maximal perturbations decrease* and the *minimal perturbations increase* within at most $2N - 1 + M_{\mathsf{sp}}$ periods, where $M_{\mathsf{sp}} = \lceil N_{\mathsf{sp}}/M \rceil$ and $\lceil x \rceil$ denotes the smallest integer larger or equal to x. We study the decrease of the maximal perturbation in detail, the increase of the minimal perturbation follows analogously.

First, suppose that there is no neural phase $\phi_1, ..., \phi_N$ with maximal perturbation after the arrival of the jth spike, but the maximal perturbation is in the spike variables $\sigma_{\kappa_1(\theta_j)}, ..., \sigma_{\kappa_1(\theta_j)-N_{\mathsf{sp}}+1}$ only. The maximal perturbation will then decrease as soon as N_{sp} spikes have been sent because the neurons' phases do not reach maximal perturbation due to Eq. (5.69) and the newly sent spikes inherit the perturbations of the phases (Eq. (5.51)), while the original spikes carrying maximal perturbation have indices $i \leq \kappa_1(\theta_j)$ and therefore do not occur in the new perturbation vector anymore. We conclude that a maximal perturbation present in the spikes only will decrease after N_{sp} spike sendings. Since in each period, M spikes are sent, the perturbation decays after $M_{\mathsf{sp}} < 2N - 1 + M_{\mathsf{sp}}$ periods if the maximal perturbation is present in the spike variables only.

Therefore, we can assume that at least one phase has maximal perturbation and that there is at least one neuron's phase or one spike in transit that is non-maximally perturbed. At the latest after the arrival of the last spike in transit there will be a phase with non-maximal perturbation because of Eqs. (5.67, 5.68) and because the network is strongly connected, so that in particular every spike is received by at least one neuron. We consider an arbitrary neuron l which is maximally perturbed after the arrival of the jth spike. To allow it to still carry perturbation $\delta_{\max}^j$ after two periods, all its presynaptic neurons $\mathrm{Pre}(l)$ must have perturbation $\delta_{\max}^j$ at the beginning of the first period. Otherwise, they have smaller perturbation also later on, in particular when they emit at least one spike in the first period which arrives before the end of the second period due to $\tau < T$. These arriving spikes then have perturbation smaller than $\delta_{\max}^j$ and decrease the perturbation of neuron l on arrival. This implies that the neurons $\mathrm{Pre}(\mathrm{Pre}(l)) := \mathrm{Pre}^2(l)$ have a perturbation of $\delta_{\max}^j$ at the beginning of the first period to allow neuron l to conserve its maximal perturbation to the end of the fourth period. Otherwise, after at most two periods, there is a neuron in $\mathrm{Pre}(l)$ having non-maximal perturbation whose spikes cause the perturbation of neuron l to decrease within two further periods.

Since the network is strongly connected, there are no neurons with presynaptic distance to neuron l larger than $N-1$. Therefore, to ensure that neuron l keeps its maximal perturbation up to the end of the $2(N-1)$th period, all N neurons have to carry perturbation $\delta^j_{\max}$ after the arrival of the jth spike. To ensure this one more period, also all spikes in transit have to carry maximal perturbation. Otherwise, within one period they cause neurons to carry a perturbation smaller than $\delta^j_{\max}$ at the end of the first period, leading after $2(N-1)$ further periods to a decrease of neuron l's perturbation. This is in contradiction to the assumption that the phase perturbations and the perturbations of the spikes in transit do not all have identical entries after the arrival of the jth spike. Since l was an arbitrary neuron carrying maximal perturbation, we conclude that all phases have non-maximal perturbation after $2(N-1)+1 = 2N-1$ periods. After further N_{sp} spike sending events all the spike variables have been replaced and inherited some non-maximal perturbation. Each period T sees M spike sending events. We defined M_{sp} to be the smallest integer multiple of the patterns period so that at least N_{sp} spikes are sent within $M_{\mathsf{sp}}T$. Therefore the *maximum perturbation decreases* within $2N-1+M_{\mathsf{sp}}$ periods.

Arguments completely analogous to the ones above, based on averaging of perturbations and strong connectivity of the network, show that the *minimal perturbation increases* within $2N-1+M_{\mathsf{sp}}$ periods.

We now show that the event-based perturbation vector converges to a vector with identical entries. We study how the perturbations evolve within multiples of $2N-1+M_{\mathsf{sp}}$ periods. The number of arrival events within one period is M. We define

$$G_j : \delta^j \to \delta^{j+(2N-1+M_{\mathsf{sp}})M}, \tag{5.70}$$

which maps an actual event-based perturbation vector to the vector $2N-1+M_{\mathsf{sp}}$ periods later. We note that due to the periodicity of the spike pattern, G_j is M-periodic in the parameter j, $G_j = G_{j+nM}$, $n \in \mathbb{N}$, in particular we will use below that $G_{j+(n-1)(2N-1+M_S)M} \circ ... \circ G_{j+(2N-1+M_S)M} \circ G_j = G_j^n$. From Eq. (5.48) we see that for the step from some spike receiving $j'-1$ to the next receiving j', event-based perturbations of the neurons' phases $\delta_l^{j'}$, $l \in \{1, ..., N\}$, depend continuously on the previous perturbation vector, namely on the previous perturbations of phases $\delta_l^{j'-1}$ and on $\zeta_{j'}$. Further, during such a step, the possibly newly sent spikes inherit the previous perturbations of the sending neurons, in particular they depend continuously on them, while the perturbations of the other spike variables stay constant or are eliminated from the perturbation vector due to later spikes. Taken together, we conclude that the map $\delta^{j'-1} \to \delta^{j'}$ is continuous for any $j' \geq \kappa_0(t)$, and therefore also G_j, the composition $\delta^j \to \delta^{j+1} \to \delta^{j+2} ... \to \delta^{j+(2N-1+M_{\mathrm{sp}})M}$ of $(2N-1+M_{\mathrm{sp}})M$ such maps. The sequence $(\max[G_j^n(\delta^j)])_n$ is strictly monotonically decreasing, $(\min[G_j^n(\delta^j)])_n$ is strictly monotonically increasing, both are bounded above by $\delta^j_{\max}$ and bounded below by $\delta^j_{\min}$. Therefore, each is convergent, say

$$\max[G_j^n(\delta^j)] \to M_0, \text{ and } \min[G_j^n(\delta^j)] \to m_0. \tag{5.71}$$

Furthermore, $(G_j^n(\delta^j))_n$ is bound and therefore has a convergent subsequence, say

$$G_j^{n_m}(\delta^j) \to \hat{\delta}. \tag{5.72}$$

The maximum of $\hat{\delta}$ is

$$\max(\hat{\delta}) = \max[\lim_{m\to\infty} G_j^{n_m}(\delta^j)] = \lim_{m\to\infty}(\max[G_j^{n_m}(\delta^j)]) = M_0, \tag{5.73}$$

where we used that max(.) is continuous and that $(\max[G_j^{n_m}(\delta^j)])_m$ is a subsequence of the sequence $(\max[G_j^n(\delta^j)])_n$ which converges to M_0. Analogously, we compute the maximum of $G_j(\hat{\delta})$,

$$\begin{aligned}\max(G_j(\hat{\delta})) &= \max[G_j(\lim_{m\to\infty}(G_j^{n_m}(\delta^j)))] \\ &= \lim_{m\to\infty}(\max[G_j(G_j^{n_m}(\delta^j))]) \\ &= \lim_{m\to\infty}(\max[G_j^{n_m+1}(\delta^j)]) \\ &= M_0,\end{aligned} \tag{5.74}$$

where we used in the second step that $\max[G_j(.)]$ is continuous and in the third that $(\max[G_j^{n_m+1}(\delta^j)])_m$ is a subsequence of the convergent sequence $(\max[G_j^n(\delta^j)])_n$. We conclude from Eqs. (5.73, 5.74) that $\max(G_j(\hat{\delta})) = M_0 = \max(\hat{\delta})$. For any vector $\hat{\delta}$ with non-identical entries however, we know from the above considerations that $\max(G_j(\hat{\delta})) > \max(\hat{\delta})$ holds. So, $\hat{\delta}$ is a perturbation vector with $N + N_{\mathsf{sp}}$ identical entries,

$$\hat{\delta} = (c_0, ..., c_0), \tag{5.75}$$

where we defined $c_0 = M_0$. The same computation as above for the minimum entries reveals $\min(G_j(\hat{\delta})) = m_0 = \min(\hat{\delta})$ (with the same $\hat{\delta}$ as in (5.72)–(5.75)). Because $\hat{\delta}$ has identical entries, $\max(\hat{\delta}) = \min(\hat{\delta}) = c_0$. Now, from Theorem 1 we infer that $\max(\delta^{j+n(2N-1+M_S)M})$ and $\min(\delta^{j+n(2N-1+M_S)M})$ are upper and lower bound for the entries of $\delta^{j'}$ for all $j' \geq j + n(2N-1)M$. Since upper and lower bound converge towards the same value c_0, the sequence $(\delta^{j'})_{j'}$ converges,

$$\delta^{j'} \to \hat{\delta}. \tag{5.76}$$

This implies

$$\tilde{t}_{j'} \to t_{j'} - c_0 \tag{5.77}$$

$$\tilde{\theta}_{j'} \to \theta_{j'} - c_0 \tag{5.78}$$

due to Eqs. (5.24, 5.28, 5.29). Thus, the spiking dynamics converges towards a spiking dynamics equivalent to the original one, namely to the original spiking dynamics shifted in time by a constant value.

Indeed, also the perturbed phase dynamics approaches the original phase dynamics shifted in time by some $-c_0$ where $|c_0| < ||\delta(0)||$ due to Theorem 1. We first consider times t which do not lie between the arrivals of the same event in the perturbed and the unperturbed dynamics. The event-based perturbation vector $\delta^{j'}$ equals the time-based perturbation vector only within the interval given by Eq. 5.33. The newly sent spikes however inherit perturbations already present in $\delta^{j'}$ as phase perturbations due to Eq. (5.28). So, the perturbations $\delta(t)$ for

$$t \in [\max(\theta_{j'}, \tilde{\theta}_{j'}), \min(\theta_{j'+1}, \tilde{\theta}_{j'+1}))\backslash \bigcup_{j:t_j \in [\theta_{j'}, \theta_{j'+1})} [\min(t_j, \tilde{t}_j), \max(t_j, \tilde{t}_j)) \quad (5.79)$$

are bound above by $\delta^{j'}_{\max}$ and bound below by $\delta^{j'}_{\min}$. Therefore, if a sequence of times $(t(j))_j$ is chosen so that $t(j)$ lies within the set given by Eq. (5.79) between the jth and $j+1$th arrival,

$$\delta(t(j)) \to \hat{\delta}, \quad (5.80)$$

when $j \to \infty$. The perturbed phase dynamics approaches the shifted phases dynamics pointwise for almost all t in the sense that $\delta(t + nT) \to \hat{\delta}$ with $n \to \infty$ for almost all t: We take the dynamics shifted in time by $-c_0$ as reference and denote the dynamical quantities by a bar, i.e. $\bar{\phi}_l(t - c_0) = \phi_l(t)$ for the spike phases, $\bar{t}_i = t_i - c_0$ for the spike times, $\bar{\theta}_i = \theta_i - c_0$ for the arrival times and $\bar{\delta}(t)$ for the time and event-based perturbation of the perturbed dynamics relative to the shifted one. Consider times t which lie between events together in the unperturbed, in the perturbed and in the shifted dynamics,

$$\begin{aligned} t \in &[\max(\theta_{j'}, \tilde{\theta}_{j'}, \bar{\theta}_{j'}), \min(\theta_{j'+1}, \tilde{\theta}_{j'+1}, \bar{\theta}_{j'+1})) \\ &\backslash \bigcup_{j:t_j \in [\theta_{j'}, \theta_{j'+1})} [\min(t_j, \tilde{t}_j, \bar{t}_j), \max(t_j, \tilde{t}_j, \bar{t}_j)). \end{aligned} \quad (5.81)$$

For large enough j', these intervals are nonempty because of Eqs. (5.77, 5.78). If times $t(j')$ are chosen within the set between the j'th and $j'+1$th arrival, we have

$$\bar{\delta}(t(j')) = \delta(t(j')) - c_0, \quad (5.82)$$

and Eq. (5.80) yields

$$\bar{\delta}(t(j')) \to 0 \quad (5.83)$$

with $j' \to \infty$. The phase perturbations $\bar{\delta}_l(t)$, $l = 1, ..., N$, are however constant for all

$$\begin{aligned} t \in \bar{S}_{j'} = &[\max(\tilde{\theta}_{j'}, \bar{\theta}_{j'}), \min(\tilde{\theta}_{j'+1}, \bar{\theta}_{j'+1})) \\ &\backslash \bigcup_{j:t_j \in [\theta_{j'}, \theta_{j'+1})} [\min(\tilde{t}_j, \bar{t}_j), \max(\tilde{t}_j, \bar{t}_j)). \end{aligned} \quad (5.84)$$

Therefore, for $t(j')$ within the set $\bar{S}_{j'}$ between j'th and $j'+1$th arrival, we have

$$\bar{\delta}(t(j')) \to 0 \quad (5.85)$$

if $j' \to \infty$. Consider $t \neq \bar{t}_i \wedge t \neq \bar{\theta}_i$ for $i \in \mathbb{N}$, i.e. t is not at the time of a shifted event. Then there is some minimal distance $\eta = \min(\min\{|t - \bar{t}_i||i \in \mathbb{Z}\}, \min\{|t-\bar{\theta}_j||j \in \mathbb{Z}\})$ separating t from any shifted event. Due to the periodicity of the dynamics, also $t + nT$ has the same finite distance from any shifted event, $\min(\min\{|t+nT-\bar{t}_i||i, n \in \mathbb{Z}\}, \min\{|t+nT-\bar{\theta}_j||j, n \in \mathbb{Z}\}) = \eta$. Because the spike dynamics converges (Eqs. (5.77, 5.78)), there is some $D' \in \mathbb{N}$ so that $|\bar{\theta}_j - \tilde{\theta}_j| < \eta$ and $|\bar{t}_j - \tilde{t}_j| < \eta$ for all $j > D'$ and therefore there is some $D'' \in \mathbb{N}$ so that $t + nT$ will not lie within any interval $[\min(\bar{t}_j, \tilde{t}_j), \max(\bar{t}_j, \tilde{t}_j))$, $[\min(\bar{\theta}_j, \tilde{\theta}_j), \max(\bar{\theta}_j, \tilde{\theta}_j))$, if $n > D''$. Thus, for large enough n, $t+nT \in \bar{S}_{j'}$ for some j'. Further, $j' \to \infty$ when $n \to \infty$, so that the times $t + nT$ form a subsequence of some sequence $(t(j'))_{j'}$. From Eq. (5.85) we infer pointwise convergence

$$\bar{\delta}(t + nT) \to 0, \tag{5.86}$$

$$\Leftrightarrow$$

$$\delta(t + nT) \to \hat{\delta}, \tag{5.87}$$

or, equivalently, pointwise convergence

$$\tilde{\phi}_l(t + nT) \to \phi_l(t + c_0 + nT), \tag{5.88}$$

$$\tilde{\sigma}_{j+nM}(t + nT) \to \sigma_{j+nM}(t + c_0 + nT), \tag{5.89}$$

where $l \in \{1, ..., N\}, j \in \{\kappa_1(t) - N_{\mathsf{sp}} + 1, ..., \kappa_1(t)\}$, for any initial t with $t \neq t_i - c_0 \wedge t \neq \theta_i - c_0$ for all $i \in \mathbb{N}$.

5.8 Unstable spike patterns

Now we demonstrate that for a different, equally important class of systems non-degenerate periodic spike patterns are guaranteed to be unstable.

Theorem 3: Consider a strongly connected network where $(H^{(l)}_{\varepsilon_{lm}})'(\phi_l) > 1$ for all $l, m \in \{1, ..., N\}$ with $\varepsilon_{lm} \neq 0$, and all $\phi_l \in (B_l, \Theta_l]$. Then, any non-degenerate periodic pattern of spikes is unstable.

Proof: We will show that for all $d_0 > 0$ there is a perturbation with $||\delta(0)|| < d_0$ that grows and exceeds any $d_1 < d_{\max}$, so the dynamics is unstable. We assume that there is a $d_0 > 0$ so that there is no perturbation with $||\delta(0)|| < d_0$ that grows and exceeds any $d_1 < d_{\max}$ and show that this leads to a contradiction. Obviously, we can further assume $d_0 \leq d_1$, otherwise there certainly is a perturbation so that $\|\delta(0)\| < d_0$ and $\|\delta(0)\| > d_1$. We will use that for all perturbations $||\delta^j|| \leq d_1 < d_{\max}$, $j \geq \kappa_0(0)-1$, the order of events does not change and for $j \geq \kappa_0(0)$ Eq. (5.51) is applicable. We track an initial perturbation $\delta(0)$ that has a nonidentical maximal and minimal perturbation in the perturbations of the phases (if it would be in the spikes only, it might decay),

$$\max_l \delta_l(0) = \delta_{\max}(0) > \delta_{\min}(0) = \min_l \delta_l(0). \tag{5.90}$$

We first show that the maximal entry of certain perturbations can only increase with time while the minimal entry can only decrease. Between zero and $\theta_{\kappa_0(0)}$ only spikes can be sent that inherit perturbations already present in the phases at time $t = 0$. Thus neither the overall maximal and minimal perturbation nor the perturbations of the phases can change. We may thus concentrate on $j \geq \kappa_0(0)$. From our presumptions, $(H^l_{\varepsilon_{lm}})'(\phi_l) \geq 1$ holds for all $l, m \in 1, ..., N$ and therefore $c_{lj} \geq 1$ for any interaction. Rewriting Eq. (5.51) as

$$\delta_l^j = (c_{lj} - 1)(\delta_l^{j-1} - \zeta_j) + \delta_l^{j-1}, \tag{5.91}$$

we directly infer that a maximal perturbation $\delta_l^{j-1} = \delta_{\max}^{j-1}$ in the neurons' phases cannot decrease due to an interaction because $(\delta_l^{j-1} - \zeta_j) \geq 0$, with $(c_{lj} - 1) \geq 0$ therefore

$$\delta_l^j \geq \delta_l^{j-1}. \tag{5.92}$$

Analogously, a minimal perturbation cannot grow, since for $\delta_l^{j-1} = \delta_{\min}^{j-1}$, $(\delta_l^{j-1} - \zeta_j) \leq 0$ implying

$$\delta_l^j \leq \delta_l^{j-1}. \tag{5.93}$$

We now show that the property that maximal and minimal perturbations are represented in the phase perturbations is conserved, i.e. holds for δ^j with $j \geq \kappa_0(0)$. We use complete induction and start with the initial perturbation $\delta_l^{\kappa_0(0)}$. For $\delta_l^{\kappa_0(0)}$ the statement holds: Just before the the spike arrival at $\min(\theta_{\kappa_0(0)}, \tilde{\theta}_{\kappa_0(0)})$, the perturbation vector $\delta(\min(\theta_{\kappa_0(0)}, \tilde{\theta}_{\kappa_0(0)})^-)$ has phase perturbation entries

$$\delta_l(\min(\theta_{\kappa_0(0)}, \tilde{\theta}_{\kappa_0(0)})^-) = \delta_l(0). \tag{5.94}$$

The spike perturbation entries are identical to the ones of $\delta(0)$, only some might have been replaced by newly sent ones at sending times $t_1, t_2, ... < \theta_{\kappa_0(0)}$. The new spike perturbations entries equal perturbations already present in the phase perturbations, so that in particular the minimal and the maximal perturbation are still represented in the phase perturbations. Due to the interaction, the maximal phase perturbations can only grow, the minimal only decrease while the spike perturbations remain unchanged due to Eqs. 5.92, 5.93). Using $\delta_l(\min(\theta_{\kappa_0(0)}, \tilde{\theta}_{\kappa_0(0)})^-) = \delta_l^{\kappa_0(0)-1}$, $l = 1, ..., N$, we conclude that for the event based perturbation after the jth arrival

$$\begin{aligned}
\delta_{\min}^{\kappa_0(0)} &= \min_l \delta_l^{\kappa_0(0)} \\
&\leq \min_l \delta_l^{\kappa_0(0)-1} \\
&= \delta_{\min}(\min(\theta_{\kappa_0(0)}, \tilde{\theta}_{\kappa_0(0)})^-) \\
&< \delta_{\max}(\min(\theta_{\kappa_0(0)}, \tilde{\theta}_{\kappa_0(0)})^-) \\
&= \max_l \delta_l^{\kappa_0(0)-1}
\end{aligned}$$

$$\leq \max_l \delta_l^{\kappa_0(0)}$$
$$= \delta_{\max}^{\kappa_0(0)}, \tag{5.95}$$

holds. In the following, we assume for $j \geq \kappa_0(0)+1$ that the maximal and minimal perturbations $\delta_{\max}^{j-1}$ and $\delta_{\min}^{j-1}$ of the perturbation vector δ^{j-1} are represented in the phase perturbations δ_l^{j-1},

$$\min_l \delta_l^{j-1} = \delta_{\min}^{j-1} < \delta_{\max}^{j-1} = \max_l \delta_l^{j-1}, \tag{5.96}$$

and show that

$$\min_l \delta_l^{j} = \delta_{\min}^{j} < \delta_{\max}^{j} = \max_l \delta_l^{j}. \tag{5.97}$$

Perturbations of spikes with indices i, $\kappa_1(\theta_{j-1}) \geq i \geq \kappa_1(\theta_{j-1}) - N_{\mathsf{sp}} + 1$ occurring in the perturbation vector δ^{j-1} are bound by $\delta_{\min}^{j-1}$ and $\delta_{\max}^{j-1}$. Their value does not change but they can be replaced by the perturbations of new spikes i, $\kappa_1(\theta_{j-1}) < i \leq \kappa_1(\theta_j)$, sent between θ_{j-1} and θ_j. Due to Eq. (5.28) these new spikes i inherit a perturbation $\zeta_i = \delta_{s_i}^{P(i)}$, $P(i) = j-1$, already present in the phases and therefore also bound by $\delta_{\min}^{j-1}$ and $\delta_{\max}^{j-1}$. When the jth spike arrives, the size of the perturbations of spike variables do not change while the perturbations of the phases change according to Eq. (5.51). Eqs. (5.92, 5.93) imply that the maximal perturbation of the phase can only increase and the minimal perturbation can only decrease, so that the new extremal perturbations of the phase are the extremal perturbations of the new perturbation vector,

$$\begin{aligned} \delta_{\min}^{j} &= \min_l \delta_l^{j} \leq \min_l \delta_l^{j-1} = \delta_{\min}^{j-1} \\ &< \delta_{\max}^{j-1} = \max_l \delta_l^{j-1} \leq \max_l \delta_l^{j} = \delta_{\max}^{j}. \end{aligned} \tag{5.98}$$

After we have seen that for the perturbations considered the maximal perturbation can only increase while the minimal perturbation can only decrease and both are always represented in the phases, we show that the maximal perturbation indeed has to grow within $2(N-1)$ periods as long as $||\delta^j|| \leq d_1$. We assume that the perturbation does not grow within $2(N-1)$ periods and show that this assumption leads to a contradiction. First, we consider the case that the perturbation of some neuron l which is maximally perturbed, $\delta_l^j = \delta_{\max}^j$, after the arrival of the jth spike, decreases. Due to Eq. (5.91), this can only happen within two periods if there was an arrival of a spike i, $j < i \leq j + 2M$, with $\zeta_i > \delta_{\max}^j$. This implies that the maximal perturbation must have grown which already contradicts our assumption. Therefore, we can assume that the perturbation of maximally perturbed neurons l does not decrease. However, Eqs. (5.53, 5.91) imply that the perturbation of neuron l stays constant only if $\delta_l^{i-1} = \zeta_i$ or $\varepsilon_{ls_i} = 0$, i.e. to ensure that neuron l keeps its perturbation $\delta_{\max}^j$, all arriving spikes ζ_i, $j < i \leq j + 2M$ with $\varepsilon_{ls_i} \neq 0$ must have maximal perturbation. This implies that all presynaptic neurons $\mathrm{Pre}(l)$ have perturbation $\delta_{\max}^j$ when they spike within the first period, because their spikes arrive before the end of the second period due to $\tau < T$ and the

spikes have inherited the sending neurons' perturbation due to Eq. (5.28). If the maximal perturbation has not yet increased, the perturbation of neurons with perturbation $\delta^j_{\max}$ cannot decrease so that neurons $\mathrm{Pre}(l)$ have maximal perturbation later on, in particular at the end of the second period. However, to ensure that the perturbation of neurons $\mathrm{Pre}(l)$ does not increase within the next two periods, also all neurons $\mathrm{Pre}(\mathrm{Pre}(l))$ have to carry perturbation $\delta^j_{\max}$ when they spike in the third period, which entails that they carry perturbation $\delta^j_{\max}$ at the end of the fourth period. To ensure that the maximal perturbation does not increase up to the $2(N-1)$th period, all neurons would have to carry perturbation $\delta^j_{\max}$ at the end of the $2(N-1)$th period in contradiction to the fact that the minimal perturbation cannot grow and is represented in the perturbations of the neurons' phases, so that there is at least one neuron m with $\delta_m^{j+2(N-1)M} \leq \delta^j_{\min} < \delta^j_{\max}$ at the end of the $2(N-1)$th period. Therefore, our assumption is wrong and the *maximal perturbation grows* within at least $2(N-1)$ periods. A completely analogous consideration shows that the *minimal perturbation decreases* within at least $2(N-1)$ periods.

Therefore, the sequence $(\max(\delta^{j+n(2N-1)M}))_n$ is strictly monotonic increasing and $(\min(\delta^{j+n(2N-1)M}))_n$ is strictly monotonic decreasing, due to our assumption they are bound from below and above by $-d_1$ and d_1 and therefore converge,

$$\max(\delta^{j+n(2N-1)M}) \to M_0, \tag{5.99}$$

$$\min(\delta^{j+n(2N-1)M}) \to m_0. \tag{5.100}$$

Furthermore, $(\delta^{j+n(2N-1)M})_n$ is bound with respect to $||.||$ by d_1 and therefore has a convergent subsequence, say

$$\delta^{j+n_m(2N-1)M} \to \hat{\delta}. \tag{5.101}$$

We define $\bar{G}_j$, which maps an actual event-based perturbation vector to the vector $2N-1$ periods later

$$\bar{G}_j : \delta^j \to \delta^{j+(2N-1)M}. \tag{5.102}$$

Like G_j defined in Eq. (5.70), $\bar{G}_j$ is continuous and M-periodic in j. With the same computations as for the proof of stability, we conclude $\max(\hat{\delta}) = M_0$, $\max(\bar{G}_j(\hat{\delta})) = M_0$, so

$$\max(\hat{\delta}) = \max(\bar{G}_j(\hat{\delta})) \tag{5.103}$$

Since $\delta^{j+n_m(2N-1)M}_{\max}, \delta^{j+n_m(2N-1)M}_{\min}$ are always represented in the finitely many phase perturbations, we can find constant indices $l', l'' \in \{1, ..., N\}$ so that

$$\delta_{l'}^{j+n_{m'}(2N-1)M} = \delta^{j+n_{m'}(2N-1)M}_{\max} \tag{5.104}$$

and

$$\delta_{l''}^{j+n_{m''}(2N-1)M} = \delta^{j+n_{m''}(2N-1)M}_{\min} \tag{5.105}$$

for subsequences $(n_{m'})_{m'} \subset (n_m)_m$, $(n_{m''})_{m''} \subset (n_m)_m$. Since max and min are continuous, $\hat{\delta}_{l'} = \max(\hat{\delta})$ and $\hat{\delta}_{l''} = \min(\hat{\delta})$ so the extremal perturbations are

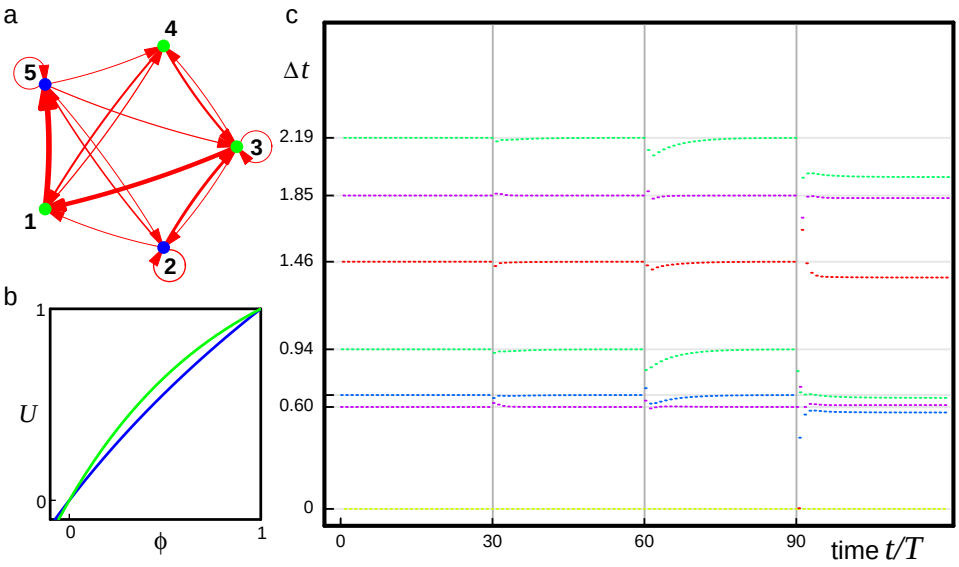

Figure 5.3: Asymptotic stability of non-degenerate periodic spike-patterns in purely inhibitory, strongly connected networks of neurons with concave rise function. Sparse inhibitory network (a) of three leaky integrate-and-fire neurons (green) and two Mirollo and Strogatz biological oscillators (blue) (cf. sec. 3.4). The rise functions are concave as displayed in (b) for neurons 2 (blue) and 4 (green). (c) displays the dynamics by showing the time difference Δt between the actual spike (colored according to the sending neuron) minus the time of last preceding spike of neuron 1 versus the total time elapsed. The network has been designed to realize a predefined pattern. At time $t = 30T$ a perturbation inside the minimal basin is applied, at $t = 60T$ a perturbation inside the basin but outside the minimal basin and at $t = 90T$ a perturbation outside the basin. (For details, see text.)

represented in the perturbations of the phases of the limit perturbation vector $\hat{\delta}$. This implies that the minimum and maximum of $\hat{\delta}$ would change under $\bar{G}_j$ if $\hat{\delta}$ had nonidentical entries. Due to Eq. (5.103), this is not the case, so $\hat{\delta}$ has identical entries. Since also $\min(\hat{\delta}) = m_0$ we conclude $M_0 = m_0$ in contradiction to $m_0 \leq \min \delta(0) < \max \delta(0) \leq M_0$. Therefore, our initial assumption is wrong and there are arbitrarily small initial perturbations that finally exceed any $d_1 < d_{\max}$, where $d_{\max} > 0$ is given in sec. 5.4.

5.9 Purely inhibitory networks with normal dissipation

Corollary 4: In purely inhibitory arbitrarily connected networks with concave rise function (i.e. normal dissipation), $U'' < 0$, any non-degenerate spike pattern is stable. In purely inhibitory strongly connected networks with concave rise function, any non-degenerate spike pattern is even asymptotically stable. The order preserving neighborhood lies within the basin of attraction, i.e. the dynamics is stable at least against perturbations smaller than $d^{\mathrm{In}}_{\max}$.

Proof: In networks with normal dissipation we have for any l and $\varepsilon < 0$

$$H^{(l)}_{\varepsilon}(\phi_l) < H^{(l)}_0(\phi_l) = \phi_l, \tag{5.106}$$

due to the monotonicity of the transfer function and

$$0 < U'_l(\phi_l) < U'_l(H^{(l)}_{\varepsilon}(\phi_l)), \tag{5.107}$$

because U is concave. This implies

$$0 < (H^{(l)}_{\varepsilon})'(\phi_l) = \frac{U'_l(\phi_l)}{U'_l(H^{(l)}_{\varepsilon}(\phi_l))} < 1, \tag{5.108}$$

and Theorem 1 yields the first part of the statement (simple stability). Further, for strongly connected networks we can apply Theorem 2 and the definition of the order preserving neighborhood Eq. (5.42) for purely inhibitory networks which yields the second part of statement (asymptotic stability and minimal basin of attraction).

Fig. 5.3 illustrates the statement of Corollary 4. The parameters in the figure are $\gamma = 0.3, 0.8, 1.2$ for the leaky integrate-and-fire neurons and $b = 0.5, 1$ for the Mirollo-Strogatz biological oscillators. The thresholds of the potentials are $\Theta_{U,l} = 1$, the connections are delayed with $\tau = 0.125$. The remaining neuron parameters I and a are chosen so that the free period is normalized to 1. Applying the methods introduced in ch. 4, the network has been designed to realize the periodic pattern of spikes $t = \{0, 0.60, 0.67, 0.94, 1.46, 1.85, 2.19\}$ (rounded to two decimal digits) with sending neurons $s = \{1, 4, 3, 2, 5, 4, 2\}$, randomly chosen from the patterns with period $T = 2.5$ and seven spike times, as invariant solution. The non-degenerate spike pattern is stable, where all trajectories with maximal distance smaller than $d^{\mathrm{In}}_{\max} \approx 0.03$ (cf. Eq. (5.42)) are certainly attracted. Around times $30T, 60T$ and $90T$ perturbations are applied. The first perturbation has maximum norm slightly smaller than $d^{\mathrm{In}}_{\max}$, the dynamics therefore stays within the minimal basin of attraction and relaxes back towards the original pattern. The second and third perturbation have maximum norm $1.8 d^{\mathrm{In}}_{\max}$. After the second perturbation the trajectory starts outside the minimal basin but still within the basin of attraction, as can be seen from the numerical simulation. The third one perturbs the trajectory out of the basin of attraction into the basin of a different non-degenerate spike pattern.

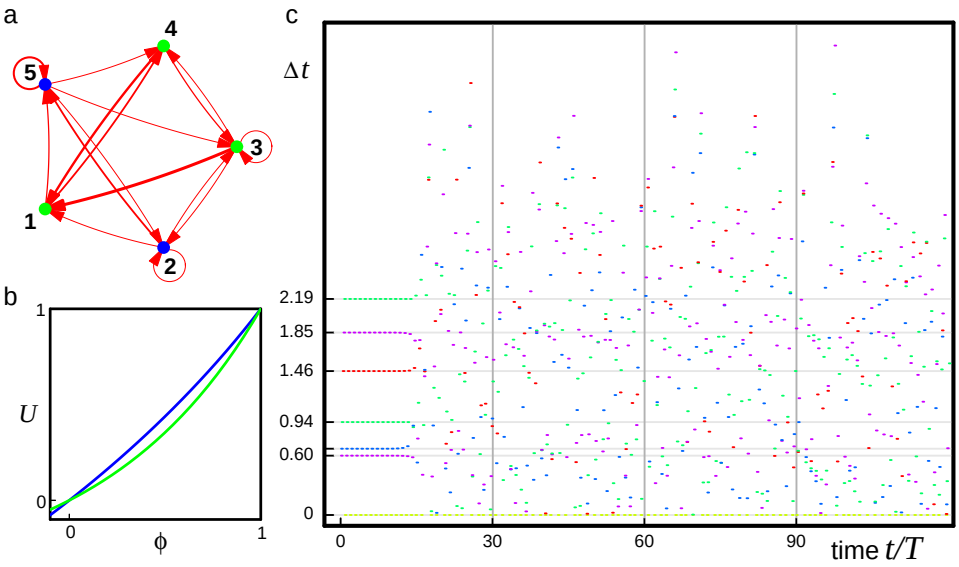

Figure 5.4: Instability of non-degenerate periodic spike-patterns in purely inhibitory, strongly connected networks of neurons with convex rise function. The inhibitory network (a) has the same rough topology, neuron types and delays as the one in Fig. 5.3 and it is designed to show the same periodic pattern of spikes as invariant dynamics. However, the rise functions (b) are now convex as displayed in (b) for neurons 2 and 4. The pattern is therefore unstable, as displayed in (c). The three perturbations do not change the irregular dynamics qualitatively. (For details, see text.)

5.10 Purely inhibitory networks with anomalous dissipation

Corollary 5: In purely inhibitory strongly connected networks with convex rise function (anomalous dissipation) any non-degenerate spike pattern is unstable.

Proof: In networks with anomalous dissipation, for $\varepsilon < 0$,

$$U_l'(\phi) > U_l'(H_\varepsilon^{(l)}(\phi)) > 0, \tag{5.109}$$

because $H_\varepsilon^{(l)}(\phi) < \phi$ due to the monotonicity of the transfer function and U_l is convex. This implies

$$(H_\varepsilon^{(l)})'(\phi) = \frac{U_l'(\phi)}{U_l'(H_\varepsilon^{(l)}(\phi))} > 1, \tag{5.110}$$

and application of Theorem 3 yields the statement.

An illustration to corollary 5 is given in Fig. 5.4. The network has been designed to realize the same pattern as in Fig. 5.3 and to have the same rough topology. The

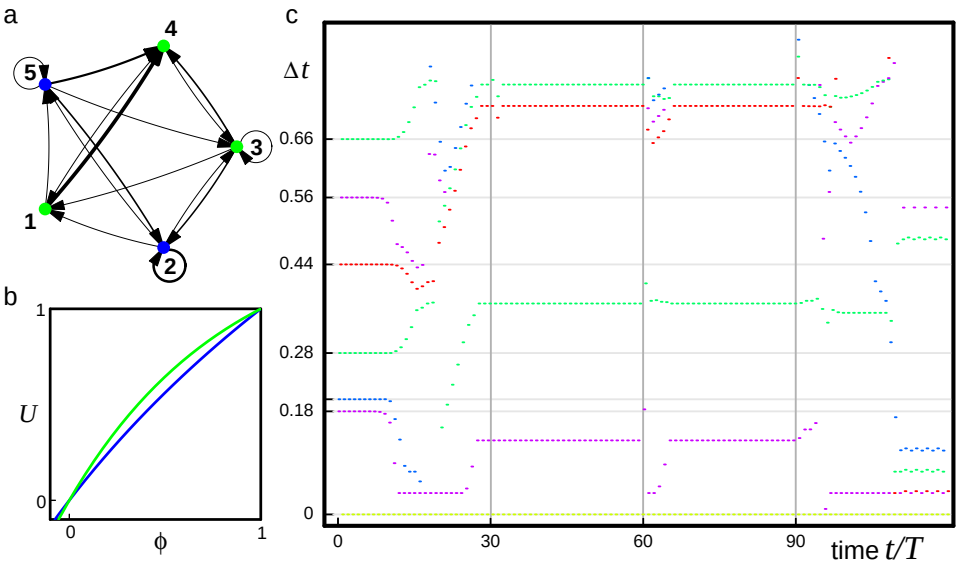

Figure 5.5: Instability of non-degenerate periodic spike-patterns in purely excitatory, strongly connected networks of neurons with concave rise function. Excitatory network (a) with rough topology, neurons and rise functions (illustrated in (b) for neurons 2 and 4) as in Fig. 5.3. The non-degenerate spike pattern is unstable (c). The dynamics converges to patterns stabilized by degenerate events. (For details, see text.)

neurons now have convex rise function: The parameters are $\gamma = -0.3, -0.8, -1.2$ for the leaky integrate-and-fire neurons and $b = -0.5, -1$ for the Mirollo-Strogatz biological oscillators. (Other network parameters as in Fig. 5.3.) Due to the convex rise function, the pattern is unstable, as displayed in (c). The dynamics quickly leaves the periodic orbit corresponding to the spike pattern already due to growth of numerical errors. For purely inhibitory networks there is no obvious stabilizing mechanism such as supra-threshold excitation, and, indeed, we find continued irregular activity. The three perturbations at times $30T, 60T$ and $90T$ do not change this dynamics qualitatively.

5.11 Purely excitatory networks with normal dissipation

Corollary 6: In purely excitatory, strongly connected networks with concave rise function (normal dissipation) any non-degenerate spike pattern is unstable.

Proof: In networks with normal dissipation we have for any l and $\varepsilon > 0$,

$$H_\varepsilon^{(l)}(\phi) > H_0^{(l)}(\phi) = \phi, \tag{5.111}$$

due to the monotonicity of the transfer function and

$$U_l'(\phi) > U_l'(H_\varepsilon^{(l)}(\phi)) > 0, \tag{5.112}$$

because U is concave. This implies

$$(H_\varepsilon^{(l)})'(\phi) = \frac{U_l'(\phi)}{U_l'(H_\varepsilon^{(l)}(\phi))} > 1, \tag{5.113}$$

and application of Theorem 3 yields the statement.

The typical dynamics of such a network is illustrated by Fig. 5.5. The rough topology and the neuron parameters are chosen as in Fig. 5.3. The delay time τ is scaled by a factor of 0.3. The network is designed so that the dynamics has the periodic random pattern of spikes $t = \{0, 0.18, 0.20, 0.28, 0.44, 0.56, 0.66\}$ with sending neurons $s = \{1, 4, 3, 2, 5, 4, 2\}$ and period $T = 0.75$ as invariant solution. This is the pattern of Fig. 5.3 scaled by a factor 0.3 so that it can be realized by a completely excitatory network with neurons of intrinsic period one. The non-degenerate spike pattern is unstable. Already due to increase of numerical error, the dynamics leaves the pattern and converges to a different pattern of spikes. This pattern is stable, as can be seen from the perturbations applied at times $30T, 60T$. It therefore must be degenerate. Indeed, it is stabilized by supra-threshold excitation: neuron 5 excites neurons $2, 4$ over the threshold to simultaneous firing, these neurons in turn excite neurons $1, 3$ over the threshold. The perturbation at $90T$ is large enough to cause the dynamics to leave its basin of attraction and to assume a different pattern, which is again stabilized by supra-threshold excitation.

5.12 Purely excitatory networks with anomalous dissipation

Corollary 7: In purely excitatory arbitrarily connected networks with convex rise function (anomalous dissipation) any non-degenerate spike pattern is stable. In purely excitatory strongly connected networks with convex rise function any non-degenerate spike pattern is asymptotically stable. The order preserving neighborhood lies within the basin of attraction, i.e. the dynamics is stable at least against perturbations smaller than $d_{\max}^{\mathrm{Ex}}$.

Proof: For $\varepsilon > 0$ in networks with convex U_l,

$$0 < U_l'(\phi) < U_l'(H_\varepsilon^{(l)}(\phi)), \tag{5.114}$$

holds because $H_\varepsilon^{(l)}(\phi) > \phi$. This implies

$$0 < (H_\varepsilon^{(l)})'(\phi) = \frac{U_l'(\phi)}{U_l'(H_\varepsilon^{(l)}(\phi))} < 1, \tag{5.115}$$

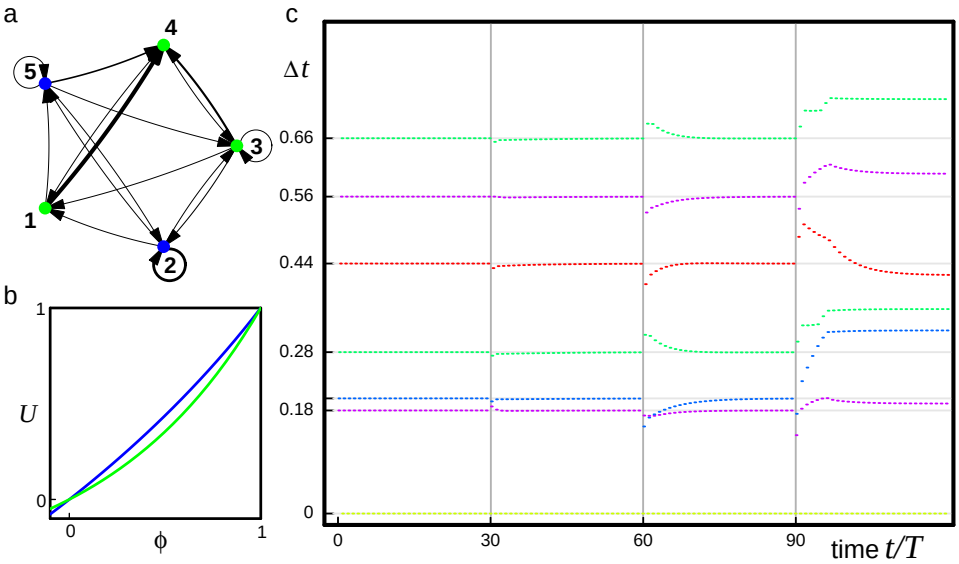

Figure 5.6: Asymptotic stability of non-degenerate periodic spike-patterns in purely excitatory, strongly connected networks of neurons with convex rise function. The excitatory network (a) has the same rough topology, neuron types and delays as the one in Fig. 5.5 and it is designed to show the same periodic pattern of spikes as invariant dynamics. The rise functions are now convex as displayed in (b) for neurons 2 and 4. The pattern is asymptotically stable. At time $t = 30T$ a perturbation inside the minimal basin is applied, at $t = 60T$ a perturbation inside the basin but outside the minimal basin and at $t = 90T$ a perturbation outside the basin are applied. (For details, see text.)

and we can apply Theorem 1 which yields the first part of the statement (simple stability). Further, for strongly connected networks, Theorem 2 and the definition of the order preserving neighborhood Eq. (5.43) for purely excitatory networks yield the statement (asymptotic stability and minimal basin of attraction).

An illustration is given by Fig. 5.6. The rough network topology and the neuron parameters are the same as in Fig. 5.4. The pattern is asymptotically stable with a basin of attraction so that any trajectory with maximal distance less than $d_{\max}^{\mathrm{Ex}} \approx 0.008$ is certainly attracted. The dynamics (c) is perturbed with a vector of maximum norm less than $d_{\max}^{\mathrm{Ex}}$ at time $t = 30T$. Indeed, it relaxes back towards the original spike pattern. At times $t = 60T$, $t = 90T$ two different perturbations with maximum norm $6d_{\max}^{\mathrm{Ex}}$ are applied. At $t = 60T$ the trajectory is perturbed outside the minimal basin (e.g. the firing times of neurons 3 and 4 are interchanged) but it lies still within the basin of attraction, at $t = 90T$, the basin of attraction is left and the dynamics converges to a different stable periodic pattern, which is in fact degenerate and additionally stabilized by supra-threshold excitation: A firing event of neuron 2 is generated by a supra-threshold input from neuron 3.

5.13 Conclusion and outlook

We have analytically studied the stability properties of a general class of periodic orbits for multi-unit systems with delayed couplings and complex connectivity structure, where particular emphasis was put on the mathematically rigorous formulation.

One of the most basic properties of a periodic pattern of spikes is its stability or instability against small perturbations. Numerical simulations have shown that in mixed networks, networks having both excitatory and inhibitory interactions, periodic patterns can be both stable or unstable (cf. ch. 4). For purely excitatory or purely inhibitory networks where the rise functions are congenerically curved, general statements about the stability properties of non-degenerate periodic patterns of spikes have been derived in the present chapter: For arbitrary underlying network connectivity we analytically showed that

(i) In purely inhibitory networks with concave rise function (normal dissipation) any non-degenerate spike pattern is stable. If the network is strongly connected, any non-degenerate spike pattern is asymptotically stable (Corollary 4, sec. 5.9).

(ii) In purely excitatory strongly connected networks with concave rise function (normal dissipation) any non-degenerate spike pattern is unstable (Corollary 6, sec. 5.11).

(iii) In purely inhibitory strongly connected networks with convex rise function (anomalous dissipation) any non-degenerate spike pattern is unstable (Corollary 5, sec. 5.10).

(iv) In purely excitatory networks with convex rise function (anomalous dissipation) any non-degenerate spike pattern is stable. If the network is strongly connected, any non-degenerate spike pattern is asymptotically stable (Corollary 7, sec. 5.12).

For asymptotically stable periodic spike patterns in strongly connected networks we also derived an analytic expression for a minimal basin of attraction.

The proof of stability is based on the observation that interactions lead to averaging of perturbations so that differences between the maximal and the minimal perturbation can only decrease at interactions. If the network is strongly connected, the averaging takes place over the entire network leading to asymptotic stability. In weakly but not strongly connected networks we cannot expect asymptotic stability in general. A simple counterexample is given by a network where several neurons do not receive any input. Their firing sub-pattern will not be asymptotically but only Lyapunov stable.[2]

The proof of instability is based on the observation that for certain arbitrarily small perturbations, the difference between the maximal and the minimal perturbation can only increase on interactions so that these perturbations grow until they are large (i.e. they have the size to interchange event order). Implications of only weakly connected network topology remain to be investigated.

A linear stability analysis employing the Frobenius and Gershgorin Theorems [125] as applied in [177] to much simpler dynamics is probably also possible. The nonlinear stability analysis has the advantage that we can derive information about the size of the basin of attraction and that it allows for a generalization to irregular dynamics (cf. ch. 6). So, we concentrated exclusively on this method.

Degenerate patterns with simultaneous events such as simultaneous spike sendings and arrivals can be unstable or stable. In particular, in networks in which all non-degenerate patterns are stable there can also be unstable periodic patterns. For excitatory coupling and concave rise function, where non-degenerate patterns are unstable, degenerate patterns can be stabilized by supra-threshold excitation, because supra-threshold excitation eliminates small perturbations, cf. [181], so these patterns are observed as attractors in numerical simulations, cf. Fig. 5.5. In contrast, in purely inhibitorily coupled networks with convex rise function, there is no such obvious stabilization mechanism (as long as no additional features are introduced) and indeed, we find continued irregular activity after the dynamics has left the unstable periodic pattern. This regime remains to be studied in detail.

Precisely timed patterns of spikes have been found in neurobiology [6, 66, 152, 67]. For their identification, statistical methods have been derived in [66, 151]. In model neural networks with currents of infinitesimal temporal extent, degenerate spike patterns that are stabilized by supra-threshold excitation can be highly robust and arbitrarily precise also when perturbations are present. In a preliminary study, together with G. Pipa, we analyzed the spike data from such model neural networks

[2]For general implications of the inherent hierarchical structure of weakly connected networks see [178].

with the method proposed in his thesis [151]. Indeed the predicted patterns were found. Future research will quantify this agreement also for non-degenerate spike patterns whose stability has been established in the recent chapter and for different model neurons. On the one hand this will test the statistical methods used in neurobiology. On the other hand it will show for which model parameters precisely timed patterns of spikes occur in the model spike trains and how appropriate the models are for the description of neural activity.

Another important direction of future research concerns the robustness of the current results against the introduction of noise or against changes of the model, e.g. introduction of few excitatory couplings in inhibitory networks or introducing synaptic couplings with finite time course. Some respective results are derived towards the end of the next chapter, in sec. 6.7.

The results presented in the recent chapter suggest the question if we can generalize our proofs and derive statements about the stability properties of irregular, non-periodic dynamics. In the next chapter, we will see that this is indeed possible. However, we will face additional complications arising, e.g., from the fact that for irregular network activity arbitrarily small time intervals between events occur with positive probability that increases with time to one.

Chapter 6

Stability of irregular dynamics

Irregular activity in high dimensional systems is often associated with chaos. For sparse balanced networks of neurons a 'balanced state' of highly irregular activity arises under different conditions. In balanced networks, excitatory and inhibitory inputs have the same order of magnitude. For neural networks of simple units the balanced state is associated with chaos, cf. [198, 199]. It was conjectured that the chaoticity is an emergent property of large, sparse balanced networks and is thus also present for networks of more detailed neuron models [198, 199]. In balanced spiking neural networks, the mean input is subthreshold so that spikes are generated by fluctuations of the membrane potential. The spike statistics is similar to a Poisson process. The balanced state in purely inhibitory and in mixed, excitatory and inhibitory, finite networks is approximated by the same mean field theory [31, 30] and has very similar statistical properties (cf. Fig. (6.1)). We analyze the irregular dynamics in purely inhibitory networks of neurons with normal dissipation and, using a Poissonian approximation, analytically show that the generic irregular dynamics is *stable* in contrast to the *chaotic* dynamics in mixed networks. The considerations are also valid for non-balanced networks as long as the dynamics is sufficiently irregular. The proof generalizes ideas presented in chapter 5 to non-periodic dynamics. We show that the stable dynamics is robust against changes of the neuron properties. Finally, a transition to chaotic dynamics occurs when sufficiently many excitatory couplings are introduced and when the decay time constant of the synaptic currents is sufficiently large. This chaotic dynamics may be transient but it dominates the network dynamics for long times. Our results highlight that chaotic and stable dynamics are equally capable of generating irregular neuronal activity.

We did this study together with S. Jahnke. Parts of the results are presented in his Diploma thesis [93] and, in Letter form, in our article [95]. An exhaustive article is currently prepared with shared first authorship [94].

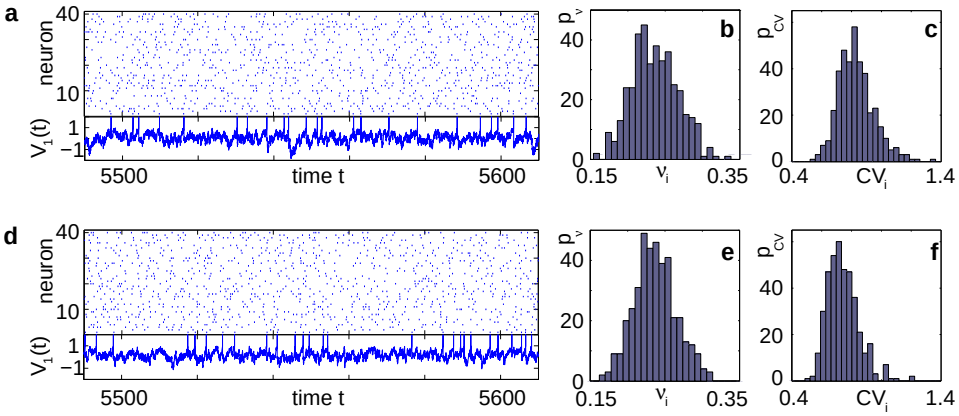

Figure 6.1: Irregular dynamics in purely inhibitorily (a-c) and inhibitorily and excitatorily (d-f) coupled recurrent random networks of leaky integrate-and-fire neurons ($N = 400$, $\gamma_i \equiv 1$, $\phi_{\Theta,i} \equiv 1$, $\tau_{ij} \equiv 0.1$, $|\mathrm{Pre}(i)| \equiv 80$). (a,d) Spiking dynamics (a) $\sum_j \varepsilon_{ij} \equiv -16$, $I_i \equiv 4$, $N_E = 0$; (d) $\sum_j \varepsilon_{ij} \equiv -11$, $I_i \hat{=} 2.95$, $N_E = 1600$, where the N_E excitatory couplings are distributed so that each neuron has the same number of excitatory inputs. The upper panel displays the spiking times (blue lines) of the first 40 neurons. The lower panel displays the membrane potential trajectory of neuron $i = 1$ (spikes of height $\Delta V = 2$ added at firing times). (b,e) Histogram of mean firing rates ν_i. (c,f) Histogram of the coefficients of variation $\mathrm{CV}_i := \sigma_i/\mu_i$; $\mu_i = \left\langle t^s_{ik+1} - t^s_{ik} \right\rangle_k$; $\sigma_i^2 := \left\langle \left(t^s_{ik+1} - t^s_{ik} - \mu_i\right)^2 \right\rangle_k$ averaged over time.

6.1 State of the art

In refs. [198, 199], the activity in a network of simple binary neurons, where excitatory and inhibitory inputs have the same order of magnitude was studied. The studies showed that for sparse networks in the large N limit, the dynamics underlying the irregular balanced state is chaotic. It was conjectured that irregular chaotic dynamics is an emergent property of balanced networks and that it occurs also in networks of more detailed neuron models.

In ref. [209] diluted, purely excitatory networks of spiking neurons of the Mirollo-Strogatz type (cf. ch. 3) with normal dissipation are considered. The irregular transients that dominate the network dynamics for sufficiently large networks are shown to be chaotic. For globally coupled purely excitatory networks, a stability analysis reveals the presence of unstable attractors [180]. These are states with a basin of attraction that has positive volume but the attracting states are surrounded by the basins of attraction of other states so that an arbitrarily small perturbation leads the dynamics to leave the original state and to switch to another state. In [208] purely inhibitory networks of leaky integrate-and-fire neurons without delay are studied. The authors prove analytically that for homogeneous, fully coupled networks the dynamics converge to the stable 'splay state' [174], characterized by evenly spaced spike times of all network neurons. Weakly diluted networks are investigated numerically. Although the dynamics is irregular, its Lyapunov exponent is negative. The irregular dynamics is stationary until it finally converges to a periodic orbit. However, the length of the transient grows exponentially with the network size so that the transient dominates the dynamics. Another article, [98], considers globally coupled networks of leaky integrate-and-fire neurons without delay, where inhibition dominates every coupling. The results indicate that the irregular dynamics is stable and converges to a periodic orbit (for further comments, see end of sec. 6.5). Numerical results derived in a related article were interpreted as indication for chaoticity of the dynamics if coupling delays are included [76], cf. appendix A.

6.2 The model

We consider Mirollo-Strogatz neurons as introduced in chapter 3. We slightly adapt our notation to our article [95]. We thus shortly recall the model using the modified notation. As in the previous chapters, networks of N neurons interact via directed couplings by sending and receiving spikes. If such a directed connection exists from neuron i to neuron j we call j postsynaptic to neuron i and write $j \in \mathrm{Post}(i)$. Neuron i is then presynaptic to neuron j, $i \in \mathrm{Pre}(j)$. The membrane potential $V_i(t)$ of some neuron i evolves according to

$$\frac{d}{dt}V_i = f_i(V_i) + \sum_{j=1}^{N}\sum_{k\in\mathbb{Z}} \varepsilon_{ij}\delta\left(t - t_{jk}^{\mathrm{s}} - \tau_{ij}\right) \tag{6.1}$$

(cf. Eq. (3.1)), where a smooth function f_i specifies the internal dynamics, $\varepsilon_{ij} \leq 0$ are the inhibitory coupling strengths from presynaptic neurons j to i, $\delta(.)$ is the Dirac delta-distribution, $\tau_{ij} > 0$ are the delay times of the connection and t^{s}_{jk} denotes the time when neuron j sends the kth spikes. Spikes sent to postsynaptic neurons with different delay times from neuron j are considered as separate spikes, so if the delays are all different, e.g. if they are chosen randomly, neuron j sends $|\mathrm{Post}(j)|$ spikes at time t^{s}_{jk}. When neuron j reaches the threshold $V_{\Theta,j}$ of the potential, i.e. $V_j(t^-) = V_{\Theta,j}$, it generates spikes at $t =: t^{\mathsf{s}}_{jk}$ for some k and is reset, $V_j(t^{\mathsf{s}}_{jk}) = 0$. Sendings or receivings of spikes are called events. Simultaneous sendings of spikes by one neuron are considered as one event as well as simultaneous receptions of spikes sent by the same neuron. The f_j for all j satisfy $f_j(V_j) > 0$ and $f_j{}'(V_j) < 0$ for all $V_j \leq V_{\Theta,j}$ so that in isolation each neuron exhibits oscillatory dynamics.

As described in ch. 3, this network dynamics can equivalently be described by a phase-like variable $\phi_j(t) \in (-\infty, \phi_{\Theta,j}]$ satisfying

$$d\phi_j/dt = 1 \tag{6.2}$$

at all non-event times (cf. sec. 3.2). When the phase threshold is reached, $\phi_j({t^{\mathsf{s}}_{jk}}^-) = \phi_{\Theta,j}$, the phase is reset, $\phi_j(t^{\mathsf{s}}_{jk}) := 0$ and spikes are generated. An individual spike sent to neuron i arrives there after a delay time τ_{ij} and induces a phase change according to

$$\phi_i(t^{\mathsf{s}}_{jk} + \tau_{ij}) = H^{(i)}_{\varepsilon_{ij}}\left(\phi_i\left(\left(t^{\mathsf{s}}_{jk} + \tau_{ij}\right)^-\right)\right) \tag{6.3}$$

with the transfer function

$$H^{(i)}_{\varepsilon}(\phi) = U_i^{-1}\left[U_i(\phi) + \varepsilon\right], \tag{6.4}$$

$U_i(t)$ is the free (all $\varepsilon_{ij} = 0$) solution of (6.1) through the initial condition $U_i(0) = 0$, yielding $U_i' > 0$ and $U_i'' < 0$ and $\phi_{\Theta,j} = U_j^{-1}(V_{\Theta,j})$.

The analysis below is valid for general $U_i(\phi)$; in the numerical simulations we employ leaky integrate-and-fire neurons, $f_i(V) = I_i - \gamma_i V$ with time scale $\gamma_i^{-1} > 0$ and equilibrium potential $\gamma_i^{-1} I_i > V_{\Theta,i}$, the membrane potential has the functional dependence $U_i(\phi) = \gamma_i^{-1} I_i(1 - \exp(-\gamma_i \phi))$ on ϕ (cf. sec. 3.4). We further note that in the simulations a homogeneous distribution of $\gamma_i = 1$, $I_i = I_0$ and $V_{\Theta,j} = V_{\Theta,0}$ was employed, and time was counted in units of $T_0 = \ln(I_0/(I_0 - 1))$ (the free period of a neuron with $V_{\Theta,0} = 1$). In Figs. 6.1, 6.9, after the simulations, time was multiplied by T_0. In the following, we consider arbitrary generic spike sequences in which all neurons are active, i.e. there is a finite constant $T > 0$, so that in every time interval $[t, t + T)$, $t \in \mathbb{R}$, every neuron fires at least once. Further, in these spike sequences the dynamics is sufficiently irregular so that two events occur with zero probability at the same time.

Due to the delay, the state space is formally infinite dimensional. However, at a given time t the network dynamics is completely determined by the phases $\phi_i(t)$ and

by the spikes which have been sent but not yet received by the postsynaptic neurons at t. Their number is bounded by some constant ND': Due to the inhibitory character of the network couplings, each neuron i needs at least the free oscillation period $\phi_{\Theta,i}$ to generate a spike after the last reset. Consequently, at most

$$D' = N \left\lceil \max_{i,j=1,\ldots,N} \left(\frac{\tau_{ij}}{\phi_{\Theta,i}} \right) \right\rceil \tag{6.5}$$

spikes per neuron are in transit and the state space stays finite, with dimensionality smaller than $N \cdot (1 + D')$ (cf. also [14]). As before, $\lceil . \rceil$ is the ceiling function.

We now introduce variables to describe spikes, which are already sent at time t by neuron j to the postsynaptic neuron i and not yet received. A single spike in transit is characterized by the state variable $\sigma_{ijk}(t) \in [0, \tau_{ij}]$. The index $k = 1, 2, 3 \ldots \leq D'/N$ numbers the different spikes traveling from neuron j to i at time t in the order of arrival at the postsynaptic neuron i, starting with $k = 1$ for the spike to arrive next. When spikes are emitted at time t^{s}_{jn} for some n, $\sigma_{ijk}(t)$ is set to $\sigma_{ijk}(t^{\mathsf{s}}_{jn}) = 0$. The spike index k equals the number of spikes already in transit plus one. It thus depends on the actual network state at time t^{s}_{jn}. Between two events, $\sigma_{ijk}(t)$ increases linearly with slope one, when $\sigma_{ijk}(t^{\mathsf{s}}_{jn} + \tau_{ij}) = \tau_{ij}$, the spike is received by the postsynaptic neuron i, where it induces a phase jump according to Eq. (6.3). After spike reception we cancel the spike arrived (which has index $k = 1$) and renumber the indices $k > 1$ as $k \to k - 1$ so that $\sigma_{ij1}(t^{\mathsf{s}}_{jn} + \tau_{ij})$ again specifies the spike which arrives next at the postsynaptic neuron i sent by neuron j (cf. Fig. 6.2a,b for illustration).

6.3 Lyapunov stability

In this section we study the stability properties of the spike sequences. We compare the microscopic dynamics of two sequences, which slightly differ in the timing of the spikes, but the ordering is the same. We show that the distance between these trajectories is bounded by the initial distance. Assuming that one sequence is generated by a perturbation of the other, this implies Lyapunov stability against perturbations that do not change the order of events.

Since the distance between trajectories only changes at event times, we can choose an event-based perspective. The time of the nth event in the entire network is denoted by t_n in the first sequence, and by $\tilde{t}_n$ in the second one. Analogously, we denote the phases of a neuron i at a given time t by $\phi_i(t)$ and $\tilde{\phi}_i(t)$ and the spikes in transit at time t by $\sigma_{ijk}(t)$ and $\tilde{\sigma}_{ijk}(t)$ in the different sequences. Let

$$\Delta_i^{(n)} = \left(\phi_i\left(t_n\right) - \tilde{\phi}_i\left(\tilde{t}_n\right) \right) - \left(t_n - \tilde{t}_n \right) := \delta_i^{(n)} - \delta t^{(n)} \tag{6.6}$$

denote the difference between the phase differences, $\delta_i^{(n)} := \phi_i\left(t_n\right) - \tilde{\phi}_i\left(\tilde{t}_n\right)$, and the temporal offset, $\delta t^{(n)} = t_n - \tilde{t}_n$, after the nth and before the $(n+1)$th event

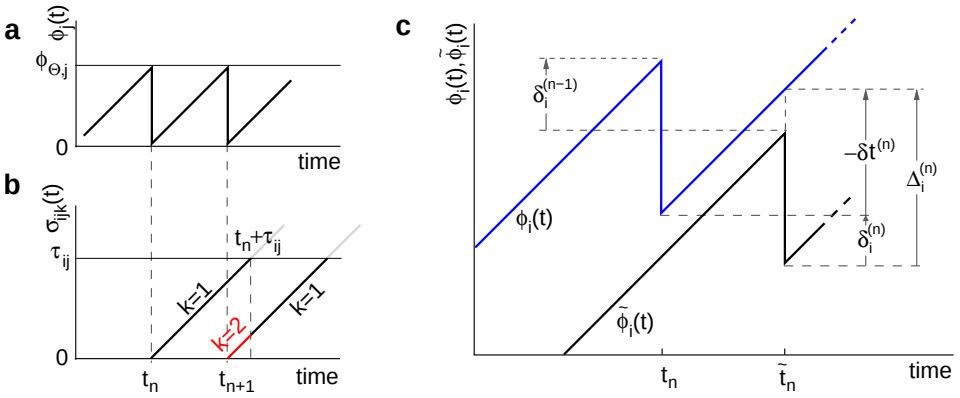

Figure 6.2: (a) Phase dynamics of neuron j. At $t = t_n$ and $t = t_{n+1}$ the phase $\phi_j(t)$ reaches the threshold and is reset to 0. (b) The spikes emitted travel to the postsynaptic neurons $i \in \mathrm{Post}(j)$. They are described by $\sigma_{ijk}(t)$. In this example we show two spikes traveling from neuron j to one specific postsynaptic neuron i, described by $\sigma_{ij1}(t)$ (black) and $\sigma_{ij2}(t)$ (red). At $t = t_n$, $\sigma_{ij1}(t_n)$ is set to 0, where $k = 1$ because there is no spike in transit at $t = t_n^-$. When neuron j spikes again at $t = t_{n+1}$, $\sigma_{ij2}(t_{n+1})$ is set to 0. At $t = t_n + \tau_{ij}$ the spike emitted at $t = t_n$ arrives at the postsynaptic neuron j and induces a phase jump in $\phi_i(t)$ (not shown, cf. Fig. 3.2). After spike reception, we renumber $k \to k - 1$ so that $\sigma_{ij2} \to \sigma_{ij1}$. (c) Definition of the phase shifts. The phase $\phi_i(t)$ of neuron i (blue) before and after the reception of a spike at $t = t_n$ is shown together with $\tilde{\phi}_i(t)$ (black). $\delta_i^{(n)} = \phi_i(t_n) - \tilde{\phi}_i(\tilde{t}_n)$ is the difference of neuron i's phases in the perturbed and the unperturbed dynamics taken at corresponding event times t_n and $\tilde{t}_n$. $\delta t^{(n)} = t_n - \tilde{t}_n$ denotes the difference of event times t_n and $\tilde{t}_n$, i.e. the temporal offset between both sequences. Finally, $\Delta_i^{(n)} = \delta_i^{(n)} - \delta t^{(n)}$ is some phase shift of neuron i with the temporal offset taken into account.

(cf. Fig. 6.2c). Similarly

$$\Delta\sigma_{ijk}^{(n)} = \left(\sigma_{ijk}\left(t_n\right) - \tilde{\sigma}_{ijk}\left(\tilde{t}_n\right)\right) - \left(t_n - \tilde{t}_n\right) := \delta\sigma_{ijk}^{(n)} - \delta t^{(n)} \tag{6.7}$$

labels the shift of the kth spike sent by neuron j and not yet arrived at neuron i after the nth and before the $(n+1)$th event, which equals the negative temporal difference of the sending times in the perturbed and the unperturbed system. Between two consecutive events both $\phi_i(t), \tilde{\phi}_i(t)$ and $\sigma_{ijk}(t), \tilde{\sigma}_{ijk}(t)$ increase linearly and only at event times the phases and spike variables are updated non-linearly as described above. Therefore, as in ch. 5, to study the stability of the system it is sufficient to consider the perturbations after events.

In the following we investigate the evolution of shifts at discrete event times. There are two different kinds of events: (i) sending and (ii) receiving of spikes. When spikes are sent, the shifts $\Delta_i^{(n)}$ and $\Delta\sigma_{ijk}^{(n)}$ stay unchanged, but new spikes with new spike variables are generated. These variables inherit the perturbation of the sending neuron. In the second case, the phase shift of the neuron which receives the spike changes and the spikes in transit are reordered. From the investigation on periodic patterns in purely inhibitory networks with concave rise function, sec. 5.9, we expect that the resulting phase shift of the neuron receiving a spike is a weighted sum of previous shifts, also for the more general networks with inhomogeneous delay and irregular dynamics. Indeed this is the case. We will now study both events in detail.

(i) If as $(n+1)$th event the phase of some neuron j^* reaches its threshold and a spike is emitted, the shifts of all neurons' phases stay unchanged,

$$\begin{aligned}\Delta_j^{(n+1)} =& \phi_i\left(t_n\right) + \left(t_{n+1} - t_n\right) - \left(\tilde{\phi}_i\left(\tilde{t}_n\right) + \left(\tilde{t}_{n+1} - \tilde{t}_n\right)\right) - \delta t^{(n+1)} \\ =& \Delta_j^{(n)}.\end{aligned} \tag{6.8}$$

Similarly, the shifts of the spikes in transit stay unchanged

$$\begin{aligned}\Delta\sigma_{ijk}^{(n+1)} =& \sigma_{ijk}\left(t_n\right) + \left(t_{n+1} - t_n\right) - \left(\tilde{\sigma}_{ijk}\left(\tilde{t}_n\right) + \left(\tilde{t}_{n+1} - \tilde{t}_n\right)\right) - \delta t^{(n+1)} \\ =& \Delta\sigma_{ijk}^{(n)}.\end{aligned} \tag{6.9}$$

Additionally, new spikes are generated $\sigma_{ij^*k^*}(t_{n+1}) = 0$ and $\tilde{\sigma}_{ij^*k^*}(\tilde{t}_{n+1}) = 0$ where $k^* = k^*(i, j^*, n+1)$ is the appropriate spike number k^*, cf. Fig. 6.2. The shifts of the new spike variables depend on the phase shift of the sending neuron j^* according to

$$\begin{aligned}\Delta\sigma_{ij^*k^*}^{(n+1)} =& -\delta t^{(n+1)} \\ =& -\left[\left(t_n + \phi_{\Theta,j^*} - \phi_{j^*}\left(t_n\right)\right) - \left(\tilde{t}_n + \phi_{\Theta,j^*} - \tilde{\phi}_{j^*}\left(\tilde{t}_n\right)\right)\right] \\ =& \Delta_{j^*}^{(n)}.\end{aligned} \tag{6.10}$$

(ii) If as $(n+1)$th event some spike arrives, say $\sigma_{i^*j^*1}(t_{n+1}) = \tau_{i^*j^*}$, it induces a phase jump in the postsynaptic neuron i^*. According to Eq. (6.3), the phase shift $\Delta_{i^*}^{(n+1)}$ can be computed as

$$\Delta_{i^*}^{(n+1)} = H_{\varepsilon_{i^*j^*}}^{(i^*)}\left(\phi_{i^*}\left(t_{n+1}^-\right)\right) - H_{\varepsilon_{i^*j^*}}^{(i^*)}\left(\tilde{\phi}_{i^*}\left(\tilde{t}_{n+1}^-\right)\right) - \delta t^{(n+1)}, \tag{6.11}$$

where $\phi_{i^*}\left(t_{n+1}^-\right) = \phi_{i^*}(t_n) + (t_{n+1} - t_n)$ and $\tilde{\phi}_{i^*}\left(\tilde{t}_{n+1}^-\right) = \tilde{\phi}_{i^*}(\tilde{t}_n) + \left(\tilde{t}_{n+1} - \tilde{t}_n\right)$ are the phases "just before" spike reception. Using the definitions (6.6) we find the identity

$$\phi_{i^*}\left(t_{n+1}{}^-\right) = \tilde{\phi}_{i^*}\left(\tilde{t}_{n+1}^-\right) + \Delta_{i^*}^{(n)} + \delta t^{(n+1)}.$$

Applying the mean value theorem in Eq. (6.11) and the relation

$$\begin{aligned}\delta t^{(n+1)} =& t_{n+1} - \tilde{t}_{n+1} \\ =& t_n + \tau_{i^*j^*} - \sigma_{i^*j^*1}(t_n) - \tilde{t}_n - \tau_{i^*j^*} + \tilde{\sigma}_{i^*j^*1}(\tilde{t}_n) \\ =& -\Delta\sigma_{i^*j^*1}^{(n)}\end{aligned} \tag{6.12}$$

yields

$$\Delta_{i^*}^{(n+1)} = c_{i^*j^*}^{(n+1)} \cdot \Delta_{i^*}^{(n)} + \left(1 - c_{i^*j^*}^{(n+1)}\right) \cdot \Delta\sigma_{i^*j^*1}^{(n)} \tag{6.13}$$

where $c_{i^*j^*}^{(n+1)}$ is given by the derivative

$$c_{i^*j^*}^{(n+1)} = \left.\frac{\partial H_{\varepsilon_{i^*j^*}}^{(i^*)}(\phi)}{\partial\phi}\right|_{\phi\in\left[\phi_{i^*}\left(t_{n+1}^-\right),\tilde{\phi}_{i^*}\left(\tilde{t}_{n+1}^-\right)\right]}, \tag{6.14}$$

for $\phi_{i^*}\left(t_{n+1}^-\right) \leq \tilde{\phi}_{i^*}\left(\tilde{t}_{n+1}^-\right)$, for $\phi_{i^*}\left(t_{n+1}^-\right) > \tilde{\phi}_{i^*}\left(\tilde{t}_{n+1}^-\right)$, ϕ takes values $\phi \in \left[\tilde{\phi}_{i^*}\left(\tilde{t}_{n+1}^-\right), \phi_{i^*}\left(t_{n+1}^-\right)\right]$. If neuron i^* would not be connected to neuron j^*, $\varepsilon_{i^*j^*} = 0$, the function $H_{\varepsilon_{i^*j^*}}^{(i^*)}(\phi) = H_0^{(i^*)}(\phi) = \phi$ would be the identity, so that the phase shift stays unchanged, $\Delta_{i^*}^{(n+1)} = \Delta_{i^*}^{(n)}$, indeed $c_{i^*j^*}^{(n+1)} = dH_0^{(i^*)}(\phi)/d\phi = 1$ independent of ϕ.
For $\varepsilon_{i^*j^*} < 0$, we find $c_{i^*j^*}^{(n+1)}$ bounded by

$$c_{\min} := \inf_{\phi,k}\left\{\frac{\partial\left(H_{\varepsilon_{\min}}^{(k)}(\phi)\right)}{\partial\phi}\right\} \leq c_{i^*j^*}^{(n+1)} \leq \sup_{\phi,k}\left\{\frac{\partial\left(H_{\varepsilon_{\max}}^{(k)}(\phi)\right)}{\partial\phi}\right\} =: c_{\max}, \tag{6.15}$$

where $\varepsilon_{\max} := \max_{i,j:\varepsilon_{ij}\neq 0}\{\varepsilon_{ij}\}$ and $\varepsilon_{\min} := \min_{i,j:\varepsilon_{ij}\neq 0}\{\varepsilon_{ij}\}$. We have used that

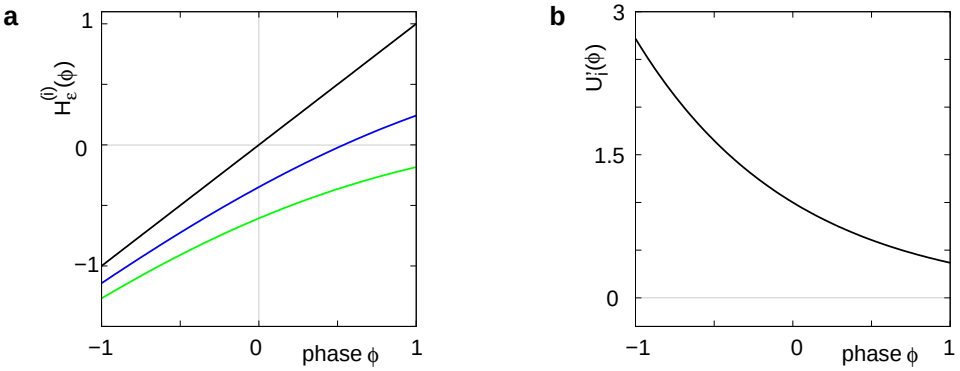

Figure 6.3: (a) The transfer function $H_\varepsilon^{(i)}(\phi)$ for a leaky integrate-and-fire neuron. For $\varepsilon = 0$ (black), $H_0^{(i)}(\phi) = \phi$ is the identity (black), for $\varepsilon < 0$ (blue: $\varepsilon = -0.5$, green: $\varepsilon = -1$) the phase ϕ after receiving an input is smaller than before. For all inhibitory inputs we find $H_\varepsilon^{(i)}(\phi) < \phi$. (b) The derivative of $U_i(\phi)$ is monotonic decreasing, therefore $\partial H_\varepsilon^{(i)}(\phi)/\partial\phi \leq 1$ for $\varepsilon \leq 0$ (cf. Eq. (6.20)).

$\partial\left(H_\varepsilon^{(k)}(\phi)\right)/\partial\phi$ is monotonic increasing with ε

$$\begin{aligned}\frac{\partial}{\partial\varepsilon}\left\{\frac{\partial H_\varepsilon^{(k)}(\phi)}{\partial\phi}\right\} &= U_k'(\phi)\frac{\partial}{\partial\varepsilon}\left(\left[U_k'(H_\varepsilon^{(k)}(\phi))\right]^{-1}\right)\\ &= -\frac{U_k'(\phi)}{\left(U_k'(H_\varepsilon^{(k)}(\phi))\right)^2}\frac{U_k''(H_\varepsilon^{(k)}(\phi))}{U_k'(H_\varepsilon^{(i)}(\phi))}\\ &> 0. \end{aligned} \tag{6.16}$$

The shifts of traveling spikes stay unchanged on spike reception,

$$\Delta\sigma_{ijk}^{(n+1)} = \Delta\sigma_{ijk}^{(n)}, \tag{6.17}$$

for all spikes with $i \neq i^* \vee j \neq j^*$. For $i = i^*, j = j^*$ the spike variables are renumbered and

$$\Delta\sigma_{i^*j^*k-1}^{(n+1)} = \Delta\sigma_{i^*j^*k}^{(n)} \tag{6.18}$$

holds, except for $k = 1$, because $\sigma_{i^*j^*1}(t)$ is the variable describing the spike received and therefore canceled.

We will now ascertain that the coefficients $c_{i^*j^*}^{(n+1)}$ in Eq. (6.13) lie in a compact interval within $(0, 1)$ so that a true averaging takes places when interactions happen. Formally, the phases of neurons can achieve values $\phi_i \in (-\infty, \phi_{\Theta,i}]$. Each neuron fires at least once within a time interval of length T, therefore the phases are

certainly bounded to the compact interval $\phi_i \in [-T + \phi_{\Theta,i}, \phi_{\Theta,i}]$. Further, in inhibitory networks the phase after an interaction is smaller than before,

$$H_\varepsilon^{(i)}(\phi) \quad = U_i^{-1}(U_i(\phi) + \varepsilon) < U_i^{-1}(U_i(\phi)) = \quad \phi, \tag{6.19}$$

because together with U_i also U_i^{-1} is strictly monotonic increasing and $\varepsilon < 0$. The concavity of $U_i(\phi)$ implies

$$0 < \frac{\partial H_\varepsilon^{(i)}(\phi)}{\partial \phi} = \frac{U_i'(\phi)}{U_i'\left(H_\varepsilon^{(i)}(\phi)\right)} < 1 \tag{6.20}$$

for any finite ϕ (cf. sec. 5.9, cf. Fig. 6.3 for an illustration). The derivative $\frac{\partial H_\varepsilon^{(i)}(\phi)}{\partial \phi}$ is continuous in ϕ, therefore the images $\frac{\partial H_{\varepsilon_{ij}}^{(i)}([-T+\phi_{\Theta,i}, \phi_{\Theta,i}])}{\partial \phi}$ are compact. Together with Eq. (6.20) it follows that

$$0 < c_{\min}, c_{\max} < 1. \tag{6.21}$$

Taken together, Eqs. (6.8, 6.9, 6.10, 6.13, 6.21) imply that a true averaging between shifts already present in the system takes place when a spike is received. For other events the shifts stay unchanged. As a consequence, the maximal and minimal shift after the nth event,

$$\Delta_{\max}^{(n)} := \max_{i,j,k} \left\{ \Delta_i^{(n)}, \Delta\sigma_{ijk}^{(n)} \right\} \quad \text{and} \quad \Delta_{\min}^{(n)} := \min_{i,j,k} \left\{ \Delta_i^{(n)}, \Delta\sigma_{ijk}^{(n)} \right\}, \tag{6.22}$$

are bounded by the initial shifts for all future events,

$$\Delta_{\max}^{(n)} \leq \Delta_{\max}^{(0)} \quad \text{and} \quad \Delta_{\min}^{(n)} \geq \Delta_{\min}^{(0)}, \tag{6.23}$$

as long as the order of events in both sequences is the same. Here the minima and maxima are taken over $i, j = \{1, \ldots, N\}$ and k numbers the spikes traveling from neuron j to i at time t_n. An initial perturbation thus cannot grow, in particular, the trajectory is Lyapunov stable.

Indeed, in the definition of Lyapunov stability def. (i) in sec. 2.7 we can choose $\delta = \min(\eta, \varepsilon)$, where the δ, ε are used in the meaning of this definition in the subsequent paragraph. Further we may choose the maximum norm for our distance measurements in def. (i) of sec. 2.7, since norms are equivalent in finite dimensional vector spaces [203]. Then,

$$|\Delta_{\min}^{(0)}| < \delta \text{ and } |\Delta_{\max}^{(0)}| < \delta \tag{6.24}$$

The time shifts of the trajectories, $\delta t^{(n)}$ for events after the initial time equal phase shifts after some event or an initial perturbation due to Eqs. (6.12, 6.10), so Eq. (6.23) leads to

$$|\delta t^{(n)}| \leq \max(|\Delta_{\min}^{(0)}|, |\Delta_{\max}^{(0)}|) < \delta \leq \eta. \tag{6.25}$$

Outside the intervals

$$\begin{aligned}\bigcup_n [\min(t^{(n)}, \tilde{t}^{(n)}), \max(t^{(n)}, \tilde{t}^{(n)})] &\subset \bigcup_n (t^{(n)} - \delta, t^{(n)} + \delta) \\ &\subset \bigcup_n (t^{(n)} - \eta, t^{(n)} + \eta), \end{aligned} \tag{6.26}$$

i.e. for all t with $|t - t^{(n')}| > \eta$ for all n', we have

$$\phi_i(t) - \tilde{\phi}_i(t) = \Delta_i^{(n)}, \tag{6.27}$$

$$\sigma_{ijk}^{(n)}(t) - \tilde{\sigma}_{ijk}^{(n)}(t) = \Delta\sigma_{ijk}^{(n)}, \tag{6.28}$$

for all i, j, k and for some n. With Eqs. (6.10, 6.23), we conclude

$$|\phi_i(t) - \tilde{\phi}_i(t)| < \delta \leq \varepsilon, \tag{6.29}$$

$$|\sigma_{ijk}^{(n)}(t) - \tilde{\sigma}_{ijk}^{(n)}(t)| < \delta \leq \varepsilon. \tag{6.30}$$

We note that we did not make assumptions about network connectivity, the results hold for any network structure and the described class of trajectories.

6.4 Asymptotic stability

In this section we prove that for strongly connected networks even asymptotic stability holds under the condition that both, the perturbed and the unperturbed sequences have the same order of events, i.e. the order of events is unchanged by small perturbations. The central idea is as follows: We study the dynamics and convergence of two neighboring trajectories. We will track the propagation of the perturbation of one specific neuron l_0 through the entire network. Since there is a directed connection between every pair of neurons in the network and any receiving spike leads to an averaging of shifts, there is an averaging over all perturbations in the network. For large times all perturbations converge towards the same value, so that both sequences become equivalent, only shifted by a constant temporal offset.

All neurons spike at least once in a sufficiently large, but finite time interval T. Moreover, after $\tau_{\max} = \max_{i,j}(\tau_{ij})$ all spikes in transit have certainly arrived at the postsynaptic neurons. We label the maximal number of events possible in the time interval $[t, t + \max\{T, \tau_{\max}\}]$ by M. For purely inhibitory networks, $M < \infty$ due to the bounded neural spike rate. We denote the set of neurons that can be reached from neuron l_0 through i directed connections (cf. sec. 2.8) by

$$\mathrm{Post}^i(l_0) = \underbrace{\mathrm{Post} \circ \mathrm{Post} \circ \ldots \circ \mathrm{Post}(l_0)}_{i \text{ times}}, \tag{6.31}$$

in other words, a neuron $l_i \in \mathrm{Post}^i(l_0)$ is connected to l_0 by a directed path of length i.

We estimate the bounds of the perturbation following one specific path from a neuron l_0 to a neuron l. In a strongly connected network, $l \in \mathrm{Post}^j(l_0)$ for some $j \leq N-1$, so there is a path between l_0 and $l = l_j$ via neurons $l_1, ..., l_{j-1}$ in the network. As the consideration holds for an arbitrary path and for any neuron l in the strongly connected network, the result is a universal bound of the perturbation. Initially, at $n = 0$, the neurons are perturbed by $\Delta_i^{(0)}$. The first spiking of neuron l_0 after $n = 0$ is labeled by $s_0 \leq M$. After a delay time $\tau_{l_1 l_0}$ this spike is received by the postsynaptic neuron $l_1 \in \mathrm{Post}(l_0)$, we call this event $r_1 \leq 2M$. After at most M further events, at $s_1 \leq 3M$, the neuron l_1 emits a spike. In general, we recursively define s_i as the first spiking event of neuron $l_i \in \mathrm{Post}^i(l_0)$ after r_i and r_i as the event when the spike generated by $l_{i-1} \in \mathrm{Post}^{i-1}(l_0)$ at s_{i-1} is received. Due to the definition of M, the relations $s_i \leq (2i+1)M$ and $r_i \leq 2iM$ hold.

Now, we prove by induction that the perturbation of the neuron l_i before sending of a spike at s_i is bounded from above by

$$\Delta_{l_i}^{(s_i-1)} \leq \left[(1-c_{\max})^i \cdot c_{\min}^{s_i-1}\right] \Delta_{l_0}^{(0)} + \left[1-(1-c_{\max})^i \cdot c_{\min}^{s_i-1}\right] \Delta_{\max}^{(0)}. \tag{6.32}$$

(i) Initially, neuron l_0 is perturbed by $\Delta_{l_0}^{(0)}$. Before l_0 generates a spike it receives at most $s_0 - 1$ inputs. According to Eq. (6.13), if neuron l_0 indeed receives inputs, the perturbation of neuron l_0 may increase. To find an upper bound, we assume that at every event $0 < n < s_0$ neuron l_0 receives an input with the maximal initial perturbation, $\Delta_{\max}^{(0)}$, and a minimal averaging constant $c_{\min}$, which moves the average into the direction of the maximal possible perturbation. Repeated application of (6.13) yields

$$\begin{aligned}
\Delta_{l_0}^{(1)} &\leq c_{\min}\Delta_{l_0}^{(0)} + (1-c_{\min})\,\Delta_{\max}^{(0)}, \\
\Delta_{l_0}^{(2)} &\leq c_{\min}\Delta_{l_0}^{(1)} + (1-c_{\min})\,\Delta_{\max}^{(0)} \leq c_{\min}^2\Delta_{l_0}^{(0)} + \left(1-c_{\min}^2\right)\Delta_{\max}^{(0)} \\
&\ldots \\
\Delta_{l_0}^{(s_0-1)} &\leq c_{\min}^{s_0-1}\Delta_{l_0}^{(0)} + \left(1-c_{\min}^{s_0-1}\right)\Delta_{\max}^{(0)}.
\end{aligned} \tag{6.33}$$

which is the inductive statement (6.32) for $i = 0$.

(ii) We assume that the statement (6.32) holds for $\Delta_{l_i}^{(s_i-1)}$, which is neuron l_i's perturbation as inherited by the spike sent at s_i (cf. Eq. (6.10)). After at most M events the spike is received by the postsynaptic neuron l_{i+1} at event r_{i+1}. In our worst-case estimate, we assume that neuron l_{i+1} is maximally perturbed before it receives the spike, $\Delta_{l_{i+1}}^{(r_{i+1}-1)} = \Delta_{\max}^{(0)}$, and that the interaction constant $c_{l_{i+1}}^{(r_{i+1})}$ is maximal, $c_{\max}$, so that again the average is moved into the direction of the maximal perturbation. Therefore the perturbation

after the interaction is bounded by

$$\begin{aligned}\Delta_{l_{i+1}}^{(r_{i+1})} &\leq c_{\max}\cdot\Delta_{\max}^{(0)} + (1-c_{\max})\,\Delta_{l_i}^{(s_i-1)} \\ &\leq \left[(1-c_{\max})^{i+1}\cdot c_{\min}^{s_i-1}\right]\cdot\Delta_{l_0}^{(0)} \\ &\quad + \left[1-(1-c_{\max})^{i+1}\cdot c_{\min}^{s_i-1}\right]\cdot\Delta_{\max}^{(0)}. \end{aligned} \tag{6.34}$$

Before its own sending at $s_{i+1} > r_{i+1} > s_i$, neuron l_{i+1} receives at most $(s_{i+1}-1-r_{i+1})$ inputs. Analogously to Eq. (6.33), we assume that with each event, neuron l_{i+1} receives a spike which is maximally perturbed (with $\Delta_{\max}^{(0)}$) and that the averaging constant is minimal, $c_{\min}$. This yields

$$\begin{aligned}\Delta_{l_{i+1}}^{(s_{i+1}-1)} &\leq \left[(1-c_{\max})^{i+1}\cdot c_{\min}^{s_i-1+s_{i+1}-1-r_{i+1}}\right]\Delta_{l_0}^{(0)} \\ &\quad + \left[1-(1-c_{\max})^{i+1}\cdot c_{\min}^{s_i-1+s_{i+1}-1-r_{i+1}}\right]\Delta_{\max}^{(0)}. \end{aligned} \tag{6.35}$$

We replace $c_{\min}^{s_i-1+s_{i+1}-1-r_{i+1}}$ by $c_{\min}^{s_{i+1}-1}$ in Eq. (6.35), thereby increasing the right-hand side, because $s_i - 1 - r_{i+1} < 0$. This directly yields the induction statement for $\Delta_{l_{i+1}}^{(s_{i+1}-1)}$.

Based on Eq. (6.32) we now derive an upper bound of the perturbation of all neurons after event s_{N-1}. After this event every neuron l_i has sent at least one spike which is influenced by the initial perturbation of neuron l_0, because the union $\bigcup_{i=1}^{N-1} \mathrm{Post}^i(l_0)$ contains all neurons of the network. After the s_ith event, the neuron l_i still receives spikes. Before the s_{N-1}th event, taken as reference, it receives in a worst case scenario $(s_{N-1}-1-s_i)$ inputs with maximal initial perturbation $\Delta_{\max}^{(0)}$ and a minimal averaging constant $c_{\min}$. Using Eq. (6.32) we repeatedly apply Eq. (6.13)$(s_{N-1}-1-s_i)$ times which leads to

$$\begin{aligned}\Delta_{l_i}^{(s_{N-1})} &\leq \left[(1-c_{\max})^{i}\cdot c_{\min}^{s_i-1+s_{N-1}-1-s_i}\right]\Delta_{l_0}^{(0)} \\ &\quad + \left[1-(1-c_{\max})^{i}\cdot c_{\min}^{s_i-1+s_{N-1}-1-s_i}\right]\Delta_{\max}^{(0)}. \end{aligned} \tag{6.36}$$

The right-hand side increases with i, therefore, the perturbation of an arbitrary neuron $j \in \{1,\ldots,N\}$ after s_{N-1} events is bounded from above by

$$\begin{aligned}\Delta_{j}^{(s_{N-1})} &\leq \left[(1-c_{\max})^{N-1}\cdot c_{\min}^{(s_{N-1}-2)}\right]\cdot\Delta_{l_0}^{(0)} \\ &\quad + \left[1-(1-c_{\max})^{N-1}\cdot c_{\min}^{(s_{N-1}-2)}\right]\cdot\Delta_{\max}^{(0)}. \end{aligned} \tag{6.37}$$

At the s_{N-1}th event there can be D' per neuron in transit which in our worst case scenario can still have maximal perturbation. Due to their arrival after the s_{N-1}th

event, the perturbation still increases. However, taking into account the arrival of these spikes using Eqs. (6.13, 6.38) we conclude that the estimate

$$\begin{aligned}\Delta_j^{(s_{N-1}+n)} &\leq \left[(1-c_{\max})^{N-1}\cdot c_{\min}^{\left(s_{N-1}-2+D'\right)}\right]\cdot\Delta_{l_0}^{(0)} \\ &\quad+\left[1-(1-c_{\max})^{N-1}\cdot c_{\min}^{\left(s_{N-1}-2+D'\right)}\right]\cdot\Delta_{\max}^{(0)}. \qquad (6.38)\end{aligned}$$

must hold for all $n \geq 1$. The bound (6.38) holds also for all spikes generated after the s_{N-1}th event (cf. Eq. (6.10)), because spikes have to inherit a perturbation present in the phases and in the worst case, all maximally perturbed spikes arrived before spike sending which is precisely accounted for by Eq. (6.38). After M further events, all spikes sent before s_{N-1} have arrived. Since $D' \leq M$, the perturbations of the neurons and the spikes in transit after $K := 2NM \geq s_{N-1} + M$ events are bounded by

$$\begin{aligned}\Delta_j^{(K)} &\leq \left[(1-c_{\max})^{N-1}\cdot c_{\min}^{2NM-2}\right]\cdot\Delta_{l_0}^{(0)} \\ &\quad+\left[1-(1-c_{\max})^{N-1}\cdot c_{\min}^{2NM-2}\right]\cdot\Delta_{\max}^{(0)}. \qquad (6.39)\end{aligned}$$

Therefore we find an upper bound for the maximal perturbation $\Delta_{\max}^{(K)}$ after K events,

$$\Delta_{\max}^{(K)} \leq c^*\cdot\Delta_{l_0}^{(0)} + [1-c^*]\cdot\Delta_{\max}^{(0)}. \qquad (6.40)$$

with

$$0 < c^* = (1-c_{\max})^{N-1}\cdot c_{\min}^{2NM-2} \leq (1-c_{\max})\cdot c_{\max} \leq 1/4. \qquad (6.41)$$

Similarly, we find a lower bound for the minimal perturbation after K events

$$\Delta_{\min}^{(K)} \geq c^*\cdot\Delta_{l_0}^{(0)} + [1-c^*]\cdot\Delta_{\min}^{(0)}, \qquad (6.42)$$

by an estimation analogous to the one above, where only $\Delta_{\max}^{(0)}$ has be replaced $\Delta_{\min}^{(0)}$and the relation "$\leq$" has to be replaced by "$\geq$". The difference of the maximal and minimal perturbation after K events is therefore given by

$$\Delta_{\max}^{(K)} - \Delta_{\min}^{(K)} \leq (1-c^*)\left(\Delta_{\max}^{(0)} - \Delta_{\min}^{(0)}\right). \qquad (6.43)$$

We note, that we did not have to specify the perturbation $\Delta_{l_0}^{(0)}$ to derive this result. The spread of any perturbation through the network has a contracting effect on the total perturbation, it leads to a decay of the difference between the extremal perturbations at least by a factor of $(1-c^*)$. Inequality (6.43) implies together with

$$3/4 \leq (1-c^*) < 1 \qquad (6.44)$$

that for the considered trajectories in the long-time limit the maximal and minimal perturbation are the same,

$$\lim_{n\to\infty} \Delta_{\max}^{(n)} = \lim_{n\to\infty} \Delta_{\min}^{(n)}. \tag{6.45}$$

Both sequences become equivalent,

$$\lim_{n\to\infty} \delta_i^{(n)} = 0, \tag{6.46}$$

and the events are just shifted by a constant temporal offset

$$\delta t = \lim_{n\to\infty} \left\{ \delta t^{(n)} \right\} = - \lim_{n\to\infty} \Delta_{\max}^{(n)} \tag{6.47}$$

for $t \to \infty$ (cf. Fig. 6.4). Thus all sequences considered are asymptotically stable. We note that we used a notion of asymptotic stability of trajectories that allows convergence to a time shifted, equivalent trajectory. It is more general than Def. (iii) in sec. 2.7 and appropriate for time translation invariant systems. Indeed, the stability is even exponential since for all strongly connected networks the perturbations decay exponentially fast with at least

$$\Delta_{\max}^{(n)} - \Delta_{\min}^{(n)} \leq (1 - c^*)^{\left\lfloor \frac{n}{K} \right\rfloor} \left(\Delta_{\max}^{(0)} - \Delta_{\min}^{(0)} \right), \tag{6.48}$$

where $\lfloor . \rfloor$ is the floor function. The numerically measured exponential decay is much faster than the estimation given by Eq. (6.48). The main reasons are that (i) the mean path length is more meaningful for estimating the number of events until all neurons have received an input from the starting one and (ii) it is impossible that the neurons receive the worst case perturbation at each receiving.

6.5 Margins

The stability results in the previous sections hold for the class of patterns, where a sufficiently small perturbation does not change the order of spikes. In this section we show that typical spike dynamics, generated by networks with a complex connectivity, belong to this class.

In heterogeneous networks with purely inhibitory interactions the occurrence of events at *identical* times has a zero probability. There is no mechanism causing simultaneous spiking, like supra-threshold inputs in excitatory coupled networks (cf. sec. 5.11, ch. 7). As long as two events do not occur at the same event time, there is a non-zero perturbation size keeping the order unchanged in any *finite* time interval. However, the requirement of an unchanged event order yields more and more conditions over time so that the allowed size of a perturbation could decay more quickly with time than the actual perturbation. This will be excluded if a temporal *margin* $\mu^{(n)}$ (cf. [98]) stays larger than the dynamical perturbation for *infinite* time. Formally, after time t_n denote the kth potential future event time

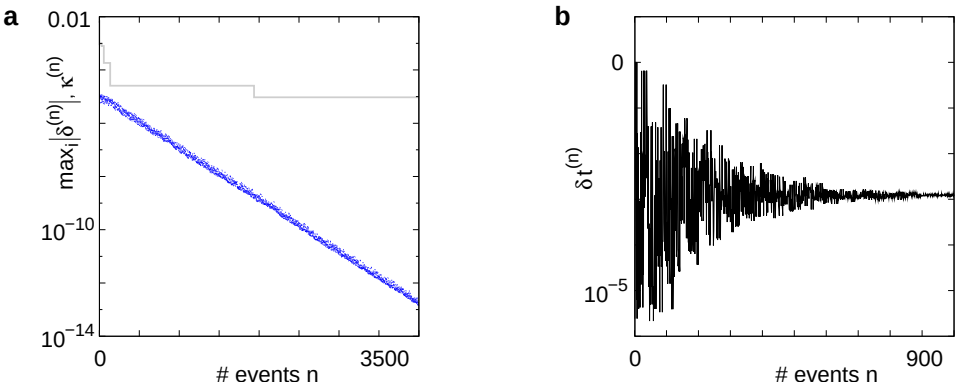

Figure 6.4: Stable dynamics in the network of Fig. 6.1a. (a) Exponential decay of the maximal perturbation $\max_i \left|\delta_i^{(n)}\right|$ (blue dots) and minimal margin $\kappa^{(n)}$ (gray line) for one microscopic dynamics. The initial perturbation $\max \left|\delta_i^{(0)}\right| \approx 10^{-5}$ decays exponential fast. (b) Exponential convergence of the temporal offset $\delta t^{(n)}$. For large n both sequences are equivalent, just shifted by a constant offset $\delta t = \lim_{n\to\infty} \left\{\delta t^{(n)}\right\}$.

(of the original trajectory) that would arise if there were no future interactions by $\theta_{n,k}$, $k \in \mathbb{N}$, and the temporal *margin* by $\mu^{(n)} := \theta_{n,2} - \theta_{n,1}$. A sufficiently small perturbation, satisfying $\Delta_{\max}^{(n)} - \Delta_{\min}^{(n)} < \mu^{(n)}$, cannot change the order of the $(n+1)$th event.

This directly implies that almost all *periodic orbits* (all those with non-degenerate event times t_n) consisting of a finite number of P events are stable because there is a minimal margin

$$\kappa^{(P)} := \min_{n\in\{1,\dots,P\}} \mu^{(n)} \tag{6.49}$$

for every non-degenerate periodic pattern (cf. sec. 5.9).

We further study the stability properties of *irregular non-periodic spike sequences* by considering the minimal margin $\kappa^{(n)}$ over the first n events. For simplicity, we consider delay distributions where τ_{ij} is independent of the spike receiving neuron i. For arbitrary inhomogeneous delay, another definition of margins has to be used, based on the margins of single neurons, since interchanges of spike arrivals at different neurons do not destroy stability. The irregular spiking dynamics of the entire network is well modeled by a Poisson point process with rate ν^{s}, where ν^{s} specifies the mean firing rate of the network [193, 31, 30, 33]. We note, however, that individual neurons are assumed to slightly deviate from Poissonian spiking due to our previous assumptions and that there are correlations between the individual spike trains, cf. sec. 6.2 and [40, 110]. We assume that, along with the irregular spiking dynamics, the temporal margins are generated by a Poisson point process

with network event rate ν. $\nu = 2\nu^s$, because any spike sending time generates one receiving event since τ_{ij} is independent from i. The distribution function of margins is given by

$$P\left(\mu^{(n)} \leq \mu\right) = 1 - e^{-\nu\mu}. \tag{6.50}$$

Therefore, the probability that the minimal margin $\kappa^{(n)}$ after n events is smaller or equal to μ is determined by the probabilities that not all individual margins $\mu^{(n)}$ are larger than μ so that

$$P\left(\kappa^{(n)} \leq \mu\right) = 1 - \prod_{m=1}^{n} P\left(\mu^{(m)} > \mu\right) = 1 - e^{-n\nu\mu} \tag{6.51}$$

with density $\rho_n(\mu) := dP\left(\kappa^{(n)} \leq \mu\right)/d\mu = n\nu \exp(-n\nu\mu)$. This implies an algebraic decay with the number n of events for the expected minimal margin

$$\overline{\kappa^{(n)}} = \int_0^\infty \mu\rho_n(\mu)d\mu = (\nu n)^{-1} \tag{6.52}$$

that depends only on the event rate and is independent of the specific network parameters. Numerical simulations show excellent agreement with this algebraic decay (6.52) of the expected minimal margin with the number of network events n; a typical example is shown in Fig. 6.5c.

Since the fluctuations are small, this strongly suggests that a sufficiently small perturbation stays smaller than the minimal margin for all times. In each step, the exponential distribution of margins has finite density for arbitrarily small values of μ, i.e. in each step the margin can fall below the level of perturbation with finite probability. We have to exclude in particular that $P\left(\exists n : \mu^{(n)} \leq \Delta_{\max}^{(n)} - \Delta_{\min}^{(n)}\right)$, the probability that there is at least one step in which the margin falls below the perturbation size, does not approach one if time goes to infinity for arbitrary perturbation. We will show that it even goes to zero if the size of the initial perturbation goes to zero. Of course, we cannot expect to reach zero for nonzero perturbation.

We derive a lower estimate for the probability that the margin stays larger than the perturbation for infinite time. We show that it converges to one when the size of perturbation goes to zero and thus prove that sufficiently small perturbations have arbitrarily high probability to stay smaller than the minimal margin for all times. We start from the upper estimate for the evolution of the perturbation, Eq. (6.48). Using $\left\lfloor \frac{n}{K} \right\rfloor \geq \frac{n}{K} - 1$ and Eq. (6.44) leads to

$$\begin{aligned}
\Delta_{\max}^{(n)} - \Delta_{\min}^{(n)} &\leq (1-c^*)^{\frac{n}{K}-1} \left(\Delta_{\max}^{(0)} - \Delta_{\min}^{(0)}\right), \\
&= \exp\left(\frac{\log(1-c^*)}{K} n\right) \frac{\Delta_{\max}^{(0)} - \Delta_{\min}^{(0)}}{1-c^*}, \\
&= C\exp(-\alpha n),
\end{aligned} \tag{6.53}$$

where we introduced

$$C = \frac{\Delta_{\max}^{(0)} - \Delta_{\min}^{(0)}}{1 - c^*}, \tag{6.54}$$

$$\alpha = -\frac{\log(1 - c^*)}{K} > 0. \tag{6.55}$$

In particular, $C \to 0$, if the initial perturbation goes to zero, i.e. $\Delta_{\max}^{(0)} - \Delta_{\min}^{(0)} \to 0$, while α is independent of the initial perturbation. The probability that all margins are larger than all perturbations is given by

$$P\left(\forall n : \mu^{(n)} > \Delta_{\max}^{(n)} - \Delta_{\min}^{(n)}\right) = \prod_{n=1}^{\infty} P\left(\mu^{(n)} > \Delta_{\max}^{(n)} - \Delta_{\min}^{(n)}\right), \tag{6.56}$$

since the margins are assumed to be independent. Using Eq. (6.53) and $P\left(\mu^{(n)} > \mu\right) = \exp(-\nu\mu)$ yields

$$\begin{aligned}
\prod_{n=1}^{\infty} P\left(\mu^{(n)} > \Delta_{\max}^{(n)} - \Delta_{\min}^{(n)}\right) &\geq \prod_{n=1}^{\infty} P\left(\mu^{(n)} > C\exp(-\alpha n)\right) \\
&= \prod_{n=1}^{\infty} \exp(-\nu C \exp(-\alpha n)) \\
&= \exp\left(-\nu C \sum_{n=1}^{\infty} \exp(-\alpha n)\right) \\
&= \exp\left(-\nu C \frac{1}{\exp(\alpha) - 1}\right),
\end{aligned} \tag{6.57}$$

which goes to one if the initial perturbation (and thus C) goes to zero.

We note that the assumption of a constant lower bound of the minimal margin is not necessary in contrast to [98]. Indeed, this assumption would be highly problematic. A spiking dynamics converging to a periodic orbit has a finite minimal margin $\kappa > 0$ if not two spikes precisely coincide which has in our networks probability zero for randomly chosen initial conditions. Also, an irregular dynamics, such as Poissonian network dynamics, has $\kappa > 0$ within a finite time interval. However, in an irregular dynamics, arbitrarily small margins naturally have small but finite probability in every step. Therefore, for infinite number of steps, these margins occur and the minimal margin falls below any lower bound $\kappa > 0$ with probability one. So, if we already assume that there is some lower bound, we exclude the generic irregular dynamics. We could only state that the network dynamics is stable if it converges to a periodic orbit, or make statements about convergence for finite time but not about generic irregular dynamics for infinite time.

Our approach allowed us to show that the generic irregular dynamics is stable.

Interestingly, as we will see below, generic dynamics indeed converges to periodic orbits. However, also in this proof we may not assume that the margins have finite

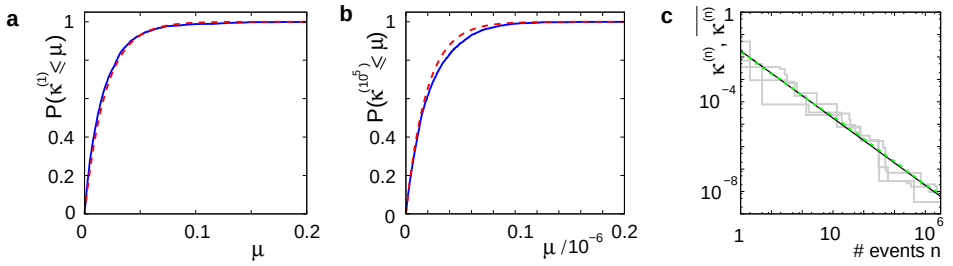

Figure 6.5: Margins in the network given in Fig. 6.1a. (a),(b) Probability distribution $P(\kappa^{(n)} \leq \mu)$ after (a) $n = 1$ and (b) $n = 10^5$ events. The blue curve is the measured distribution over 2500 samples, the red dotted line is the analytical prediction (no free fit parameter, rate ν is measured; cf. Eq. (6.51)). (c) Algebraic decay of the average minimal margin, $\overline{\kappa^{(n)}}$ (green dashed line, averaged over 250 random initial conditions) and the analytical prediction (no free fit parameter) of $\overline{\kappa^{(n)}}$ (black solid line). Additionally, we show the minimal margin $\kappa^{(n)}$ for three exemplary initial conditions (gray lines), including that of figure 6.4a.

lower bound: We might first be tempted to consider a finite time interval. There, we take the almost surely existing lower bound of the dynamics and then show that the dynamics becomes periodic. The problem is that the time after which the dynamics becomes periodic, grows when the lower bound for the margin decreases [98]. If we thus choose a finite interval, it might be too short for the dynamics to converge. When choosing a longer interval, there is more time for convergence but also the lower bound for the margin will usually be lower, so that still no convergence appears. Thus, just considering finite intervals with lower bound of the margin does not lead to a result. As soon as we consider infinite time however, we cannot assume a finite lower bound for the margin because this excludes generic irregular dynamics.

6.6 Convergence to periodic orbits

Interestingly, the slow algebraic decay of the minimal margin and its small fluctuations provides a strong argument that generic spike sequences have to converge to a periodic orbit after a finite time. Indeed, this convergence is found numerically.

Consider two sequences in the same network, which share the order of at least E events. We have shown that for $0 \leq n \leq E$, both sequences converge exponentially fast against each other. Both the phases and the variables encoding the spikes in transit are bounded to a finite interval, $\phi_i(t) \in [-T + \phi_{\Theta,i}, \phi_{\Theta,i}]$ and $\sigma_{ijk}(t) \in [0, \max_{ij}\{\tau_{ij}\}]$ at any given time t. Therefore, the maximal initial distance between

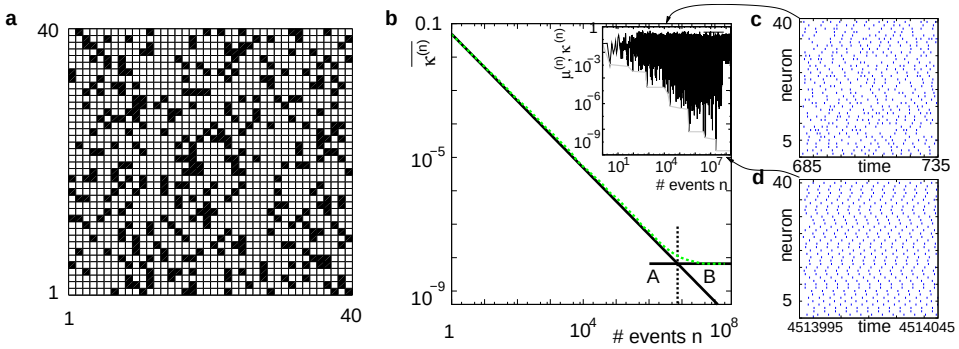

Figure 6.6: Convergence towards a periodic orbit in a random network ($N = 40$, $\gamma_i \equiv 1$, $I_i \equiv 3.0$, $\phi_{\Theta,i} \equiv 1.0$, $\tau_{ij} \equiv 0.1$, $|\mathrm{Pre}(i)| \equiv 8$, $\sum_j \varepsilon_{ij} \equiv -3.3$). (a) Coupling matrix, each realized connection is indicated by a black square. (b) Average minimal margin $\overline{\kappa^{(n)}}$ (averaged over 250 random initial conditions, cf. Fig. 6.5a) decays as a power-law (region A) and saturates after about 10^7 events (region B) when the periodic orbit is reached. Inset: Margin $\mu^{(n)}$ (black) and minimal margin $\kappa^{(n)}$ (gray) for a trajectory started from one specific initial condition. The margin $\mu^{(n)}$ fluctuates strongly on the transient and is comparatively large after the sequence becomes periodic; here the minimal margin $\kappa^{(n)}$ does not decrease further for future events n. (b),(c): Snapshots of irregular spike sequences (c) after $n \approx 15000$ events on the transient and (c) after $n \approx 10^8$ events on the periodic orbit.

two trajectories is bounded by

$$\Delta^{(0)}_{\max} - \Delta^{(0)}_{\min} \leq \max_{i,j} \{T, \tau_{ij}\} =: \Phi_{\max}. \tag{6.58}$$

For generic irregular sequences, the minimal margin $\kappa^{(n)}$ decays slower than the perturbation. This implies that there is a certain number of events E^*, after which the maximal initial distance $\Phi_{\max}$ has decayed to the same size as the minimal margin at E^* if the order of events remains unchanged. Our analytical consideration yield an upper estimate for E^*,

$$(1 - c^*)^{\left\lfloor \frac{E^*}{K} \right\rfloor} \Phi_{\max} \approx (\nu \cdot E^*)^{-1}. \tag{6.59}$$

If $E \gtrsim E^*$, even for $n > E$ the order of events in the considered trajectories are the same, because the perturbation stays smaller than the margin also for future events. Consequently, a trajectory which contains two identical subsequences of minimal length E^* is trapped into a periodic orbit, since the subsequence already determines the order of all future events.

The considered system is finite dimensional with dimension maximal $N + ND'$. Thus, any sequence with

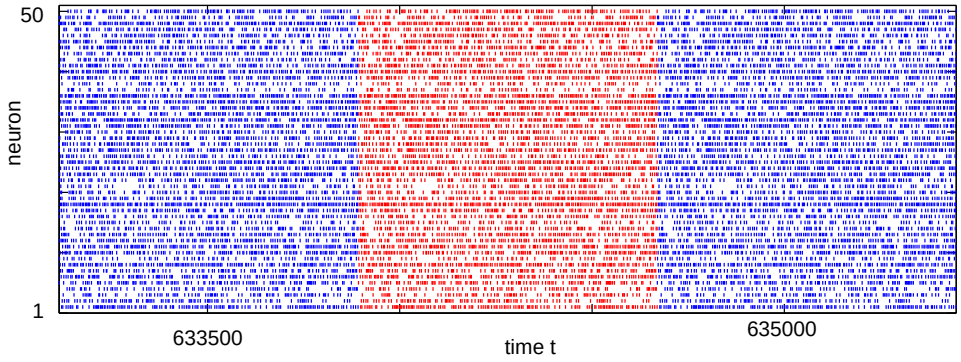

Figure 6.7: Long periodic orbit in a random network ($N = 50$, $\gamma_i \equiv 1$, $I_i \equiv 1.2$, $\phi_{\Theta,i} \equiv 1.0$, $\tau_{ij} \equiv 0.1$). The coupling strengths are randomly and uniformly drawn from $[-1, 0]$ and normalized afterwards ($\sum_{j=1}^{N} \varepsilon_{ij} = -6.5$). The final spike pattern repeats every 11012 events and is highly irregular.

$$E^{**} = (N + ND')^{E^*} + E^* \tag{6.60}$$

events contains at least two copies of an identical subsequence of length E^*: The system converges to a periodic spike sequence after at most E^{**} events. In Fig. 6.6 we show a typical example: The mean margin, $\overline{\kappa^{(n)}}$, decays algebraically on the transient and saturates after the periodic orbit is reached. The periodic attractor shown in Fig. 6.6d differs slightly from the "splay state" [174], where the firing pattern is characterized by equally spaced inter-spike-intervals. We have seen that it is possible to design networks, which exhibit more complex periodic spike patterns (cf. ch. 4). Indeed, in different parameter regimes we observe such complex periodic orbits, with a large periodicity, cf. the heterogeneous globally coupled network in Fig. 6.7, where the periodic orbit is reached after a small number of events, compared to sparse networks.

Although the attractor is reached after a finite number of events, the transient becomes very important in systems with strong inhibition or large number of neurons. As formerly found in networks with excitatory coupling [209], and also in weakly diluted networks with purely inhibitory interactions [208], the transient length grows rapidly with network size so that the dynamics is determined by the transient for large timescales. We studied inhibitory random networks with an arbitrary network structure, typically far away from the weakly diluted topology. Since Eqs. ((6.59), (6.60)) yield an upper bound which is typically much larger than the actual transient length, we perform numerical measurements of the transient length dependent on network size N. To avoid the choice of a parameter defining the neighborhood of the periodic orbit, we define the length of the transient, t_r by the number of events after which the order of events stays periodic. When increasing the network size N, we leave the external current I_i and the normalization of

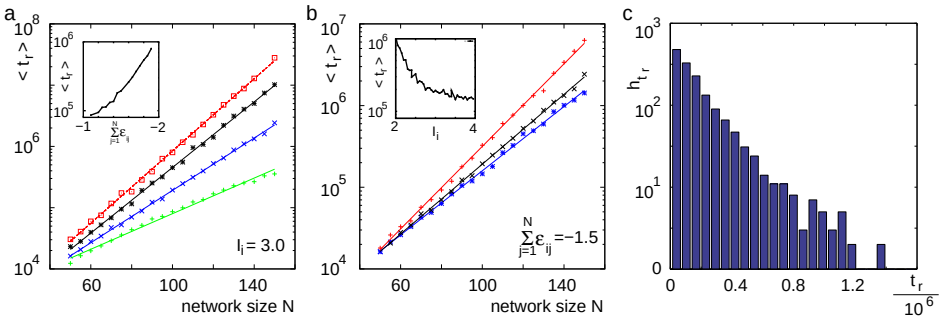

Figure 6.8: Transient lengths for different parameters in sparse random networks ($|\mathrm{Pre}(i)| = \lfloor N/4 \rfloor$). (a) The external current $I_i \equiv 3.0$ is fixed and the internal coupling is normalized to $\sum_{j=1}^{N} \varepsilon_{ij} \equiv -1.1$ (green), -1.5 (blue), -1.75 (black), -1.9 (red), so that the mean firing rate, $< \nu_i >$, of the single neurons stays approximately constant for each curve. We observe an exponential increase of the mean transient length, $< t_r >$, with network size. The inset shows the fast increase of the transient length with inhibitory coupling strength; in this figure $N = 100$, $I_i \equiv 3.0$. (b) Also for a fixed normalization and different external currents $I_i \equiv 2.5$ (red), 3.0 (black), 3.5 (blue) there is an exponential increase of $< t_r >$. The inset shows the transient length for $N = 100$ dependent on the external current I_i. With increasing external current the transient length decreases. This is consistent with the results in subfigure (a): the transient length increases when the internal inhibition increases relative to the external current. (c) The transient lengths t_r are broadly distributed. The histogram shows the number of transients lengths h_{t_r} per bin found in 2500 trials ($N = 100$, $I_i \equiv 3.0$, $\sum_{j=1}^{N} \varepsilon_{ij} \equiv -1.5$).

the internal interactions $\sum_{j=1}^{N} \varepsilon_{ij}$ constant. Thus, on average, each neuron receives a constant effective input independent of N and the mean firing rate of a single neuron ν_i is approximately conserved. Fig. 6.8a,b shows the increase of transient lengths with N for different internal normalizations $\sum_{j=1}^{N} \varepsilon_{ij}$ and different external currents I_i respectively. We observe an exponential increase of the mean transient length with network size N and no qualitative change compared to the weakly diluted case which confirms a conjecture in [208]. If the network is in the balanced state (cf. Fig. 6.1), the stable transients typically dominate the network dynamics over large time scales and the periodic attractor becomes less important.

6.7 Robustness and transition to chaos

In the following we will check the robustness of our results. The considerations above hold for networks with inhibitory interactions with infinitesimal synaptic time constants. We investigate the influence of excitatory interaction and of synap-

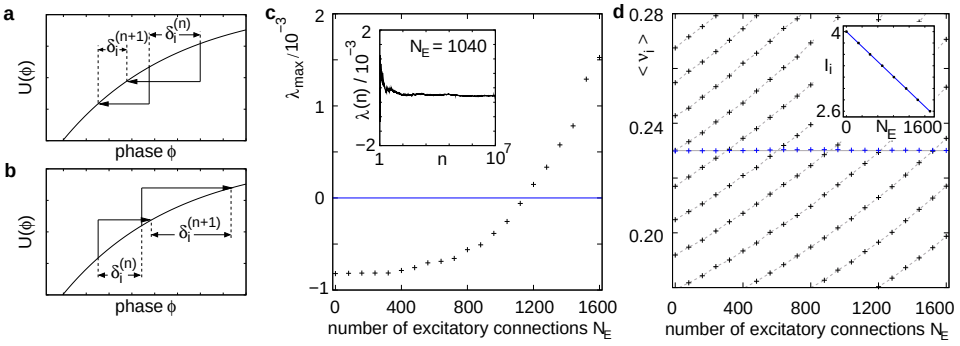

Figure 6.9: Destabilizing effect of excitation. (a) Receiving an inhibitory input decreases the phase shift. (b) Receiving an excitatory input increases the phase shift. (c) Largest Lyapunov exponent measured for an increasing fraction of excitatory neurons starting with the network of Fig. (6.1)a-c and ending with the network of Fig. (6.1)d-f. (d) Average firing rates of a single neuron $< \nu_i >$ versus number of excitatory connections in the network. The neurons' firing rate stays almost constant, if we reduce the external current linearly with the number of excitatory neurons (blue crosses for $< \nu_i > \approx 0.23$). Inset displays current strength needed to maintain network frequency $< \nu_i > \approx 0.23$. (Further details see text.)

tic currents with finite duration. For small deviation from the networks considered above the stability properties are similar, for large fractions of excitatory neurons and large temporal extent of synaptic currents, we observe a transition to a chaotic regime. For temporally extended synaptic currents we assume that after a neuron is reset all previous input is lost. Therefore, the state of a neuron is specified by its last spike time and the spikes it has received afterwards. The phase representation is thus not meaningful anymore and we track two trajectories by comparing the differences in the last spike time of the neurons and in the spike arrival times since the last spikes. To keep the section consistent, we adopt this view when studying the Lyapunov exponents of the excitatory dynamics.

Excitation

We have shown that in networks with purely inhibitory interactions trajectories underlying irregular spiking dynamics are typically stable. If the connection between two neurons is excitatory, the phase shift of the postsynaptic neuron after the interaction may exceed its previous shift and the shift of the received spike. Fig. 6.9a,b gives an illustration: A spike is simultaneously received in the perturbed and in the unperturbed dynamics. The phase shift before and after application of the transfer function $H_\varepsilon^{(i)}(\phi)$ is shown for (a) an inhibitory input (cf. Eq. (6.3) and (6.4)) and (b) and excitatory input. For inhibitory input the phase shift $\delta_i^{(n)}$ is reduced, this leads to the stable dynamics in purely inhibitorily coupled networks.

The effect of excitation is destabilizing. The phase shift $\delta_i^{(n)}$ can increase when a spike is received, the perturbations can grow.

The inverse of $U_i(\phi)$ is monotonically increasing with ϕ, therefore we find for a given $\varepsilon > 0$

$$H_\varepsilon^{(i)}(\phi) = U_i^{-1}(U(\phi) + \varepsilon) > U_i^{-1}(U_i(\phi)) = \phi. \tag{6.61}$$

In contrast to Eq. (6.20) the derivative of the transfer function $H_\varepsilon^{(i)}(\phi)$ is bounded from below by

$$\frac{dH_\varepsilon^{(i)}(\phi)}{d\phi} = \frac{U_i'(\phi)}{U_i'\left(H_\varepsilon^{(i)}(\phi)\right)} > 1. \tag{6.62}$$

(cf. sec. 5.11). This destabilizes the trajectory, because for the upper bound of $c_{ij}^{(n)}$, $c_{\max} < 1$ (cf. Eq. (6.21)) does not hold. However, in a network with a small fraction of excitatory connections, the trajectory is still stable. At an interaction the perturbation may increase, but the stabilizing effect of inhibitory inputs dominates the dynamic. We study the transition from the stable regime to chaotic dynamics (a discussion of the chaotic dynamics in networks with purely excitatory interactions can be found in [209]). When increasing the number of excitatory couplings, we increase the mean effective input current to the neurons. Thus we additionally decrease the external input I_i to keep the network rate ν constant. Indeed, in good approximation, the current has to be decreased linearly with N_E, the number of excitatory connections $I_i \equiv I - kN_E$ where I is the original input current.

To quantify the transition we estimate the largest Lyapunov exponent of the system: At the nth event, we denote with $n - W(n)$ the earliest event which still influences the future dynamics of the system explicitly. We apply an initial perturbation of size $\|\Delta_0\|_\infty$ to the event times $t_0, t_{-1}, \ldots, t_{-W(0)}$, where

$$\Delta_n = (\Delta t_n, \Delta t_{n-1}, \ldots, \Delta t_{n-W(n)}) \tag{6.63}$$

is the perturbation vector at the nth event time and Δt_i is the perturbation of t_i. We evolve the system and rescale the perturbation vector Δ_n by a_n after each event, so that the rescaled perturbation vector is of the same size as the initial perturbation, $\|\Delta_n'\|_\infty = \|\Delta_n \cdot a_n\|_\infty = \|\Delta_0\|_\infty$. The largest Lyapunov exponent, $\lambda_{\max}$, is then given by

$$\lambda_{\max} = \lim_{n\to\infty} \lambda(n) \quad \text{with} \quad \lambda(n) := \frac{1}{n}\sum_{i=1}^{n} \ln(a_i^{-1}). \tag{6.64}$$

We observe a transition from a stable to a chaotic regime, characterized by a positive Lyapunov exponent. For small fraction of excitatory neurons the dynamics is typically stable, the effect of the inhibitory pulses dominates the dynamics and on average a perturbation does not grow over time. With increasing N_E, the Lyapunov exponent increases until the dynamic becomes chaotic. Of course, in our numerical simulations we can only study finite time Lyapunov exponents with very large n. The chaotic dynamics may thus be transient. However, it dominates the

network dynamics for very long times. Fig. 6.9c,d shows some numerical results: (c) The largest Lyapunov exponent is measured for an increasing fraction of excitatory neurons starting with the network of Fig. (6.1)a-c and finishing with the network of Fig. (6.1)d-f. The number of excitatory neurons is increased by successively choosing one incoming inhibitory connection per neuron to be excitatory. The external current, I_i, is reduced linearly to keep the network rate unchanged according to $I_i \equiv I - kN_E$, where $I = 4.0$ is the initial external current, $k \approx 0.05$ and N_E is the number of excitatory neurons. For a larger fraction of excitatory couplings we observe a transition to an unstable,chaotic regime. The inset demonstrates the convergence of $\frac{1}{n}\sum_{i=1}^{n} \ln(a_i^{-1}) \to \lambda_{\max}$(exemplary shown for $N_E = 1040$). (d) Average firing rate of a single neuron $< \nu_i >$. For a constant external current the rate increases with increasing fraction of excitatory neurons (black crosses, for $I_i = 2.6, 2.8, 3.0, 3.2, 3.4, 3.6, 3.8, 4.0, 4.2, 4.6$). The neurons' firing rate stays almost constant if we reduce the external current linearly with the number of excitatory neurons (blue crosses). We determined the value of N_E at the intersection point of the $< \nu_i >$ versus I_i curves with the desired frequency by linear interpolation. The values (I_i, N_E) that give rise to the desired frequency lie in good approximation on a straight line with slope $-k \approx -0.05$ (cf. Inset to (d)).

The results are particularly remarkable since in mean-field descriptions of balanced networks, as long as the mean input to each cell is the same, the regime where $N_E = 0$ is comparable to the regime where N_E reaches the number of realized couplings (with appropriately reduced external excitatory current I_i).

Temporally extended interactions

Up to now, we considered δ-coupling, where the response to an action potential is instantaneous. However, in biological neuronal systems the postsynaptic current has finite temporal extent. Thus, we investigate the influence of temporally extended interactions. The analysis gets more complicated, because neurons are permanently influenced by incoming signals. In our model we assume that the neuron looses the information about previously received spikes when it reaches the threshold and is reset.

We modify Eq. (6.1) by introducing an temporally extended interaction kernel $g(t)$ (cf. sec. 2.5) so that the evolution of the membrane potential is given by

$$\frac{d}{dt}V_i = f_i(V_i) + \sum_{j=1}^{N}\sum_{k\in\mathbb{Z}} \varepsilon_{ij} g\left(t - t_{jk}^{\mathrm{s}} - \tau_{ij}\right). \tag{6.65}$$

In the following analysis we consider single exponential couplings, $g(t) = \Theta(t) \cdot \beta e^{-\beta t}$ with time scales $\gamma^{-1} > \beta^{-1} > 0$, the time constant of the postsynaptic current is shorter than the membrane time constant (cf. sec. 2.2). As an exemplary neuron model we study the leaky integrate-and-fire neuron, $f_i(V_i) = -\gamma V_i(t) + I_i$, (cf. secs. 2.4, 2.6) but the analysis can be easily extended to more complex neuron models and interaction kernels.

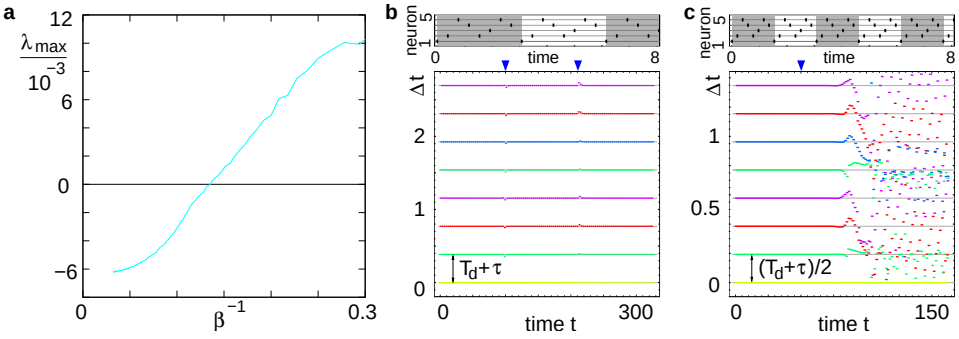

Figure 6.10: Robustness and transition to chaos with increasing temporal extent of the synaptic current. (a) Largest Lyapunov exponent versus time constant of synaptic current. (b) Stable periodic pattern in a network with temporally extended interactions. (c) Time compressed, unstable pattern in a network with temporally extended interactions. (For details see text.)

Numerical simulations show that the stability of the dynamics is robust against introduction of synaptic currents with small temporal extent, but on increase of temporal extension a transition to chaos occurs. In Fig. 6.10, the largest Lyapunov exponent, $\lambda_{\max}$, in a random network ($N = 50$, $|\mathrm{Pre}(i)| \equiv 10$, $\gamma = 1$, $I_i \equiv 4.0$, $\tau = 0.125$, $\sum_j \varepsilon_{ij} \equiv -3.3$, $\tau_{ij} \equiv 0.1$) is estimated in dependence of the decay time constant β of the synaptic current. For small time constant β^{-1}, the dynamics behaves similar to the dynamics in with δ-pulse interactions, in particular it is stable, the largest Lyapunov exponent is negative. For increasing β^{-1} the temporal extension becomes more and more influential and there is a transition to an unstable, chaotic regime with positive largest Lyapunov exponent.

We now study the stability properties analytically. We denote the last spiking time of neuron i before t_n by

$$t_0(n,i) = \max_{k\in\mathbb{Z};\, t_{ik}^{\mathrm{s}} \le t_n} \left(t_{ik}^{\mathrm{s}}\right); \tag{6.66}$$

at $t = t_0(n,i)$ the potential of neuron i was reset to zero. The solution of Eq. (6.65) together with the initial condition $V_i(t_0(n,i)) = 0$ is then given between the nth and $(n+1)$th network event by

$$\begin{aligned} V_{i,n}(t) \quad = \quad & \frac{I_i}{\gamma}\left(1 - e^{-\gamma(t-t_0(n,i))}\right) \\ & + \frac{\beta}{\beta-\gamma} \sum_{j=1}^{N} \sum_{k\in\mathbb{Z}} \varepsilon_{ij} \Theta\left(t_{ijk}^{\mathrm{r}} - t_0(n,i)\right) \Theta\left(t - t_{ijk}^{\mathrm{r}}\right) \\ & \times \left(e^{-\gamma\left(t-t_{ijk}^{\mathrm{r}}\right)} - e^{-\beta\left(t-t_{ijk}^{\mathrm{r}}\right)}\right), \end{aligned} \tag{6.67}$$

where $t_{ijk}^{\mathrm{r}} = t_{jk}^{\mathrm{s}} + \tau_{ij}$ is the reception time of the spike sent at t_{jk}^{s} by neuron j to

neuron i. The sum in Eq. (6.67) takes into account all spikes which are received by neuron i between $t_0(n,i) \leq t \leq t_n$ and therefore influence the potential $V_{i,n}(t)$. In the limit of very short temporal extension of the postsynaptic current, $\beta \to \infty$, Eq. (6.67) becomes a solution of Eq. (6.1). After the nth event, neuron i would reach the threshold at t' under the assumption that there are no further inputs after t_n. According to Eq. (6.67), t' is implicitly given by

$$V_{\Theta,i} - V_{i,n}(A, t = t') = 0, \tag{6.68}$$

where A is the vector of the original event times $t_n, \ldots, t_{n-W}$,

$$A = (t_n, ..., t_{n-W}), \tag{6.69}$$

where we introduced $W = \max_n(W(n))$. To estimate the effect of a small perturbation $\Delta t_n, \ldots, \Delta t_{n-W}$ of the event times $t_n, \ldots, t_{n-W}$ on the hypothetical event time t' we linearize Eq. (6.68) at (A, t'). The Jacobian of t, Dt, with respect to former spike times, $t_n, \ldots, t_{n-W}$, is given by

$$\begin{aligned} Dt\,(A,t') &= \left(\frac{\partial t}{\partial t_n}\,(A,t'), \ldots, \frac{\partial t}{\partial t_{n-W}}\,(A,t') \right) \\ &= -\left(\frac{\partial V_{i,n}}{\partial t}\,(A,t') \right)^{-1} \cdot DV_{i,n}\,(A,t')\,. \end{aligned} \tag{6.70}$$

The linearized estimation of the displacement $\Delta t'$ of t' is then given by

$$\begin{aligned} \Delta t' &\doteq Dt\,(A,t') \cdot \begin{pmatrix} \Delta t_n \\ \vdots \\ \Delta t_{n-W} \end{pmatrix} \\ &= \left(\frac{\partial V_{i,n}}{\partial t}\,(A,t') \right)^{-1} \cdot \sum_{k=n-W}^{n} \left(-\frac{\partial V_{i,n}}{\partial t_k}\,(A,t') \right) \cdot \Delta t_k. \end{aligned} \tag{6.71}$$

The special structure of $V_{i,n}(t)$ (cf. Eq. (6.67)), more precisely the fact that $V_{i,n}(t)$ depends on t via $t - t_k$ for $k = n - W, \ldots, n$, yields the identity

$$\sum_{k=n-W}^{n} -\frac{\partial V_{i,n}}{\partial t_k}\,(A,t') = \frac{\partial V_{i,n}}{\partial t}\,(A,t')\,. \tag{6.72}$$

Under the condition

$$\frac{\partial V_{i,n}}{\partial t_k}\,(A,t') \leq 0 \quad \text{for all}\, k = n - W, \ldots, n, \tag{6.73}$$

we can combine Eq. (6.71) and Eq. (6.72) and find bounds for the the displacement

$$\min_{k=n-W,\ldots n}\,(\Delta t_k) \leq \Delta t' \leq \max_{k=n-W,\ldots n}\,(\Delta t_k)\,. \tag{6.74}$$

Condition (6.73) implies that if neuron i sends or receives a spike earlier, also the threshold is crossed earlier. This always holds for δ-couplings, for interactions with finite temporal extent it restricts the class of patterns as we show below. Eq. (6.74) is an analog to Eq. (6.23), sufficiently small perturbations stay bounded by the initial ones for finite times. This directly implies Lyapunov stability for periodic orbits. For general irregular dynamics and to prove asymptotic stability, the propagation of pulses through the network has to be studied as for the nonlinear stability analysis in the main part.

We now want to specify a class of periodic patterns which are stable in a network with temporally extended synaptic currents. The influences of various events on the $V_{i,n}(A,t')$ are as follows: For an influential spike receiving t_k, Eq. (6.67) yields

$$\frac{\partial V_{i,n}}{\partial t_k}(A,t') = \frac{\beta}{\beta-\gamma}\varepsilon^* \left(\gamma e^{-\gamma(t'-t_k)} - \beta e^{-\beta(t'-t_k)}\right), \tag{6.75}$$

where $\varepsilon^* < 0$ is the coupling strength from the sending neuron. For the last spike sending of neuron i, $t_k = t_0(n,i)$,

$$\frac{\partial V_{i,n}}{\partial t_0(n,i)}(A,t') = -I_i e^{-\gamma(t-t_0(n,i))} < 0. \tag{6.76}$$

For any other event t_k a displacement of t_k has no influence on $V_{i,n}(t)$, here

$$\frac{\partial V_{i,n}}{\partial t_k}(A,t') = 0. \tag{6.77}$$

Therefore, condition (6.73) reduces to a condition on Eq. (6.75) and can be reformulated as

$$t' - t_k > \frac{1}{\beta-\gamma}\ln\left(\frac{\beta}{\gamma}\right) := T_d, \tag{6.78}$$

where t_k are the spikes arrival times at neuron i since the last reset $t_0(n,i)$. This means that the class of patterns where each neuron i does not cross the threshold for a time T_d after receiving a spike are stable. For $\beta \to \infty$ the system tends to the δ - pulse coupled system and indeed T_d vanishes, $\lim_{\beta\to\infty} T_d = 0$ so that any non-degenerate orbit is stable. This is consistent with the nonlinear analysis of chapter 5 and of the previous sections. However, for temporally extended interactions unstable periodic orbits corresponding to non-degenerate patterns exists and also chaotic dynamics is possible (cf. Fig. 6.10a).

To illustrate our analytical findings, in Fig. 6.10b,c, we used a generalization of the method introduced in chapter 4 and designed networks of five neurons with temporally extended couplings ($\beta = 8$, delay $\tau_{ij} = \tau = 0.125$) that realize two predefined spike patterns (upper panel). Both patterns are the same, but with different inter-spike-intervals. In (b) all spikes are separated by $\Delta T = T_d + \tau$, which ensures that a neuron never spikes within a time period T_d after receiving a spike; in (c) we choose the inter-spike-intervals smaller $\Delta T = (T_d + \tau)/2$. The lower panels illustrates the stability properties: The spike times of the different

neurons are plotted relative to the spiking of neuron 1 in vertical direction. The horizontal direction is simulated time, different colors indicate spike times of the five different neurons. At certain points in time (blue arrows) the network dynamics is perturbed. Indeed, in agreement with our analytical findings the dynamics in (b) is stable: After a perturbation of size ≈ 0.2 (maximum norm), the dynamics converge towards the periodic orbit. The dynamics in (c) is unstable: a perturbation of size $\approx 10^{-12}$ leads to a divergence from the unstable periodic orbit.

6.8 Conclusion and outlook

We have shown that generic trajectories which give rise to the irregular balanced state are exponentially stable in purely inhibitory strongly connected networks of neurons with delayed couplings and with infinitesimal synaptic time course.

Analytically, we have shown that the generic irregular dynamics, well described by the Poissonian approximation, is generated by exponentially stable trajectories. The proof is based on the observation that interactions lead to averaging between perturbations. Following the detailed spread of perturbations through a strongly connected network, we have shown that this leads to an exponential decay of perturbations as long as events are not interchanged. Using a Poissonian approximation, we observed that the minimum of the margins between potential future events decays much more slowly, namely algebraically, in agreement with numerical simulations. This allows sufficiently small perturbations to stay smaller than the minimal margin between events and to decay without changing event order and generating a large perturbation. We argued that the dynamics ultimately has to converge to a periodic orbit. In the previous chapter, ch. 5, it was not necessary to show the exponential decay for stable dynamics. This is ultimately a consequence of the existence of a minimal margin in non-degenerate periodic dynamics.

We numerically illustrated and refined our analytical results. For rather small, sparse networks we showed that indeed the dynamics converges to a periodic orbit, the irregular stable transient however grows exponentially with network size so that the transient dynamics dominates for larger networks.

Finally, we studied the robustness of our results against changes in the model numerically and analytically by introduction of excitatory couplings and by introducing finite synaptic decay time constants and specified the transition to chaotic dynamics.

Previous numerical simulations (cf. sec. 6.1) on a subclass of the networks considered were interpreted as suggesting unstable dynamics [76]. In contrast, in simpler networks without coupling delay, stable dynamics was found when numerically investigating weakly diluted or analytically investigating fully connected networks [208, 98]. We have now analytically shown that the dynamics is stable for networks with more general topology and with coupling delay. The results presented allow to explain the mechanisms leading to the numerical observations given in Ref. [76]. Details are given in appendix A.

Our results yield new insights in the balanced state of neural networks which is considered a model for the ground state of cortical dynamics [10]. We have seen that in a large and important class of networks the dynamics is irregular but stable and may thus be predictable (cf. the concept of stable chaos [156, 208]). The consequences of stable irregular dynamics for neural systems, especially computational issues remain to be investigated. Also, it is necessary to find more detailed models with this type of dynamics.

Another interesting direction for future research is to study the large N limit. If the number of inputs stays constant when N tends to infinity (the network becomes arbitrarily sparse) we expect that the size of basin of attraction of the trajectories might not tend to zero since only interchanges of potential future events at a particular neuron causes neighboring trajectories to deviate.

Our results shed new light on irregularity in neural networks which is often associated with chaotic dynamics. In the networks considered, the dynamics is stable. The origin of the highly irregular dynamics has to be further investigated. The fact that in small and in homogeneous networks the dynamics quickly converges to periodic orbits suggests an important role of high dimensionality and network heterogeneities.

Chapter 7

Propagation of synchrony in random neural networks

Recent experiments show that excitatory inputs simultaneously arriving at a neuron can lead to a somatic EPSP that is supra-linearly enhanced compared to the linearly added EPSPs in response to individual inputs [82, 13, 157, 71, 70]. In the following chapter, we study the dynamics of random recurrent networks of spiking neuron models that interact synaptically with dendritic integration that is supra-additive. We replace the commonly used linear and additive coupling of excitatory synaptic inputs by experimentally observed, nonlinear, supra-additive coupling [13, 157, 71, 70]. We find that purely random networks are capable of stably propagating synchronous spiking activity within a recurrent network if the coupling is supra-additive.

Using analytical arguments and numerical simulations, we study conditions for networks with propagating dynamics and the transition from networks with non-propagating dynamics. In a deterministic approximation, upon increasing the strength of non-additivity, a tangent bifurcation creates a stable fixed point for the mean size of a synchronous pulse, enabling propagation. Our results in particular suggest that additional structural features of the network connectivity, such as super-imposed feed-forward structures in 'synfire chains' [3, 83, 54], which have been proposed as a model for the generation of precise spike timing, may not be required for the propagation of synchronous spiking activity and the generation of precise spike timing in recurrent networks.

7.1 State of the art

A famous model for the propagation of synchrony through neural networks are 'synfire chains'. Synfire chains consist of groups of neurons that are feedforwardly connected via excitatory connections to a chain. When these feedforward structures

are embedded in an otherwise random network, they allow synchronous activity to successively propagate from one group in the chain to the next [3, 83, 54, 18]. A related modeling study investigated if strengthening of already existing connections in a random network could lead to propagation of synchrony in networks of leaky integrate-and-fire neurons with temporally extended synaptic currents. While firing rate signals propagate over six groups of neurons when the connecting excitatory synapses are significantly strengthened (by a factor of $12-16$ compared with other connections), this does not lead to propagation of precise synchrony since the strong excitatory connections lead to multiple spikes in response to synchronous pulses and thus to lengthening of pulse packets. Propagation of synchrony over six groups of neurons can be achieved by strongly increasing synapse strength (factor 30) and additionally decreasing the responsiveness of neurons within the groups (factor 10 compared to neurons that do not belong to a group) [201].

Several models for neurons exist that incorporate nonlinear dendritic interactions. There are highly detailed multi-compartment models of neurons in CA1, that reflect the detailed morphology and ion channel distribution of neurobiological neurons [13, 153, 71]. These models also show dendritic spikes and the response properties agree with those of neurobiologically recorded neurons. Also more abstract models suited for studies in discrete time and in rate models have been derived (e.g. [127, 128, 130, 129, 12, 154]). In the two-layer model of synaptic integration, segments of the dendritic tree act as separate thresholded sub-units. The outputs of these subunits are gathered in a second layer and thresholded to produce the overall response of the cell. (The extension to the multi-layer model with more than two layers is straightforward.) For sigmoidal threshold functions that act on linearly summated inputs, this simple model predicts the rate response properties of a highly detailed compartmental model very well [154]. Also the computational abilities of dendritic nonlinearity in different neural microcircuits have been studied (e.g. [130, 12], cf. [129, 112] for reviews). However, up to now, no spiking single compartment model that incorporates nonlinear dendritic enhancement has been established and there is no study about the influence of nonlinear dendritic interactions on the dynamics of recurrent spiking neural networks.

7.2 The model

How can we incorporate non-additive coupling in single compartment spiking neural network models? Non-additive coupling due to fast dendritic spikes is observed for synchronous inputs, where 'synchronous' means 'with time difference of about 2ms or less' [13]. We idealize this by considering *exactly* synchronous inputs, i.e. spikes that arrive at identical times.

Usually, the input strength due to several exactly synchronous inputs is considered to be the sum of the input strengths of the individual inputs (cf. sec. 4.4). We model nonlinear enhancement and saturation by modulating the linearly summed strengths of excitatory inputs with a nonlinear, sigmoid-like function σ

(cf. [128, 129, 154]). We further assume that the synapses have infinitesimal time course and that the delay τ between spike sending and somatic response is constant for all neurons. In particular, firing due to supra-threshold excitation occurs precisely after the delay time τ. These assumptions are appropriate for the description of neurons with fast dendritic spikes: Action potentials mediated by fast dendritic spikes [13] occur $\tau = 5$ms after stimulation with sub-millisecond inter- and intra-neuronal jitter while the action potential timing strongly varies in time if no dendritic spike is elicited. Indeed, the supra-threshold excitation of interest in our model network will mostly be due to nonlinearly enhanced excitatory inputs. Further, we will include a constant input current guaranteeing that spiking does not only occur due to supra-threshold excitation and thus also imprecise responses exist.

Since the synaptic currents have infinitesimal time course, precisely synchronous spiking and receiving occurs in the networks. If a neuron sends a spike, due to the constant delay, all postsynaptic neurons will receive the input at the same time. If two of the postsynaptic neurons receiving an excitatory input are sufficiently close to the threshold, the input can be supra-threshold for both neurons, and they fire simultaneously. The generated spikes in turn simultaneously arrive at the postsynaptic targets and neurons postsynaptic to both sending neurons receive exactly synchronous inputs.

In general, if a group of neurons fires simultaneously, a subset of neurons in the network will receive spikes precisely after the delay time τ. The neurons for which this input is supra-threshold fire simultaneously and thus can in turn excite a further group and so on. In this way, chains of synchronous pulses occur in the network. We consider chains generated by stimulating an initial group of neurons to fire simultaneously and analyze their evolution. We will see that they quickly die out (i.e. the pulse-sizes decay to the level of spontaneously synchronous pulses) in linearly coupled random networks. In contrast, in nonlinear coupled random networks with similar parameters, they can persist embedded in the background activity.

To allow for theoretical predictions based on the diffusion approximation, sec. 2.10, in this chapter we specialize on networks of leaky integrate-and-fire neurons introduced in sec. 2.6. The scheme of incorporating nonlinear coupling in the networks by modulating precisely synchronous inputs is of course applicable to any network model with instantaneous synaptic coupling, in particular to networks of Mirollo-Strogatz neurons (ch. 3) and we expect the described effects of nonlinear coupling to be largely independent of the neuron model.

We consider recurrent random networks of N leaky integrate-and-fire neurons. The probability for the existence of a directed synaptic coupling between two neurons is p_0, the probabilities for the coupling being excitatory and inhibitory are p_{Ex} and $p_{\mathrm{In}} = 1 - p_{\mathrm{Ex}}$, respectively. The dynamics of the membrane potential V_l of neuron l in a network with linear coupling is given by Eq. (2.18). We now collect

the spike events into pulses of simultaneously sent spikes and rewrite Eq. (2.18) as

$$\frac{dV_l(t)}{dt} = -\gamma V_l(t) + \sum_{f\in\mathbb{Z}} \sum_{j\in M(f)} \varepsilon_{lj}\delta(t - t^f - \tau) + I_0, \tag{7.1}$$

where f labels the sending times in the network and t^f is the network's fth sending time. Further, we introduced the set $M(f)$ collecting the neurons sending a spike at the fth sending time,

$$M(f) = \{j : \exists n : t^{\mathsf{s}}_{jn} = t^f\}, \tag{7.2}$$

where t^{s}_{jn} are the spike times of neuron j. As in the preceding chapters, the inverse membrane time constant $\gamma = 1/\tau_{\text{mem}}$ measures the dissipation of the system, ε_{lj} is the coupling strength from neuron j to neuron l and τ the transmission delay. Each neuron receives some constant external input I_0. When the membrane potential reaches or exceeds the threshold, $V_l(t^-) \geq \Theta$, it is reset to $V_l(t) = V_{\text{r}}$. We now introduce the sets $M_{1,l}(f)$, collecting the spikes sent at t^f that have an excitatory effect on neuron l, and $M_{2,l}(f)$, collecting the spikes sent at t^f that have an inhibitory effect on neuron l,

$$M_{1,l}(f) = \{j : (\varepsilon_{lj} > 0 \wedge \exists n : t^{\mathsf{s}}_{jn} = t^f)\}, \tag{7.3}$$
$$M_{2,l}(f) = \{j : (\varepsilon_{lj} < 0 \wedge \exists n : t^{\mathsf{s}}_{jn} = t^f)\}. \tag{7.4}$$

Introducing these definitions, Eq. (7.1) reads

$$\begin{aligned}\frac{dV_l(t)}{dt} =& -\gamma V_l(t) \\ &+ \sum_f \Big[\sum_{j\in M_{1,l}(f)} \varepsilon_{lj} + \sum_{j\in M_{2,l}(f)} \varepsilon_{lj}\Big]\delta\left(t - t^f - \tau\right) + I_0.\end{aligned} \tag{7.5}$$

Since inhibition and excitation often act at different places at a single neuron, we assume that the inhibition has no influence on the nonlinear dendritic effects. We further do not account for the influence of synaptic position on the nonlinear dendritic interactions. This influence can be strong due to the diversity of dendritic branches [157]. We consider model neurons with one nonlinear dendrite where the excitatory contacts of the presynaptic neurons considered end and nonlinearly interact. The nonlinear coupling is modeled by a nonlinear function σ which modulates the total excitatory input,

$$\begin{aligned}\frac{dV_l(t)}{dt} =& -\gamma V_l(t) \\ &+ \sum_f \Big[\sigma\Big(\sum_{j\in M_{1,l}(f)} \varepsilon_{lj}\Big) + \sum_{j\in M_{2,l}(f)} \varepsilon_{lj}\Big]\delta\left(t - t^f - \tau\right) + I_0\end{aligned} \tag{7.6}$$

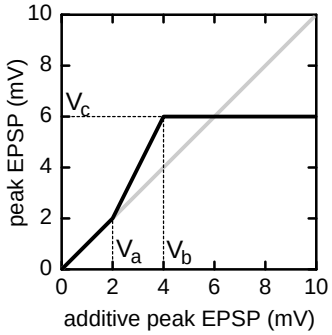

Figure 7.1: Sigmoidal dendritic summation function. The interaction function maps the somatic peak EPSP expected for additive interaction of inputs to the actual peak EPSP strength. Due to the presence of fast dendritic spikes (cf. sec. 2.1), there is nonlinear enhancement of inputs when the input strength passes a threshold V_a. The values for V_a, V_b and V_c are chosen in agreement with biological data [157].

which reduces for $\sigma(\varepsilon) = \varepsilon$ to the usual leaky integrate-and-fire network model with linear additive coupling. Interestingly, the function σ can be directly read off the experimental literature. Due to the infinitesimal rise time of the membrane potential in response to arriving spikes, the coupling strength of some excitatory coupling ε_{lj} equals the peak excitatory postsynaptic potential (EPSP) in a stimulation paradigm where all other inputs, in particular I_0, are set to zero. Also, since our model is current based and linear in V_l, the sum of the EPSPs in response to separate inputs $\varepsilon_1, ..., \varepsilon_n$ equals the EPSP in response to one input with strength $\varepsilon_1 + ... + \varepsilon_n$. The nonlinear coupling function σ now has a straightforward interpretation: It maps the peak EPSP strength expected from linearly adding the coupling strengths $\sum_{j \in M_{1,l}(f)} \varepsilon_{lj}$ to the actual value. This is given in instances of experimental literature as characterization of nonlinear dendritic enhancement [157]. The function $\sigma(\varepsilon)$ was experimentally found to have a sigmoidal shape, a linear part with slope one for small values of ε and saturation at high values. We thus model the non-additive coupling by a linear behavior $\sigma(\varepsilon) = \varepsilon$ at low values $\varepsilon \leq V_a$, a constant saturation $\sigma(\varepsilon) = V_c$ at high values $\varepsilon \geq V_b$, and linearly interpolate σ between these values, cf. Fig. 7.1. If not stated otherwise, the parameters used in the examples below are $V_a = 2$mV for the onset of supra-additivity, $V_b = 4$mV for the onset of saturation and $V_c = 6$mV for the level of saturation, in agreement with experimental measurements[1] [157]. The network parameters are $N = 1000$, $p_0 = 0.3$, $p_{\text{Ex}} = p_{\text{In}} = 0.5$, $\tau_{\text{mem}} = 8\text{ms} = 1/\gamma$, $\tau = 5$ms, $I_0 \tau_{\text{mem}} = 17.6$mV,

[1] The values orient at [157] derived for slow dendritic spikes. In [13], the onset of nonlinearity and the level of saturation lie higher, the values are used in ch. 8. Employing different parameter values does not change the qualitative results of the recent chapter.

$\Theta = 16\text{mV}$, $V_\text{r} = 0\text{mV}$ and $\varepsilon_{lj} = 0.2\text{mV}$ if the coupling from neuron j to neuron l is excitatory and $\varepsilon_{lj} = -0.2\text{mV}$ if it is inhibitory. Isolated neurons show spiking with period $T_{0,l} \approx 19.2\text{ms}$.

7.3 Synchrony in linearly and non-linearly coupled networks

At time t_0, we excite a group of neurons with size g'_0 to fire synchronously. This may cause a subgroup of the neurons which are postsynaptic to group 0 to fire an exactly synchronous pulse since they receive supra-threshold excitation. These neurons in turn potentially cause a subgroup of their postsynaptic neurons to synchronously fire etc. We study the chains of firing events resulting from this mechanism. Due to the identical coupling delays τ and the infinitely short rise time of the EPSPs, such a chain can be easily separated from background activity: The g'_k members of the kth pulse are the only neurons to fire precisely at $t_0 + k\tau$, $k \in \mathbb{N}$.

First, we consider the propagation of synchronous pulses in networks with purely linear, additive coupling. For such networks, we find that chains of synchronous spiking activity rapidly die out, i.e. the pulse-sizes reduce to the level of spontaneous synchronization, cf. Fig. 7.2, 7.4, consistent with previous studies [54, 201].

In a nonlinearly coupled network, for a broad set of parameters V_a, V_b, V_c, propagation of synchrony is stable. A chain started with a large enough, but not too large pulse-size can persist for a long time. After a few steps the pulse-sizes reach a level where they fluctuate around some mean value (cf. Fig. 7.3). Spontaneously synchronized pulses are small and do not reach the size-threshold for stable propagation.

This stable propagation of synchrony can be intuitively understood. Small pulses behave as for linear, additive coupling, i.e. the chains usually die out after a few steps and do not give rise to larger pulses. Thus, the probability for larger pulses to occur spontaneously is sufficiently small so that the background activity is stable. If a larger initial pulse is excited, e.g. by external stimulation, postsynaptic neurons get sufficient excitatory input so that the nonlinearity becomes effective. Since inhibition only increases linearly, the number of postsynaptic neurons for which excitation dominates is larger than in the linearly coupled networks. This causes more neurons to fire in response to the pulse. For pulses with certain sizes g', the mean number of neurons usually firing in response to it can then exceed g' so that the number of neurons synchronized in each step of the chain grows. However, if the pulse-size becomes too large, saturation of the excitatory inputs sets in while inhibition still grows. Thus the size of the responding neuron group decays. Additionally, if the membrane time constant τ_mem is larger than the transmission delay τ, neurons that were active in the previous pulse are in a relative refractory period when the spikes arrive. Indeed, in Figs. (7.2, 7.3) neurons firing synchronously at t_0 do not send spikes at $t_0 + \tau$. So the number of neurons able to respond decreases if the previous pulse grows. Taken together, the pulse-size

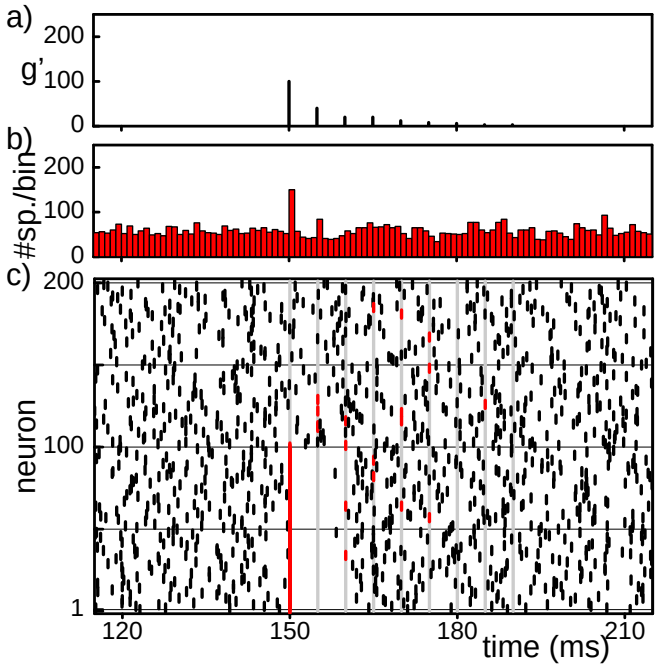

Figure 7.2: Synchrony does not propagate in networks of linearly coupled neurons. Panel (c) shows the spiking activity of the first 200 neurons in a network of 1000 neurons (parameters of the network, see text) versus time. A chain of synchronous pulses is initiated by applying external supra-threshold inputs to the first 100 neurons at time $t_0 = 150$ms. Red colored spikes are sent as part of a synchronous pulse within the chain. Gray lines indicate the times $t_0 + k\tau$, $k \in \{0, ..., 8\}$, where pulses of the chain of size larger than zero are present. The decay of pulse-sizes is illustrated by part (a), showing the size of pulses isolated from the background activity. (b) displays the number of spikes per bin of 1ms taken over the entire network. Only for the first two pulses the spike rate (measured per bin of 1ms) is enhanced due to presence of large synchronous pulses and the pulse activity is distinguishable from background activity.

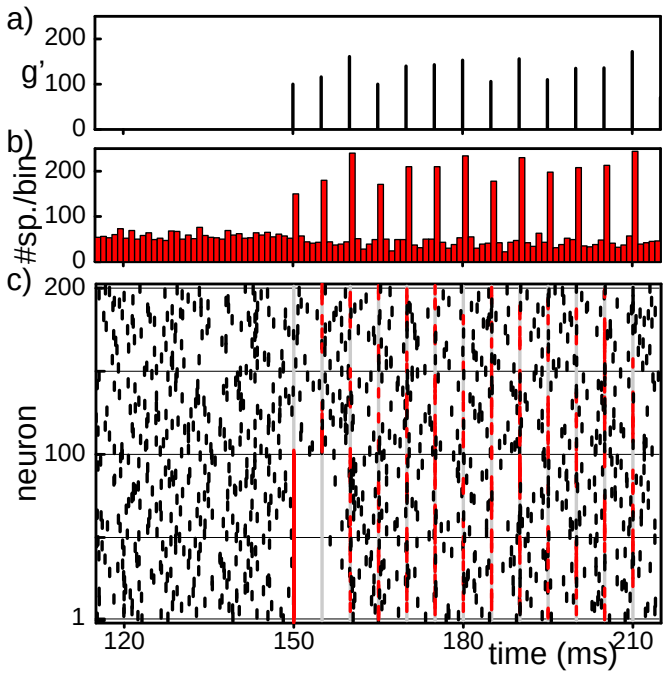

Figure 7.3: Synchrony propagates in networks with supra-additive coupling. Panel (c) shows the spiking activity of the first 200 neurons in a network of 1000 neurons (parameters see text). At time $t_0 = 150$ms a synchronous pulse of 100 neurons is initiated by external supra-threshold inputs. The pulse-sizes of the initiated chain are illustrated in part (a) of the figure. (b) The presence of larger synchronized pulses is reflected by changes in the network rate. The histogram displays the number of spikes sent per bin of 1ms. (See Fig. 7.2 for further description).

within the chain can stay stably within a certain range of pulse-sizes g'.

7.4 Analysis of propagating and non-propagating states

We studied the evolution of pulse-sizes numerically and analytically. Numerically, we measured $P(g_{i+1}|g_i)$, with random variables g_{i+1}, g_i, $i \in \mathbb{N}_0$, describing the pulse-sizes and assuming values in $\{1, ..., N\}$. $P(g_{i+1} = g'_{i+1}|g_i = g'_i)$ is the probability that the ith pulse with g'_i simultaneously firing neurons causes a pulse of g'_{i+1} neurons to fire simultaneously in response [144, 7]. From the conditional probabilities, the mean size of a pulse following a pulse of size g'_i can be derived, i.e. the conditional expectation

$$E(g_{i+1}|g_i = g'_i) = \sum_{j=1}^{N} jP(g_{i+1} = j|g_i = g'_i). \tag{7.7}$$

Both in networks of linearly and nonlinearly coupled neurons, the distributions of transition probabilities between the sizes g_0 and g_1 of the initial and the first pulse (Figs. 7.4, 7.5) are qualitatively similar to the transition probabilities between sizes of later pulses. Further, they are expected to approximately fulfill the Markov property. As an example, Fig. 7.6a,b,e show the transition probabilities $P(g_2 = g'_2|g_1 = g'_1, g_0 = g'_0)$ for different values of g'_0. Indeed, the probability distributions are largely independent from g'_0, $P(g_2|g_1 = g'_1, g_0 = g'_0) \sim P(g_2|g_1 = g'_1)$.

In general, neurons participating in pulse $i-1$ are close to being equilibrated, i.e. the probability density of their membrane potential $P(V)$ is close to the one of non-participating neurons, when the spikes from pulse i arrive. This is a consequence of the choice of parameters τ and γ and the balance between excitation and inhibition (We note that total excitation dominates due to the presence of supra-threshold input current I_0 to each neuron). If $\tau_{\text{mem}} = 1/\gamma$ approaches $k\tau$ with $k = 2$, sizes of earlier pulses influence the transition probabilities from g_i to g_{i+1} since neurons firing in earlier pulses are still relatively refractory and not excitable.

The results displayed in Fig. 7.6 were derived initiating synchronous pulses of size g'_0, twice (with different initial conditions and at different times t_0) in 1500 different random networks. In Fig. 7.6a,c,e, only a section of the transition matrix is displayed since stimulation of an initial pulse of size g'_0 evokes responses with the rather localized probability distribution $P(g_1|g_0 = g'_0)$ (g_1 cannot be predefined). In contrast, the probability distributions $P(g_{10}|g_0 = g'_0)$ are better extended over the interval of interest so that Fig. 7.6b,d,f shows the entire distribution in the interval of interest. In Fig. 7.6b, chains that already decayed to the level of spontaneous synchronization lead for larger g'_{10} to sparser data for $P(g_{11}|g_{10} = g'_{10})$. The figure shows that the transition probabilities are still qualitatively similar to $P(g_1|g_0 = g'_0)$ despite the fact that the presence of large synchronous pulses of course influences

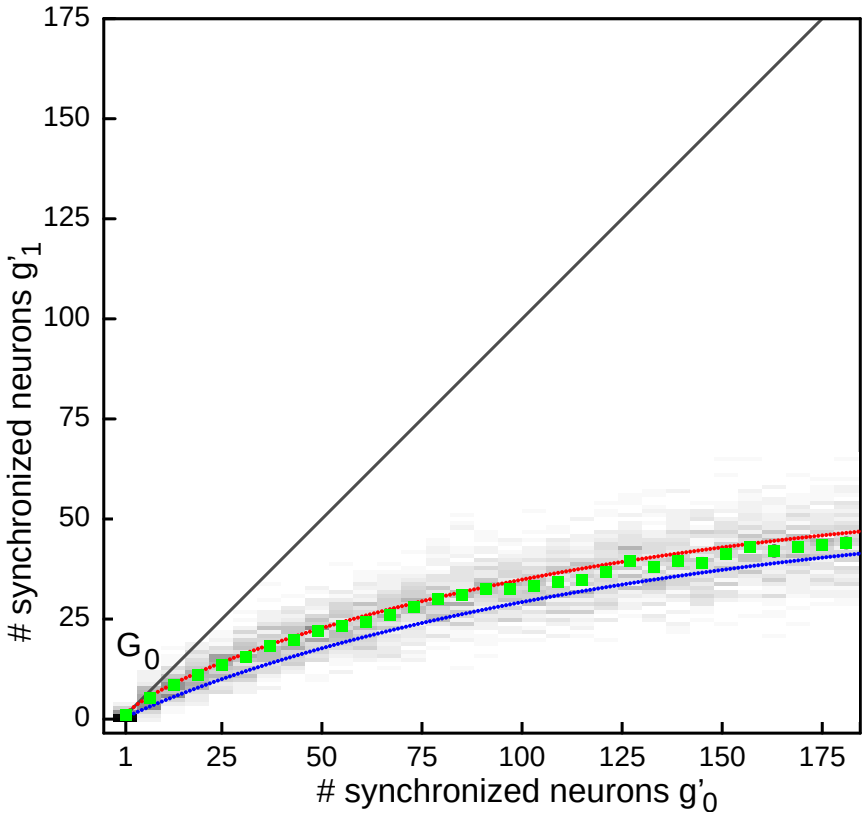

Figure 7.4: Evolution of synchronous pulses in linearly coupled networks. Probability distributions $P(g_1|g_0 = g_0')$, i.e. distribution of pulse-size g_1 at $t_0+\tau$ in response to a pulse of size $g_0 = g_0'$ and mean responses $E(g_1|g_0 = g_0')$ (green squares) are plotted against the initial pulse-size. Error of the mean (2σ-confidence interval) has the size of the plot symbol. Numerical results were derived by initiating synchronous pulses of size $1, 7, 13, ..., 181$, twice (with different initial conditions and at different times t_0) in 50 different random networks (parameters as in Fig. 7.2). An analytical result for $E(g_1|g_0)$ derived from diffusion approximation is given by the blue dots. The result of a semi-analytical approach (see text) is given by red dots. Under stationary and Markovian assumption this representation can be interpreted as a statistical iterated map, i.e. as the transition matrix of a homogeneous Markov chain (cf. 2.9). There is no area from where the pulse-sizes do not quickly converge with high probability to the level of spontaneously synchronized neuron groups.

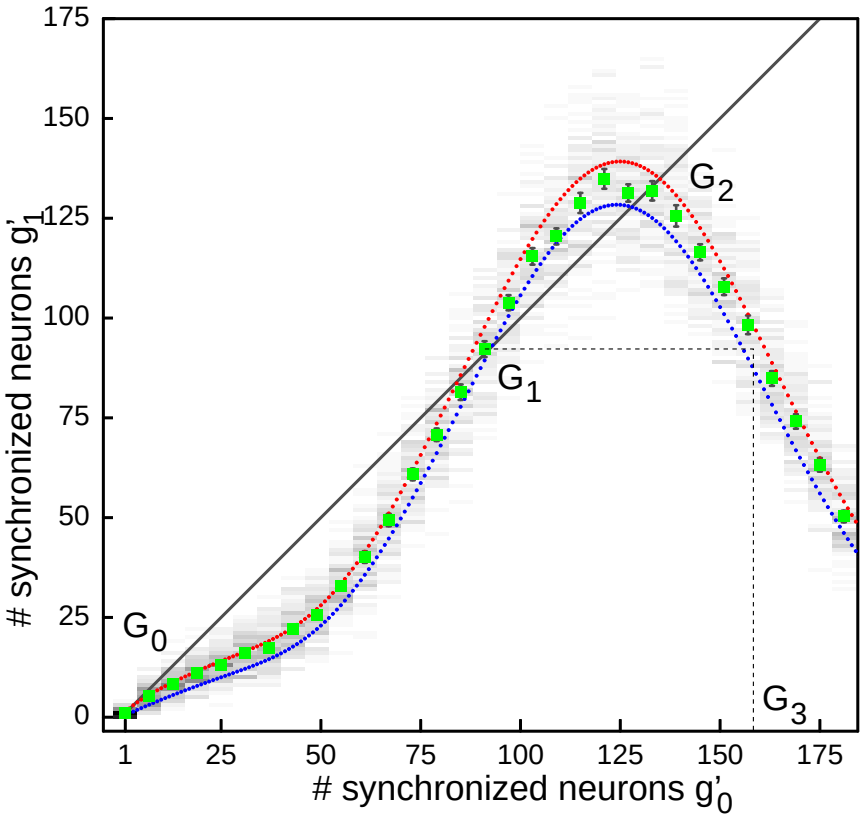

Figure 7.5: Evolution of synchronous pulses in nonlinearly coupled networks. Probability distributions $P(g_1|g_0 = g_0')$, and mean responses $E(g_1|g_0 = g_0')$ (green squares) are plotted against the initial pulse. Numerical results were derived by initiating synchronous pulses of size $1, 7, 13, ..., 181$, twice (with different initial conditions and at different times t_0) in 50 different random networks (parameters as in Fig. 7.3). An analytical estimate derived from diffusion approximation and connectivity properties of the random network for $E(g_1|g_0)$ is given by blue dots. Red dots give the values derived from a semi-analytical approximation. In contrast to Fig. 7.4, the probability for chains with pulse-sizes between G_1 and G_3 to converge to the level of spontaneously synchronized pulses is rather low (see also Fig. 7.6): There is a stable propagating state in the network.

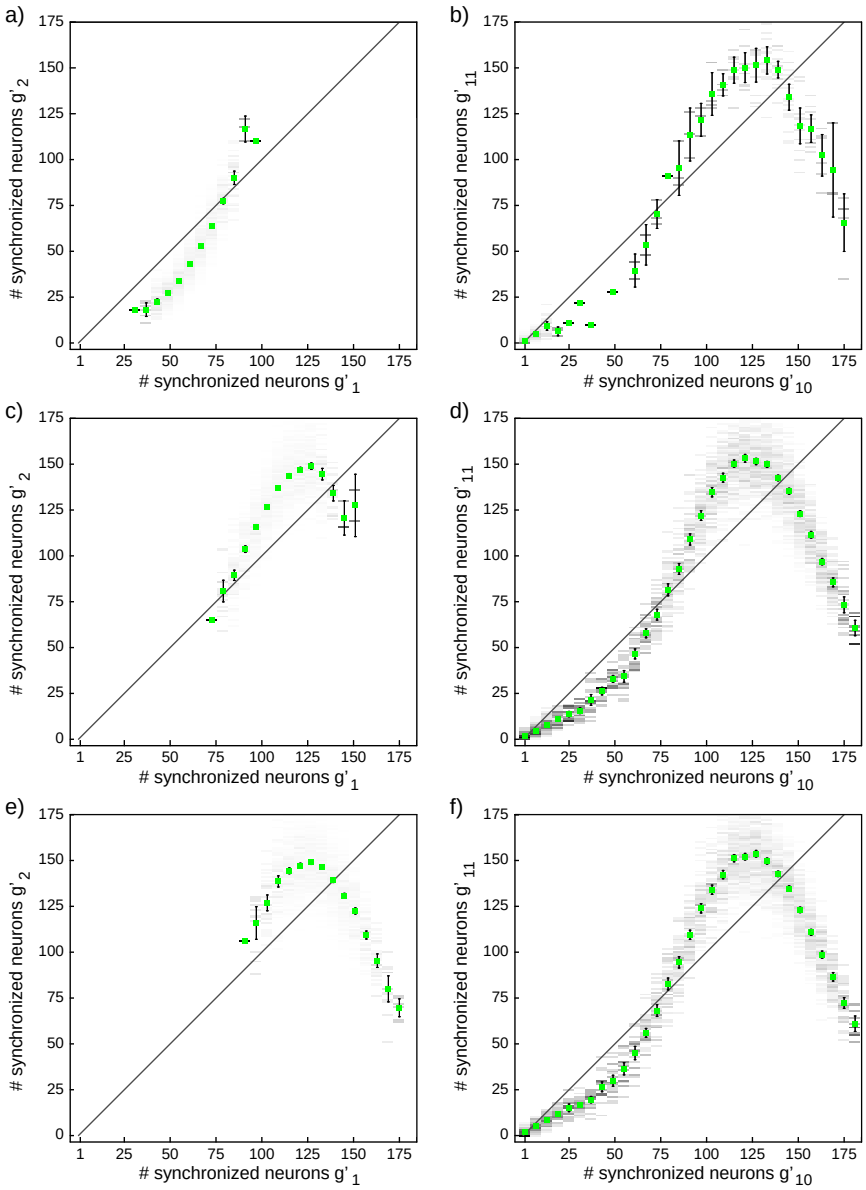

Figure 7.6: Later evolution of synchronous pulses in nonlinear networks. Panels a,c,e: Section of the transition matrix $P(g_2 = g_2'|g_1 = g_1', g_0 = g_0')$ from pulse 1 to pulse 2 for fixed values of g_0', (a) $g_0' = 75$, (c) $g_0' = 100$, (e) $g_0' = 125$ (gray shaded) and conditional expectations $E(g_2|g_1 = g_1', g_0 = g_0')$ (green boxes). Panels b,d,f: Transition matrix $P(g_{11} = g_{11}'|g_{10} = g_{10}', g_0 = g_0')$ from pulse 10 to pulse 11 for fixed values of g_0', (b) $g_0' = 75$, (d) $g_0' = 100$, (f) $g_0' = 125$ (gray shaded) and conditional expectations $E(g_{11}|g_{10} = g_{10}', g_0 = g_0')$ (green boxes). Errors of the conditional expectations (2σ confidence interval) are highlighted by error bars.

the overall network dynamics. Indeed, quantitatively, there are differences: The pulse-sizes are shifted to larger values.

For the first steps of evolution, $E(g_1|g_0)$ and $P(g_1|g_0)$ yield a good understanding of the mechanism that leads to stable propagation of synchronization (cf. also sec. 7.6). For networks of linearly coupled neurons, each pulse of $g_0' \geq G_0 \approx 4$, where G_0 is the intersection point of the interpolated $E(g_1|g_0 = g_0')$-values with the diagonal (cf. Fig. 7.4), excites on average pulses with smaller size. Indeed, due to similarity of transition matrices in later steps, all such pulses die out quickly. Also for different network parameters investigated, the shape of the curve stays the same. Increase of excitation for example only shifted G_0 to higher values, which could lead to instability in the background dynamics (every spike evokes a chain of large synchronous pulses) but not to propagation of synchrony in front of a stable background of asynchronous spikes. In contrast, in networks of nonlinearly coupled neurons there can be a zone of propagation where chains with larger pulse-sizes persist. These are roughly bounded by the second intersection point with the diagonal G_1 and by G_3 (cf. 7.5). Pulses with size between G_1 and G_2 are expected to lead to responses between G_1 and G_3. Pulses with size between G_1 and G_3 are expected to evoke pulses with size between G_1 and G_3 again. However, if the probability distribution allows pulses between G_1 and G_3 to assume values larger than G_3 with sufficiently high probability, the chains will die out rather quickly: Pulses with sizes larger than G_3 typically evoke pulses with sizes smaller than G_1 and these have a high probability to decay to zero. Thus, the emergence of a narrower peak in $E(g_{i+1}|g_i = g_i')$ shifted to higher values as seen for later stages of evolution (cf. Fig. 7.6) can promote dying out of chains if it becomes too pronounced.

7.5 Analytical derivation of the transition probabilities

The analytical derivation of $P(g_{i+1}|g_i)$ is based on the diffusion approximation in the large N limit (in particular, we did not consider quenched disorder, i.e. differences between neurons due to network heterogeneity). We approximate the inputs from background activity with Poissonian spike trains. Then, no simultaneous spikes occur due to background activity and therefore no nonlinear enhancement of inputs. In this approximation, the mean and the variance of the input are given by Eqs. (2.20, 2.21). Taking the constant external input current into account and rewriting the equations in the notation of this chapter, yields for the mean input and its variance

$$\mu = I_0 + p_0 N \nu (p_{\mathrm{Ex}} \varepsilon_{\mathrm{Ex}} + p_{\mathrm{In}} \varepsilon_{\mathrm{In}}), \tag{7.8}$$

$$\sigma^2 = p_0 N \nu (p_{\mathrm{Ex}} \varepsilon_{\mathrm{Ex}}^2 + p_{\mathrm{In}} \varepsilon_{\mathrm{In}}^2), \tag{7.9}$$

where ν is the network frequency, that is determined by the self-consistency equation Eq. (2.30),

$$1 = \nu \frac{\sqrt{\pi}}{\gamma} \int_{\frac{\gamma V_r - \mu}{\sqrt{\gamma}\sigma}}^{\frac{\gamma \Theta_U - \mu}{\sqrt{\gamma}\sigma}} \exp(u^2)(1 + \mathrm{erf}(u))du. \tag{7.10}$$

Finally, the probability density $P(V)$ is given (cf. sec. 2.29) by

$$P(V) = \frac{2\nu}{\sigma^2} \exp\left(-\frac{(\gamma V - \mu)^2}{\gamma \sigma^2}\right) \int_V^{\Theta_U} \Theta\left(s - V_\mathrm{r}\right) \exp\left(\frac{(\gamma s - \mu)^2}{\gamma \sigma^2}\right) ds, \tag{7.11}$$

for $V \leq \Theta_U$ and $P(V) = 0$ for $V > \Theta_U$. Since the synapses have infinitesimal time course, the arrival of a spike with strength ε at some neuron leads to an instantaneous jump in the membrane potential about ε. Thus, the probability $F(\varepsilon)$ that a neuron is excited above threshold when it receives an input of strength ε, is the probability that its membrane potential is larger than $\Theta_U - \varepsilon$. In terms of $P(V)$, this probability is given by

$$F(\varepsilon) = \int_{\Theta_U - \varepsilon}^{\Theta_U} P(V) dV, \tag{7.12}$$

cf. Fig. 7.7, the cumulative distribution function from the right (since $P(V) = 0$ for $V > \Theta_U$ we could replace the upper bound by $+\infty$). We now derive the probability that a neuron receives an input of strength ε from a synchronized neuron group of size $g_i = k$. Our network has the topology of an Erdös-Rényi random graph with probability p_0 for the existence of a coupling, p_Ex for the probability that this coupling is excitatory and $p_\mathrm{In} = 1 - p_\mathrm{Ex}$ that it is inhibitory. In particular, there are no separate excitatory and inhibitory neuron populations (cf. sec. 2.2). Thus, the coupling received from a specific neuron in the synchronized group can be interpreted as the result of a generalized Bernoulli Experiment with three possible outcomes, excitatory coupling, inhibitory coupling and no coupling, with corresponding probabilities $p_0 p_\mathrm{Ex}$, $p_0 p_\mathrm{In}$, $(1 - p_0)$. The probability that a neuron receives j_1 excitatory, j_2 inhibitory connections and no connections from $k - j_1 - j_2$ neurons of the synchronized group, is given by the the multinomial distribution

$$M(k, j_1, j_2) = \left(\begin{array}{c} k \\ j_1, j_2, k - j_1 - j_2 \end{array} \right) (p_0 p_\mathrm{Ex})^{j_1} (p_0 p_\mathrm{In})^{j_2} (1 - p_0)^{k - j_1 - j_2}, \tag{7.13}$$

with the multinomial coefficient

$$\left(\begin{array}{c} k \\ j_1, j_2, k - j_1 - j_2 \end{array} \right) = \frac{k!}{j_1! j_2! (k - j_1 - j_2)!}. \tag{7.14}$$

The effective input resulting from these connections in a network where the simultaneous excitatory inputs are modulated with the coupling function σ (cf. Eq. 7.6) is then given by

$$\varepsilon(j_1, j_2) = \sigma(j_1 \varepsilon_\mathrm{Ex}) + j_2 \varepsilon_\mathrm{In}. \tag{7.15}$$

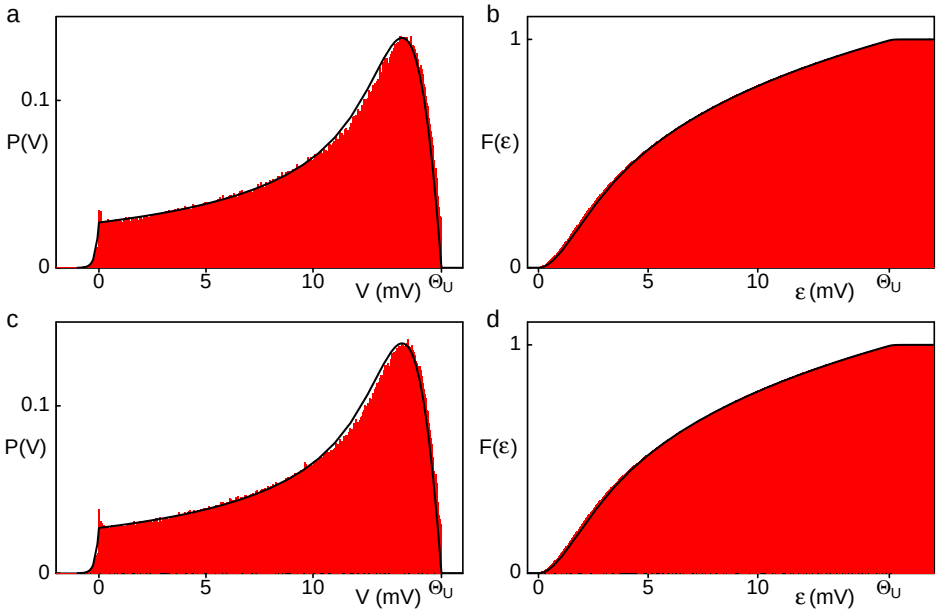

Figure 7.7: Probability density $P(V)$ of the membrane potentials during background activity in networks of linearly (a) and nonlinearly (c) coupled neurons. Red bars show probability density $P_{\mathrm{act}}(V)$ as measured in a network of 1000 neurons (parameters see text). Black curves show the theoretical prediction from Poissonian approximation $P(V)$. In Poissonian approximation no precisely synchronous spikes occur, so the theoretical prediction is identical in both cases. Further, since the spontaneously synchronized neuron groups do not reach sufficient size to generate input pulses larger than the threshold V_a, also the measured probability densities are indistinguishable. The measured distribution deviates from the theoretical prediction due to finite size effects. The corresponding distributions $F(\varepsilon)$, integrated backwards from threshold, are given in (b) (linear coupling) and in (d) (nonlinear coupling). $F_{\mathrm{act}}(\varepsilon)$ as derived from the measured $P_{\mathrm{act}}(V)$ (red bars) deviates from the theoretical predictions (black curves) near $V = 0$ as a consequence of the deviations of $P_{\mathrm{act}}(V)$ from $P(V)$ near threshold.

The joint probability that a neuron receives j_1 excitatory inputs and j_2 inhibitory inputs and is excited above threshold is then given by $F(\varepsilon(j_1, j_2))M(k, j_1, j_2)$. We note that this probability is zero if inhibition dominates, since $F(\varepsilon) = 0$ for $\varepsilon < 0$. The total spike sending probability for an equilibrated neuron in response to a previous pulse of size k is the sum

$$P^{\mathsf{s}}(k) = \sum_{j_1=0}^{k} \sum_{j_2=0}^{k-j_1} F(\varepsilon(j_1, j_2))M(k, j_1, j_2). \tag{7.16}$$

If in the simultaneously spiking group $g_i = k$ neurons were active, after the delay time τ there are $N-k$ neurons that are excitable enough to react to the synchronous input with supra-threshold firing (as mentioned above, this depends on the size of $\tau_{\mathrm{mem}} = 1/\gamma$ relative to τ). We will further assume that these neurons are equilibrated. Then, the firing of one of these neurons can be considered as result of a Bernoulli experiment with probability $P^{\mathsf{s}}(k)$. The probability that $g_{i+1} = j$ neurons fire in response to a synchronous pulse of k neurons is then binomially, $B(N-k, P^{\mathsf{s}}(k))$, distributed,

$$P(g_{i+1} = j | g_i = k) = \left(\begin{array}{c} N-k \\ j \end{array} \right) P^{\mathsf{s}}(k)^j (1 - P^{\mathsf{s}}(k))^{N-k-j}. \tag{7.17}$$

The expected number of neurons firing in response to a synchronous pulse of size k is the conditional expectation $E(g_{i+1}|g_i = k)$,

$$\begin{aligned} E(g_{i+1}|g_i = k) &= \sum_{j=0}^{N-k} jP(g_{i+1} = j|g_i = k) \\ &= (N-k)P^{\mathsf{s}}(k) \\ &= (N-k) \sum_{j_1=1}^{k} \sum_{j_2=0}^{k-j_1} F(\varepsilon(j_1, j_2)) \left(\begin{array}{c} k \\ j_1, j_2, k-j_1-j_2 \end{array} \right) \times \\ &\quad (p_0 p_{\mathrm{Ex}})^{j_1} (p_0 p_{\mathrm{In}})^{j_2} (1-p_0)^{k-j_1-j_2}. \end{aligned} \tag{7.18}$$

The analytically derived values for $E(g_{i+1}|g_i)$ with $i = 0$ agree well with the numerically derived values as shown in Fig. 7.4 for the network with linear couplings and in Fig. 7.5 for network with nonlinear couplings. Deviations are due to the deviations of $P(V)$ from the actual probability $P_{\mathrm{act}}(V)$ in the network (cf. Fig. 7.7), due to the fact that the neurons are not absolutely refractory and not completely equilibrated, due to other finite size effects (quenched disorder) and due to changes of the network dynamics in presence of synchronous pulses. For later pulses, the changes in the network dynamics are more severe, so that we see a less good agreement (cf. Fig. 7.6). To eliminate errors due to Poissonian approximation, we derived the probability density of the membrane potentials $P_{\mathrm{act}}(V)$ numerically from background activity. Replacing $F(\varepsilon)$ by $F_{\mathrm{act}}(\varepsilon)$,

$$F_{\mathrm{act}}(\varepsilon) = \int_{\Theta_U - \varepsilon}^{\Theta_U} P_{\mathrm{act}}(V) dV, \tag{7.19}$$

in Eqs. (7.17, 7.18) yields $P(g_{i+1}|g_i)$ and $E(g_{i+1}|g_i)$ in a semi-analytical way. The agreement with the numerically measured expectation values is better than in the purely analytical approach, however some error sources as described above remain. Comparison between the numerically measured $P_{\mathrm{act}}(V)$ and $P(V)$ reveals small differences (cf. Fig. 7.7). In particular, due to the finite size network with constant input current, there is a finite density $P_{\mathrm{act}}(V)$ arbitrarily close to threshold in contrast to the theoretical prediction with $P(\Theta_U^-) = 0$, cf. sec. 2.10. This also leads to a peak at reset $V = 0$, where neurons with membrane potentials exceeding the threshold are set in again. Due to the deviations near threshold, $F_{\mathrm{act}}(\varepsilon)$ is larger than the analytical prediction $F(\varepsilon)$ near $\varepsilon = 0$. Since small input sizes often occur in the network, these deviations are responsible for the larger values of $E(g_{i+1}|g_i = g_i')$ in the semi analytical approach compared with the analytically derived values Fig. (7.4, 7.5).

7.6 Transition to the propagating state

In this section we investigate the transition from linear networks to networks that give rise to stable propagation of synchrony. We will consider the first steps of time evolution that are well described by the transition matrix $P(g_1 = g_1'|g_0 = g_0')$ and by $E(g_1|g_0 = g_0')$. We note that also changes of background dynamics due to the presence of synchronous pulses might stabilize or destabilize propagation. These effects have to be investigated separately. To obtain analytical insights into the transition to networks that give rise to stable propagation of synchrony, as an approximation we consider the evolution of pulse-sizes as deterministic, where the number of neurons responding to a pulse of size g_0' is given by the expected value $E(g_1|g_0 = g_0')$ which can be analytically derived from diffusion approximation. Since $E(g_1|g_0 = g_0')$ is in general not an integer, we consider a polynomial interpolation of $E(g_1|g_0 = g_0')$. This determines an iterative map ruling the evolution of chains in our approximation. For additive coupling, the map has only one stable fixed point G_0 at small pulse-sizes (which can be distinct from the trivial fixed point at 0). Any initial pulse-size will lead to a chain decaying to pulse-sizes of the order of spontaneous synchronization. For certain non-additive coupling, there are two stable fixed points G_0 and G_2, and one unstable fixed point G_1. Chains starting with sizes in the basin of G_2 thus propagate stably with pulse-sizes around G_2. The approximation allows to analytically determine the bifurcation from unstable to stable propagation. As parameter, we use the inverse of V_a, $V_a^{-1} \in [0, \frac{2}{3}\mathrm{mV}^{-1}]$, and $V_b = V_a + 2\mathrm{mV}$ and $V_c = V_b + 2\mathrm{mV}$. Due to the small size of spontaneously synchronized groups, we can assume that for the considered range of V_a the background activity is in the linear regime and thus well described by $P(V)$ in Poissonian approximation or by $P_{\mathrm{act}}(V)$. We vary $V_a^{-1} \in [0, \frac{2}{3}\mathrm{mV}^{-1}]$, apply the semi-analytical approach, derive and interpolate $E(g_1|g_0 = g_0')$ and solve for the fixed points of the resulting iterated map. This yields the bifurcation diagram Fig. 7.8d. The case $V_a^{-1} = 0$, equivalent to $V_a = \infty$, means that the coupling is linear additive. The

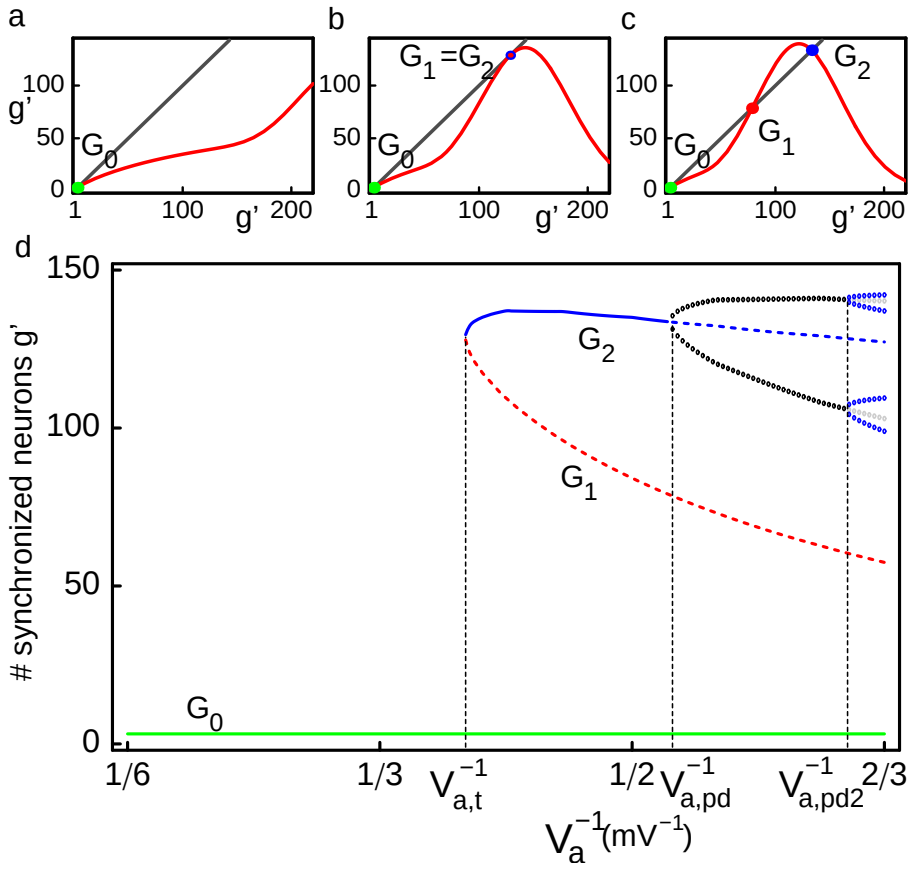

Figure 7.8: Transition to stable propagation of synchrony with increasing non-additivity. Panels (a)–(c) show analytically derived iterated maps approximating the time evolution of pulse sizes for three different values of V_a. Solving for the fixed points of the iterated maps leads to a bifurcation diagram, plotted as a function of V_a^{-1} in panel (d). Small groups of spontaneously synchronized neurons at G_0 exist for all V_a^{-1}. At $V_{a,t}^{-1}$ a tangent bifurcation creates a region of pulse-sizes where stable propagation is possible. At $V_{a,pd}^{-1}$ a period doubling bifurcation leads to a stable orbit of period two (black circles). At $V_{a,pd2}^{-1}$ a second period doubling bifurcation occurs, leading to a stable orbit of period four (blue circles), while the orbit with period two becomes unstable (gray circles). At all sufficiently small V_a (suff. large V_a^{-1}) appropriate initial pulse-sizes enable propagation of synchrony. (See text for further details.)

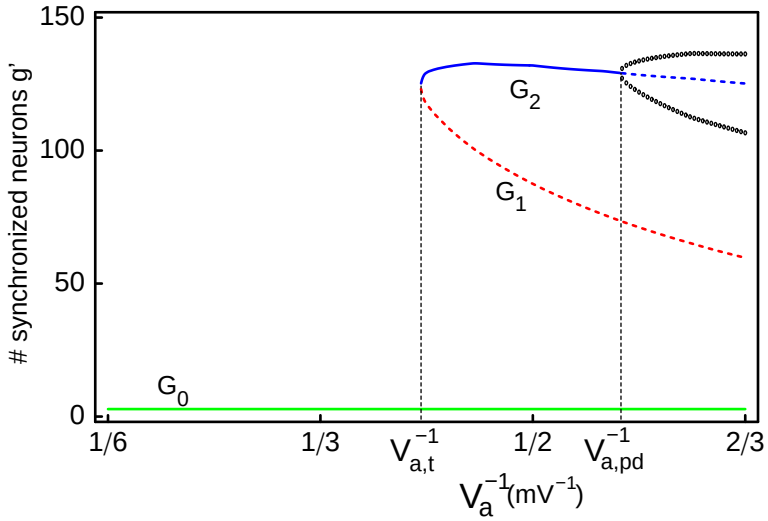

Figure 7.9: Transition to stable propagation of synchrony with increasing non-additivity as in Fig. 7.8. Bifurcation diagram for $\tau = 7$ms and $1/\gamma = 10$ms. The qualitative agreement with the diagram in Fig. 7.8 shows the robustness of the scheme against changes of the parameters.

value of G_0 does not change in the entire range considered since small groups are not influenced by the nonlinearity. When increasing V_a^{-1} this remains the only fixed point, cf. Fig. 7.8a until at $V_{a,t}^{-1} \approx 0.39\text{mV}^{-1}$ (or $V_{a,t} \approx 2.6$mV) a tangent bifurcation occurs, cf. Fig. 7.8b, and two fixed points, one unstable at G_1 and one stable at G_2 emerge. G_2 remains stable until $V_{a,pd}^{-1} \approx 0.53\text{mV}^{-1}$ (or $V_{a,pd} \approx 1.9$mV). At $V_{a,pd}^{-1}$ the fixed point at G_2 becomes unstable, due to a period doubling bifurcation and a stable orbit of period two emerges, cf. Fig. 7.8d, followed by further period doubling bifurcations for larger parameter values. Here, oscillation of pulse-sizes due to the deterministic evolution and statistical fluctuations lie upon each other. The bifurcation diagram explains the stable propagation of synchrony at $V_a = 2$mV, cf. Fig. 7.3, when the first pulse has a size around $g' = 100$, i.e. lies in the interval bounded by the two preimages G_1 and G_3 of $G_1(V_a = 2\text{mV}) \approx 84$, i.e. in the basin of G_2. The scheme of transition to a propagating state is robust against changes of the parameters (cf. Fig. 7.9 for an illustration).

7.7 Conclusion and outlook

Implementing non-additive coupling in model networks of spiking neurons we have demonstrated that stable propagation of synchronous spiking activity is possible even if the network is purely randomly connected and has no additional structural features. In particular, highly non-random feed-forward structures or systemati-

cally adapted strengths of specific synapses are not needed.

We studied idealized model networks with constant delay times between neurons and post-synaptic responses in form of delta-currents. As established in sec. 7.2, these choices are appropriate for the description of neurons with fast dendritic spikes. They further make the model computationally accessible and strongly simplify both data evaluation and mathematical analysis. We could thus study the propagation of synchrony, i.e. the evolution of chains of synchronous pulses, both numerically and analytically.

Numerically, we derived the transition matrices determining the evolution of pulse-sizes. We argue that the transition probabilities fulfill an approximate Markov property. The transition matrices are however not stationary, i.e. the Markov chain is not homogeneous, since the presence of large synchronized pulses changes the network activity. Interestingly, the background activity is sufficiently stable so that transition matrices at later stages are qualitatively similar to the early ones.

We analytically derived the complete transition matrix valid for early stages in the evolution of a chain. The background activity was described in the Poissonian approximation. The transition probabilities could then be computed using the statistical properties of the underlying network topology and the nonlinear coupling function σ. Further, to eliminate errors originating from diffusion approximation, the essential features of background activity were measured numerically and we derived the transition probabilities in a semi-analytical approach using the statistics of network connectivity and the coupling function only. We compared the resulting expectation values with the numerically derived ones and found good agreement. Finally, we approximated the statistical evolution of the chain by a deterministic iterative map based on the analytically derived conditional expectations for the pulse-sizes and demonstrated that the propagating zone is generated by a tangent bifurcation.

Previous modeling work on nonlinear dendritic interactions (cf. sec. 4.1) was dedicated either to very detailed or to highly abstract models [127, 128, 154] and studied single neurons or very small networks (cf. [129, 112] for reviews). We introduced a single compartment spiking neuron model that incorporates supra-additive dendritic summation as found in experiments [13, 157] and allows to study the implications of nonlinear dendritic enhancement for spiking dynamics of larger recurrent spiking neural networks. We find that supra-additive dendritic summation gives rise to stable propagation of precise synchrony even in random networks. Propagating, precise synchrony is considered a possible explanation for precise timing in biological neural networks (cf. e.g. [6]). Previous work investigating the propagation of synchrony in neural networks (cf. sec. 4.1) assumed that strongly excitatory feedforward structures are embedded in otherwise random neural networks. Precisely synchronous pulses can then propagate along these structures [83, 54, 201]. However, up to now, there is no experimental evidence for the presence of such structures in cortical neural networks.

We have numerically studied networks of up to 1000 neurons whereas biologically realistic size of a local circuit is two orders of magnitude larger (these larger

networks usually do not have the topology of an Erdös-Rényi random graph). Our theoretical predictions made above are based on mean field arguments, strictly valid only in the limit of infinite network size. Already for moderately sized networks these predictions are in good agreement with measured data from simulations. We expect that the agreement with the mean field predictions will get even better with larger network sizes. Nevertheless, the absolute sizes of synchronous pulses as well as their sizes relative to that of the total network may vary strongly with parameters such as network size, connection probability, and effective total input coupling strengths. These points need to be investigated in more detail.

Preliminary studies show that propagation enabled by non-additive coupling is robust against changes of the model. In particular, the phenomenon is insensitive against changing the precise form of non-additivity (i.e. the sigmoidal function used above) or including NMDA-like synaptic currents with long decay time constant. Structural stability has to be further studied, in particular with regard to inhomogeneous parameters such as inhomogeneous delays and finite synaptic time constants (cf. also ch. 8). We expect that the inclusion of noise sources will not change the qualitative dynamics. Synaptic noise will increase the fluctuations of pulse-sizes, larger pulse-sizes lead to an averaging effect so that the total additional noise will stay small. Noise, e.g. also due to random neuronal inputs, will even prove beneficial, because it stabilizes background activity and leads to a fast equilibration of neurons after a synchronous pulse. Thus, the analytical predictions and the Markov property might be even better fulfilled. A network dominated by stationary noise might lead to stationary transition matrices and to a homogeneous Markov chain of synchronous pulses.

In our model dynamics, no specific propagation paths of synchronous neurons exist; non-additive coupling can ensure that synchronous activity propagates but it is a priori unknown, where it will propagate. This is very unlike synfire-chain models where the propagation paths of synchronous activity are predefined by the embedded feed-forward networks and can be experimentally tested. In preliminary studies, together with P. Bittihn we started to investigate how distance dependent connectivity influences the dynamics of propagating pulses. Also more specifically structured network connectivity and distributed synaptic strengths are expected to be reflected in pulse propagation. In particular with respect to computational abilities of the considered networks it will be important to see whether and how non-random network structure is actually relevant for the dynamics.

One of the most important questions is if propagation of synchrony, as predicted by our rather abstract, idealized model, exists in biological neural networks. If the pulse-sizes are large enough, we expect that the propagating synchronous activity is reflected by specific patterns in mass signals of cortical activity as measured by local field potential recordings. Further, the brain regions where we expect the patterns is delimited. It should be the regions where neurons with strong and fast nonlinear dendritic enhancement exist, and thus include in particular the region investigated in ref. [13] (Hippocampal region CA1). Indeed, in this region, patterns as expected from our theoretical predictions have been experimentally measured,

cf. ch. 8.

Chapter 8

Towards a frequency-predicting model for sharp wave/ripples

Knowing about the preceding chapter, we have to ask if there are experimental findings in which the propagation of synchrony based on nonlinear dendritic interaction might be reflected. Refs. [13, 71, 70] found that pyramidal neurons in the proper Hippocampus, more precisely in the CA1 region show the described high dendritic excitability and coincidence detection. How would propagating synchrony appear in experiments? If the synchronized neuron groups are large enough, we expect a detectable pattern of synchronous firing activity even in neuronal mass signals such as the local field potential. According to Ref. [13], action potentials are generated 5ms after sufficiently large inputs. Accounting for the time to collect the input until it is large enough and the axonal conduction delay which is in the sub-millisecond range for the small distances considered, we expect the peaks of maximally synchronized activity to be separated by time intervals of slightly more than 5ms. Taken together, we expect an oscillation with frequency slightly below 200Hz in CA1 and related regions. Indeed, phases of increased activity, so called *sharp waves*, with superimposed *ripples*, oscillations with frequencies between $180 - 200$Hz have been found in the local field potential in the hippocampal regions CA1 and CA3 [206, 116, 37]. The troughs of the oscillation (temporal distance about 5ms) are assumed to be generated by precisely synchronous spiking of pyramidal neurons. The origin of the phenomenon is still unclear.

In this chapter we present a more detailed model of a neural network with dendritic nonlinearities. In particular, we take into account the non-instantaneous time course of post-synaptic currents. We show that in this model indeed activity patterns resembling sharp wave/ripples *spontaneously* occur. The sharp wave and the superimposed ripples, which are often considered to have different causes, appear as one phenomenon. We present the two already existing, competing models for sharp wave/ripples and discuss experimental findings in the context of the new model and the existing ones.

8.1 State of the art

Up to now there are two different modeling approaches to assess sharp wave/ripples (SPW/Rs).

Model 1 assumes that networks of inhibitory neurons entrain excitatory neurons to fire in a phase locked manner [206, 39]. Sharp wave and ripples are considered as two distinct phenomena, the sharp wave is in the original model generated in hippocampal region CA3, the ripples are onmodulated in region CA1. Indeed, in many studies ripples have not been found in CA3 or they were of lower and variable frequency (cf. [206] and references therein). The sharp wave is explained as a population burst in excitatory pyramidal neurons. The excitatory input leads to oscillatory spiking in interneurons. Experimental and theoretical studies show that oscillatory neurons which are coupled by fast inhibitory connections tend to synchronize (see, e.g. [204, 58]) so that the entire inhibitory population exhibits an oscillatory activity pattern. Also, some types of interneurons are coupled by gap junctions, whose ability to instantaneously transmit (low pass filtered) changes even in the subthreshold membrane potential additionally strengthens their tendency to synchronize [108]. Pyramidal cells now can only fire when the inhibition is not too strong, i.e. between the arrival of the inhibitory barrage originating from phases of high activity in the interneurons. The pyramidal cells are thus entrained by inhibitory neurons to fire synchronously and phase locked to the oscillation of the interneurons.

Model 2 is based on the assumption that there are gap junctions between the axons of pyramidal neurons of region CA1 connecting the pyramidal neurons to a sparse network [184, 186, 115]. Indeed, there is indirect evidence for the existence of such axo-axonal gap junctions given in [168], for some special axons in the hippocampus direct evidence exists [78]. In the model, it is assumed that the electric coupling is strong enough so that a spike in one axon can induce a spike in the other axon. Since the axons are highly excitable and small in diameter, such gap junctions would have strengths in the physiological range (in contrast e.g. to gap junctions coupling two somata). Further, the gap junction coupling in the network has to be above the percolation limit for the network so that a giant coupled component exists. Finally, it is assumed that some background spikes exist in the neural network which may occur with low frequency. If a spike reaches a gap junction, it induces a spike in the next axon which in turn i) induces spikes in further axons through gap junctions, thus spikes multiply and ii) travels antidromically to the soma. Due to the multiplication of spikes in the axonal bulk entire populations of spikes are excited to fire. Numerical simulations show that this mechanism leads to bursts of rhythmic network spiking activity, with intra-burst frequencies easily reaching values of 200Hz [186].

The spike activity as described in both models has to be translated into the local field potential (LFP) measured in biological experiments. This is a non-trivial task and subject to current research, since the measured LFP depends on the position of the electrode, the spatial distribution of currents and the filtering properties of the

tissue. The following paragraph has thus the character of a rough approximation. In the extracellular potential, due to the influx of current into the neuron and subsequent outflux [74], an action potential results in a sharp negative excursion with subsequent flat positive hill. Since the LFP measures the superposition of many of these extracellular potentials and also has low pass filter properties, only highly synchronous action potentials are reflected by sharp negative excursions in the LFP, while non-synchronous action potentials will not be seen. In contrast, due to their larger time extent as compared with action potentials, already slightly synchronous synaptic currents and potassium rectifying currents are reflected in the LFP, so that sufficient current outflux from neurons due to activation of inhibitory synapses leads to a rise in the measured LFP, while it decreases if there is sufficient current influx due to activation of excitatory synapses. The "ripples" are then due to highly synchronous action potentials in the principal neurons which lead to troughs, in the LFP [206]. The increase in the LFP, the sharp wave, is due to an increase of overall activity and slightly synchronous activity of interneurons [35].

Up to now, there is no concluding experimental evidence for either model 1 or model 2, despite a number of experimental studies (cf. sec. 8.6). Further, the models do not predict the frequency of ripple oscillations. We were thus led to propose a new model for SPW/Rs which is consistent with present experimental knowledge, predicts the frequency of ripple oscillations and might fit well with the role assumed for SPW/Rs in learning.

8.2 The model

We consider a random network of N conductance based leaky integrate-and-fire neurons (cf. sec. 2.6), divided into two populations of N_E excitatory neurons and $N_I = N - N_E$ inhibitory neurons (cf. sec. 2.2). Without dendritic nonlinearity, the time course of neuron l's membrane potential is determined by

$$\begin{aligned}\tau_{\mathrm{mem}}\frac{dV_l(t)}{dt} =& V_{\mathrm{rest}} - V_l(t) + g_A(t)(E_{\mathrm{Ex}} - V_l(t)) + g_N(t)(E_{\mathrm{Ex}} - V_l(t)) \\ &+ g_G(t)(E_{\mathrm{In}} - V_l(t)),\end{aligned} \tag{8.1}$$

cf. Eq. (2.6). The synaptic conductances have single exponential time course (cf. sec. 2.5), the free dynamics is given by

$$\begin{aligned}\tau_A\frac{dg_A(t)}{dt} &= -g_A(t), \\ \tau_N\frac{dg_N(t)}{dt} &= -g_N(t), \\ \tau_G\frac{dg_G(t)}{dt} &= -g_G(t).\end{aligned} \tag{8.2}$$

We concentrate on three classes of synaptic currents: Fast and slow excitatory and fast inhibitory currents. The excitatory, fast decaying conductance $g_A(t)$ with

decay time constant $\tau_A = 7$ms ([11], p. 214) models the conductance due to AMPA receptors[1]. $g_N(t)$, fast rising and slowly decaying with time constant $\tau_N = 200$ms ([11], p. 215), models the conductance due to the activation of NMDA receptors[2]. Both AMPA and NMDA channels give rise to mixed cation currents with reversal potential around $E_{\mathrm{Ex}} = 0$mV ([48], p. 179). The NMDA receptors activates a bit slower than the AMPA receptor (about 1.5ms rise time) and is also voltage dependent, cf. sec. 2.2. To concentrate on the essentials, we do not consider the slower rise of the conductance and also neglect the voltage dependence which would lead to changes up to a factor two in the NMDA conductances ([48], p. 183). Finally, $g_G(t)$ are fast decaying inhibitory conductances with decay time constant $\tau_G = 10$ms ([187]) modeling the conductance due to the activation of $\mathrm{GABA_A}$ receptors[3]. We set the reversal potential for the current through $\mathrm{GABA_A}$ receptors to $E_{\mathrm{In}} = -75$mV. Indeed, AMPA and NMDA receptors have been shown to be important for the generation of dendritic spikes [13]. Also, together with $\mathrm{GABA_A}$ receptors (and in contrast e.g. to $\mathrm{GABA_B}$ receptors mediating slow inhibition), they influence the properties of SPW/R activity [117, 45, 22]. Further, the slow NMDA current stabilizes the asynchronous activity in leaky integrate-and-fire networks [202] (as also a sufficiently strong constant input current would), it is however not necessary for sustained irregular activity [201, 105], cf. also [79].

In our model, a spike sent at time t_0 arrives at the postsynaptic neurons after a delay time τ, i.e. at time $\theta_0 = t_0 + \tau$. There, it evokes a jump in the conductances. If the spike was sent by an excitatory neuron, this jump is about Δg_A and Δg_N in the fast and slow excitatory conductances and adds up linearly to the existing conductances,

$$\begin{aligned} g_A(\theta_0) &= g_A(\theta_0^-) + \Delta g_A, \\ g_N(\theta_0) &= g_N(\theta_0^-) + \Delta g_N, \end{aligned} \tag{8.3}$$

a spike from an inhibitory neuron enhances the inhibitory conductances according to

$$g_G(\theta_0) = g_G(\theta_0^-) + \Delta g_G. \tag{8.4}$$

Each neuron additionally receives high frequency random input trains of excitatory and inhibitory spikes. The input spike trains have Poissonian statistics and are uncorrelated for different neurons. They introduce noise in our model and stabilize

[1] AMPA receptors are fast activating (in the sub-ms range, [48], p. 182) and deactivating ionotropic Glutamate receptors (i.e. the neurotransmitter activating these channels is Glutamate, cf. also sec. 2.2) predominantly permeable for $\mathrm{Na^+}$ and $\mathrm{K^+}$. Unlike e.g. NMDA receptors, they can also be activated by AMPA, α-amino-3-hydroxy-5-methyl-4-isoxazolepropionic acid, a substance that does not occur as neurotransmitter in nature ([104], p. 157f).

[2] NMDA receptors are ionotropic Glutamate receptors that can be selectively activated by the amino-acid NMDA, *N*-methyl-*D*-aspartic acid, which also does not occur as neurotransmitter in nature. NMDA receptors are permeable for $\mathrm{Na^+}$, $\mathrm{Ca^{2+}}$ and $\mathrm{K^+}$.

[3] $\mathrm{GABA_A}$ receptors are $\mathrm{Cl^-}$-permeable ionotropic receptors that are activated by GABA, γ-aminobutyric acid.

the irregular background dynamics. We note that a similar model was considered e.g. in [201] (cf. sec. 7.1).

The excitatory neurons now have nonlinear dendrites. Highly detailed models for such neurons in CA1 exist as well as non-spiking neuron models [128, 129, 13, 154, 153]. However, to study network dynamics and in particular precise spike timing, the appropriate model is a single compartment spiking neuron model, because it combines a reasonable degree of accuracy with a rather simple time evolution that allows simulations also of larger networks. Further, it allows to introduce features of nonlinear dendritic enhancement as found in [13] in a simple manner. Due to the performed abstraction, we can study the influences of features considered as crucial on network dynamics, where the underlying mechanisms are not obscured by a too detailed description (cf. sec. 2.4). We thus construct a model incorporating nonlinear dendritic enhancement on the basis of the conductance based leaky-integrate-and fire model Eq. (8.1). In a simple multi-compartment model, we might describe the dendrite by a separate compartment, with its own membrane potential and its own gating variables and with a resistive coupling to the soma (cf. e.g. [48], p. 218). If the compartment is sufficiently depolarized, sodium spikes are generated due to voltage gated channels via the positive feedback process described in sec. 2.1. The resulting stereotypical depolarization in the dendritic compartment leads to a depolarizing current flowing through the resistive coupling into the soma. In the single-compartment model, we include this current pulse. In order to include only essential features, we model it as stereotypic, neglecting dependencies of the current strength on the state of the soma and the dendrite. Nonlinear interaction takes place for inputs that occur within a window of $\Delta t \approx 2$ms [13]. We therefore sample excitatory inputs within a window of length Δt and compare the strength of the excitatory input with some threshold. If the strength of the total input is larger than the threshold, we assume that a dendritic spike is elicited and the current pulse is applied to the soma. Since we want to first study networks of medium size we do not distinguish between different basal dendrites and compartments that receive the inputs. In order to keep the differential equations that are to be integrated simple, we model the current pulse as the difference of two exponentially decaying currents, one, with shorter time constant, as excitatory, the other as inhibitory. The behavior of the current is thus analogous to two current based channel populations with different inactivation times opening at the same time. We thus add two current based terms to above conductance based equation,

$$\begin{aligned}\tau_{\mathrm{mem}}\frac{dV_l(t)}{dt} =& V_{\mathrm{rest}} - V_l(t) + g_A(t)(E_{\mathrm{Ex}} - V_l(t)) + g_N(t)(E_{\mathrm{Ex}} - V_l(t)) \\ &+ g_G(t)(E_{\mathrm{In}} - V_l(t)) \\ &+ g_{\mathrm{NL,Ex}}(t)(E_{\mathrm{Ex}} - V_{\mathrm{rest}}) + g_{\mathrm{NL,In}}(t)(E_{\mathrm{In}} - V_{\mathrm{rest}}),\end{aligned} \tag{8.5}$$

and complete the equations for the conductances Eqs. (8.2) by

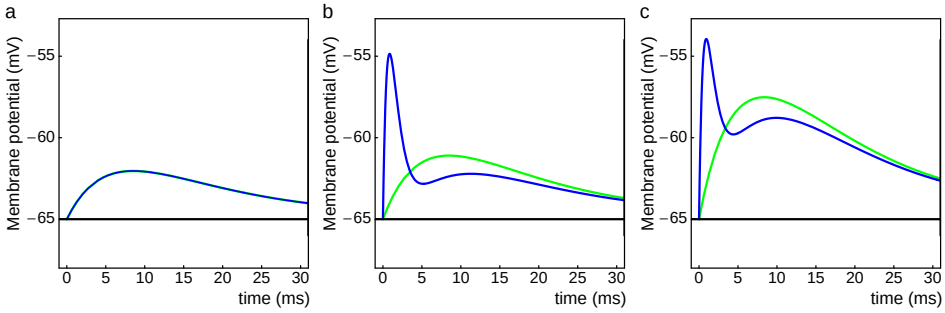

Figure 8.1: Voltage traces of a single compartment model neuron with nonlinearly enhanced inputs due to a fast dendritic spike (blue curves) in comparison to the response without dendritic spike (green curves). (a) Below the threshold for the dendritic spike, inputs result in conventional excitatory postsynaptic currents and somatic responses. (b) Above threshold, a dendritic spike is generated, whose effect is modeled as a current pulse into the soma. The dendritic spike evokes a sharp peak in the membrane potential ((b), blue curve). (c) Further increase of input strength does not result in a large further increase in the peak potential ((c), blue curve), but increases the slower afterpotential. (Details see text.)

$$\tau_{\mathrm{NL,Ex}} \frac{dg_{\mathrm{NL,Ex}}(t)}{dt} = -g_{\mathrm{NL,Ex}}(t),$$
$$\tau_{\mathrm{NL,In}} \frac{dg_{\mathrm{NL,In}}(t)}{dt} = -g_{\mathrm{NL,In}}(t). \tag{8.6}$$

Decay times for the excitatory and the inhibitory current were chosen $\tau_{\mathrm{NL,Ex}} = 0.75\mathrm{ms}$ and $\tau_{\mathrm{NL,In}} = 1\mathrm{ms}$ to generate rise and decay times of the somatic response in the biological range. Initial current strengths after initiation of a dendritic spike were chosen $\Delta g_{\mathrm{NL,Ex}} \approx 933\mathrm{mVms}/(\tau_{\mathrm{NL,Ex}}(E_{\mathrm{Ex}} - V_{\mathrm{rest}})) \approx 19$ for the excitatory and $\Delta g_{\mathrm{NL,In}} \approx -933\mathrm{mVms}/(\tau_{\mathrm{NL,In}}(E_{\mathrm{In}} - V_{\mathrm{rest}})) \approx 93$ for the inhibitory current (in units of the resting conductance) to generate biologically realistic peak potential sizes ($\approx 10\mathrm{mV}$) of somatic voltage traces [13]. Further specific parameters used in the simulations are given in sec. 8.5. Together with the sodium spikes, also NMDA spikes can occur. Indeed, there are two neuron populations with different response properties, one where only a small NMDA component accompanies the Na-spike and one where there is a proper NMDA spike[4]. For simplicity, we do not take NMDA spikes into account. Resulting membrane potentials $V(t)$ in response to inputs of different strength are displayed in Fig. 8.1: The figure shows responses of the conductance based neuron Eq. (8.5) with membrane time constant $\tau_{\mathrm{mem}} = 10\mathrm{ms}$. Below the threshold for generation of a dendritic spike, arriving synchronous spikes (three synchronous inputs

[4] J. Schiller, personal communication.

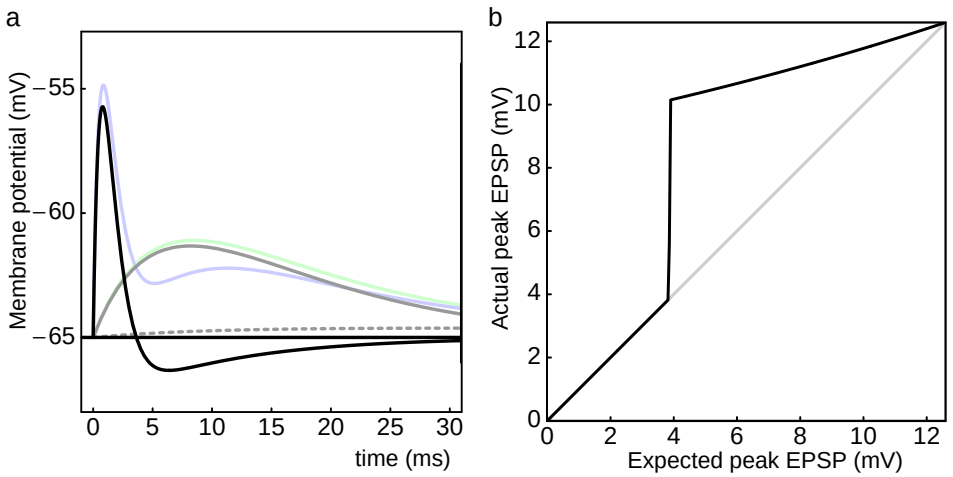

Figure 8.2: Contributions to the membrane potential in response to an input generating a dendritic spike (a) and relation between actual peak EPSP and peak EPSP expected without influence of a dendritic spike (b). (a) The membrane potential (faint blue, cf. Fig. 8.1b) in response to an input generating a dendritic spike is composed of components due to conductance based excitatory inputs and the current pulse modeling the effect of the dendritic spike. Individual voltage traces in response to only fast excitation (gray curve), only slow excitation (gray dashed curve), to the expected EPSP without dendritic spike, i.e. to fast and slow excitation together (faint green curve), are displayed. The effect of the dendritic spike alone is given by the black curve. We note that due to the conductance based character of the model, the overall response (faint blue curve) slightly differs from the sum of the contributions. (b) Strengthening of the EPSP by occurrence of a dendritic spike is illustrated by relating the actual peak EPSP including the influence of the dendritic spike to the expected peak EPSP without this influence. In the subthreshold region, actual and expected peak EPSP are equal (cf. also Fig. 8.1a). Inputs which would generate expected peak EPSPs larger than ≈ 3.9mV from the resting potential evoke a dendritic spike which results in a peak EPSP around 10mV in agreement with biological data [13] (cf. also Fig. 8.1b). This peak EPSP only weakly increases with further increase of input strength (cf. also Fig. 8.1c).

with the model parameters of secs. 8.4, 8.5) generate only a jump in the excitatory conductances to initial values $\Delta g_A = 3 \times 22\text{mVms}/(\tau_A(E_{\text{Ex}} - V_{\text{rest}})) \approx 0.15$, $\Delta g_N = 3 \times 22\text{mVms}/(\tau_N(E_{\text{Ex}} - V_{\text{rest}})) \approx 0.005$ (in units of the resting conductance, the single input strength is chosen so that the peak EPSP is 1mV), cf. Fig. 8.1a. Above threshold (four synchronous inputs), a dendritic spike is generated, whose effect is modeled as a current pulse into the soma which evokes a sharp peak in the membrane potential, (cf. Fig. 8.1b (blue curve), the EPSP due to pure channel activation is displayed for comparison (green curve)). The actual EPSP is composed of the effect of the dendritic spike and the depolarization due to conductance based channels with initial conductances $\Delta g_A = 4 \times 22\text{mVms}/(\tau_A(E_{\text{Ex}} - V_{\text{rest}})) \approx 0.19$, $\Delta g_N = 4 \times 22\text{mVms}/(\tau_A(E_{\text{Ex}} - V_{\text{rest}})) \approx 0.007$ and exponential decay (cf. also Fig. 8.2). Further increase of coupling strength (eight synchronous inputs) does not result in a large increase in the peak potential (Fig. 8.1c (blue curve)), the stronger channel activation ($\Delta g_A \approx 0.39$, $\Delta g_N \approx 0.014$, cf. also Fig. 8.1c (green curve)) leads to a larger after-potential. The firing thresholds in our simulations lie between -50mV and -47mV, i.e. above the potentials reached due to a dendritic spike when the neuron is at resting potential. Fig. 8.2a illustrates how the different conductances and currents contribute to the trace. The relation of actual and expected peak EPSP[5] is shown in Fig. 8.2b.

8.3 Sharp wave/ripples in neurobiology

The Hippocampus is a part of the allocortex located in the medial temporal lobe of mammalian brains. It is considered to play a central role in the creation and in the consolidation of memories (see, e.g. [11] chs. 12, 13). Dependent on the behavioral state of the animal, distinct forms of activity are generated. The two most prominent patterns are i) the theta/gamma rhythm, regular oscillations of population activity on frequencies of about $4-10$Hz, with superimposed oscillations of $40 - 100$Hz, occurring during phases of high active behavior or REM sleep and ii) SPW/Rs, large sharp waves of activity with durations about $50 - 100$ms and onmodulated oscillations of ~ 200Hz occurring irregularly with inter-event-intervals in the second range during slow wave sleep or at rest. We note that also sharp waves without detectable ripples are observed *in vitro* [117]. Approximately $5 - 15\%$ of the local pyramidal neuron population and the entire population of some types of interneurons participate at an event ([37], p. 345). This means that SPW/Rs are a very strong event. While the pyramidal neurons fire at most a few spikes per event, some types of interneurons discharge at rates of $150 - 200$Hz [206]. The probability for a single pyramidal cell to participate in a SPW/R event strongly depends on the individual cell. Some neurons participate in a large fraction (up to

[5] We note that the expected EPSP differs slightly from an additive EPSP as given in literature (cf. e.g. [157]). If the expected EPSP is generated by two simultaneous inputs, it will be slightly lower than the additive EPSP, the sum of two voltage traces generated by the two separate inputs. In a conductance based model the conductances add linearly, but the EPSPs add sublinearly due to the factor $(E_{\text{Ex}} - V(t))$ in Eq. 8.1 which is larger for smaller $V(t)$.

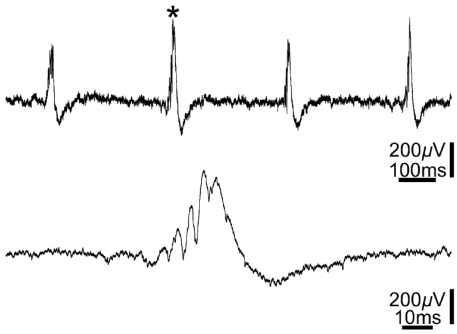

Figure 8.3: Local field potential recording in the CA1 region *in vitro*. Upper trace shows spontaneous occurrence of sharp wave/ripple events. Closeup of the single event indicated by an asterisk in the upper trace reveals ripple structure superposed to sharp wave. Reproduced from [117], with permission.

40%) of events, others participate very rarely.

The patterns of activity are detected by measuring the LFP: When ionic currents flow in or out of a neuron due to activation of transmembrane channels, charge differences and thus electric fields are generated in particular in the extracellular medium. For an entire population of neurons the electric fields superpose and the resulting mean potential over some area, the LFP, can be measured by an extracellular electrode ([37], p. 89).

Sharp wave/ripples occur when the animal has no or very little interaction with the environment [35], they are thus considered as "ultimate self-organized endogenous hippocampal events" ([37], p. 344). Indeed, they also persist in the functionally disconnected hippocampus, and in *in vitro* preparations, the latter even if subregions (CA1, CA3) of the hippocampus are isolated [117].

The function of SPW/Rs is unknown. Since this pattern of activity only occurs at rest, it might be just the idling state of the hippocampus, assumed when it is released from states of high activity characterized by other patterns like theta waves accompanying exploratory behavior or foraging. Indeed, SPW/Rs start with a few seconds delay after beginning to rest, they are usually interrupted as soon as stimuli occur and they also occur when the hippocampal formation is functionally disconnected.

The discharge of a large fraction of neurons with millisecond precision is, however, likely to be a significant event for the brain [36]. Further, the inter-ripple-intervals of 5ms are in the optimal range for the induction of synaptic modification [121, 24]. Indeed, SPW/Rs are conjectured to be important for learning processes: One hypothesis is that during SPW/R activity, existing synaptic connections are strengthened and thus memory is consolidated. Evidence is provided by experiments showing that sequences of spiking activity that occur during earlier

behavioral activity (e.g. exploration) also occur during SPW/R events (cf. [11], p. 484, [109, 53]). Supported by observations of neocortical activity correlated to SPW/Rs [171], the 'two stage model of memory consolidation', assumes that during this replay of activity information is transferred to the neocortex where it is stored persistently [36].

8.4 Sharp wave/ripple-like events in networks with nonlinear dendritic interaction

For biologically realistic parameters (cf. secs. 8.5, 8.6), the conductance based leaky integrate-and-fire model with temporally extended nonlinear dendritic interactions as described in sec. 8.2 shows SPW/R-like events, occurring spontaneously cf. Fig. 8.4[6]. Fig. 8.5 shows a closeup of a SPW/R-like event and the corresponding spike-time histogram. Occasionally, paired SPW/R-like events occurred in our simulations. These are also observed in experiments [38]. Fig. 8.6 shows a paired SPW/R-like event detail. In our network simulations nearly all excitatory neurons participate at each event. This is in contrast to experimental results (cf. sec. 8.6) and might suggest that the connectivity in biologically realistic neural networks is more structured than our networks which have random topology as described in sec. 8.5.

The mechanism leading to SPW/Rs in our model can be described as follows (cf. Fig. 8.5): First, comparably small groups of excitatory neurons are synchronized spontaneously due to fluctuations in the network dynamics or due to changes in the network dynamics on longer timescales such as decay of NMDA currents.[7] If these groups are large enough, they induce some dendritic spiking activity in excitatory neurons. In response, larger groups of excitatory neurons send their well synchronized spikes and thus excite further larger and better synchronized groups of excitatory neurons. Parallel, since excitatory neurons strongly project on inhibitory neurons, also activity of inhibitory neurons is increased. Since there is no strong synchronizing mechanism, their synchronization is however less precise. In the following, there are still synchronous groups of excitatory neurons but inhibition accumulates, favored by its longer decay time constant and the weak mutual inhibition of interneurons. Finally, the inhibition dominates the dynamics and membrane potentials of excitatory neurons are far from threshold so that even excitation due to dendritic spikes is not sufficient to excite them to fire. The

[6] We note that for some choices of parameters we observed epileptic activity (frequency $\approx$ 200Hz) occurring after several seconds of simulated time. We did not observe this for the parameters chosen below, where we also checked that background activity and frequency were stationary (60s of simulated time).

[7] Also other mechanisms of initiating an event are possible, based on neural properties which are not included in our model. E.g. short term synaptic plasticity is known to promote synchronous spiking of neuron groups [189, 191, 111]. Indeed, short term synaptic plasticity is known to be present in the hippocampus, also in region CA1 ([52], [11], ch. 10). It might be possible to differentiate the mechanisms by considering the statistics of occurrences.

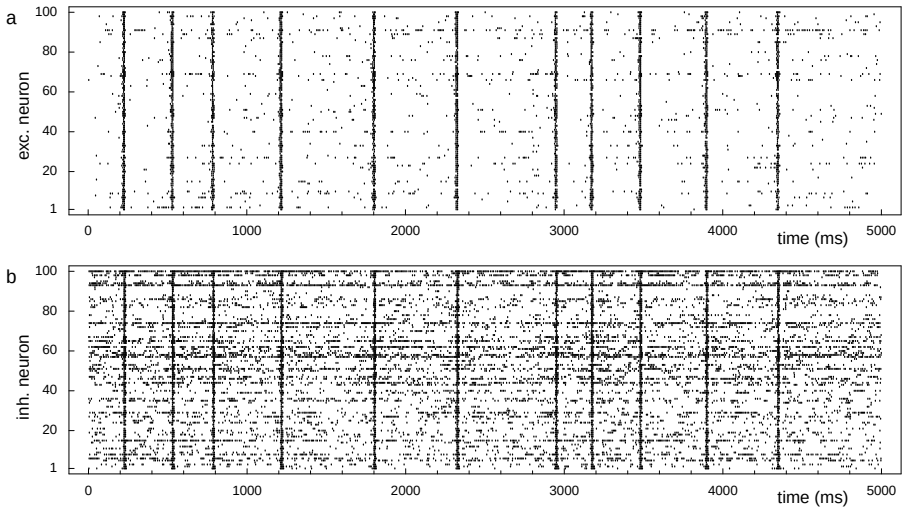

Figure 8.4: Sharp wave/ripple-like events in a network model of neurons with nonlinear dendritic interactions. Figure shows five seconds of the spiking dynamics of (a) 100 excitatory and (b) 100 inhibitory neurons in a network of 1000 neurons (500 excitatory, 500 inhibitory, see text for further network parameters). The events occur spontaneously with a frequency of about 2.2Hz due to spontaneous synchronization of groups and have a length of about 50ms in agreement with neurobiological data. The fine structure of a event is displayed in Fig. 8.5. The pattern of spiking activity can be translated into an LFP pattern resembling SPW/R events as described in the text.

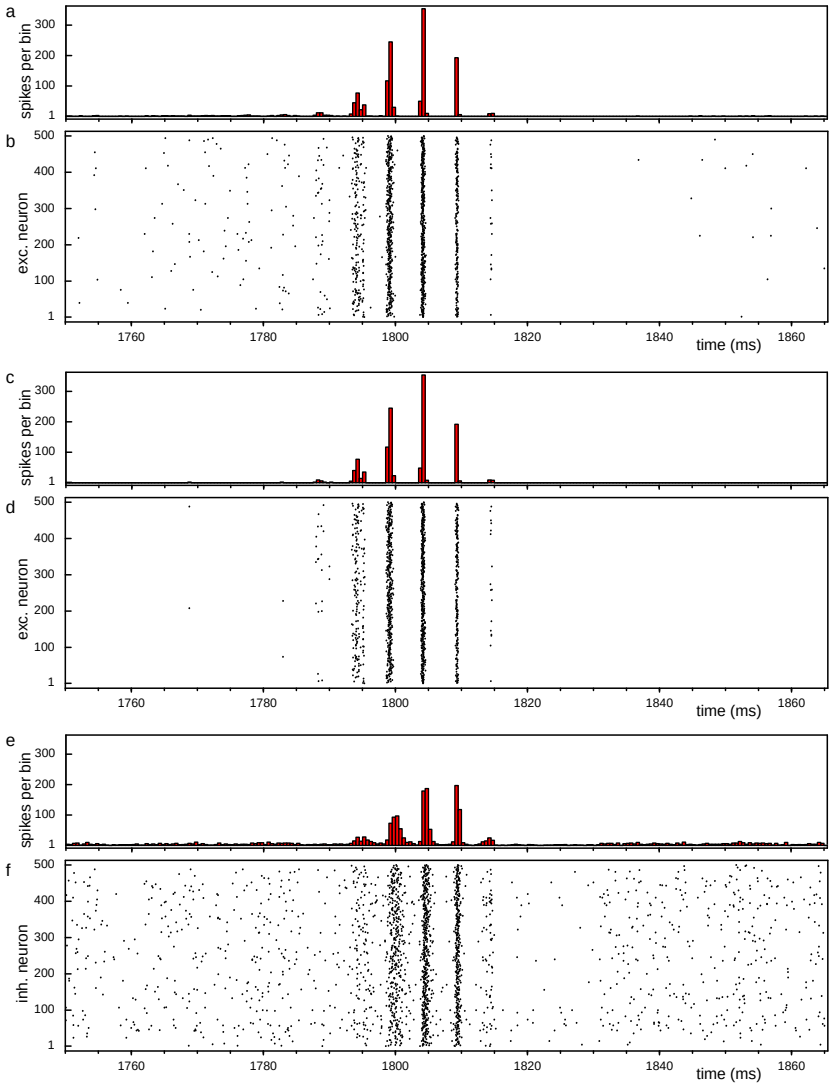

Figure 8.5: Closeup of the sharp wave/ripple-like event around $t = 1800$ms in the dynamics displayed in Fig. 8.4. The event lasts from $t \approx 1770$ms to $t \approx 1830$ms. (b) shows spiking of excitatory neurons in the network versus time. Synchronously spiking groups of excitatory neurons have temporal distance about 5ms (cf. Fig. 8.8). Precise synchronization is illustrated by histogram (a) displaying the number of spikes per bin of 1ms. (c), (d) show the filtered version of excitatory dynamics, where the background level of spiking has been removed (details see text). Spiking dynamics of inhibitory neurons (e) is less synchronous, histogram (e) shows one main peak of activity. At this event 99% of excitatory and 99% of inhibitory neurons participate.

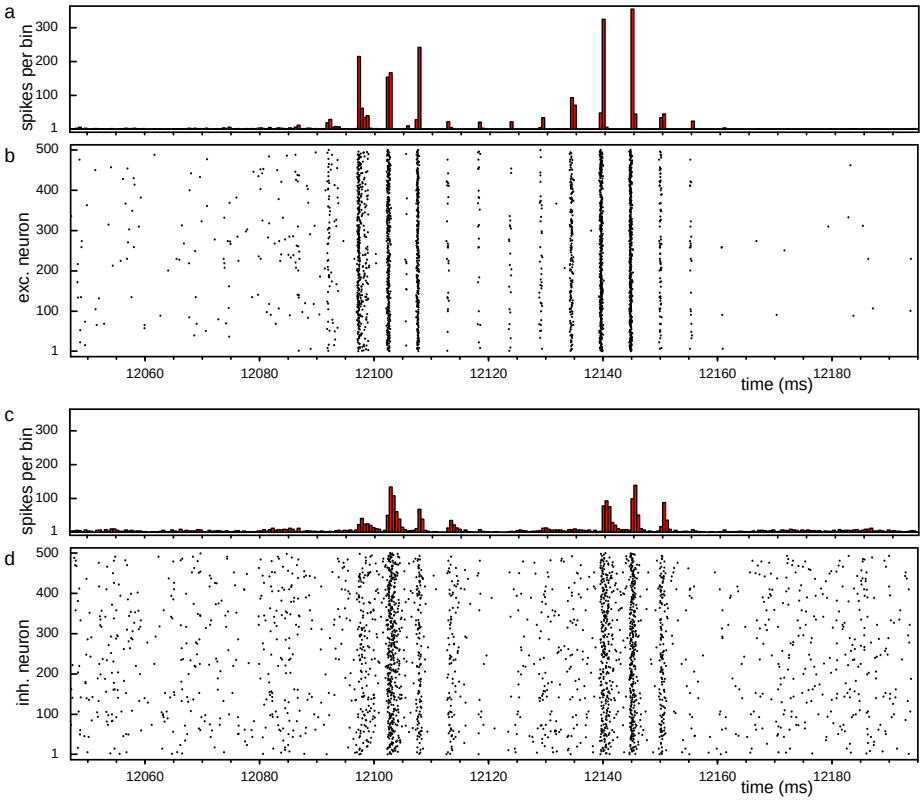

Figure 8.6: Paired sharp wave/ripple-like event found in our simulations. Figure shows number of firing excitatory (a) and inhibitory (c) neurons per bin of 1ms and spiking dynamics of the excitatory (b) and the inhibitory (d) population (see text for network parameters). In such an event, the late, well synchronized pulses of the previous event initiate a second event.

dominating inhibition thus leads to a period of low activity that finishes the event. We note that towards the end excitatory neurons will often be hyperpolarized, and that in experiment strongly hyperpolarized neurons have been shown to produce no dendritic spikes which would strengthen the effect of inhibition [13].

The spike activity can be translated into the LFP as described for the existing models in sec. 8.1. There are highly synchronous action potentials in the excitatory neurons which lead to troughs in the LFP. The time difference between the troughs is slightly above 5ms due to axonal transmission delay, synaptic transmission delay and the time for the membrane potential to reach firing threshold. Further, we will expect an increase in the LFP, a 'sharp wave' since the synchronous activity leads to a strong increase of overall and in particular interneuron neural activity (and thus to inhibitory post-synaptic currents) to balance the strong excitation due to synchronous excitation and to avoid epileptic firing.

We will refer to the model described in this section in the following as to model 3.

8.5 Analyzing the sharp wave/ripple like events

How can we quantify the evolution of a SPW/R-like event? In chapter 7, synchronization was exact. Therefore, only one parameter, the number of firing neurons g characterized a synchronous pulse (we need no distinction between a random variable g and its value g' in the recent chapter). In the presence of temporally extended couplings, the synchronous pulse will have a positive width. We can thus characterize the synchronization by the size g of the synchronized pulse and by the standard deviation σ of the firing times. Synchrony gets stronger if the number of participating spikes grows and the standard deviation from the mean firing time in an isolated pulse decreases. Instead of the evolution of the pulse-sizes as analyzed in sec. 7.4 by a transition matrix, we then have an evolution in the two dimensional σ-g space, i.e. in each step a mapping of σ-g space on itself. A similar approach has been used to study the propagation of synchronous activity along synfire chains in ref. [54].

We first have to separate the synchronous pulses from background activity. We concentrate on the population of excitatory neurons. The SPW/R-like events are easily distinguishable from the background activity because the spike rates during an event are much higher. We introduced a threshold of 100 excitatory spikes per ms for this separation which is far from background activity and easily reached by all events as was confirmed by visual inspection. To roughly isolate SPW/R-like events from background activity, around any bin at time t_0 with an excess of threshold, an interval $[t_0 - 40\text{ms}, t_0 + 20\text{ms}]$ was defined. The union of all these intervals was considered the 'event containing' part and the complement was considered to contain only background dynamics. It was checked that the incidence of SPW/R-like events is stationary over the simulation. From each interval with background activity, the mean spike frequency was derived and stationarity of the dynamics was checked. Further, the mean inter-spike-interval time $\bar{t}_{\text{ISI}}$ of back-

ground activity in excitatory neurons was derived (in the simulation $\bar{t}_{\mathrm{ISI}} \approx 0.75$ms for the excitatory population). Since background activity is approximately Poissonian with low rate (in the simulation ≈ 2.7Hz per neuron for the excitatory and ≈ 18.7Hz for the inhibitory population), synchronous pulses have a significantly higher degree of synchrony than background activity. This allows to pulses of excitatory activity in an SPW/R-like event to be separated from background activity by declaring any spike which is isolated in a time bin of some time t_θ as a spike of background activity and to delete it for the investigation of synchronous pulses [73]. Quality of separation, of course, depends on the choice of t_θ. Choosing t_θ too small leads to a loss of spike events at the vicinity of a synchronized pulse, choosing it too large leaves too much noise in the data. In contrast to the pulse packages traveling in synfire chains, we do not have distinct neuron populations which only contribute to one synchronized pulse. Therefore, we additionally have to separate the different pulses. Too much noise in the data makes this difficult. We thus found a value $t_\theta = 0.01\bar{t}_{\mathrm{ISI}}$ or smaller appropriate, which is stricter (the prefactor is six times smaller) than the value chosen in [73]. Different synchronous pulses could then be distinguished by introducing another time threshold, $t'_\theta = 2$ms and to declare spike pulses separated by more than t'_θ as different. Also here, the quality of separation depends on the choice of the threshold. For too large t'_θ, different pulses are merged, for too small t'_θ, single pulses are divided. This is however only a problem for smaller pulses before the neuron groups fire precisely synchronous. For the isolated and separated pulses, σ and g were derived and the evolution of the SPW/R-like events was visualized in the $\sigma - g$-plane revealing a rather stereotyped evolution of events, cf. Fig. 8.7. Although inputs within a window of $\Delta t = 2$ms contribute to dendritic spikes, the pulse widths are much smaller and the time differences between successive pulses are only slightly larger than 5ms with small fluctuations.

The parameters employed in the simulation are partially already given in sec. 8.2. The network has $N = 1000$ neurons, $N_E = 500$ are excitatory, $N_I = 500$ are inhibitory. Spikes arriving from excitatory neurons lead to a jump in the fast and slow excitatory conductances about $\Delta g_A = 22\mathrm{mVms}/(\tau_A(E_{\mathrm{Ex}} - V_{\mathrm{rest}})) \approx 0.048$, $\Delta g_N = 22\mathrm{mVms}/(\tau_N(E_{\mathrm{Ex}} - V_{\mathrm{rest}})) \approx 0.0017$ (measured in multiples of the resting conductance) which generates a peak EPSP of approximately 1mV from resting potential for a neuron with membrane time constant $\tau_{\mathrm{mem}} = 10$ms. Spikes from inhibitory neurons lead to jumps in the inhibitory conductances about $\Delta g_G = -10\mathrm{mVms}/(\tau_G(E_{\mathrm{In}} - V_{\mathrm{rest}})) = 0.1$. The probability for the existence of a connection from an excitatory to an excitatory neuron is $p_{\mathrm{ExEx}} = 0.08$, thus the excitatory-excitatory network is very sparse, for an excitatory→inhibitory connection $p_{\mathrm{InEx}} = 0.13$, for an inhibitory→excitatory connection $p_{\mathrm{ExIn}} = 0.13$ and for an inhibitory→inhibitory connection $p_{\mathrm{InIn}} = 0.1$. Connections between neurons are randomly and independently realized according to these probabilities. The resting and reset potentials are put to $V_{\mathrm{rest}} = V_{\mathrm{r}} = -65$mV. The membrane time constants $\tau_{\mathrm{mem},l}$ and somatic firing thresholds $\Theta_{U,l}$ are uniformly distributed within

$\tau_{\mathrm{mem},l} \in [8\mathrm{ms}, 12\mathrm{ms}]$ and $\Theta_{U,l} \in [-50\mathrm{mV}, -47\mathrm{mV}]$ (cf. [11], p. 139)[8]. The simulation shown in Fig. 8.6 has parameters $\Delta g_A = 14.4\mathrm{mVms}/(\tau_A(E_{\mathrm{Ex}} - V_{\mathrm{rest}})) \approx 0.032$, $\Delta g_N = 14.4\mathrm{mVms}/(\tau_N(E_{\mathrm{Ex}} - V_{\mathrm{rest}})) \approx 0.0011$ (single excitatory coupling generates an EPSP with peak 0.7mV at $\tau = 10\mathrm{ms}$), the threshold for the dendritic spike is at 2.6mV peak EPSP so that still four simultaneous excitatory inputs generate a dendritic spike and the initial current strengths after initiation of a dendritic spike are $\Delta g_{\mathrm{NL,Ex}} \approx 19$ and $\Delta g_{\mathrm{NL,In}} \approx 91$. External input to each neuron is modeled by uncorrelated Poisson spike trains with frequency 8kHz, 70% of the inputs are excitatory, leading to conductance jumps of $\Delta g_A = 8\mathrm{mVms}/(\tau_A(E_{\mathrm{Ex}} - V_{\mathrm{rest}})) \approx 0.018$ and $\Delta g_N = 8\mathrm{mVms}/(\tau_A(E_{\mathrm{Ex}} - V_{\mathrm{rest}})) \approx 0.0006$ and 30% are inhibitory leading to conductance jumps of $\Delta g_G = 0.08$. Neurons and dendrites have a total refractory period of 3ms. During the refractory period of the neuron after a somatic spike, the membrane potential stays constant at the resting potential. Spikes received during the dendritic refractory period after a dendritic spike do not contribute to dendritic spikes, in particular no dendritic spikes are generated. The delay between spike sending and somatic reaction in the postsynaptic neuron is $\tau = 5\mathrm{ms}$.

The rather stereotyped time course of an SPW/R-event allows the congeneric synchronous pulses of excitatory spikes to be collected within the different events. An event usually consists of some large synchronous pulses, preceded and followed by some small synchronous pulses. We further note that there are usually about $n = 7$ sufficiently clearly synchronous distinct pulses. We take the last large pulse as reference. It was suitable to define 'large' as 'containing more than 25 spikes'. This in particular defines the border between pulse 6 (red) and pulse 7 (blue green) parallel to the σ-axis at $g = 25$ and determines the clustering structure in Fig. 8.8. We tag this last large pulse by number 6. Previous pulses are numbered backwards down to 1 (if enough pulses are present, otherwise we stop at a higher number) and the subsequent pulse (if present) is numbered 7. Possible remaining unnumbered pulses are neglected. Congeneric synchronized pulses in different events have similar properties concerning standard deviation, size and distance to the next pulse, cf. Figs. 8.8 and 8.9.

Time differences between pulses become shorter towards later events where also the pulses are larger and then grow slightly. The fluctuations in time difference and standard deviation become very small towards the end of an event. Indeed, we expect that with increasing pulse-size the time difference between the mean firing times of synchronous pulses decreases, since only a short period of input sampling is necessary before dendritic spikes are generated. Further, we expect that pulses with larger standard deviation generate larger fluctuations in the time between pulses but also an earlier succeeding pulse, because there is a large number of spikes sent before the mean firing time of the pulse and these spikes can already generate early responses.

[8] We note that at the best, for membrane constant $\tau_{\mathrm{mem},l} = 8\mathrm{ms}$ and threshold $\Theta_{U,l} = -50\mathrm{mV}$, 12 simultaneous excitatory inputs would be necessary to excite the neuron from rest to spiking.

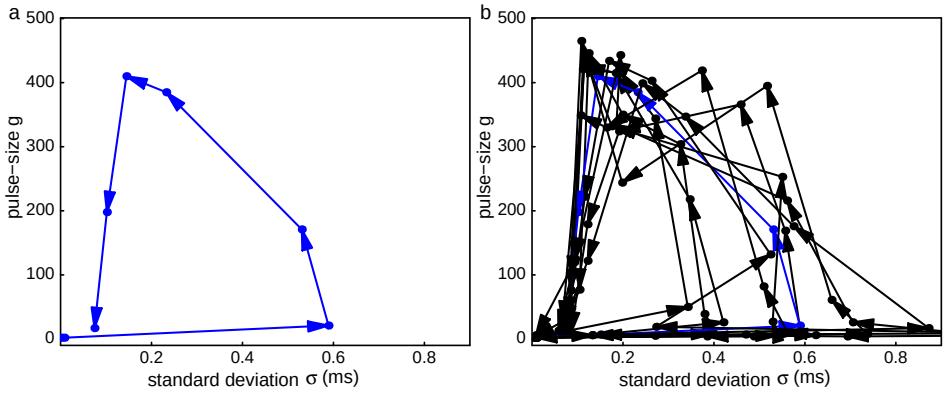

Figure 8.7: SPW/R-like events in the σ-g representation. After isolating the events, removing the background activity (cf. Fig. 8.5 for an illustration) and splitting the event into its different synchronous pulses, it is possible to characterize the evolution of the event in terms of synchronous pulse-sizes g (number of spikes in the pulse) and standard deviation of pulses σ. Single event (a) as displayed in 8.5. Each dot represents a synchronized pulse of the event in terms of its size and its standard deviation. Successive pulses are connected by an arrow which allows the time evolution of the event to be followed: Pulse-sizes and standard deviations in the beginning are not far from background synchronization, the low standard deviation is a consequence of the small pulse-size and the filtering method: Small pulses at the beginning of an event often have smaller standard deviations, because the filtering procedure removes the events at the edges of the pulse. After first slightly increasing, the pulse-sizes grow significantly larger and pulses become highly synchronized. Towards the end of the event, the size of the pulses decays back to very small values due to dominating inhibition, while synchrony still increases. Displaying all events between $t = 0$ms and $t = 5000$ms in one figure (b) reveals the remarkably stereotypical structure of the events. (Event displayed in (a) also colored blue in (b) for comparison.)

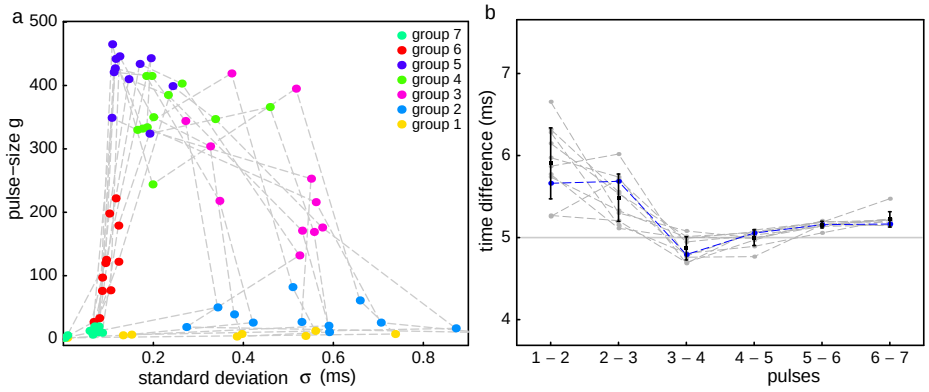

Figure 8.8: Stereotypical event evolution allows separation of the main part of the event in congeneric synchronous pulses. (a) In the σ-g plane, congeneric pulses are clustered (different pulses highlighted with different colors, dashed lines connect pulses of the same event). This shows that sorting relative to the last large pulse indeed divides the events into pulses with similar properties. Time differences between mean firing times in congeneric synchronized pulses are displayed in (b). Particular differences between mean firing times of subsequent synchronous pulses are given by gray dots, differences belonging to the same SPW/R-like event are connected by gray dashed lines. The event displayed in Fig. 8.5 is highlighted by blue color. The mean time differences of congeneric pulses taken over all events are indicated by black boxes, error bars give standard deviation of the mean. Time differences are slightly above 5ms and are expected to decrease with increasing pulse-size and to increase with increasing synchrony (see text).

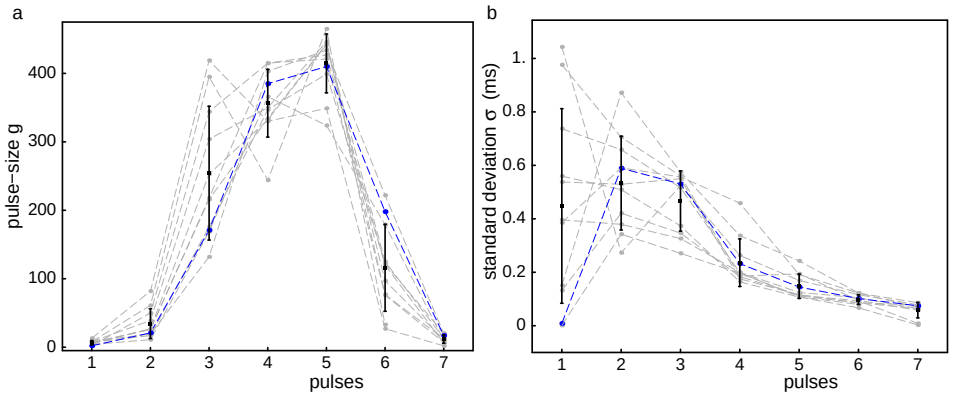

Figure 8.9: (a) Pulse-sizes g and (b) standard deviations σ of congeneric synchronous pulses in different events. Pulse-sizes and standard deviations of individual events are given by gray dots connected by dashed gray lines. Mean values of pulse-sizes and standard deviations for congeneric pulses are taken over all trials. Error bars are standard deviations of the mean. Plots show the increasing and finally decreasing pulse-size during an event and the increasing synchrony.

8.6 Comparison with some experimental results

In this section, we put our model 3 to test by checking its compatibility with experimental results. We partially also discuss the compatibility of models 1 and 2. We will focus in particular on the CA1 region. SPW/R events have been detected in hippocampal slices in the isolated CA1 region and the results about nonlinear dendrites our model is based on have have been derived in this region [13]. However, in the CA3 region neurons are structurally similar and strong collateral pyramid-pyramid connections are known to be present. Thus, although in CA3 dendritic excitability is less well studied ([11], p. 159), our model might in particular also apply to this region. Indeed, in the intact hippocampus, SPW/R events are usually initiated in the CA3 region and occur with higher incidence than in the functionally isolated CA1 region [143].

Pyramidal neurons in CA1 are coupled via axon-to-basal-dendrite synapses [52]. The interval between a stimulation of a dendritic spike in the basal dendrite and the somatic spike is 5.0 ± 0.1ms if the input strength is so that an action potential is generated with 20% reliability and 5.1 ± 0.1ms if the spike is generated with 100% reliability (standard deviation gives the jitter between recorded neurons as derived from a measurement with $n = 5$ neurons). The temporal jitter between trials is 0.14 ± 0.02ms and 0.12 ± 0.05ms [13]. This means that the timing of spikes has sub-millisecond intra- and inter-neuronal precision and is nearly independent from the input strength. In contrast, if action potentials are generated without dendritic spiking by pairing basal and apical dendrite stimulation, the timing of evoked action

potentials shows a strong dependence on the strength and number of inputs.[9] Our simulations show that when dendritic spikes lead to action potential timing with this remarkable precision, SPW/R-like events are seen in the network dynamics[10]. Further, in contrast to the existing models 1 and 2, our model based on [13] predicts the frequency of ripples to be about 200Hz. Interestingly, also epileptic activity in the absence of inhibition in the CA3-CA1 system has this frequency which might also be explainable by the mechanisms of our model [117]. The interval between stimulation and response also depends on the axonal length the spike has to travel before reaching the synapse, and the synaptic delay. Therefore it is expected to depend on the species and the hippocampal region studied (see, e.g. [117]). The inter-ripple interval might also slightly depend on the strength of coupling, the number of synchronized neurons and the strength of synchronization cf. Fig. 8.8. During sharp wave ripples, an increased number of dendritic spikes has been found in CA3-CA1 neurons [103] which supports our model based on dendritic spikes.

Sharp waves in hippocampal slices often do not carry detectable ripples (see, e.g. [117]). This might support the view that sharp waves and ripples have different causes. It might, however, also be be due to the filtering properties of the LFP or due to the occurrence of less well synchronized events. Such events occasionally occurred in our simulations as well.

In our model, convergent inputs from synchronized groups of excitatory neurons lead to dendritic spikes in further excitatory neurons whose firing then generates the subsequent synchronous group. In the hippocampal regions CA1 and CA3 where ripples have been most studied, excitatory microcircuits exist [43], but the connectivity between its principal neurons is known to be very sparse. For CA1, the estimate is that 1% of the possible local pyramidal-pyramidal connections are realized [52]. The result was derived from paired recordings of cells where the pairs were randomly chosen with distance of 200μm[11]. In CA3, the connectivity of principal neurons is estimated to be $2-6\%$ ([9],[185], p. 62). Individual couplings are however strong. In CA1, the amplitude of EPSPs in a pyramidal cell generated by a presynaptic pyramidal cell were measured as 0.7 ± 0.5mV [52], in CA3 amplitudes lie between $0.6-1.3$mV ([185], p. 49). Thus, since the threshold for the generation of a dendritic spike is only about 3.9mV [13], already a few strong synchronous inputs may be sufficient to generate such an event. The precise number is still unknown ([13], cf. also the estimation of $4-30$ inputs needed in neocortical apical dendrites given in [205]). It will also depend on the position and on the clustering of the activated synapses. In particular, synapses at the same compartment are expected to have largest effect [128, 154, 153, 157]. The patterned arrangement of pairs found to be connected in CA1 might indicate that the apparently low

[9] It decreases from 8.81 ± 2.23ms with temporal jitter 1.83 ± 0.55ms at 20% AP generation probability to 5.94 ± 1.3ms with temporal jitter 0.87 ± 0.34ms at 100% AP generation probability [13].

[10] If distributed apical EPSPs are paired with basal dendritic spikes, the action potential timing decreases down to 4.39 ± 0.15ms (80% action potential reliability), we did not include this in our model, although there is background stimulation of the neurons [13].

[11] A. Thomson, personal communication.

connectivity masks a structured organization of couplings [52], indeed for regions in CA3 it is known that the connection probability between neurons decays exponentially with distance [9]. This might also be indicated by the fact that the participation of pyramidal neurons in SPW/R events varies a lot and by the fact that during one event only a small fraction of neurons participates (cf. sec. 8.3). Additionally, electric couplings between neighboring pyramidal neurons have been shown to exist at the dendrite close to the soma which might increase the tendency of neurons to form synchronized groups [133] together with possible influences of field effects (ephaptic effects) of the LFP increasing the excitability of neurons [96]. In our simulations, where connections are randomly distributed with equal probability, we have thus chosen a sparse network with connection probability of 8% and an EPSP amplitude of 1mV. Four excitatory inputs within a time window of $\Delta t = 2$ms are then sufficient to evoke a dendritic spike where a dependence on synaptic positions was neglected. We did, however, not explore the lower limiting values for these parameters. Couplings from excitatory to inhibitory neurons and from inhibitory to excitatory neurons are found to be strong in CA1 and CA3 ([11], pp. 138,156), this has been included in our model and is necessary to overcome the strong effect of excitatory synchronous inputs, to finish SPW/R events and to avoid epileptic dynamics.

Electrophysiological studies have established the dependence of SPW/Rs on chemical synapses. Blocking fast excitatory AMPA receptors (20μM AMPA/Kainate receptor antagonist CNQX or 20μM AMPA receptor antagonist GYKI) abolishes both spontaneous and stimulus induced SPW/Rs. The phenomenon thus crucially depends on AMPA synaptic interaction. Light block of NMDA receptors (30μM D,L-APV[12]) has no influence while a strong block increases the size of SPW/Rs and the ripple amplitude (100μM D-APV) [117, 116, 45]. This might suggest that excitatory chemical transmitter systems are directly involved in the generation of SPW/Rs. To interpret these results in the context of model 3, we first note that the generation of dendritic spikes also crucially depends on AMPA synaptic interactions. Blocking AMPA receptors (20μM CNQX) abolishes the fast component of the dendritic spikes (after NMDA was blocked). Further, there is an NMDA receptor dependence, in the form that dendritic spikes can still be generated also if NMDA receptors are strongly blocked (100μM D-APV) provided that the input strength is sufficiently increased (factor 2)[13]. In this case also NMDA spikes are missing [13]. The increase of incidence and amplitude in SPW/Rs when NMDA is blocked might be due to less excitation of inhibitory neurons and thus more frequent spontaneous synchronization of excitatory neurons. Indeed, very recently such an "opposite" effect of NMDA blockade has been found in the neocortex [87]. Also, the number of inputs needed to generate a dendritic spike increases. The influence of both effects remains to be studied. The amplitude increase could also be a direct consequence of missing excitatory NMDA dependent currents due to

[12]We note that the L-enantiomer has no influence on NMDA channels.

[13]Up to now, there is no data about the influence of light NMDA block. J. Schiller, personal communication.

missing NMDA spikes, which leads to increased LFP amplitudes. The influence of excitatory chemical transmission might also be explainable in the context of models 1 and 2, by indirect influences due to changed network spiking dynamics, by direct influences on the LFP shape or direct influences on the chemical transmission dependent sharp wave.

In the absence of relevant chemical coupling (40μM $GABA_A$ antagonist Bicuculline, 20μM AMPA/Kainate receptor antagonist NBQX, 40μM D-APV) or upon total block of chemical synapses by bathing in nominally calcium free solution, spontaneous ripple like oscillations at frequencies around 200Hz still spontaneously occur in the LFP [55]. Further, ripples can be induced when blocking fast chemical coupling (10μM Gabazine, 20μM CNQX, 30μM D,L-APV[14]) when strong stimulation of neurons by KCl is applied [143]. In both cases the ripple frequency is less precise and the characteristics of the events are a bit different [55]. Further, the sharp wave is missing, which might suggest that it is indeed due to inhibitory synaptic currents (cf. sec. 8.1). These results cannot be explained by model 3 or by model 1. They form the basis of model 2. The oscillations in absence of chemical coupling might however have a different origin as the ripples observed under physiological conditions.[15]

Application of agents blocking electrical coupling reduces the incidence of sharp wave ripple events. The uncoupling agents carbenoxolone (200μM) and octanol (1mM) reduce the spontaneous occurrence of sharp waves and strongly reduce the fraction of sharp waves carrying ripples. Both uncoupling agents had no systematic effect on the frequency of the remaining ripples [117]. Further, the anesthetic halothane, which is also an uncoupling agent, abolishes the ripples superimposed to sharp waves in vivo [206]. It has to be noted however, that gap junction blockers are not very selective and have a many side effects. Further, since the sharp wave persists under block of gap junctions with halothane, it cannot be just a consequence of oscillations of pyramidal neurons that are electrically coupled. The assumption of a separate source for the sharp wave in model 2 is necessary. In model 3, the reduced incidence in SPW/Rs might be due to less spontaneous synchronization. Gap junctions tend to synchronize neurons, so blocking of gap junctions reduces the size of spontaneously synchronized groups of neurons and thus the incidence of SPW/Rs. The loss of ripple incidence might be due to side effects that lead to less synchronization or the agents change the LFP pattern in response to a certain activity. In the context of models 1 and 2, one might argue in a similar way to explain loss of incidence of population spikes leading to sharp waves. Model 2, however, also predicts that the frequency of ripples decreases with decreasing strength and with decreasing number of gap junctions. This is in contradiction to the observation that addition of uncoupling agents had no systematic effect on the

[14] We note that it is unclear if chemical transmission by NMDA channels is really completely blocked by 30μM D,L-APV since it had no influence on the ripple incidence in contrast to 100μM D-APV.

[15] It has to be noted that bursts of single neurons have frequencies around 200Hz and are sometimes hard to distinguish from population events and that bathing in Ca-free solution makes neurons highly excitable and prone to bursting ([11], p. 157).

frequency of the remaining ripples.

Finally, sharp wave ripples are supposed to be involved in learning. Indeed, firing patterns during sharp wave ripples are similar to firing patterns during running activity preceding rest (cf., e.g., [109, 53]). During repeated running of an animal through an environment, sequences of place cell groups are successively activated. Hebbian learning together with time compression mechanisms then might lead to modification of excitatory connections, in particular to strengthening of connections from the preceding group of excitatory place cells to the successive group [147]. During sharp waves, the sequences of activation are then replayed in a time compressed way (e.g. [109, 53]). We expect a model based on excitatory connections such as model 3, to reflect the differences in excitatory coupling strengths in firing activity which might lead to replay of stored sequences (cf. the modeling study [16] and the concepts of synfire chains [3, 4] and strengthened pathways [201]).

8.7 Conclusion and outlook

We have shown that in networks of model neurons incorporating nonlinear dendritic enhancement, sharp wave/ripple-like patterns spontaneously occur. We analyzed the pattern and found that it agrees with the spike pattern assumed to underlie sharp wave/ripples in local field potential. In contrast to the two existing models for sharp wave/ripples, our model predicts the frequency of the ripple oscillations and explains the entire sharp wave/ripple complex as one phenomenon and not as consisting of two parts, sharp wave and superposed ripples. Also, the role sharp wave/ripples are assumed to have in learning might fit well with our model [37]. We discussed our model and partially the existing models in the context of neurophysiological experiments on sharp wave/ripples and neuroanatomical knowledge about the brain regions in question. We emphasized that also a combination of the mechanisms described by the three existing models might be responsible for the pattern of activity. We concluded that, taking into account present knowledge, our model provides a plausible explanation for the occurrence of sharp wave/ripples.

Our study opens a new field of theoretical research in neural network dynamics, namely research on the spiking dynamics of recurrent neural networks with supralinear dendritic interactions (cf. sec. 2.1). We addressed the implications of fast nonlinear dendritic enhancement as found in hippocampal CA1 pyramidal neurons [13]. Fast nonlinear dendritic enhancement has been also found in the neocortex [142]. The implications remain to be studied. In other neurons (neocortical layer-5 pyramidal neurons) and dendrites, nonlinear dendritic enhancement was found that takes place on longer timescales. Here, also inputs with larger temporal distances summate supra-linearly [157]. Future research needs to study the implications of such nonlinearities on the dynamics of neural networks both with rate models, employing the multi-layer neuron model developed in [128, 129, 154, 153] and spiking single compartment neuron models where nonlinear dendritic effects are taken into account. Such models were developed in secs. 7.2, 8.2. We will also study larger

networks and more detailed neurons such as interneurons which can also possess nonlinear dendrites and response properties [101]. Larger networks with perhaps more structured connectivity are expected to lead to a smaller participation rate of excitatory neurons in single sharp wave/ripple-like events in quantitative agreement with experimental findings. Further, the size of nonlinearity is assumed to depend on the positions of the active synapses on the dendrites. This can be implemented in our models. Even for highly detailed models (cf., e.g., [13, 153]) it might be possible to study the propagation of synchrony without the need to simulate larger networks using methods employed in chapters 8.

Further, future research needs to study the influence of network topology and connection strengths on the propagation of synchrony. The connection probability in a larger neural network depends on the spatial distance between neurons. The spread of synchronous pulses through such a network remains to be studied. Also, the participation of neurons in synchronous pulses has to be studied for random networks and for networks with underlying structure. We have seen that in networks with supra-linear dendritic interaction, synchronous pulses propagate through the network without being bound to certain groups. However, from previous research on synfire chains and related networks [18, 124, 175, 201, 139], we expect that sequences of neuron groups with strengthened directed excitatory connections give rise to sequences of spikes occurring with higher probability. In the context of our model for sharp wave/ripples, this would have important consequences for the assumed role of this pattern during learning.

Another question concerns networks with dynamical topology, i.e. networks that continue learning when synchrony propagates. On the one hand, due to probabilistic replay of sequences, propagation of synchrony might lead to strengthening of synaptic connections. On the other hand, random propagation of synchrony or replay of many different sequences might lead to elimination of structure and thus to the erasure of memories. Both possibilities are conjectured for neurobiological networks (cf. e.g. [126] and references therein).

We have seen that, with respect to present knowledge, our model for sharp wave/ripples is plausible. It thus has to be further examined to clarify the mechanism underlying this prominent pattern of activity. A related task is to derive the local field potential from the spiking activity of the different models. The investigations will also yield further insight into the role of sharp wave/ripples in learning.

Chapter 9

Conclusion and outlook

In this thesis, we have studied precise spike timing in complex neural network models from different perspectives. For a general class of neuron models, we analytically derived the networks that give rise to predefined precisely timed patterns of spikes. We investigated the stability properties of trajectories underlying periodic and irregular precise spiking dynamics and checked the degree of robustness of our statements. Further, we analytically and numerically showed that in networks with nonlinear dendritic interaction, pulses of precisely synchronized spikes propagate through the network, which led to a quantitative model for experimentally found sharp wave/ripples in the Hippocampus.

We studied the dynamics of networks of spiking neurons from an uncommon perspective by predefining an arbitrary spiking dynamics and designing the networks so that they give rise to the dynamics as a solution of the dynamical system through an appropriate initial condition (chapter 3). Indeed, the idealization of infinitely fast responses of neurons (the synaptic currents have infinitesimal rise and decay time) makes is possible to analytically determine the class of networks that gives rise to a predefined pattern. The very general methods developed are applicable to networks with predefined topology and allow the selection of networks optimized with respect to given criteria, such as wiring costs. They are useful, e.g. to numerically investigate the stability properties of periodic patterns of spikes or to illustrate analytically derived results; a generalization of the methods for couplings of finite temporal extent is used in chapter 6.

Future research will consider networks with dynamical network topology, i.e. deal with learning of patterns and the stability of patterns in networks with changing network topology. This is particularly important with regard to patterns generated by biological neural networks which exhibit spike timing dependent plasticity such as cortical networks. The possibility to select networks with predefined structure that are optimized with respect to given criteria suggests the application of the generalized and further complemented network design method to biological neural

networks where the entire coupling structure as well as the desired dynamics are known (see e.g. [146]). A comparison of the class of possible networks with those realized in nature could reveal optimizing principles underlying network topology found in natural systems.

We studied the stability of spiking dynamics from a general perspective (chapters 5 and 6). In chapter 5, we assessed periodic spike patterns, where particular emphasis was put on mathematically strict formulation. We analytically showed stability, asymptotic stability or instability of arbitrarily complicated non-degenerate patterns (i.e. pattern where no simultaneous events occur) for different, large classes of networks. We numerically illustrated and interpreted our results. The exact, nonlinear proof of stability is based on the fact that interactions lead to averaging of finite size perturbations, the dynamics is even asymptotically stable in strongly connected networks where perturbations of all neurons necessarily average over time. The proof of instability establishes that a class of arbitrarily small perturbations can only grow upon interaction. In chapter 6, we generalize our ideas to the irregular balanced state in purely inhibitory networks. We analytically showed the asymptotic stability of trajectories underlying the generic irregular spiking activity. In contrast to the periodic dynamics, we had to explicitly study the decay of a small but finite size perturbation and to ensure that it is fast enough so that the order of events does not change, which would result in a large perturbation. We gave analytical and numerical evidence that the irregular activity finally converges to a periodic orbit, and investigate the borders of stable to chaotic dynamics. We conclude that the highly irregular dynamics in purely inhibitory networks with delayed couplings and synaptic currents of infinitesimal temporal extent is stable for a class of neuron models covering e.g. leaky integrate-and-fire neurons. This contrasts to mixed networks with sufficient excitatory coupling. The results are particularly interesting since the balanced state is often associated with chaotic dynamics [198, 199] and the mean field descriptions [199, 30] of purely inhibitory and mixed, excitatory and inhibitory networks are nearly identical. In a recent study, numerical simulations using a network model which is contained in the class investigated in chapter 6 were interpreted as showing a chaotic balanced state [76]. This would contradict our analytical findings. We refute the interpretation in the appendix. We further describe the mechanism which underlies the switching dynamics whose observation is the main result of the article [76].

Future research will address the application of statistical methods derived for the isolation of recurrent patterns of spikes in neurobiology [66, 151] to our models. Preliminary studies have shown that indeed the stored stable patterns can be found. This will test the statistical methods and show for which network model parameters precisely timed patterns of spikes are generated and thus how appropriate the models are for the description of neural activity.

We considered a specific type of precisely timed spiking activity, propagating synchrony (chapters 7 and 8). Synchrony is known to stably propagate along strongly excitatory feed-forward structures (synfire chains) [3, 83, 54, 18]. Up to now, however, there is no neurobiological evidence for the existence of such struc-

tures. We studied – for the first time – the dynamics of larger recurrent networks of spiking neurons that incorporate nonlinear dendritic interactions as found in neurobiological experiments [13, 157, 142]. In chapter 7, we developed an appropriate neuron model and studied both numerically and analytically that fast nonlinear dendritic enhancement as found in [13] can lead to stable propagation of synchrony even in random neural networks without embedded feedforward structure. We analytically investigated the bifurcation to stable propagation which arises when nonlinearity is increased. From the experimental data, the temporal distance between synchronized groups is determined to 5ms which leads to oscillations of 200Hz superposed to network activity [13]. Interestingly, in the hippocampal region considered in ref. [13], a prominent pattern of activity, sharp waves with superposed ripples of 200Hz involving synchronous activity of excitatory neurons is found in neural mass signals [206, 116, 37]. We were thus led to conjecture a connection between propagation of synchrony and this pattern and examined it in chapter 8. To exclude possible model artefacts, we developed a more detailed neuron model based on [13]. We showed with numerical simulations that in networks of these neurons, sharp wave/ripple-like patterns spontaneously occur. We analyzed the pattern and found that it agrees with the spike pattern assumed to underlie sharp wave/ripples. In contrast to existing models for sharp wave/ripples, our model predicts the frequency of the ripples based on neurophysiological data [13]. We discussed our model and also the two existing models in the context of neurophysiological experiments on sharp wave/ripples and neuroanatomical knowledge of the hippocampal regions where they occur. We finally concluded that, with regard to present knowledge, our model provides a plausible explanation for sharp wave/ripples.

This study opens a new field of theoretical research in neural network dynamics, namely research on the dynamics of recurrent spiking networks with supra-linear dendritic interactions. The study is based on fast nonlinear dendritic interactions as described in [13]. One direction of future research will address other forms of supra-linear dendritic summation described e.g. in [157], employing both rate models [128, 129, 154, 153] and single compartment spiking neuron models (secs. 7.2, 8.2). Also, larger networks and more detailed neuron models can be studied using the methods of chapters 7 and 8. Another direction of future research concerns the influence of network topology and connection strengths on the propagation of synchrony. Vice versa, in networks with dynamical topology, propagating synchrony changes the coupling strengths in the network. In the context of our model, these studies will reveal further insight in the role of sharp wave/ripples in learning. Finally, we have seen that, with respect to present knowledge, our model for sharp wave/ripples is plausible. It thus has to be further examined. Is the described mechanism underlying sharp wave/ripples? Is a combination of the mechanisms given by the three existing models responsible for this prominent pattern of activity? What is the role of sharp wave/ripples in learning? Only further theoretical and experimental research can answer these questions.

Appendix A

Remark on ref. [76]

On the basis of our analytical stability analysis for the balanced state (chapter 6), we refute the interpretation of recent numerical results as showing a chaotic balanced state. The numerical results and the interpretation were given in the article "Dynamically maintained spike timing sequences in networks of pulse-coupled oscillators", ref. [76]. As the main result, the article describes switching between regular patterns of activity in networks with very long delay, the origin of the phenomenon was unclear. We describe the underlying mechanism in sec. A.3.

We derived the results of this appendix together with S. Jahnke.

A.1 The model

The model used in ref. [76] is a network of $N = 100$ leaky integrate-and-fire neurons. In the notation of ch. 6, the dynamics is given by

$$\frac{dV_l(t)}{dt} = -\gamma V_l + \sum_{j=1}^{N} \sum_{k\in\mathbb{Z}} \varepsilon_{lj}\delta(t - t^{\mathrm{s}}_{jk} - \tau) + I_0. \tag{A.1}$$

The model is contained in the class of models considered in this chapter. We adopt the parameters of ref. [76], the neuron threshold $V_\Theta = 10\mathrm{mV}$, the reset potential $V_\mathrm{r} = 0$, the membrane time constant $1/\gamma = 40\mathrm{ms}$ and the current $I_0/\gamma = 50\mathrm{mV}$. Since $I_0/\gamma > V_\Theta$, all neurons intrinsically oscillate with the same period $T_0 \approx 8.926\mathrm{ms}$. The networks are purely inhibitory, the probability for the existence of a coupling is $p_0 = 0.08$. The coupling strength is normalized, $\varepsilon_{lj} = \varepsilon/|\mathrm{Pre}(l)|$, for $j \in \mathrm{Pre}(l)$, where $\varepsilon = -18\mathrm{mV}$. The coupling delays are either $\tau = 1.2\mathrm{ms}$ (short delay) or $\tau = 72\mathrm{ms}$ (long delay).

A.2 Dynamics with short delay

For short delay, ref. [76] states that "the finite time Lyapunov exponents [...] remain positive all the time. Here, chaotic collective dynamics makes spike timing patterns variable and irregular, which is known as balanced state". The authors use a different definition of phase,

$$\phi_{\mathrm{GL},i}(t) = 2\pi \frac{t - t_i^k}{t_i^{k+1} - t_i^k}, \tag{A.2}$$

where t_i^k denotes the last firing time of neuron i before t, and t_i^{k+1} denotes the first firing time of neuron i after t [150]. The perturbation is applied by choosing a spike time t_0 of a reference oscillator and adding a random perturbation uniformly distributed in $[-\sigma/2, \sigma/2]$, where $\sigma = 0.6$ms [76] to the last previous spike times of the neurons.[1] The phase distance at time t_n, the nth firing time of the reference neuron after t_0, is defined by

$$D_n^{\mathrm{GL}} = \sum_{i=1}^{N} |\phi_{\mathrm{GL},i}(t_n) - \phi'_{\mathrm{GL},i}(t_n)|, \tag{A.3}$$

where $\phi'_{\mathrm{GL},i}(t_n)$ are the phases in the perturbed dynamics at the firing time t_n of the unperturbed reference oscillator. Finally, the finite-time Lyapunov exponent is defined as

$$\lambda^{\mathrm{GL}}(t_0) = \frac{1}{M} \ln \left(\frac{D_M^{\mathrm{GL}}}{D_0^{\mathrm{GL}}} \right), \tag{A.4}$$

where $M = 20$ is chosen. $\lambda^{\mathrm{GL}}(t_0)$ is then given for different firing instances t_0 of the reference neuron.

We use the Mirollo-Strogatz phase representation,

$$\phi_i(t) = U_{\mathrm{IF}}^{-1}(V_i(t)), \tag{A.5}$$

where U_{IF} is the rise function of the leaky integrate-and-fire neuron (cf. sec. 3.4). This allows us to use analytical results derived in ch. 6 about the evolution of perturbations in this representation. For the free dynamics both phase representations only differ by a constant factor. Of course, a change in the representation of the dynamics does not change the stability properties of the trajectories. Indeed, we qualitatively reproduce the numerical results found in [76]. We have to slightly modify the definition of phase differences by taking the perturbed phases ϕ'_i at the firing times t'_n of the perturbed reference oscillator,

$$D_n = \sum_{i=1}^{N} |\phi_i(t_n) - \phi'_i(t'_n)|. \tag{A.6}$$

[1] Personal communication, P. Gong.

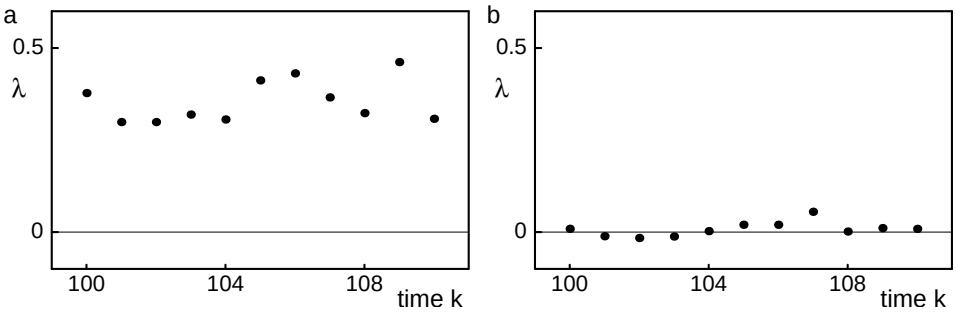

Figure A.1: $\lambda(t_0)$ measured after a perturbation with standard deviation $\sigma = 0.6$ms has been applied to the phases at t_0, where t_0 is the kth firing time of the reference oscillator. $\lambda(t_0)$ has been measured using (a) the L_1-norm (cf. Eq. (A.7)) and (b) the L_∞-norm (cf. Eq. (A.9)) for the phase distances. In both norms, some perturbations grow over time, which is reflected by the positive values of $\lambda(t_0)$.

Otherwise, due to the hybrid character of our dynamical system, we face a complication already familiar from sec. 2.7 and chapters 5, 6: If the unperturbed reference oscillator fires an arbitrarily short time before the perturbed reference oscillator, the perturbed oscillator is reset at time t_n, while the unperturbed oscillator is close to threshold, so that we measure a large perturbation in the phase of the reference oscillator. This is especially important if we measure the maximal perturbation as in Eq. A.8 (see below). However, in any norm the measurement would lead to fluctuations in the measured phase differences and thus in derived quantities. Furthermore, in definition A.3, a dynamics which is equivalent, only shifted in time with respect to the original dynamics will appear as different. The finite-time Lyapunov exponent is defined analogously to A.4 as

$$\lambda(t_0) = \frac{1}{M} \ln \left(\frac{D_M}{D_0} \right), \tag{A.7}$$

with $M = 20$. $\lambda(t_0)$ is computed for different firing instances t_0 of the reference neuron, cf. Figs. A.1a, A.2a. We did not reproduce the exact perturbation paradigm, but applied uniformly distributed jitter to the Mirollo-Strogatz phases of the neurons at time t_0. For free time evolution of each neuron, both perturbation paradigms are identical, interactions reduce the perturbation of the last spike time in the phase representation (cf. ch. 6). Our numerical simulations with perturbations uniformly distributed with $\sigma = 0.6$ms show that the perturbation is a large perturbation (cf. Fig. A.1) that causes the dynamics to leave the basin of attraction of the original trajectory (see below). Also for significantly smaller perturbation, e.g. $\sigma = 0.01$ms, this is often the case, which suggests that a uniformly distributed perturbation with width $\sigma = 0.6$ms applied to the last spike times before time t_0 is a large perturbation. If this is indeed the case, the measured exponents are not finite-time Lyapunov exponents but rather a kind of finite-size finite-time Lyapunov

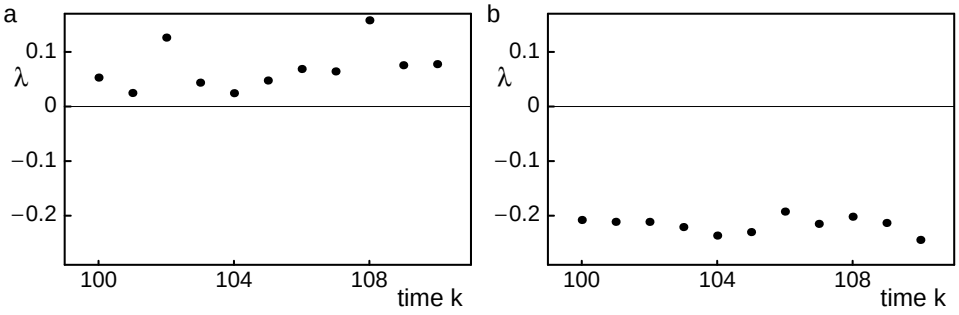

Figure A.2: $\lambda(t_0)$ measured after a perturbation with standard deviation $\sigma = 0.00001$ (a) with the L_1-norm (cf. Eq. (A.7)) and (b) with the L_∞-norm (cf. Eq. (A.9)). In (a), Lyapunov exponents $\lambda(t_0) > 0$ exist reflecting the fact, that the perturbation grows in L_1 norm when it spreads into the network. In (b), the Lyapunov exponents fulfill Eq. A.10 as shown in ch. 6.

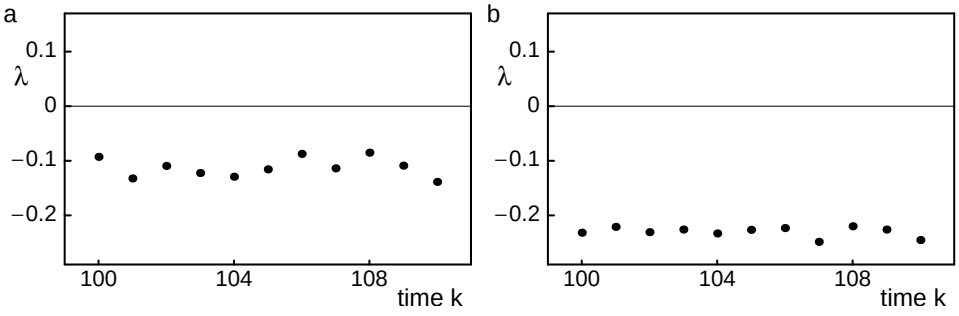

Figure A.3: $\lambda(t_0)$ measured $M = 50$ steps after a perturbation with standard deviation $\sigma = 0.00001$ with (a) the L_1-norm (cf. Eq. (A.7)) and with (b) the L_∞-norm(cf. Eq. (A.9)). In both (a) and (b) the Lyapunov exponents are negative $\lambda(t_0) < 0$.

exponents (cf. [17]) measuring the evolution of finite-size perturbations, which in general does not yield information about local stability.

Due to chapter 6, we know that for a sufficiently small perturbation in Mirollo-Strogatz phase representation, the maximal perturbation cannot grow and the minimal perturbation cannot decrease, in particular the maximum-norm L_∞ of the perturbation vector cannot increase. (A random realization of a network with above parameters is typically strongly connected.) In particular, if we initially only perturb the phases and not the spikes in transit, the maximum-norm of the phase-perturbations cannot grow. We therefore introduce another phase distance based on the maximum norm

$$D_n^\infty = \max_{i=1,\dots,N} |\phi_i(t_n) - \phi_i'(t_n')|, \tag{A.8}$$

and the corresponding finite-time Lyapunov exponent

$$\lambda^{\mathrm{L}\infty}(t_0) = \frac{1}{M} \ln\left(\frac{D_M^\infty}{D_0^\infty}\right), \tag{A.9}$$

for which

$$\lambda^{\mathrm{L}\infty}(t_0) \leq 0 \tag{A.10}$$

holds according to chapter 6. Fig. A.1 shows that in contradiction to Eq. (A.10), for $\sigma = 0.6$ms there are exponents $\lambda^{\mathrm{L}\infty}(t_0) > 0$. We checked that also for a larger number of time steps ($M = 200, 500$) $\lambda(t_0) > 0$ and $\lambda^{\mathrm{L}\infty}(t_0) > 0$. We thus conclude that the applied perturbation was large and led to an interchange of events. Now we consider a small perturbation with zero mean and $\sigma = 0.00001$ms. Numerical simulations show that Eq. A.10 is fulfilled, cf. Fig. A.2b. In the L1 norm, the perturbation may grow as long as it is in process of equilibrating. Indeed, for $M = 20$ steps, there are finite-time Lyapunov exponents $\lambda(t_0) > 0$, indicating that this happens, cf. Fig. A.2a. Since the exponent was only measured over (a rather short) finite time, this shows that in the L_1-norm the perturbation grows while it spreads and equilibrates in the network after it has been applied at t_0, but it does not indicate instability of trajectories. Numerical simulations for longer times ($M = 50, 100, 200, 500$) give exponents $\lambda(t_0) < 0$, independent of the norm we choose for the derivation of the Lyapunov exponent, cf. Fig. A.3, since for longer times decrease of perturbation dominates. This agrees with our analytical findings in chapter 6. Indeed, the dynamics is even asymptotically stable and converges against an equivalent dynamics only shifted in time. The time shift is smaller than the extremal original perturbations as a consequence of the averaging of perturbations at interactions (cf. sec. 6.3). Thus, stability also holds if time shifted trajectories are considered as different. We conclude that generic trajectories underlying the irregular balanced state in the considered networks are stable, in particular there is no chaotic dynamics.

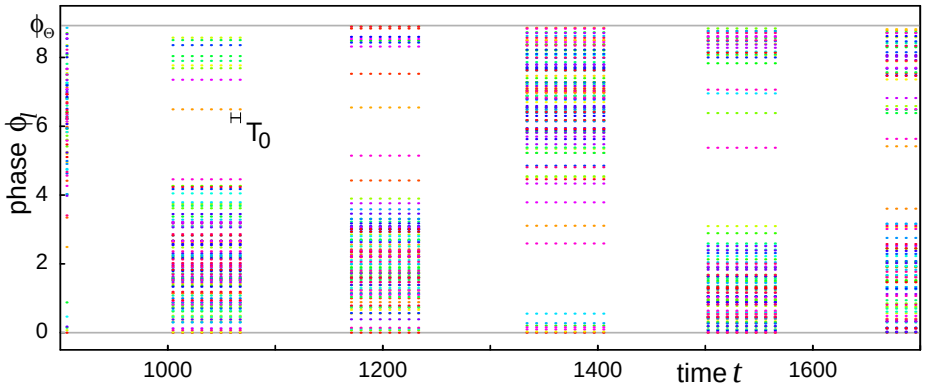

Figure A.4: Phases ϕ_l of neurons l in the network (different colors for different neurons) at the firing times of a reference neuron. Within a period of activity, all phase relations are conserved. The time differences between firings of the reference neuron equal the free period T_0. Periods of regular activity are interrupted by periods of silence, where the reference oscillator does not fire.

A.3 Dynamics with long delay

The main result of ref. [76] is the observation of switching between regular phase patterns in networks with very long delay $\tau = 72$ms. In that article, the dynamics is characterized via the phases of the neurons Eq. A.2 at the kth firing time of a reference oscillator and the phases are given versus discrete time k. This makes it harder to understand the underlying mechanism. Plotting the phases of the neurons at the kth firing time of a reference oscillator versus simulated time t shows also the regular phase patterns but reveals large gaps between the firings of the reference oscillator, cf. Fig. A.4.

In Fig. A.5a, we display the spike sending times of the neurons versus time t. In Fig. A.5b, we display the spike arrival times at the neurons versus time t. Comparison of both panels shows that periods of spiking activity alternate with periods of silence. During periods of spiking activity no spike arrives. Thus, all neurons fire with their intrinsic frequency which is identical. Therefore the phase relation between neurons is unchanged and the phase pattern is regular. (We recall that for the free dynamics, the phase definition Eq. (A.2) equals the Mirollo-Strogatz representation up to a constant factor.) A period of activity has duration slightly above the delay time τ. The spikes sent at the beginning t_b of a phase of activity arrive at $t_b + \tau$, they finish the phase of activity by starting to suppress the firing of neurons. Approximately after time τ, all spikes in transit have arrived, the neurons need some time to recover and then start the next period of activity characterized by free oscillating and sending of every neuron. When spikes arrive, the phase relations are changed due to interactions with arriving spikes so that the phase and spike patterns at different periods of activity are different. We checked

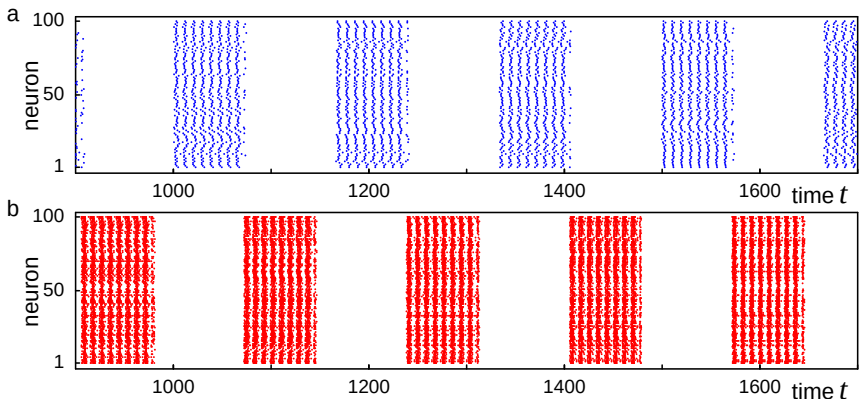

Figure A.5: Spike sendings (a) and spike arrivals (b) of the same dynamics as in Fig. A.4 versus time. Periods of regular activity, in which the neurons oscillate and send their spikes freely according to their intrinsic frequency, alternate with periods of spike arrivals, where the neurons are silent and the phase relations are changed due to incoming spikes.

that for different initial conditions this kind of dynamics was assumed.

A.4 Conclusions

The model considered in ref. [76] is contained in the class of models considered in chapter 6, cf. sec. 6.2. As in ch. 6, trajectories that underlie the irregular balanced state are studied. The authors of ref. [76] report that they numerically find positive finite-time Lyapunov exponents for these trajectories. This result is interpreted as indication of a chaotic balanced state which would contradict our analytical proof showing the stability of generic trajectories. However, the finding of positive finite-time Lyapunov exponents does not contradict our results. We reproduce the qualitative numerical results given in ref. [76] using a slightly different representation of the dynamics and show that the positive finite-time Lyapunov exponents arise since (i) the L_1 norm was chosen for the measurement of perturbation size and in this norm the perturbation increases when it initially spreads into the network and (ii) during the finite interval over which the evolution of the perturbation is measured, the decrease of perturbation does not yet dominate the initial increase. Further, our simulations suggest that the perturbation applied in ref. [76] is large, i.e. the perturbation causes the dynamics to leave the basin of attraction of the original trajectory. We conclude that our simulations confirm the stability of trajectories against sufficiently small perturbations in agreement with the analytical proof in chapter 6, in particular the dynamics is not chaotic.

We also give an explanation for the main result of the article, the observation of switching between regular patterns of activity in networks with very long delay. We

find that in networks with very long delay, periods of firing activity alternate with periods of silence. During periods of activity no spikes arrive (cf. Fig. A.5), the neurons oscillate freely and, due to the identical intrinsic frequency of all neurons, the phase relations are conserved which leads to the observed regular patterns. During periods of activity, spikes are sent. When these spikes arrive, they suppress any neural activity which leads to a period of silence that lasts until all spikes have arrived. During such a period of spikes arrivals, phase relations between neurons are changed due to interactions. The regular phase patterns thus ultimately occur since all neurons have identical free period.

Bibliography

[1] L. Abbott. Lapicque's introduction of the integrate-and-fire model neuron (1907). *Brain Res. Bull.*, 50:303–304, 1999.

[2] L. Abbott and C. van Vreeswijk. Asynchronous states in networks of pulse-coupled oscillators. *Phys. Rev. E*, 48:1483–1490, 1993.

[3] M. Abeles. *Local Cortical Circuits: An Electrophysiological Study*. Springer, Berlin, 1982.

[4] M. Abeles. *Corticonics: Neural Circuits of the Cerebral Cortex*. Cambridge University Press, Cambridge, 1991.

[5] M. Abeles. Time is precious. *Science*, 304:523–524, 2004.

[6] M. Abeles, H. Bergman, F. Margalit, and E. Vaadia. Spatiotemporal firing patterns in the frontal cortex of behaving monkeys. *J. Neurophysiol.*, 70:1629–1638, 1993.

[7] M. Abeles, G. Hayon, and D. Lehmann. Modeling compositionality by dynamic binding of synfire chains. *J. Comp. Neurosci.*, 17:179–201, 2004.

[8] H. Alle and J. Geiger. Combined analog and action potential coding in hippocampal mossy fibers. *Science*, 311:1290–1293, 2006.

[9] D. Amaral, N. Ishizuka, and B. Claiborne. Neurons, numbers and the hippocampal network. *Prog. Brain Res.*, 83:1–11, 1990.

[10] D. Amit and N. Brunel. Model of global sontaneous activity and local structured activity during delay periods in the cerebral cortex. *Cereb. Cortex*, 7:237–252, 1997.

[11] P. Andersen, R. Morris, D. Amaral, T. Bliss, and J. O'Keefe. *The Hippocampus Book*. Oxford University Press, Oxford, 2007.

[12] K. Archie and B. Mel. An intradendritic model for computation of binocular disparity. *Nat. Neurosci.*, 3:54–63, 2000.

[13] G. Ariav, A. Polsky, and J. Schiller. Submillisecond precision of the input-output transformation function mediated by fast sodium dendritic spikes in basal dendrites of CA1 pyramidal neurons. *J. Neurosci.*, 23:7750–7758, 2003.

[14] P. Ashwin and M. Timme. Unstable attractors: Existence and robustness in networks of oscillators with delayed pulse coupling. *Nonlinearity*, 18:2035–2060, 2005.

[15] P. Ashwin and M. Timme. When instability makes sense. *Nature*, 436:36–37, 2005.

[16] D. August and W. Levy. Temporal sequence compression by an integrate-and-fire model of hippocampal area CA3. *J. Comp. Neurosci.*, 6:71–90, 1999.

[17] E. Aurell, G. Boffetta, A. Crisanti, G. Paladin, and A. Vulpiani. Growth of noninfinitesimal perturbations in turbulence. *Phys. Rev. Lett.*, 77:1262–1265, 1996.

[18] Y. Aviel, C. Mehring, M. Abeles, and D. Horn. On embedding synfire chains in a balanced network. *Neural Comp.*, 15:1321–1340, 2003.

[19] D. Bainov and P. Simeonov. *Systems with Impulse Effect. Stability, Theory and Applications.* Horwood, London, 1989.

[20] J. Bang-Jensen and G. Gutin. *Digraphs. Theory, Algorithms and Applications.* Springer, London, 2002.

[21] C. Behrens, L. van den Boom, L. de Hoz, A. Friedman, and U. Heinemann. Induction of sharp wave/ripple complexes in vitro and reorganization of hippocampal networks. *Nat. Neurosci.*, 8:1560–1567, 2005.

[22] C. Behrens, L. van den Boom, and U. Heinemann. Effects of the $GABA_A$ receptor antagonists bicuculline and gabazine on stimulus induced sharp wave-ripple complexes in adult rat hippocampus in vitro. *Europ. J. Neurosci.*, 25:2170–2181, 2007.

[23] M. Bennett and R. Zukin. Electrical coupling and neuronal synchronization in the mammalian brain. *Neuron*, 41:495–511, 2004.

[24] G.-Q. Bi and M.-M. Poo. Synaptic modifications in cultured hippocampal neurons: Dependence on spike timing, synaptic strength, and postsynaptic cell type. *J. Neurosci.*, 18:10464–10472, 1998.

[25] S. Boyd and L. Vandenberghe. *Convex Optimization.* Cambridge Univ. Press, Cabridge, UK, 2004.

[26] V. Braitenberg and A. Schüz. *Cortex: Statistics and Geometry of Neuronal Connectivity.* Springer, Berlin, 1998.

[27] M. Branicky. Studies in hybrid systems. Modeling, analysis and control. ScD thesis, Department of Electrical Engineering and Computer Science, Massachusetts Institute of Technology, 1995.

[28] M. Branicky. Introduction to hybrid systems. In D. Hristu-Varsakelis and W. Levine, editors, *Handbook of Networked and Embedded Control Systems*. Birkhauser, 2005.

[29] R. Brette and W. Gerstner. Adaptive exponential integrate-and-fire model as an effective description of neuronal activity. *J. Neurophysiol.*, 94:3637–3642, 2005.

[30] N. Brunel. Dynamics of sparsely connected networks of excitatory and inhibitory spiking neurons. *J. Comp. Neurosci.*, 8:183–208, 2000.

[31] N. Brunel and V. Hakim. Fast global oscillations in networks of integrate-and-fire neurons with low firing rates. *Neural Comp.*, 11:1621–1671, 1999.

[32] J. Buck. Synchronous rhythmic flashing of fireflies. II. *Quart. Rev. Biol.*, 63:265–289, 1988.

[33] A. Burkitt. A review of the integrate-and-fire neuron model: I. Homogeneous synaptic input. *Biol. Cybern.*, 95:1–19, 2006.

[34] A. Burkitt. A review of the integrate-and-fire neuron model: II. Inhomogeneous synaptic input and network properties. *Biol. Cybern.*, 95:97–112, 2006.

[35] G. Buzsáki. Hippocampal sharp waves: Their origin and significance. *Brain Res.*, 398:242–252, 1986.

[36] G. Buzsáki. Two-stage model of memory trace formation: A role for "noisy" brain states. *Neuroscience*, 31:551–570, 1989.

[37] G. Buzsáki. *Rhythms of the Brain*. Oxford University Press, Oxford, 2006.

[38] G. Buzsáki, D. Buhl, K. Harris, J. Csicsvari, B. Czéh, and A. Morozov. Hippocampal network patterns of activity in the mouse. *Neuroscience*, 116:201–211, 2003.

[39] G. Buzsáki and J. Chrobak. Temporal structures in spatially organized neuronal ensembles: A role for interneuronal networks. *Curr. Opinion. Neurobiol.*, 5:504–519, 1995.

[40] H. Câteau and A. Reyes. Relation between single neuron and population spiking statistics and effects on network activity. *Phys. Rev. Lett.*, 96:058101, 2006.

[41] G. Chartrand and L. Lesniak. *Graphs and Digraphs*. Chapman and Hall, Boca Raton, 2000.

[42] D. Chklovskii. Exact solution for the optimal neuronal layout problem. *Neural Computation*, 16:2067–2078, 2004.

[43] E. Christian and F. Dudek. Electrophysiological evidence from glutamate microapplications for local excitatory circuits in the CA1 area of rat hippocampal slices. *J. Neurophysiol.*, 59:110–123, 1988.

[44] B. Clark, P. Monsivais, T. Branco, M. London, and M. Häusser. The site of action potential initiation in cerebellar Purkinje neurons. *Nat. Neurosci.*, 8:137–139, 2005.

[45] L. Colgin, Y. Jia, J.-M. Sabatier, and G. Lynch. Blockade of NMDA receptors enhances spontanoues sharp waves in rat hippocampal slices. *Neurosci. Lett.*, 385:46–51, 2005.

[46] B. Connors and M. Long. Electrical synapses in the mammalian brain. *Annu. Rev. Neurosci.*, 27:393–418, 2004.

[47] E. Curti, G. Mongillo, G. La Camera, and D. Amit. Mean field and capacity in realistic networks of spiking neurons storing sparsely coded random memories. *Neural Comp.*, 16:2597–2637, 2004.

[48] P. Dayan and L. Abbott. *Theoretical Neuroscience: Computational and Mathematical Modeling of Neural Systems*. MIT Press, Cambridge, 2001.

[49] J. de la Rocha, B. Doiron, E. Shea-Brown, K. Josić, and A. Reyes. Correlation between neural spike trains increases with firing rate. *Nature*, 448:802–807, 2007.

[50] M. Denker, M. Timme, M. Diesmann, F. Wolf, and T. Geisel. Breaking synchrony by heterogeneity in complex networks. *Phys. Rev. Lett.*, 92:074103, 2004.

[51] A. Destexhe, Z. Mainen, and T. Sejnowski. Synthesis of models for excitable membranes, synaptic transmission and neuromodulation using a common kinetic formalism. *J. Comp. Neurosci.*, 1:195–230, 1994.

[52] J. Deuchars and A. Thomson. CA1 pyramid-pyramid connections in rat hippocampus *in vitro*: Dual intracellular recordings with biocytin filling. *Neuroscience*, 74:1009–1018, 1996.

[53] K. Diba and G. Buzsáki. Forward and reverse hippocampal place cell sequences during ripples. *Nat. Neurosci.*, 10:1241–1242, 2007.

[54] M. Diesmann, M.-O. Gewaltig, and A. Aertsen. Stable propagation of synchronous spiking in cortical neural networks. *Nature*, 402:529–533, 1999.

[55] A. Draguhn, R. Traub, D. Schmitz, and J. Jefferys. Electrical coupling underlies high frequency oscillations in the hippocampus *in vitro*. *Nature*, 394:189–192, 1998.

[56] B. Drossel and A. McKane. Modeling food webs. In S. Bornholdt and H. Schuster, editors, *Handbook of Graphs and Networks: From the Genome to the Internet*. Wiley-VCH, 2002.

[57] B. Ermentrout and N. Kopell. Parabolic bursting in an excitable system coupled with a slow oscillation. *SIAM J. Appl. Math.*, 2:233–253, 1986.

[58] U. Ernst, K. Pawelzik, and T. Geisel. Synchronization induced by temporal delays in pulse-coupled oscillators. *Phys. Rev. Lett.*, 74:1570–1573, 1995.

[59] U. Ernst, K. Pawelzik, and T. Geisel. Delay induced multistable synchronization of biological oscillators. *Phys. Rev. E*, 57:2150–2162, 1998.

[60] C. Eurich, K. Pawelzik, U. Ernst, J. Cowan, and J. Milton. Dynamics of self-organized delay adaptation. *Phys. Rev. Lett.*, 82:1594–1597, 1999.

[61] J. Fellous, P. Tiesinga, P. Thomas, and T. Sejnowski. Discovering spike patterns in neuronal responses. *J. Neurosci.*, 24:2989–3001, 2004.

[62] T. Fiacco and K. McCarthy. Astrocyte calcium elevations: Properties, propagation and effects on brain signaling. *Glia*, 54:676–690, 2006.

[63] R. Fields and B. Stevens-Graham. New insights into neuron-glia communication. *Science*, 298:556–562, 2001.

[64] N. Fourcaud-Trocmé, D. Hansel, C. van Vreeswijk, and N. Brunel. How spike generation mechanisms determine the neuronal response to fluctuating inputs. *J. Neurosci.*, 23:11628–11640, 2003.

[65] M. Galarreta and S. Hestrin. Electrical synapses between GABA-releasing interneurons. *Nat. Rev. Neurosci.*, 2:425–433, 2001.

[66] K. Gansel and W. Singer. Replay of second-order spike patterns with millisecond precision in the visual cortex. Soc. Neurosci. Abstr. 276.8, 2005.

[67] K. Gansel and W. Singer. Recurring second-order spike patterns concur with increased symmetry in functional neuronal couplings. Soc. Neurosci. Abstr. 634.25, 2006.

[68] K. Gansel and W. Singer. Repeating spatiotemporal spike patterns reflect functional network states in the visual cortex. NCCD Meeting Abstr., 2007.

[69] C. Gardiner. *Handbook of Stochastic Methods*. Springer, Berlin, 2002.

[70] S. Gasparini and J. Magee. State-dependent dendritic computation in hippocampal CA1 pyramidal neurons. *J. Neurosci.*, 26:2088–2100, 2006.

[71] S. Gasparini, M. Migliore, and J. Magee. On the initiation and propagation of dendritic spikes in CA1 pyramidal neurons. *J. Neurosci.*, 24:11046–11056, 2004.

[72] W. Gerstner and W. Kistler. *Spiking Neuron Models: Single Neurons, Populations, Plasticity*. Cambridge Univ. Press, Cambridge, 2001.

[73] M.-O. Gewaltig. Evolution of synchronous spike volleys in cortical networks. PhD thesis, Ruhr University of Bochum, 1999.

[74] C. Goldman, D. Henze, C. Koch, and G. Buzsáki. On the origin of the extracellular action potential waveform: A modeling study. *J. Neurophysiol.*, 95:3113–3128, 2006.

[75] J. Goncalves, A. Megretski, and M. Dahleh. Global analysis of piecewise linear systems using impact maps and quadratic surface Lyapunov functions. *IEEE Trans. Autom. Contr.*, 48:2089–2106, 2003.

[76] P. Gong and C. van Leeuwen. Dynamically maintained spike timing sequences in networks of pulse-coupled oscillators with delays. *Phys. Rev. Lett.*, 98:048104, 2007.

[77] S. Grillner. Biological patern generation: The cellular and computational logic of networks in motion. *Neuron*, 52:751–766, 2006.

[78] F. Hamzei-Sichani, N. Kamasawa, W. Janssen, T. Yasumura, K. Davidson, P. Hof, S. Wearne, M. Stewart, S. Young, M. Whittington, J. Rash, and R. Traub. Gap junctions on hippocampal mossy fiber axons demonstrated by thin-section electron microscopy and freeze fracture replica immunogold labeling. *Proc. Natl. Acad. Sci.*, 104:12548–12553, 2007.

[79] D. Hansel and G. Mato. Existence and stability of persistent states in large neuronal networks. *Phys. Rev. Lett.*, 86:4175–4178, 2001.

[80] J. Hasty, D. McMillen, F. Isaacs, and J. Collins. Computational studies of gene regulatory networks: In numero molecular biology. *Nat. Rev. Genet.*, 2:268–279, 2001.

[81] M. Häusser and B. Mel. Dendrites: Bug or feature? *Curr. Op. Neurobiol.*, 13:372–383, 2003.

[82] M. Häusser, N. Spruston, and G. Stuart. Diversity and dynamics of dendritic signaling. *Science*, 290:739–744, 2000.

[83] M. Herrmann, J. Hertz, and A. Prügel-Bennett. Analysis of synfire chains. *Network*, 6:403–414, 1995.

[84] J. Hertz, A. Lerchner, and M. Ahmadi. Mean field methods for cortical network dynamics. Proceedings of the Erice School on Cortical Dynamics, 2004.

[85] A. Herz and J. Hopfield. Earthquake cycles and neural reverberations: Collective oscillations in systems with pulse-coupled threshold elements. *Phys. Rev. Lett.*, 75:1222–1225, 1995.

[86] B. Hille. *Ion channels of excitable membranes.* Sinauer, Sunderland, 2001.

[87] H. Homayoun and B. Moghaddam. NMDA receptor hypofunction produces opposite effects on prefrontal cortex interneurons and pyramidal neurons. *J. Neurosci.*, 27:11496–11500, 2007.

[88] J. Hopfield. Neural networks and physical systems with emergent collective computational abilities. *Proc. Natl. Acad. Sci.*, 79:2554–2558, 1982.

[89] Y. Ikegaya, G. Aaron, R. Cossart, D. Aronov, I. Lampl, D. Ferster, and R. Yuste. Synfire chains and cortical songs: Temporal modules of cortical activity. *Science*, 304:559–564, 2004.

[90] E. Izhikevich. *Dynamical Systems in Neuroscience: The Geometry of Excitability and Bursting.* MIT Press, Cambridge, 2007.

[91] J. Jack, D. Noble, and R. Tsien. *Electric current flow in excitable cells.* Clarendon, Oxford, 1985.

[92] G. Jacobson, K. Diba, A. Yaron-Jakoubovitch, Y. Oz, C. Koch, I. Segev, and Y. Yarom. Subthreshold voltage noise of rat neocortical pyramidal neurons. *J. Physiol.*, 564:145–160, 2005.

[93] S. Jahnke. Stable spike timing in complex neural networks. Diploma thesis, Department of Physics, Georg-August University of Göttingen, 2006.

[94] S. Jahnke, R.-M. Memmesheimer, and M. Timme. How chaotic is the balanced state? in preparation, 2008.

[95] S. Jahnke, R.-M. Memmesheimer, and M. Timme. Stable irregular dynamics in complex neural networks. *Phys. Rev. Lett.*, 100:048102, 2008.

[96] J. Jefferys. Influence of electric fields on the excitability of granule cells in guinea-pig hippocampal slices. *J. Physiol.*, 319:143–152, 1981.

[97] G. Jetschke. *Mathematik der Selbstorganisation.* VEB Deutscher Verlag der Wissenschaften, Berlin, 1989.

[98] D. Jin. Fast convergence of spike sequences to periodic patterns in recurrent networks. *Phys. Rev. Lett.*, 89:208102, 2002.

[99] D. Jin and H. Seung. Fast computation with spikes in a recurrent neural network. *Phys. Rev. E*, 65:051922, 2002.

[100] R. Jolivet, A. Rauch, H.-R. Lüscher, and W. Gerstner. Integrate-and-fire models with adaptation are good enough: Predicting spike times under random current injection. In M. Taketani and M. Baudry, editors, *Advances in network electrophysiology using multi-electrode arrays.* Springer, 2006.

[101] P. Jonas, J. Bischofberger, D. Fricker, and R. Miles. Interneuron diversity series: Fast in, fast out: Temporal and spatial signal processing in hippocampal interneurons. *Trends Neurosci.*, 27:30–40, 2004.

[102] D. Jungnickel. *Graphs, Networks and Algorithms*. Springer, Heidelberg, 1999.

[103] A. Kamondi, L. Acsádi, and G. Buzsáki. Dendritic spikes are enhanced by cooperative network activity in the intact hippocampus. *J. Neurosci.*, 18:3919–3928, 1998.

[104] E. Kandel, J. Schwartz, and T. Jessell. *Principles of Neural Science*. Prentice Hall, London, 1995.

[105] A. Kumar, S. Schrader, A. Aertsen, and S. Rotter. The high-conductance state of cortical networks. *Neural Comp.*, 20:1–34, 2007.

[106] C. Landisman and B. Connors. Long-term modulation of electrical synapses in the mammalian thalamus. *Science*, 310:1809–1813, 2005.

[107] L. Lapicque. Recherches quantitatives sur l'excitation electrique des nerfs traiteé comme une polarisation. *J. Physiol. Pathol. Gen.*, 9:357, 1907.

[108] F. LeBeau, R. Traub, H. Moyer, M. Whittington, and E. Buhl. The role of electrical signaling via gap junctions in the generation of fast network oscillations. *Brain Res. Bul.*, 62:3–13, 2003.

[109] A. Lee and M. Wilson. Memory of sequential experience in the hippocampus during slow wave sleep. *Neuron*, 36:1183–1194, 2002.

[110] B. Lindner. Superposition of many independent spike trains is generally not a Poisson process. *Phys. Rev. E*, 73:022901, 2006.

[111] A. Loebel and M. Tsodyks. Computation by ensemble synchronization in recurrent networks with synaptic depression. *J. Comp. Neurosci.*, 13:111–124, 2002.

[112] M. London and M. Häusser. Dendritic computation. *Annu. Rev. Neurosci.*, 28:503–532, 2005.

[113] W. Maass and C. Bishop. *Pulsed neural networks*. MIT Press, Cambridge, 1999.

[114] W. Maass and T. Natschläger. Real-time computing without stable states: A new framework for neural computation based on perturbations. *Neural Comp.*, 14:2531–2560, 2002.

[115] R. Maex and E. De Schutter. Mechanism of spontaneous and self-sustained oscillations in networks connected through axo-axonal gap junctions. *J. Neurosci.*, 25:3347–3358, 2007.

[116] N. Maier. Elektrophysiologische Untersuchungen zu sharp-wave-ripple Komplexen im Hippocampus der Maus in vitro. Doctor of Medicine thesis, Institute of Physiology, Department of Medicine, Charité Berlin, 2006.

[117] N. Maier, V. Nimmrich, and A. Draguhn. Cellular and network mechanisms underlying spontaneous sharp wave-ripple complexes in mouse hippocampal slices. *J. Physiol*, 550.3:873–887, 2003.

[118] Z. Mainen and T. Sejnowski. Reliability of spike timing in neocortical neurons. *Science*, 268:1503–1506, 1995.

[119] V. Makarov, F. Panetsos, and O. de Feo. A method for determining neural connectivity and inferring the underlying network dynamics using extracellular spike recordings. *J. Neurosci. Meth.*, 144:265–279, 2005.

[120] H. Markram. The blue brain project. *Nat. Rev. Neurosci.*, 7:153–160, 2006.

[121] H. Markram, J. Lübke, M. Frotscher, and B. Sakmann. Regulation of synaptic efficacy by coincidence of postsynaptic APs und EPSPs. *Science*, 275:213–215, 1997.

[122] H. Markram, M. Toledo-Rodriguez, Y. Wang, A. Gupta, G. Silberberg, and C. Wu. Interneurons of the neocortical inhibitory system. *Nature Reviews Neuroscience*, 5:793–807, 2004.

[123] I. Matus Bloch and C. Romero Z. Firing sequence storage using inhibitory synapses in networks of pulsatil nonhomogeneous integrate-and-fire neural oscillators. *Phys. Rev. E*, 66:036127, 2002.

[124] C. Mehring, U. Hehl, M. Kubo, M. Diesmann, and A. Aertsen. Activity dynamics and propagation of synchronous spiking in locally connected random networks. *Biol. Cybern.*, 88:395–408, 2003.

[125] M. Mehta. *Matrix theory: Selected topics and useful results.* Hindustan Publishing Corporation, Delhi, 1989.

[126] M. Mehta. Cortico-hippocampal interaction during up-down states and memory consolidation. *Nat. Neurosci.*, 10:13–15, 2007.

[127] B. Mel. The clusteron: Toward a simple abstraction for a complex neuron. In J. Moody, S. Hanson, and R. Lippmann, editors, *Advances in Neural Information Processing.* Morgan Kaufmann, 1992.

[128] B. Mel. Synaptic integration in an excitable dendritic tree. *J. Neurophysiol.*, 70:1086–1101, 1993.

[129] B. Mel. Why have dendrites? A computational perspective. In G. Stuart, N. Spruston, and M. Häusser, editors, *Dendrites.* Oxford University Press, 1999.

[130] B. Mel, D. Ruderman, and K. Archie. Translation-invariant orientation tuning in visual 'complex' cells could derive from intradendritic computations. *J. Neurosci.*, 17:4325–4334, 1998.

[131] R.-M. Memmesheimer and M. Timme. Designing complex networks. *Physica D*, 224:182–201, 2006.

[132] R.-M. Memmesheimer and M. Timme. Designing the dynamics of spiking neural networks. *Phys. Rev. Lett.*, 97:188101, 2006.

[133] A. Mercer, A. Bannister, and A. Thomson. Electrical coupling between pyramidal cells in adult cortical regions. *Brain Cell Biol.*, 35:13–27, 2006.

[134] T. Metzinger. Einleitung: Das Problem des Bewusstseins. In T. Metzinger, editor, *Bewusstsein. Beiträge aus der Gegenwartsphilosophie.* Schöningh, 1996.

[135] R. Milo, N. Kashtan, S. Itzkovitz, M. Newman, and U. Alon. On the uniform generation of random graphs with prescribed degree sequences. http://arxiv.org/abs/cond-mat/0312028, 2003.

[136] R. Mirollo and S. Strogatz. Synchronization of pulse coupled biological oscillators. *SIAM J. Appl. Math.*, 50:1645–1662, 1990.

[137] A. Mokeichev, M. Okun, O. Barak, Y. Katz, O. Ben-Shahar, and I. Lampl. Stochastic emergence of repeating cortical motifs in spontaneous membrane potential fluctuations in vivo. *Neuron*, 53:413–425, 2007.

[138] G. Mongillo, D. Amit, and N. Brunel. Retrospective and prospective persistent activity induced by Hebbian learning in a recurrent cortical network. *Eur. J. Neurosci.*, 18:2011–2024, 2003.

[139] A. Morrison, A. Aertsen, and M. Diesmann. Spike-timing-dependent plasticity in balanced random networks. *Neural Comp.*, 19:1437–1467, 2007.

[140] B. Naundorf, T. Geisel, and F. Wolf. Action potential onset dynamics and the response speed of neuronal populations. *J. Comp. Neurosci.*, 18:297–309, 2005.

[141] B. Naundorf, F. Wolf, and M. Volgushev. Unique features of action potential initiation in cortical neurons. *Nature*, 440:1060–1063, 2006.

[142] T. Nevian, M. Larkum, A. Polsky, and J. Schiller. Properties of basal dendrites of layer 5 pyramidal neurons: A direct patch-clamp recording study. *Nat. Neurosci.*, 10:206–214, 2007.

[143] V. Nimmrich, N. Maier, D. Schmitz, and A. Draguhn. Induced sharp wave-ripple complexes in the absence of synaptic inhibition in mouse hippocampal slices. *J. Physiol.*, 563.3:663–670, 2005.

[144] J. Norris. *Markov Chains.* Cambridge University Press, Cambridge, 1997.

[145] L. Nowak, M. Sanchez-Vivez, and D. McCormick. Influence of low and high frequency inputs on spike timing in visual cortical neurons. *Cereb. Cortex*, 7:487–501, 1997.

[146] M. Nusbaum and M. Beenhakker. A small systems approach to motor pattern generation. *Nature*, 417:343–350, 2002.

[147] J. O'Keefe and M. Recce. Phase relationship between hippocampal place units and the EEG theta rhythm. *Hippocampus*, 3:317–330, 1993.

[148] M. Oram, M. Wiener, R. Lestienne, and B. Richmond. Stochastic nature of precisely timed spike patterns in visual system neuronal responses. *J. Neurophysiol.*, 81:3021–3033, 1999.

[149] P. Parra, A. Gulyás, and R. Miles. How many subtypes of inhibitory cells in the hippocampus? *Neuron*, 20:983–993, 1998.

[150] A. Pikovsky, M. Rosenblum, and J. Kurths. *Synchronization: A Universal Concept in Nonlinear Sciences.* Cambridge Univ. Press, Cambridge, MA, 2001.

[151] G. Pipa. The neuronal code - development of tools and hypotheses for understanding the role of synchronization of neuronal activity. Doctoral thesis, Faculty for Electrical Engineering and Computer Sciences, Technical University of Berlin 2002.

[152] G. Pipa, A. Riehle, and S. Grün. Validation of task-related excess of spike coincidences based on NeuroXidence. *Neurocomputing*, 70:2064–2068, 2007.

[153] P. Poirazi, T. Brannon, and B. Mel. Arithmetic of subthreshold synaptic summation in a model CA1 pyramidal neuron. *Neuron*, 37:977–987, 2003.

[154] P. Poirazi, T. Brannon, and B. Mel. Pyramidal neuron as two-layer network. *Neuron*, 37:989–999, 2003.

[155] G. Pola, M. Bujorianu, J. Lygeros, and M. D. Benedetto. Stochastic hybrid models: An overview. In *Proceedings IFAC Workshop on Analysis and Design of Hybrid Systems*, 2003.

[156] A. Politi, R. Livi, G.-L. Oppo, and R. Kapral. Unpredictable behavior in stable systems. *Europhys. Lett.*, 22:571–576, 1993.

[157] A. Polsky, B. Mel, and J. Schiller. Computational subunits in thin dendrites of pyramidal cells. *Nat. Neurosci.*, 7:621–627, 2004.

[158] A. Prinz. Insights from models of rhythmic motor systems. *Curr. Opin. Neurobiol.*, 16:615–620, 2006.

[159] A. Prinz, D. Bucher, and E. Marder. Similar network activity from disparate circuit parameters. *Nat. Neurosci.*, 7:1345–1352, 2004.

[160] D. Purves, G. Augustine, D. Fitzpatrick, L. Katz, A.-S. LaMantia, and J. McNamara. *Neuroscience*. Sinauer, Sunderland, 1997.

[161] R. Rao and T. Sejnowski. Spike-timing-dependent Hebbian plasticity as temporal difference learning. *Neural Comp.*, 13:2221–2237, 2001.

[162] A. Rauch, G. LaCamera, H. Lüscher, W. Senn, and S. Fusi. Neocortical pyramidal cells respond as integrate-and-fire neurons to in vivo like input currents. *J. Neurophysiol.*, 90:1598–1612, 2003.

[163] M. Ren, Y. Yoshimura, N. Takada, S. Horibe, and Y. Komatsu. Specialized inhibitory synaptic actions between nearby neocortical pyramidal neurons. *Science*, 316:758–761, 2007.

[164] A. Riehle, S. Grün, M. Diesmann, and A. Aertsen. Spike synchronization and rate modulation differentially involved in motor function. *Science*, 278:1950–1953, 1997.

[165] H. Risken. *The Fokker Planck Equation. Methods of Solution and Applications.* Springer, Berlin, 1996.

[166] A. Roxin, N. Brunel, and D. Hansel. Role of delays in shaping spatiotemporal dynamics of neuronal activity in large networks. *Phys. Rev. Lett.*, 94:238103, 2005.

[167] A. Schaft and J. Schumacher. *An introduction to hybrid dynamical systems.* Springer, London, 2000.

[168] D. Schmitz, S. Schuchmann, A. Fisahn, A. Draguhn, E. Buhl, E. Petrasch-Parwez, R. Dermietzel, U. Heinemann, and R. Traub. Axo-axonal coupling: A novel mechanism for ultrafast neuronal communication. *Neuron*, 31:831–840, 2001.

[169] M. Shadlen and W. Newsome. The variable discharge of cortical neurons: Implications for connectivity, computation, and information coding. *J. Neurosci.*, 18:3870–3896, 1998.

[170] Y. Shu, A. Hasenstaub, A. Duque, Y. Yu, and D. McCormick. Modulation of intracortical synaptic potentials by presynaptic somatic membrane potential. *Nature*, 441:761–765, 2006.

[171] A. Siapas and M. Wilson. Coordinated interactions between hippocampal ripples and cortical spindles during slow wave sleep. *Neuron*, 21:1123–1128, 1998.

[172] W. Softky and C. Koch. The highly irregular firing of cortical cells is insonsistent with temporal integration of random EPSPs. *J. Neurosci.*, 13:334–350, 1993.

[173] N. Spruston, G. Stuart, and M. Häusser. Dendritic integration. In N. Spruston, G. Stuart, and M. Häusser, editors, *Dendrites*. Oxford Univ. Press, 2002.

[174] S. Strogatz and R. Mirollo. Splay states in globally coupled Josephson arrays: Analytical prediction of floquet multipliers. *Phys. Rev. E*, 47:220–227, 1993.

[175] T. Tetzlaff, A. Morrison, T. Geisel, and M. Diesmann. Consequences of realistic network size on the stability of embedded synfire chains. *Neurocomputing*, 58-60:117–121, 2004.

[176] M. Timme. *Collective Dynamics in Networks of Pulse-Coupled Oscillators*. PhD thesis, Georg-August-Universität zu Göttingen, 2002.

[177] M. Timme. Collective dynamics in networks of pulse coupled oscillators. Doctoral thesis, Department of Physics, Georg-August University of Göttingen, 2002.

[178] M. Timme. Does dynamics reflect topology in directed networks? *Europhys. Lett.*, 76:367–373, 2006.

[179] M. Timme, F. Wolf, and T. Geisel. Coexistence of regular and irregular dynamics in complex networks of pulse-coupled oscillators. *Phys. Rev. Lett.*, 89:258701, 2002.

[180] M. Timme, F. Wolf, and T. Geisel. Prevalence of unstable attractors in networks of pulse-coupled oscillators. *Phys. Rev. Lett.*, 89:154105, 2002.

[181] M. Timme, F. Wolf, and T. Geisel. Unstable attractors induce perpetual synchronization and desynchronization. *Chaos*, 13:377, 2003.

[182] M. Timme, F. Wolf, and T. Geisel. Topological speed limits to network synchronization. *Phys. Rev. Lett.*, 92:074101, 2004.

[183] S. Titz and B. Keller. Rapidly deactivating AMPA receptors determine excitatory synaptic transmission to interneurons in the nucleus tractus solitarius from rat. *J. Neurophysiol.*, 78:82–91, 1997.

[184] R. Traub and A. Bibbig. A model of high frequency ripples in the hippocampus based on synaptic coupling plus axon-axon gap junctions between pyramidal neurons. *J. Neurosci.*, 20:2086–2093, 2000.

[185] R. Traub and R. Miles. *Neuronal Networks of the Hippocampus*. Cambridge University Press, Cambridge, 1991.

[186] R. Traub, D. Schmitz, J. Jefferys, and A. Draguhn. High frequency population oscillations are predicted to occur in hippocampal pyramidal neuronal networks interconnected by axoaxonal gap junctions. *Neuroscience*, 92:407–426, 1999.

[187] R. Traub, M. Whittington, S. Colling, G. Buzsáki, and J. Jefferys. Analysis of gamma rhythms in the rat hippocampus *in vitro* and *in vivo*. *J. Physiol. (Lond.)*, 493:471–484, 1996.

[188] J. Trommershäuser, S. Titz, B. Keller, and A. Zippelius. Variability of excitatory currents due to single-channel noise, receptor number and morphological heterogeneity. *J. theor. Biol.*, 208:329–343, 2001.

[189] M. Tsodyks and H. Markram. The neural code between neocortical pyramidal neurons depends on neurotransmitter release probability. *Proc. Natl. Acad. Sci.*, 94:719–723, 1997.

[190] M. Tsodyks, I. Mitkov, and H. Sompolinsky. Pattern of synchrony in inhomogeneous networks of oscillators with pulse interactions. *Phys. Rev. Lett.*, 71:1280–1283, 1993.

[191] M. Tsodyks, K. Pawelzik, and H. Markram. Neural networks with dynamics synapses. *Neural Comp.*, 10:821–835, 1998.

[192] H. Tuckwell. *Introduction to theoretical neurobiology: Volume 1. Linear cable theory and dendritic structure*. Cambridge Univ. Press, Cambridge, 1988.

[193] H. Tuckwell. *Introduction to theoretical neurobiology: Volume 2. Nonlinear and stochastic theories*. Cambridge Univ. Press, Cambridge, 1988.

[194] G. Uhlenbeck and L. Ornstein. On the theory of the Brownian motion. *Phys. Rev.*, 36:823–841, 1930.

[195] C. van Vreeswijk. Partial synchronization in populations of pulse-coupled oscillators. *Phys. Rev. E*, 54:5522–5537, 1996.

[196] C. van Vreeswijk. Analysis of the asynchronous state in networks of strongly coupled oscillators. *Phys. Rev. Lett.*, 84:5110, 2000.

[197] C. van Vreeswijk, L. Abbott, and G. Ermentrout. When inhibition not excitation synchronizes neural firing. *J. Comp. Neurosci.*, 1:313–321, 1996.

[198] C. van Vreeswijk and H. Sompolinsky. Chaos in neuronal networks with balanced excitatory and inhibitory activity. *Science*, 274:1724–1726, 1996.

[199] C. van Vreeswijk and H. Sompolinsky. Chaotic balanced state in a model of cortical circuits. *Neural Comp.*, 10:1321, 1998.

[200] A. Verkhratsky and E. Toscu. Neuronal-glial networks as substrate for cns integration. *J. Cell. Mol. Med.*, 10(4), 2006.

[201] T. Vogels and L. Abbott. Signal propagation and logic gating in networks of integrate-and-fire neurons. *J. Neurosci.*, 25:10786–10795, 2005.

[202] X.-J. Wang. Synaptic basis of cortical persistent acitivity: The importance of NMDA receptors to working memory. *J. Neurosci.*, 19:9587–9603, 1999.

[203] D. Werner. *Funktionalanalysis*. Springer, Berlin, 1997.

[204] M. Whittington, R. Traub, and J. Jefferys. Synchronized oscillations in interneuron networks driven by metabotropic glutamate receptor activation. *Nature*, 373:612–615, 1995.

[205] S. Williams and G. Stuart. Dependence of EPSP efficacy on synapse location in neocortical pyramidal neurons. *Science*, 295:1907–1910, 2002.

[206] A. Ylinen, A. Bragin, Z. Nádasdy, G. Jandó, I. Szabó, A. Sik, and G. Buzsáki. Sharp wave-associated high-frequency oscillation (200Hz) in the intact hippocampus: Network and intracellular mechanisms. *J. Neurosci.*, 15:30–46, 1995.

[207] J. Zhang, K. Johansson, J. Lygeros, and S. Sastry. Dynamical systems revisited: Hybrid systems with zeno executions. In N. Lynch and B. Krogh, editors, *Hybrid Systems: Computation and Control*. Springer, 2000.

[208] R. Zillmer, R. Livi, A. Politi, and A. Torcini. Desynchronization in diluted neural networks. *Phys. Rev. E*, 74:036203, 2006.

[209] A. Zumdieck, M. Timme, T. Geisel, and F. Wolf. Long chaotic transients in complex networks. *Phys. Rev. Lett.*, 93:244103, 2004.

Acknowledgments

I am particularly grateful to

- Prof. Dr. Theo Geisel for always taking the time to answer scientific and other questions and to discuss our recent results. I would also like to thank him for the excellent research conditions in his department.
- Dr. Marc Timme for supervising this thesis, for the excellent collaboration, for the opportunity to learn from him and for his fruitful ideas. Further, for his constant support when writing publications and this thesis. I am indebted to him for proposing such an interesting topic for the thesis, and also for giving me the chance to develop my own ideas, in particular those chapters 7 and 8 are based on.
- Sven Jahnke for the excellent collaboration, his tenacity, many discussions, support, and, in particular, that he was prepared to interrupt his world-trip to complete our publication.
- Dr. Fred Wolf for highly fruitful discussions and for giving me the opportunity to learn from him.
- Kai Gansel, Dr. Gordon Pipa and Prof. Dr. Wolf Singer from the MPI for brain research, Frankfurt/Main, for helpful discussions and support on precisely timed patterns of spikes.
- Dr. Nikolaus Maier and Prof. Dr. Dietmar Schmitz from the Charité Berlin for helpful discussions and support on sharp wave/ripples. I would also like to thank Dr. Nikolaus Maier for proof-reading parts of this thesis.
- Dr. Abgail Morrison, Dr. Birgit Kriener, Michael Denker, Dr. Markus Diesmann, Prof. Dr. Stefan Rotter from the BCCN Freiburg and from the RIKEN, Tokio, for helpful discussions.
- Prof. Dr. Jackie Schiller from the Technion, Haifa, for inspiring discussions about nonlinear dendrites.

- Dr. Michael Herrmann for stimulating discussions and for sharing the experience of teaching the neuroscience course together with him and Prof. Dr. Theo Geisel.
- Christoph Kirst for numerically checking some results in chapter 8.
- Philip Bittihn for his studies and programming work during his internship in our group.
- Anna Levina and Georg Martius for many valuable discussions.
- Tatjana Tchumachenko, Min Huang, Wei Wei and Michael Kreissl for interesting discussions and their hospitality during Fred's group meetings.
- Dorothea Hämmerer for proof-reading parts of the thesis and for interesting discussions about cognitive neurosciences.
- Sibylle Jane Kalz and Eleanor Livesey for proof-reading parts of the thesis.
- Holger Hennig for the friendly atmosphere in our office and his patience with me occupying three quarters of the desk space available during the last months.
- Oliver Bendix for being so understanding whenever I had to skip fitness sessions during the last few weeks.
- Lishma Anand, Jens Arnold, Yorck-Fabian Beensen, Dr. Dirk Brockmann, Kai Bröking, Dr. Markus Butz, Vincent David, Hecke Degering, Dr. Ragnar Fleischmann, Dr. Denny Fliegner, Frank Hesse, Dr. Matthias Kaschube, Christoph Kolodziejski, Dr. Björn Naundorf, Lars Reichl, Dr. Holger Schanz, Michael Schnabel, Benjamin Schwenker and Dr. Dr. Fabian Theis for interesting discussions and support.
- all members of our group for the friendly atmosphere.
- my flatmates, Lisa Nortmann, Xenia von Schönebeck, Christina Templin, Frauke Urban, Alejandro Morales and Eliu Schmitt for their patience when I neglected WG life and WG duties because of my work.
- my sister and my parents for many valuable discussions about philosophy and neurosciences, for support and advice.